A LABORATORY INVESTIGATION OF SHEAR WAVE VELOCITY IN STABILISED SOFT SOILS

by

CHEE-MING CHAN
B.Sc. Civil Eng.
(University of Technology, Malaysia)

A THESIS SUBMITTED FOR THE DEGREE OF *DOCTOR OF PHILOSOPHY*

DEPARTMENT OF CIVIL AND STRUCTURAL ENGINEERING
UNIVERSITY OF SHEFFIELD

JANUARY 2006

For my loving parents, brother, sister and
K. W. Chok;
and all my teachers, then and now...

Acknowledgements

With the completion of this thesis comes the long overdue moment for expressing my gratitude and appreciation to all whom I am indebted to. I cannot fully thank my supervisor, Dr. Charles Hird, for his constant teaching, guidance and moral support, way back from day one. His immense patience with me and dedication to my work were... unsurpassable!

I also take pleasure in recording much generous help from the Geotechnical Engineering technical support staff, Paul Osborne and Mark Foster, as well as Tim Robinson from the Electronics section. My laboratory work and equipment set-up were greatly assisted by their superb skills, knowledge and experience. Of course, there was always a helping hand in times of need from the others too- my sincere thanks to David Hobbart, David Callaghan, Mick Moore, and all the others. Thank you also to all my friends and colleagues in the Geotechnical Engineering Group, for their friendship and sharing of knowledge.

Special thanks to my family and friends back home in Malaysia, for their inimitable love and faith in me, which kept me going when the goings were rough. They were always there with me in this roller-coaster ride, all the way... Thank you.

My sincere gratitude especially to Prof. Ismail bin Bakar, the Rector of KUiTTHO, for being such a wonderful and supportive mentor. Thanks also to Assoc. Prof. Azizan bin Abd. Aziz (KUiTTHO), for his kind words and encouragement when I first embarked on this journey. Not forgetting Madam Noor Azizah binti Ibrahim, who first introduced me to Soil Mechanics in the Polythechnic of Port Dickson (PPD) and sowed the seed for my interest today. *Terima kasih, Puan...*

Not less importantly, my appreciation goes to the Ministry of Science, Technology and Environment (MOSTE), Malaysia, for funding my studies here to fulfil a dream, which would have remained one without the financial support.

Finally, to all those who have assisted me along this journey, in any way at all, please accept my sincere thanks. Should I have failed to include a name here, pray forgive my absent-mindedness but please rest assured that your assistance and thoughtfulness were, and will always be greatly appreciated.

Any mistakes or inaccuracies in this thesis are solely, and entirely mine.

Abstract

The stabilisation of soft clay soils is intended to increase their shear strength and to reduce their compressibility. The possibility exists of using geophysical methods to monitor changes in these properties.

Laboratory experiments were carried out on stabilised clays to study the relationships between shear wave velocity, and hence small strain shear stiffness, and shear strength or one-dimensional compressibility. One artificial clay, Speswhite kaolin, and two natural clays, from Malaysia and Sweden, were used as the base clays. Either ordinary Portland cement or a 1:1 mix of the cement with unslaked lime was added to the base clays in order to stabilize them.

In the first part of the investigation, samples of stabilised clay were initially subjected to a non-destructive bender element test to obtain the shear wave velocity and then to an unconfined compressive strength test or vane shear strength test. It was evident that small stabiliser amounts (less than 10 % of the dry weight of the base clay) could significantly improve both the strength and stiffness of the originally soft material. In addition, good correlations between the shear strength and the shear wave velocity (or small strain shear stiffness) of the stabilised clays were established.

In the second part of the investigation, an instrumented oedometer was used to simultaneously monitor shear wave velocity and one-dimensional compression during tests on samples cured for a set period. Lateral stresses were also measured. Complementary tests were conducted in standard oedometers, to study the effect of the curing period. In these tests yield stresses were identified and corresponded to the onset of changes in shear wave velocity. After yield, the constrained moduli could be correlated with shear wave velocity. Tests were also carried out on samples of clay in which a central stabilised column had been created. Equal strain predictions of the compression of these samples, based on the results of separate tests on the two components, were relatively successful.

The results of the research suggest that shear wave velocity measurements could be useful in practice to enable the shear strength and post-yield compressibility of stabilised clay soil to be estimated.

Table of Contents

List of Notations

BE	Bender element
c_u	Undrained shear strength
C	Curing period
$CC_{TR}(t_s)$	Coefficient of cross-correlation
CPT	Cone penetration test
C_c	Compression index
C_r	Recompression index
C_α	Secondary compression index
D	Diameter of sample
e	Void ratio
e_f	Final void ratio
e_o	Initial void ratio
e_{100}	Void ratio at the end of 100 kPa loading stage
E	Young's Modulus
f	Frequency
f_x	Frequency at point 'x' for a sampled signal
FFT	Fast Fourier Transform
FFT^{-1}	Inverse Fast Fourier Transform
F_r	Friction losses correction factor
G_o	Maximum or small strain shear modulus
$G_{o\ initial}$	Initial maximum or small strain shear modulus
G_s	Specific gravity
$G_{xy}(f)$	Cross-power spectrum
H	Height of sample
I	Current
K	Coefficient of earth pressure ($K = \sigma_h/\sigma_v$)
K	Bulk modulus ($K = \rho v_p^2$)
K_{COL}	Coefficient of earth pressure for the column
K_o	Coefficient of earth pressure at rest ($K_o = \sigma_h/\sigma_v'$)

K_o'	Corrected coefficient of earth pressure at rest ($K_o' = K_o/F_r$)
K_{SOIL}	Coefficient of earth pressure for the soil surrounding the column
L	S-wave travel distance
LI	Liquidity index
LL	Liquid limit
m_v	Coefficient of volume compressibility
M_o	Constrained Modulus
N	N-value from SPT test
NC	Normally consolidated
NCL	Normal consolidation line
NF	Near-field
N_k	Cone bearing capacity factor
OCR	Over-consolidation ratio
Oedo-BE	Oedometer-bender element
OPC	Ordinary Portland cement
PI	Plasticity index
PL	Plastic limit
P-wave	Compression / Longitudinal wave
q_t	Cone resistance
q_u	Unconfined compressive strength
r	Radius
R	Resistance
R(t)	Received signal (in time domain)
SPT	Standard penetration test
S_r	Degree of saturation
S_{ro}	Initial degree of saturation (before test, at the beginning of curing)
S_{rf}	Final degree of saturation (after test)
S-wave	Shear / Transverse wave
t	Wall thickness
t_{cc}	Shear wave arrival time determined by cross-correlation method
t_{cs}	Shear wave arrival time determined by cross-spectrum method
t_{gr}	Group velocity travel time
t_o	Shear wave arrival time determined by visual inspection

t_{ph}	Phase velocity travel time
$t_{pk\text{-}pk}$	Shear wave arrival time based on time lapse between the first major positive peaks of the transmitted and received signals
t_s	Time shift between two signals
T(t)	Transmitted signal (in time domain)
T_r	Time record for a signal
UCS	Unconfined compressive strength
v_{cc}	Shear wave velocity based on cross-correlation
v_{cs}	Shear wave velocity based on cross-spectrum analysis
v_{gr}	Group velocity
v_o	Shear wave velocity based on visually picked travel time
v_{ph}	Phase velocity
$v_{pk\text{-}pk}$	Shear wave velocity based on time lapse between the first major positive peaks of the transmitted and received signals
v_s	Shear wave velocity
V	Voltage
VS	Vane shear
V_{in}	Input voltage
V_{out}	Output voltage
w	Natural water content
w_i	Initial water content
w_f	Final water content
W	Initial weight of sample
W_s	Dry weight of sample
W_c	Dry weight of cement
X(f)	FFT of received signal, R(t)
Y(f)	FFT of transmitted signal, T(t)
Y*(f)	Complex conjugate of Y(f)
ΔH_c	Back calculated final settlement
ΔH_m	Measured final settlement
ϕ	Phase angle
ϕ'	Angle of shearing resistance

ε_c	Hoop strain
ε_f	Axial strain at failure
ε_{pl}	Plastic vertical strain
ε_v	Vertical strain
λ	Wave length
ν	Specific volume ($\nu = 1 + e$)
ν	Poisson's ratio
σ_c	Hoop stress
σ_h	Total lateral / radial stress
σ_v	Total vertical stress
σ_h'	Effective lateral / radial stress
σ_v'	Effective vertical stress
σ_{vAVG}'	Average effective vertical stress acting on soil and column (back calculated)
σ_{vCOL}'	Effective vertical stress acting on column
σ_{vSOIL}'	Effective vertical stress acting on soil (surrounding column)
σ_{vTEST}	Average vertical stress acting on soil and column during a test (recorded)
σ_{vTEST}'	Average effective vertical stress acting on soil and column during a test (recorded)
σ_y'	Effective yield stress
$\sigma_y'_{AVG}$	Average effective yield stress of composite system (based on σ_{vTEST}')
$\sigma_y'_{COL}$	Effective yield stress of column
ω	Angular frequency ($\omega = 2\pi f$)
$\varnothing$	Diameter

List of Equations

Chapter 1 Introduction

Chapter 2 Literature Review

Chapter 4 Results: Interpretation, Analysis and Discussions

List of Tables

List of Figures

Chapter 3 Experimental Equipment, Methods and Procedures

Chapter 4 Results: Interpretations, Analysis and Discussions

Chapter 1
Introduction

1.1 Research context

The term 'stabilisation', as used in this thesis, refers to the addition of chemical substances known as 'binders' or 'stabilisers', in wet or dry conditions, to existing soft soil in order to increase its strength and reduce its compressibility (e.g. Kawasaki et al. 1981, Schaefer et al. 1997, Lin and Wong 1999, Miura et al 2001). This chemical modification of the original ground can either be carried out to form columns in the soil or a mass stabilised area, or a combination of both (Figure 1.1). Stabilised columns on land are usually not more than 30 m deep, but in offshore applications they can be up to 50 m deep. Mass stabilisation, which was originally developed to treat upper layers of organic soils, is normally used up to a depth of about 5 m (Toth 1993).

The first laboratory and field research in deep mixing was initiated in Japan and Sweden back in the mid 1960s (Holm 2001). When the formation of stabilised columns or deep stabilisation with cement was first introduced in Japan, its intended use was for port and harbour structures in offshore reclamation schemes to overcome land shortage due to industrialization. Subsequently land-based columns were implemented for inland development on soft ground. At the same time Sweden was developing lime-stabilised columns, which also functioned as vertical drains, for the same purpose of strength and stiffness improvement. The lime was added to the soil in dry powder form. Today, the implementation of deep stabilisation encompasses a wide scope, including:

- the construction of foundations and embankments on soft soils (Andersson et al. 2001, Raju and Arulrajah 2003, Rampello and Callisto 2003).
- the reduction of active pressure on retaining structures (Nicholson, et al. 1998).
- the prevention of liquefaction by providing alternative drainage paths (Ando et al. 1995, Porbaha et al. 1999).
- the mitigation of excessive track and surrounding ground vibrations with stabilised barrier trenches, as in high-speed railway track construction (Bahrekazemi et al. 2003).

- environmental applications such as remediation of contaminated ground using solidification and stabilisation techniques (Al-Tabbaa and Boes 2002).

In comparison with other ground improvement methods, for example vertical drains with preloading, piling and weight reduction in embankments, deep stabilisation has several major advantages (EuroSoilStab 2002) as follows:

- It is economical in terms of raw material, especially when industrial waste products are incorporated in the binders.
- It is less labour-intensive as compared to most other methods.
- It is less time-consuming.
- It offers more flexibility in terms of construction and improved engineering properties.
- It has less impact on the environment (e.g. minimal spoil with dry mixing).
- It causes minimal disturbance to the surroundings during installation in terms of noise and vibration levels.

Accumulated knowledge and experience have brought forth inventions and innovations of various machinery and techniques, which enable the formation of deep columns as well as mass stabilisation of a large region. Besides, there is no lack of sound understanding of the stabilisers or binders, namely cement, lime and industrial waste products like blast furnace slag, in terms of choice, properties and the performances in different soils (Kitazume 2005).

The area of quality assurance and control has developed in parallel with the above development. However most of the methods involve retrieval of samples for subsequent strength and one-dimensional compressibility tests in the laboratory, whose results are highly dependent on the quality of the samples collected and whether they are representative. Errors could arise from inhomogeneity within the sample, disturbance of the sample throughout the sampling process and also bedding errors during the laboratory tests. For in situ measurements, on the other hand, sample quality is not an issue as these tests are conducted on initially undisturbed ground in selected locations to provide a more representative overview of the soil properties. Examples of these field test methods include penetration tests with direct and reversed column probes (Boman et al. 1980, Rathmayer

1996), standard penetration tests (Nishikawa et al. 1996, Goto et al. 2000), cone penetration tests (Huidén 1999) and vane tests (Halkola 1983, Axelsson and Larsson 1994). Recently experiments have been carried out with geophysical tests using seismic methods, notably the down-hole and up-hole techniques as illustrated in Figure 1.2.

Matthews and Clayton (2000) gave a concise description of the wave modes employed in seismic tests. Seismic methods employ either body or surface waves, similar to the types generated in an earthquake. Body waves propagate through the interior of the ground as compression or P-waves, which cause a volumetric strain, and shear or S-waves, which produce shear distortion. The P-wave velocity is related to the bulk modulus (K) of the soil while the shear wave velocity is linked to the maximum shear modulus (G_o). Surface waves such as Rayleigh waves on the other hand, being dispersed energy from the main seismic events, attenuate quickly with depth and only propagate near the surface of the ground. The surface waves are therefore not particularly useful for the evaluation of column properties.

In the context of deep stabilisation, Larsson (2005) aptly pointed out the benefits of supplementing existing physical probing and sampling with geophysical (e.g. seismic) techniques, to monitor the integrity and properties of the stabilised material. Indeed, recent development of seismic testing and interpretation methods (e.g., Hiraide et al. 1996, Nishikawa et al. 1996, Goto et al 2000) has highlighted their potential in the determination of strength and deformation properties of stabilised material. Nevertheless seismic methods are not adopted without apprehension by geotechnical engineers. This is partly due to unfamiliarity with the interpretation of seismic test results, and the uncertain relationship to statically measured strength and stiffness, e.g. in terms of the strain levels (Foti and Butcher 2004).

Prior to the research described in this thesis, linking of seismic methods using shear waves with strength measurements began to be recognized as being feasible in the testing of stabilised soils. Early attempts, which involved mainly field tests, indicated the possibility of a relationship between shear wave velocity and unconfined compressive strength, though these correlations were site specific with a dependency on the soil mineralogy and climatic conditions (e.g. Hiraide et al. 1996, Goto et al 2000).

Much less effort has been expended in studying the relationship between shear wave velocity and compressibility of stabilised material. As settlement of a stabilised column is generally assumed to follow a one-dimensional compression path, compressibility studies

are routinely carried out with oedometer tests (e.g. Miura et al. 2001, Feng 2002, Horpibulsuk et al. 2004). However only Fam and Santamarina (1995) have monitored the shear wave velocity simultaneously in an oedometer test and no report was made on the relationship mentioned above.

Many of the laboratory seismic testing methods using shear waves involve piezoelectric transducers, for example shear plates and bender elements. The transducers are either used on their own in unconfined samples (e.g. Yesiller et al. 2000) or incorporated in conventional test apparatus, especially the triaxial cell (e.g. Viggiani and Atkinson 1995) and the oedometer (e.g. Fam and Santamarina 1995). They are used in pairs: a transmitter and a receiver. Typically, the transmitter would vibrate with a voltage excitation, the shear motion then being transferred through the soil to the receiver, which in turn picks up the vibration and generates a voltage output. By recording the time required for the wave motion to travel from the transmitter to the receiver, the wave velocity can be obtained. From the shear wave velocity, it is then possible to determine G_0.

Bender elements were employed for the present research, because they could be manufactured in-house with a reasonable amount of time and effort, and also because a much lower voltage was required for motion generation as compared to other piezoelectric transducers, i.e. shear plates. In addition, there was the advantage of much published work on laboratory shear wave velocity measurement with bender elements, which served as a useful guide.

The bender element test method is simple in principle, but definition of the shear wave arrival time can be rather subjective (Brignoli et al. 1996, Lings and Greening 2001, Pennington et al. 2001). Various signal manipulation and analytical methods may be employed to make the determination of shear wave arrival time less susceptible to ambiguity. These methods are based in either the time domain, such as distortion of the input signal (e.g. Jovičić et al. 1996), cross-correlation of input to output signals (e.g. Mancuso et al. 1989); or the frequency domain, for example the cross-spectrum analysis (e.g. Viggiani and Atkinson 1995). Detailed descriptions of these refined techniques are included in Chapter 2.

With the maturity of bender element test techniques, as well as the refinement of the interpretation methods, there is a very encouraging future for their application to stabilised soils. Therefore this thesis focuses on testing stabilised soils with bender elements for quality control of the improved properties, namely strength and compressibility.

1.2 Research objectives

The research programme was conceived to achieve the following specific objectives, namely to:

- develop bender element testing techniques for shear wave velocity measurement in laboratory tests on stabilised soils;
- establish with confidence the form of relationship between shear wave velocity, or maximum shear modulus, and shear strength for stabilised soils;
- investigate whether one-dimensional compressibility (constrained modulus) of stabilised soils can be correlated with shear wave velocity or maximum shear modulus;
- investigate whether vertical yield stress of stabilised soils can be correlated with shear wave velocity or maximum shear modulus;
- investigate the variation of lateral stress during one-dimensional compression of stabilised soils.

1.3 Research methods

The test materials consist of one artificial and two natural clays as the base clays, with ordinary Portland cement and unslaked lime as the stabilisers. The artificial clay came in the form of dried Speswhite kaolin clay powder, while the natural clays, Malaysian and Swedish clays, were retrieved as bulk samples from their respective sites. Samples of the artificial clay were made with dried clay powder and pre-determined amounts of water and stabiliser. On the other hand, the natural clays were remoulded at their natural water contents prior to addition of the stabilisers.

Relatively small quantities of stabiliser, less than 10 %, were used in most of the test samples as compared to the 10 – 30 % commonly used for in situ stabilisation (Feng 2002). This enabled safe recovery of the bender elements after tests, and also ensured that the settlements were measurable with reasonable accuracy with the equipment available in the one-dimensional compression tests.

Unconfined tests on stabilised soils were conducted with the bender element probes, made in-house, and a triaxial compression machine or laboratory vane shear apparatus, while one-dimensional compression tests were carried out both in standard oedometers and

in a specially instrumented oedometer, the 'oedo-BE' device. Compressibility, lateral stress and shear wave velocity were simultaneously measured in the oedo-BE tests.

For a medium that is homogeneous and elastic, the maximum shear modulus, G_o, can be obtained from the shear wave velocity, v_s, in the following way:

$$G_o = \rho v_s^2 \qquad \text{(Eq.1.1)}$$

where, ρ = bulk density.

It is useful to evaluate the maximum shear modulus because there is substantial information from previous work on the relationship of G_o with other parameters (e.g. stress history, compressibility, shear strength), providing scope for comparisons with findings from this research.

1.4 Outline of thesis

Chapter 2 reviews the literature relating to the research, which includes literature on deep mixing techniques, design philosophy, existing seismic testing methods, laboratory testing and the mechanical properties of stabilised samples. **Chapter 3** gives a detailed description of the experimental work in terms of sample preparation, test equipment and procedures. The development of devices and techniques are also carefully elaborated in the chapter to ensure good conveyance of the practical experience and knowledge. In **Chapter 4**, the test results are analyzed, compared to information from the literature and discussed in detail. Correlations between the various parameters that were established in the research are also presented and references to other related work are made where appropriate. This is followed by **Chapter 5** which lists the main conclusions from the present work. It also lays out recommendations for future work based on the Author's experience, in the hope that further work will yield beneficial results. A complete list of **References** is included and finally, **Appendices** of relevant topics can be found at the end of the thesis. These include a step-by-step guide for making bender element probes.

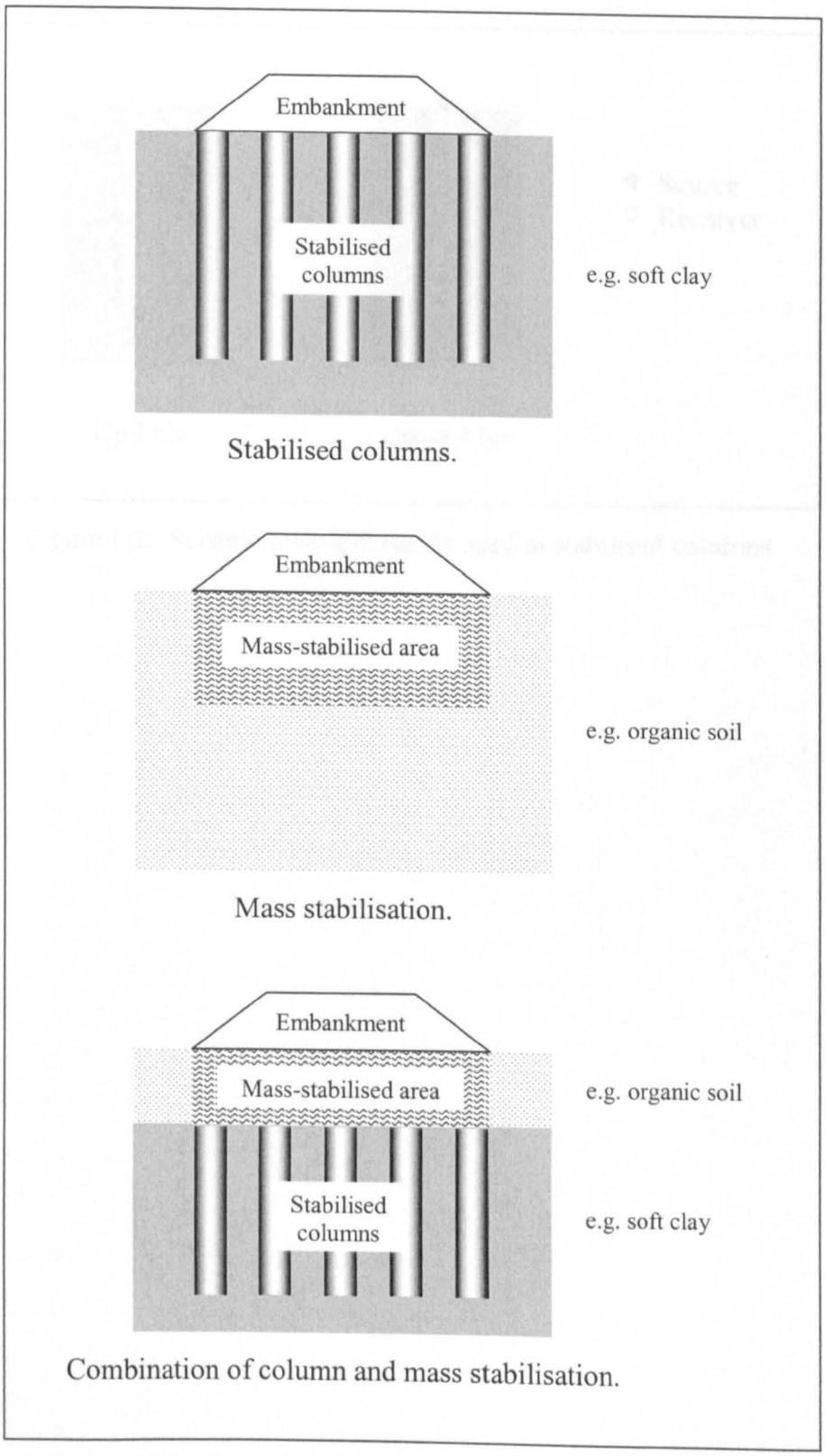

Figure 1.1: Types of deep stabilisation as used for embankments.

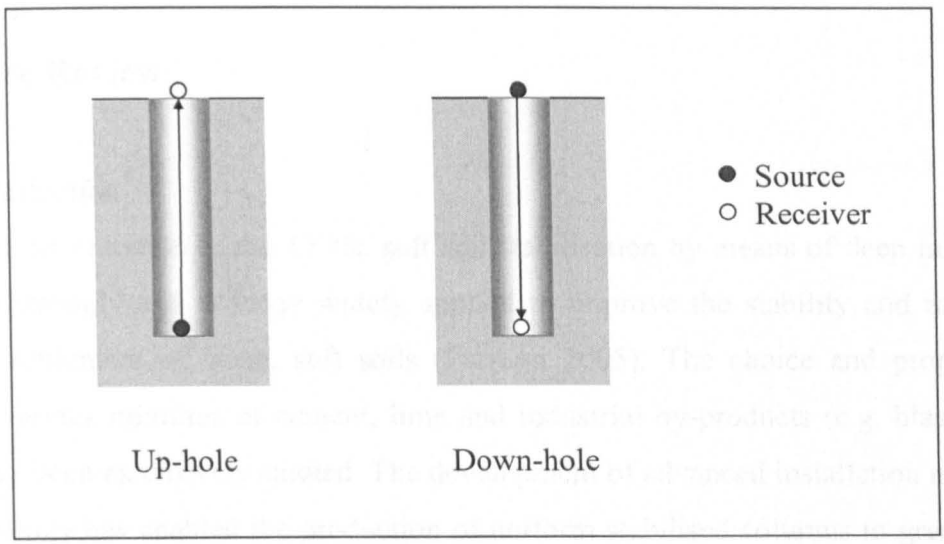

Figure 1.2: Seismic testing methods used in stabilised columns.

Chapter 2
Literature Review

2.1 Introduction

Since its initiation in the 1970s, soft soil stabilisation by means of deep mixing has developed strongly and is today widely applied to improve the stability and reduce the excessive settlement of weak, soft soils (Larsson 2005). The choice and properties of binders - various mixtures of cement, lime and industrial by-products (e.g. blast furnace slag) - have been extensively studied. The development of advanced installation machinery and technology has enabled the production of uniform stabilised columns to great depths. Besides, continuous research has provided a better understanding of the complex behaviour of the stabilised material, and its interaction with the surrounding unstabilised soils.

As explained in Chapter 1, the research described in this thesis is mainly focused on quality control of stabilised soils, by assessing the mechanical properties of the stabilised material with shear waves. Following an overview of the deep mixing stabilisation method, the literature review is therefore written to present the relevant quality control and assurance methods, as well as the laboratory investigation of the improved properties. Emphasis is given to the measurement of shear wave velocity in stabilised materials. A review of the one-dimensional compressibility behaviour of stabilised soils is also included.

2.2 Soft soil stabilisation with deep mixing

The deep mixing method was first developed by the Japanese in 1970s for offshore construction (Toth 1993). The stabilisation method was initially applied when erecting port and harbour structures but was later applied in land reclamation projects due to the shortage of land. At the same time Sweden introduced deep mixed lime columns which functioned as vertical drains to accelerate the consolidation of embankments (Broms and Boman 1977). The Japanese and Swedish methods both used dry powder as a binder. Wet mixing, which involved adding the binder in a slurry form to the soil was not developed until the late 1980s in the United States of America (Burke et al. 2002).

2.2.1 Deep mixing machinery and process

Topolnicki (2004) has summarised the different methods of deep mixing in a diagram as shown in Figure 2.1. As the present work is related to dry-mixed soils, the following review is primarily focused on that subject.

In dry deep mixing the machinery usually consists of a track mounted installation rig fitted with a leader and a drill motor. There are two main categories of machinery, depending on the mixing tool affixed to the rig: blade-based and auger-based mixing. The chemical stabiliser or binder is stored in pressurised tanks, either mounted on the rig or on a separate shuttle. The mixing process is achieved via the mixing tool connected to the drill motor by a Kelly bar. The mixing tool is first drilled and lowered to the depth where the base of the column is intended to be. The tool is then withdrawn with simultaneous injection of the binder using pressurised air. The quality of the mix is dependent on several factors: the number of blades (for a blade-based mixing tool only), the rotational speed, the rate of withdrawal of the mixing tool, as well as the rate of injection of the binder (Larsson 2005). An optimum combination of the factors would ensure maximum strength achieved and minimal inhomogeneity in the mixed product.

The sequence of the installation process is schematically shown in Figure 2.2. According to Larsson (2003), the mixing process mainly comprises three phases, namely penetration of the mixing tool to the required depth, dispersion of the binder, and molecular diffusion. It was also reported that due to the complexity and various influencing factors affecting the mixing process, the mechanisms involved in each phase are not distinctly separated. Nevertheless, the final result is a cylindrical column of soil-binder matrix, with improved strength and stiffness. The diameter of the column typically ranges from 600 to 800 mm, and the spacing is generally 1.0 - 1.5 m centre to centre. The maximum treatment depth in normal practice on land is limited to 30 m, but offshore deep mixing projects often reach depths of 50 – 70 m.

Control over the amount of binder introduced into the mix is based on continuous monitoring of the weight of the binder storage tank using load cells. This close monitoring ensures that the intended amount of binder is utilised uniformly over the length of the column. The quality control task is fully computerised, with electronic recording devices on the deep mixing machines keeping track of the production parameters.

2.2.2 Some problems with column installation

A commonly encountered problem is the formation of 'craters' near the surface of the ground, where the cap of the column is not properly formed (Larsson 2005). Such defects may be due to two factors, one being site related and the other being a technical limitation. Firstly, craters are almost unavoidable where a layer of dry crust overlays the ground being stabilised. Secondly, the mixing process is usually terminated 0.5 – 1.0 m below the surface of the ground to avoid 'blow-outs'. The resulting holes or 'craters', ranging from a few centimetres to a couple of metres deep can be backfilled with granular material, but appropriate compaction is necessary to ensure the transfer of loading to the columns and not to the surrounding unstabilised soil (Figure 2.3).

Lateral ground movement has been reported during the installation of deep mixed columns, especially with wet mixing (Hirai et al. 1996, Vähääho 2000). Kakihara et al. (1996) have conducted a study of both dry and wet mixing, concluding that the latter produces more significant lateral displacement. Larsson (2005) compiled records from several sources in Japan and showed that the lateral movement is most severe when the measuring point is under the stabilised area, Figure 2.4. It seems that the magnitude of the lateral movement can reach up to 500 mm, at points as far as three quarters of the stabilised depth, measured from the boundary of the stabilised area. However such large movements could be due to the combined effect of a column group, the extremely soft condition of the original ground, and the mixing method itself (e.g. wet mixing further increases the water content of the soil). If consideration is limited to a single column, the zone of lateral movement is likely to be much less. Several countermeasures have been developed to mitigate the problem, one of which is the removal of a soil mass which equals the volume of slurry injected (Kamimura et al. 2005). Ironically the method loses a major advantage of deep mixing, which is the production of minimal spoil for disposal. Kakihara et al. (1996) and Masuda et al. (1996) proposed the construction of stabilised columns in sequential rows to avoid excessive lateral movements. However, it is acknowledged that in a column group, lateral expansion of the intermediate columns could have the positive effect of 'tightening up' the ground being stabilised.

Column installation has been reported to significantly increase pore pressure in the surrounding soil (Shen and Miura 1999, Vriend et al. 2000). The increased pore pressure was thought to contribute to the lateral expansion of surrounding soil. On the other hand, the effect may be temporary if the columns function as vertical drains to improve the

excess pore water dissipation. Larsson (2005) suggested that clay fracturing due to the build-up of pore pressure could actually help in providing pathways for the binder to be distributed within the soil mass.

2.2.3 Load distribution in a stabilised system

Bergado et al (2003) pointed out that the main aim of deep mixing is to produce a modified soil mass that has mechanical interaction with the surrounding natural and unstabilised soil. The intention is a semi-rigid stabilisation, which is different from rigid pile-like elements which carry the entire imposed structural load. This is referred to as the 'soft treatment', and has been widely adopted in most deep mixing design philosophies.

'Soft treatment' is achieved by producing a soil-binder matrix of low binder contents, sufficient to provide improved undrained shear strengths of 100 to 250 kPa, depending on the characteristics of the original soil. The applied load is shared between the columns and the unstabilised soil between the columns. A system that is too rigid would prevent an effective interaction between the stabilised soil mass and the surrounding natural soil in terms of load distribution.

EuroSoilStab (2002) published by the European Commission adopts similar principles for deep mixing design. The design approach aims at producing a 'semi-hard' column, with the maximum shear strength taken as 150 kPa, irrespective of the possible higher values obtained in field or laboratory trials. This is because field mixing is not as effective as laboratory mixing, often resulting in strengths lower than those of laboratory mixed material. Kitazume (2005) reported the difference to range between 20 and 50 %.

The stabilised columns, though improved in terms of strength and stiffness, are generally inhomogeneous to varying degrees. They are commonly found to have irregular structures and properties, varying in different directions. As the columns are intended to be axially loaded for effective interaction with surrounding soil, any other types of loading could impair their performance. Tensile stress is considered the most detrimental and must be avoided at all times.

Settlement estimations for column-stabilised systems are generally based on the assumption that the same compression occurs in both columns and the unstabilised soil at every level (Baker 2000). In other words, the columns and soil behave as a composite unit which is subject to equal vertical strain.

2.3 Quality control and assurance

In order to ensure optimal performance of the stabilised columns, quality control and assurance are crucial before, during and after the construction (Kitazume 2005). It is therefore normal practice to perform quality control and monitoring for the entire process of a deep mixing project, as depicted in the flowchart in Figure 2.5. Apart from being divided into field and laboratory tests, the relevant test methods may also be subdivided into conventional or destructive test, and non-destructive test categories.

2.3.1 Field tests

Field measurements are carried out to validate either the mechanical properties or the uniformity of the columns. They have the major advantage of testing the actual material in situ, without any adverse effects of sampling and transportation. The test methods are generally similar to those used in normal site investigations, but some specific tests have been developed for stabilised soils. Table 2.1 gives a summary of the field tests for stabilised soils (Hosoya et al 1996). However, only the more commonly executed ones are discussed in this section. Others such as electrical logging, pile load test and integrity test are not included but can be readily referenced in the published literature.

2.3.1.1 Conventional tests

Penetration tests

The standard penetration test (SPT) is one conventional in situ test method which is perhaps most widely used for stabilised soils (Nishikawa et al. 1996, Goto et al. 2000), although it is usually accompanied by other complementary measurements, field or laboratory based, for the purpose of making comparisons and establishing the relevant correlations. The SPT is essentially a simple test of repeatedly dropping a standard hammer of known weight from a specific height. The number of blows to achieve 300 mm depth penetration of the split spoon sampler, the N-value, is correlated with the unconfined compressive strength. It is worth noting that the word 'standard' in the name of the test is misleading as the hammer weight and drop height do vary with corresponding correction factors (Budhu 2000). The weight and drop height of the hammer do not always conform to the standard specifications (hammer weight 64 kg, drop height 760 mm) and vary from region to region (Hosoya et al. 1996, Huttunen et al. 1996). For a standard test set-up, the N-values are reported to correlate well with values of unconfined compressive strength

obtained from laboratory tests, q_u = 1/4 to 1/3 N (Nishibayashi et al. 1985, after Kitazume 2005). However, inconsistency in the SPT assessment of column strength is not uncommon. Boman et al. (1980) attributed the unreliability of SPTs to the uncertain location of the probe and the relatively small volume tested within the column.

The cone penetration test (CPT) is another conventional testing method. The CPT provides information on the strength as well as continuity of the column. However the CPT is reported to have two major weaknesses: firstly, the slender shaft makes it extremely difficult to maintain verticality of the cone in the column during a test (Huidén 1999); and secondly, the fine tip limits the measurement to a localised area within the column (Larsson 2005). Improvisations have been made to make CPT a more reliable test method, like carrying out pre-boring to maintain the verticality of the cone. Porbaha et al. (2001) have developed a frictionless bar CPT probe, FRICON, to improve control over the vertical alignment of the probe. The authors found that the FRICON results agreed better with measurements by direct shear tests than those from the unconfined compressive strength tests. The correlations between the cone resistance, q_t, and undrained shear strength, c_u, from unconfined compressive strength tests ($c_u = q_u/2$) and direct shear tests, are reported to be $q_t = 18\ (q_u/2)$ and $q_t = 22 - 23\ c_u$ respectively.

A winged penetrometer has been developed in the Nordic countries for evaluating the variation of shear strength with depth of stabilised columns, and the method is named the 'column penetration test' (Figure 2.6). The initiative was largely driven by the inability of static penetration tests to produce a reliable strength evaluation of the stabilised material. The winged device, with two vanes or blades affixed to opposite sides of its shaft (400 mm in total width), is pushed into the column at 20 mm/s and the penetration resistance is registered continuously (Rathmayer 1996). This method is found to be effective for columns with a strength of up to 300 kPa. For columns deeper than 8 m, pre-boring to provide a penetration channel for the probe is found to be feasible, but inadvertently results in disturbance of the tested column. For deep columns (e.g. 12 – 15 m) with high strengths (e.g. 600 – 700 kPa), the test method is adapted by inverting the probe and planting it at the base of the column prior to installation (Ekström 1992, as cited by Larsson 2005). A sturdy cable or rope, attached to the probe and running through the column to the ground surface, is used to pull the probe out at 20 mm/s, and the variation of shear strength with decreasing depth is recorded. Thus the name 'reversed column penetration test' was given to the method.

Halkola (1999) proposed using a multiple-blade penetrometer for better vertical control, and also larger coverage of the test area within the column. Based on his studies, Larsson (2005) reported a suggestion of the incorporation of a load cell (e.g. pressure gauge) to measure the strength without the effect of bar friction, and an inclinometer to monitor the vertical alignment of the probe. In spite of the efforts expended on modifying and improving the probe, the column penetration test is routinely conducted on the central portion of the column's cross-sectional area, ignoring the possible non-uniform strengths of the outer regions. Kitazume (2005) cautioned that penetrometer tests should be treated as a guide to the variation of shear strength within the column and not as providing absolute values.

The vane shear test using modified vanes is popular in assessing the strength of stabilised columns. Such modified vanes vary in dimensions but are generally sturdier than those used for unstabilised soils. The one developed in Finland is 132 mm in diameter and 65 mm in height, with varying thickness along the vanes, from 6 mm at the shaft to 3 mm at the tip (Halkola 1983). However as in the conventional test, the accuracy of measurements in stabilised material is also limited by the strength. Halkola (1999) reported that the maximum shear strength measurable to be 200 kPa, while Axelsson and Larsson (2003) showed that a good correlation between vane shear and column penetration tests only extended as far as about 100 kPa. Although being a quick and simple test to carry out, the vane shear test is known to underestimate the actual strength considerably due to significant disturbance of the stabilised soil during penetration of the vane (Axelsson and Larsson 2003). Uncertainty of the shearing surfaces can also account for the underestimated strength, especially in stiff material.

The pressuremeter test is able to concurrently measure the strength and stiffness of stabilised soils based on cavity expansion principles, but it is not a widely used method due to the high costs and difficulties in interpreting the results (Hughes et al. 2001). Nevertheless the test does have the advantage of being capable of assessing high strength columns. The pressuremeter is placed in a pre-drilled hole at the centre of the column and displacement of the membrane with pressure is related to the strength. Comparison between results from the pressuremeter and unconfined compressive strength tests on samples from the same column was reported to be unsatisfactory by Hughes et al. (2001), Figure 2.7. The scatter was appreciable and the pressuremeter was almost consistently producing much lower strengths than unconfined compressive strength tests.

Load tests

Load tests are routinely carried out to assess the compressibility of stabilised soils. The most common load test is perhaps the plate load test, either conducted on a single column (Kivelö 1998) or a column group (Raju and Arulrajah 2003). A variation of the load test on a single column uses two plates, one at the top and the other at the base of the column (Baker et al. 1997). The bottom plate has a tension cable that runs through the column to the top and is connected to a hydraulic jack. With the top plate fastened in place, the column is loaded on both ends by an upward force applied to the bottom plate using the hydraulic jack. Baker et al. (1997) reported that the modified test set-up provides better evaluation of column uniformity. In general, interpretation of load test results on a single column is complicated by boundary conditions that are not properly defined, whereas a load test on a column group is perhaps more useful for assessing the compressibility behaviour of the stabilised system as a whole.

2.3.1.2 Non-destructive tests

Seismic test methods are relatively new for stabilised soil, and most of the tests carried out have been of an exploratory nature. These tests employ seismic waves: compression or P-waves, shear or S-waves and Rayleigh waves (also known as surface waves), and the techniques essentially differ in terms of the arrangement of the source and receiver (Figure 1.2). Seismic tests agitate the soil particles within a very small and transient strain range of 10^{-6} - 10^{-4} %, presumed to correspond with the linear-elastic phase of soil deformation (Matthews et al. 2000).

Testing with P-waves is unsuitable for evaluating the stiffness of saturated soils due to the presence of pore water in the voids (Yessiler et al. 2000). The skeletal bulk modulus, $K = \rho v_p^2$ (Eq. 2.1), where ρ is the bulk density and v_p is the P-wave velocity, of the soil is generally similar to or less than that of water. With typical v_p of approximately 1480 m/s for water, the bulk modulus measured is really a function of the stiffness of the pore water rather than the soil skeleton (Matthews et al. 2000). S-waves on the other hand induce shear distortion in the soil without volumetric changes, and shear wave velocity, v_s is exclusively a function of the maximum shear modulus, $G_o = \rho v_s^2$ (Eq. 1.1).

Hiraide et al. (1996) and Nishikawa et al. (1996) conducted in situ suspension type P-S logging on stabilised columns and related the compression and shear wave velocities to corresponding unconfined compressive strengths. The test method was developed by

Kitsunezaki (1980) and is essentially an up-hole method with two or more geophones functioning as receivers (Figure 2.8). The measurements are made in a pre-drilled borehole at the centre of the column. The device is suspended in the water in the borehole without any attachments to the wall, enabling it to be set to the desired depth with ease and accuracy.

Plots from the work of Nishikawa et al. (1996) in Figure 2.9 do not all show convincing correlations between the ultrasonic wave velocity and unconfined compressive strength. The considerable scatter of data, especially in plot (i) and the P-wave data in plot (ii), is suggestive of inaccurate measurement methods as well as the effect of sample disturbance (for the unconfined compressive strength test samples). However, it is apparent in all plots that v_p is greater than v_s by a factor of approximately two.

The unconfined compressive strength, bulk density and wave velocity profiles compiled from the P-S logging test by Hiraide et al. (1996) are shown in Figure 2.10a. The trends of the strength and both v_s and v_p follow a consistent and matching pattern, suggesting a close relationship between these parameters. Also, for a particular soil layer with a certain binder content, the wave velocity profile itself could be a good indicator of the uniformity of the mix. The field shear wave velocities, v_{sF}, agree well with laboratory measured values at matching depths, v_{sL} (Figure 2.10b).

By comparing the shear wave velocities measured with P-S logging in situ and laboratory based pulse transmission methods on natural soil, Nishikawa et al. (1996) have similarly reported good agreement between the two measurements. Nevertheless, the slight mismatch observed between the field and laboratory measurements was attributed to the following factors:

- Differences in sample size and homogeneity.
- Differences in wave lengths used in situ and in the laboratory test methods.
- Differences in the sensitivity among the testing techniques.
- Different stress paths in situ and in the laboratory.
- Differences in sample disturbance.
- Differences in the method of loading.
- Differences in sample deformation during testing.
- Differences in wave paths (e.g. ray path bending in the field).

A plot of v_{sL}^2 versus q_u is illustrated in Figure 2.10c, where Hiraide et al. (1996) fitted a linear regression line through the data irrespective of the soil type and binder content in each layer. Such generalisation of the correlation may mask a distinction between the stabilised soil types. There are probably insufficient data to show if separate correlations existed for each soil type.

Porbaha et al. (2005) conducted suspension type P-S logging tests on wet-mixed cement-stabilised columns. The variations of compression and shear wave velocities and the corresponding stiffnesses with depth for three columns are illustrated in Figure 2.11a. The natural ground was made up of multiple layers of fine and coarse grained soils. However the wave velocities do not appear to be sensitive to the soil stratification, especially so with v_p where the variation in soil strata is almost indiscernible. The authors also plotted v_p and v_s versus q_u (Figure 2.11b), with the upper and lower bounds included to envelope the scatter of data points. In spite of the limited and rather scattered data, linear correlations with very small gradients were established between the wave velocities and strength. It is not immediately clear as to why the authors correlated wave velocities measured in situ at 7 days after installation of the columns with unconfined compressive strengths of core samples retrieved and cured until the age of 28 days.

Pile integrity test (PIT) has been carried out by Goto et al. (2000) to assess the in situ stiffness of deep mixed columns, accompanied by laboratory measurements of the unconfined compressive strength and ultrasonic wave velocities (P-waves), Figure 2.12a. The PIT works on the pulse echo method, where a hand held hammer is struck on the column head to send P-waves down the length of the column. Reflections from the column base are recorded as a function of time and travel distance; hence the velocity can be calculated. The method has the additional benefit of detecting anomalies in the column which can indicate non-uniformities. An example of the profiles for unconfined compressive strength, ultrasonic P-wave velocity and SPT N-value is presented in Figure 2.12b. It is apparent that the variation of strength through the depth of the column is reflected in the wave velocity profile. Significant decreases in the strength and wave velocity profiles indicate possible weak zones in the column (e.g. at 4 m depth). Unfortunately Goto et al. (2000) did not include the wave velocity versus strength plot for the field measurements, but similar data obtained from laboratory measurements were presented (Figure 2.12c) and the correlation is clear despite the scatter.

Mattsson et al. (2005) conducted field measurements of shear wave velocity in single columns of Swedish soft clay stabilised with lime-cement. It was based on the down-hole method, using a piezoelectric borehole source powered by an impulse generator at the top of the column and three sets of five equally spaced geophones as receivers. The test set-up and the shear wave velocity profile are as illustrated in Figure 2.13a. The scatter of data for each column was reported to be occasionally high but in general, the consistency within and between the columns tested was fairly good, indicating uniformity of the soil-binder composition. The average shear wave velocity was observed to be 2 – 6 times of that in the natural soil and it also increased with depth within the column, Figure 2.13b. The approximately 40 % increase in v_s with depth from the ground surface to 11 m depth is most likely due to the increase in confining pressure of the surrounding soil with depth.

Massarsch (2005) carried out seismic down-hole tests on lime-cement columns of Swedish soft clay too. Two columns with different amounts of lime-cement binder, 99 kg/m^3 and 156 kg/m^3, were tested. Instead of geophones functioning as receivers, purpose-built displacement sensors were installed along the column. The 'reverse impact' method was adopted where a shear impulse was generated by striking a plate affixed to the top of the column with a hammer horizontally twice in opposite directions. The received signals were then amplified and captured on an oscilloscope. Intersection of the first major deflection of both the received signals was taken to be the shear wave arrival time. The author also tested samples from the same column in the laboratory using bender elements and a comparison of the two measurements showed fairly good agreement (Figure 2.36). An interesting observation was that the higher binder content, 156 kg/m^3, did not seem to have a significant effect on the properties of the soil, as compared to the column stabilised with 99 kg/m^3 of lime-cement.

The seismic cone penetration test has been conducted in stabilised columns by Hansson et al. (2001). This device has the advantage of simultaneously measuring strength (via resistance to penetration) and stiffness (via down-hole shear wave velocity measurement with a series of geophones) of the stabilised column.

2.3.2 Laboratory investigations

Laboratory experiments are mainly carried out to evaluate the strength and stiffness properties of stabilised soil, either on samples retrieved from site or prepared in the

laboratory. It is worth noting that some of the work discussed below was published recently while the research described in this thesis was still being conducted.

In situ samples are obtained in several different forms, depending on the sampling method and condition of the stabilised material when collected. Coring is effective in retrieving high strength samples but is sensitive to the sampling device and technique (Porbaha 2002), and the results of tests conducted on these samples are dependent on the sample size (Futaki et al. 1996, Hosoya et al. 1996). Wet grab samples are collected from the fresh mix of the stabilised column, but significant variation in the measured strengths (after curing) is reported (Burke 1998, O'Rouke and McGinn 2004). Samples retrieved with auger boring and piston sampling are limited to low strength columns (Braaten et al. 1999, Lawson et al. 2005). On the other hand, samples prepared in the laboratory are made under better controlled conditions (e.g. in respect of the uniformity of the mix).

The conventional test most frequently performed in the laboratory is probably the unconfined compressive strength test. The test acquires information on the unconfined compressive strength (q_u), stiffness (quoted as Young's modulus, which is usually taken at 50 % of the failure stress, E_{50}) and residual strength (Kitazume 2005). The stress-strain plot from a stabilised sample is usually characterised by a high peak strength and a small strain at failure, whereas an unstabilised soil sample yields at relatively low strength and undergoes large strain (e.g. Uddin et al. 1997, Lee et al. 2005); an example of this behaviour is shown in Figure 2.14. The peak strength value derived from such a plot is defined as the unconfined compressive strength. Terashi et al. (1980) (after Kitazume 2005) compiled the axial strain at failure of two Japanese clays stabilised with different binders, Figure 2.15. Also, Saitoh et al. (1985) and Terashi et al. (1997) (both after Kitazume 2005) showed that for clays stabilised with both cement and lime, the upper bound for E_{50} is $1000q_u$, but the lower bound for lime-stabilised clay ($E_{50} = 75q_u$) is much lower than that of cement-stabilised clay ($E_{50} = 350q_u$), Figure 2.16.

Based on one-dimensional compression data of several cement-stabilised clays, Horpibulsuk et al. (2003) concluded that there is a common relationship between the normalised strength, q_D/q_{28} (q_D = unconfined compressive strength after D days, q_{28} = unconfined compressive strength after 28 days) and the curing period or age for clays with a liquidity index between 1.0 and 2.5 (Figure 2.17). It was claimed that the generalised expression requires data from only one trial mix to predict the strength of the mix at a certain age, regardless of the clay type, clay water content and cement content.

Triaxial compression tests are not routinely conducted for quality assurance but are used for research purposes (Kitazume 2005). The test condition is usually consolidated-undrained (CU). Although it is ideal to simulate in situ stress conditions with a triaxial apparatus, the vertical and lateral stresses acting on a column are relatively low prior to loading. Therefore the strength values for a freshly mixed column sample obtained from the unconfined compressive strength test and a (suitably confined) triaxial test are very similar (Mattsson et al. 2005). Since the unconfined compressive strength test requires less time and effort to conduct, it remains the preferred choice of test for trial mixes as well as samples retrieved from the site.

Other tests that have been performed in the laboratory are mostly adaptations of conventional tests developed for unstabilised soils. As reported by Kitazume (2005), these include permeability tests, needle penetration tests, tensile strength tests and one-dimensional compressibility tests (see Section 2.5). The main laboratory based non-destructive testing method discussed in the next section is the bender element test, which has been adopted in the present work, and is therefore considered to be worthy of a separate detailed review.

It is important to determine the void ratio (e) and degree of saturation (S_r) of a stabilised sample in the studies of compression behaviour of stabilised soils. The physical properties of a treated soil are changed by both remoulding and cementation induced by the binder added. Lorenzo and Bergado (2004) demonstrated that the specific gravity, G_s, decreased with increased cement content in the treatment of Bangkok clay, Figure 2.18. The effects of remoulding water content and curing period are not discernible, leaving the cement content as the primary influencing factor. No explanation was given of why the G_s values of the composite material decreased with higher cement content.

The degree of saturation, S_r, has direct influence on the strength and stiffness of a stabilised clay. Tan et al. (2002) carried out compaction and unconfined compressive strength tests on cement-treated Singapore marine clay to demonstrate the adverse effect of entrapped air on strength development. By varying the compaction effort, samples with different air void contents were created and subjected to unconfined compressive strength tests. From Figure 2.19, approximately 5 % of strength reduction is caused by a 1 % increase in air voids. Clearly, minimisation of entrapped air in the voids of treated soil is important for its strength development.

2.4 Bender element (BE) test

The bender element (BE) test is a non-destructive test that has gained popularity in the laboratory determination of maximum shear modulus, G_0. Bender elements are essentially a pair of piezoelectric bimorph transducers: the 'transmitter' generates a bending motion when excited with a small voltage, while the 'receiver' detects the vibration propagated through the medium and produces a voltage output (see Figure 3.3). The transmitted and received electrical signals are recorded as waveforms on an oscilloscope for further examination. The BE test can be carried out on unconfined samples, or more commonly, in a test apparatus (e.g. triaxial cell, oedometer and resonant column apparatus) to provide shear wave velocity measurements.

The increasing interest in BE tests may be accounted for by the relatively quick and simple test procedure. As the same sample can be tested at different intervals, the number of samples required is very minimal. Also, recent advances in the quality of digital signal recording and sophisticated analysis methods have further increased its appeal.

2.4.1 Working principle of bender elements

Bender elements come from the family of piezoelectric ceramics or piezoceramics, which generate an electrical output when subjected to a mechanical deformation and vice versa. Piezoelectric characteristics are found naturally in quartz and tourmaline salt, but the material used in industry is usually artificially produced in the form of lead zirconate titanate (PZT), barium titanate and lead titanate (Fioravante and Capoferri 2001). Figure 2.20 shows the various transducers made from piezoceramic strips (Strassburger 1982). The deformation of the piezoelectric ceramic depends on the several factors, namely the shape and composition of the ceramic, the direction of poling and the location of the applied electrical field.

In general, the piezoceramic is intended for generating or sensing either compression (P-) or shear (S-) waves. Although spurious deformation is almost always inevitable, it is taken to be negligible. For instance, a wide bender element, when excited with an electrical input, can constrain the deflection along its length, and produce bending motion across its width, due to the differential expansion and contraction of the double layers. Sanchez-Salinero et al. (1986) reported a similar abnormality with bender elements in shear wave transmission, where the finite nature of the shear wave source tends to lead to the creation of compression wave energy.

The core of a bender element consists of two thin piezoelectric plates sandwiching a metallic (usually brass) centre shim, bonded together with thin layers of adhesive, and two thin conductive layers are applied on the outer surfaces (see Figure 2.20b). An even layer of epoxy coating is usually applied on the piezoceramic as a coating for electrical insulation and waterproofing purposes.

Based on wiring connections to the double polarised ceramic, the bender element can either function as a transmitter or a receiver (Brignoli et al. 1996). A series connection of the two plates makes a better receiver, as it generates a higher electrical output for a given deflection. This is because the total of the potentials available on each plate is equal to the output voltage. On the other hand, a parallel connection gives a higher deformation when subjected to a given voltage, thus making it more efficient as a transmitter.

2.4.2 Development of BE test in geotechnical testing

Lawrence (1963, 1965) was probably the first to apply piezoelectric transducers in shear wave testing of soil specimens. The test was carried out on clay and sand specimens, with shear plate transducers housed in the base pedestal and top cap of a triaxial apparatus. Later, Shirley and Anderson (1975) introduced bender ceramics in place of the shear plates for testing dry sand. These were preferable due to the generation of stronger signals with lower electrical excitation.

Dyvik and Madshus (1985) successfully developed bender elements for testing saturated soils. They introduced an epoxy-coating of the ceramics for insulation against the potentially conductive nature of soil, which could adversely affect the received signals. This breakthrough eventually led to a great expansion of BE testing in laboratories.

A prerequisite to the development of excellent shear wave velocity measurement techniques was a substantial improvement in the quality of the received signal (Jovičić et al. 1996). This was achieved by careful shielding of the cables connecting the bender elements to avoid external interference, so that the signals did not require amplification, filtering or averaging of data. Pennington et al. (2001) found that the most stable signals were obtained if the receiver BE's ground was in electrical connection with the soil sample, and that all earthing routes were avoided for the transmitter BE to prevent earth induction loops through the sample to the receiver.

Jovičić et al. (1996) reported that to capture a bender element signal that can be interpreted objectively, a sinusoidal wave pulse is preferable to a square wave one. Square

waves proved to be too complex for analysis compared with traces triggered with sinusoidal waves (Figure 2.21). Near-field effects (see Section 2.4.3) are almost inevitable as square wave pulses consist of a wide spectrum of frequencies.

It is now common to incorporate bender elements in the triaxial apparatus. For example, Jovičić et al. (1996) used a single pair of bender transducers embedded in the top and bottom platens to investigate the anisotropy within reconstituted kaolin samples. A multi-directional bender element transducer set-up was incorporated in triaxial tests by Fioravante and Capoferri (2001) to measure the shear wave velocities propagating along the vertical, horizontal and oblique directions in Ticino sand specimens. The experiments were aimed at evaluating the inherent and stress-induced anisotropy of the specimens. Pennington et al. (2001) studied the anisotropic modulus of clay specimens with horizontally-mounted bender transducers in housing pads attached to a radial strain belt. The bender probes consisted of a pair of ceramics positioned in a T-shape perpendicular to each other, so that measurements of shear wave polarisation in both the vertical and horizontal directions could be made simultaneously. Lings and Greening (2001) successfully introduced a convertible bender / extender element, where the electrical connections of the piezoelectric ceramics were reversed according to the polarisation of the ceramics, enabling the measurement of both compression and shear wave velocity with a single transducer.

Less commonly bender transducers have also been incorporated in oedometer tests. Jamiolkowski et al. (1995) installed bender elements to measure G_o in both vertical and horizontal directions following one-dimensional strain paths. Fam and Santamarina (1997) conducted consolidation tests with an instrumented oedometer cell to investigate G_o of soil under vertical stress in a confined condition. Observations on the dielectric permittivity were also carried out.

To date BE tests have been conducted on natural soils with no special attention given to cementation or cemented soils. The one exception is the work by Fam and Santamarina (1995, 1996) who studied the hardening and pore pressure diffusion of soil-cement slurries in an instrumented oedometer (Section 2.5).

2.4.3 Interpretation of measurements

Measurement of the shear wave velocity in laboratory soil samples is usually based on the assumption of wave propagation in an infinite medium (Stephenson 1977). The

wavelength of the pulse in the specimen should be as small as possible compared to the specimen dimensions in order to minimize the effects of the specimen size. This sets an upper limit of the wavelength in a specimen of a particular size. For a known material wave velocity, the maximum wavelength, λ_{max}, is given by the following equation:

$$\lambda_{max} = v\,T_{max} = v / f_{min} \qquad \text{(Eq. 2.2)}$$

where λ_{max} = maximum wavelength acceptable to assume infinite media

v = wave velocity in material being tested

T_{max} = period length corresponding to λ_{max}

f_{min} = minimum frequency corresponding to λ_{max}

A high enough excitation frequency is necessary to avoid a near-field effect, one of the most widely reported interfering factors affecting accurate visual determination of the shear wave arrival time. Brignoli et al. (1996) experimented with bender elements as well as flat-plate transducers with a varying distance between the transmitter and receiver. Some typical results from the research are shown in Figure 2.22. The specimens were undisturbed saturated soft clay, 50 mm in diameter and 100 mm in height, isotropically consolidated to a pressure of 25 kPa. The input and corresponding output frequencies, together with the wavelengths, are listed to the right of the figure. It was suggested that due to the energy-absorbing nature of the soil, and the dynamic interaction between the transducers and the surrounding soil, the predominant received signal frequency, f_{out}, is considerably lower than the input frequency, f_{in}, for $f_{in} \geq 5$ kHz.

Referring to the same figure, it was pointed out that, firstly, the signal component with negative polarity (denoted as 'X') preceding the arrival of the shear wave is strongest at low f_{in}. However this signal component tends to fade with increasing input frequency (increasing the number of wavelengths between the transducers). Secondly, the arrival of this near-field component is not sharply defined. Thirdly, tests with dry specimens exhibit a similar but sharper initial excursion, and the arrival time corresponds with those measured with compression transducers.

The 'X' arrival preceding S-wave arrival, which represents the near-field effect, can be theoretically accounted for by the finite dimensions of the shear wave sources, Sanchez-

Salinero et al. (1986). Near-field energy generates transverse motion with several characteristics as follows:

- Propagation with the (constrained) compression wave velocity.
- Initial polarity opposite to the component travelling with the actual S-wave velocity.
- Rapid decay with increasing number of wavelengths between the source and receiver.

It is useful to define a quantity R_d to ascertain that the near-field effects are avoided (Sanches-Salinero et al. 1986).

$$R_d = L / \lambda \qquad \text{(Eq. 2.3)}$$

where L = shear wave travel distance (tip to tip of the BEs)

λ = wavelength = v_s / f

v_s = shear wave velocity

f = frequency of the signal

Sanches-Salinero et al. (1986) recognised that the R_d ratio controls the shape of the received signal through observation of the degree of attenuation that occurs as the wave propagates through the soil specimen. R_d depends not only on the frequency of the signal, but also on the shear wave velocity. It was recommended that R_d be kept between 2 and 4, where the lower limit was to avoid near-field effects, while the upper limit was to cater for attenuation via damping. On the other hand, based on parametric studies of the propagation of elastic waves in an elastic medium, it has been shown that the actual arrival of shear waves can be significantly masked if R_d is between 1/4 and 4 (Mancuso and Vinale 1988).

Nevertheless, using a high input frequency to attain a sufficiently high R_d ratio is not always applicable. At high frequencies, as often required in testing stiffer material, 'overshooting' of the transmitter BE can occur (Jovičić et al. 1996). The limiting frequency at which overshooting begins depends on the relative impedances of the soil and bender element, making it a more serious problem in stiffer material. It is also worse for square waves, due to the rise time of the wave which is ideally zero corresponding to an infinite

frequency. Figure 2.23 shows the received trace for a test conducted on a soft rock specimen using a square wave. The correct arrival time, marked by line A-A, is lost within the noise resulting from overshooting.

To avoid overshooting, under certain circumstances, it is necessary to apply lower frequencies and tolerate the presence of a near-field effect. The methods suggested by Jovičić et al. (1996) to deal with this problem include the following:

- Distortion of the input sinusoidal wave by reducing the amplitude of the first upward cycle of the wave (Figure 2.24a). This will effectively cancel out the near-field effect and give a distinct arrival of the shear wave at the receiver. Note that the time scale is normalised so that the arrival time is 1.0.
- Adjustment of the input frequency so as to give forced oscillation of the receiver at its resonant frequency (Figure 2.24b). The arrival time can then be picked from one peak or trough on the transmitted signal to the corresponding point on the received trace. Again, the time scale is normalised so that the arrival time is 1.0.

Material dispersion, which is mostly accounted for by the fluid interaction in soils, used to be considered a major cause of problematic shear wave arrival time determination (Arroyo 2001). Analysing his own results, Arroyo observed that, for practically impermeable material like Gault clay, Biot dispersion happens in a frequency range well above that of usual BE testing, eliminating it as a potential problem in the definition of shear wave arrival time in BE testing. Arroyo also pointed out that the effect of specimen size can be more prominent than expected, when effects from the end rebound and the cylindrical boundary are considered. Interference of the received signal by these rebounds, resulting in a composite signal with various frequency components, is termed 'geometry dispersion'. The solution taken by Arroyo was a linear approach for the transfer function, developed to account for all rebounds and bender element length effects, which showed good agreement between his bench-top test results and the overall predicted shape of the amplitude spectra.

In Arroyo (2001), interaction of the propagating shear waves with the cylindrical boundary of the specimen was accounted for by waveguide theory, which models wave propagation in infinitely long cylinders. The basic principle of the waveguide theory is that, when wavelengths are comparable with the size of the propagating structure, lateral

rebounds produce an interfered signal where each frequency travels at a different velocity. Using a computer program developed for ultrasonic testing purposes, Arroyo observed from the dispersion curves for Gault clay cylinders that the propagation modes most likely to be excited by bender elements were flexural modes. Signals propagating with flexural modes displayed an amount of dispersion compatible with the observations. It was suggested that there could be a range of diameter sizes and frequencies where the problem may be magnified, and that this range substantially overlaps the usual testing range.

2.4.4 Determination of shear wave arrival time

This section reviews in detail the various methods commonly employed to determine shear wave arrival time, all of which are examined with the present test results in Section 4.2.2. In spite of the seemingly simple and direct measurement method with bender elements, the actual shear wave arrival time is perhaps more elusive than imagined. Past researchers have experimented with various techniques to ascertain the arrival time with more accuracy, and the methods can be grouped into two main categories: time domain and frequency domain.

Time domain methods are direct measurements based on plots of the electrical signals versus time (e.g. Viggiani and Atkinson 1995, Arulnathan et al. 1998, Clayton et al. 2004, Porbaha et al. 2005), whereas the frequency domain methods involve analyzing the spectral breakdown of the signals and comparing phase shifts of the components (e.g. Viggiani and Atkinson 1995, Brocanelli and Rinaldi 1998, Arroyo 2001). There is however, no method yet proven to be superior to the others.

2.4.4.1 Visual picking

This is the most commonly used method of interpretation, where the first major deflection of the received signal is taken as the shear wave arrival time (t_o) (Viggiani and Atkinson 1995, Jovičić et al. 1996, Lings and Greening 2001 and others). The method owes its popularity to being straightforward. An example of this method is shown in Figure 2.25, where the visually picked shear wave arrival time is labelled as t_o.

The first significant departure from zero amplitude could be positive or negative, depending on the arrangement and polarity of the bender elements. In order to facilitate easier identification, Teachavorasinskun and Amornwithayalax (2002) suggested employing a pair of oppositely polarised signals, obtained by changing the polarisation of

the transmitter (Figure 2.26). This is similar to the down-hole seismic field test where the received shear wave signal is captured twice by striking the hammer in opposite directions (Section 2.3.1.2).

The major disadvantage of the visual picking method is the uncertainty when the received signal does not display a distinct and sharp deflection point. Quite often this first point or arrival is masked by near-field effects (Section 2.4.3) or other interference, like background noise.

2.4.4.2 First major peak-to-peak

The first major peak-to-peak method (e.g. Viggiani and Atkinson 1995) is based on the assumption that the received signal bears a high resemblance to the transmitted one. The time lapse ($t_{pk\text{-}pk}$) between the peak of the transmitted signal and the first major peak of the received signal is taken as the shear wave travel time, as shown in Figure 2.25.

Due to the dispersion effect caused by sample geometry, and the energy-absorbing nature of soil, the received signal is usually distorted to various extents while attenuating with distance. In these circumstances, defining the first major peak becomes more difficult, as when the signal has several consecutive peaks of very slight differences in amplitude. As with the visual picking method, this technique is also significantly affected by the quality of received signals.

2.4.4.3 Cross-correlation

Cross-correlation, an adaptation of conventional signal analysis methods, was first introduced by Viggiani and Atkinson (1995) in the context of BE tests in soils. An example of the cross-correlation function, corresponding to the transmitted and received signals shown in Figure 2.25, is presented in Figure 2.27.

The cross-correlation analysis method measures the level of correspondence or interrelationship between two signals, transmitted, T(t) and received, R(t), as expressed by the cross-correlation coefficient, $CC_{TR}(t_s)$:

$$CC_{TR}(t_s) = \lim_{T_r \to \infty} \frac{1}{T_r} \int_{T_r} T(t + t_s) R(t) dt \qquad \text{(Eq. 2.4)}$$

where T_r is the time record and t_s is the time shift between the two signals.

In order to apply this technique, it is convenient to convert the time domain signals to the frequency domain, whereby decomposition of the signals produces groups of harmonic waves with known amplitude and frequency. A common algorithm used for this purpose is the Fast Fourier Transform (FFT).

The transmitted and received signals, T(t) and R(t), are transformed to their linear spectrums respectively via FFT. The linear spectrum is a vector in complex form, giving the magnitude and phase shift of each harmonic component in the signal.

The linear spectrum of the transmitted signal is

$$Y(f) = FFT\,[T(t)], \qquad \text{(Eq. 2.5)}$$

where f = frequency

The linear spectrum of the received signal is

$$X(f) = FFT\,[R(t)] \qquad \text{(Eq. 2.6)}$$

Next the complex conjugate of the linear spectrum of the transmitted signal is computed, $Y^*(f)$. The cross-power spectrum of the two signals can now be established by simple multiplication:

$$G_{xy}(f) = X(f)\,Y^*(f) \qquad \text{(Eq. 2.7)}$$

The magnitude and phase of the cross-power spectrum, $G_{xy}(f)$, are the products of the magnitudes and phase differences of the components in the two signals at that particular frequency. Therefore the range of common frequencies can be deduced from the magnitude of the cross-power spectrum.

To obtain $CC_{TR}(t_s)$, an inverse Fast Fourier Transform is executed on $G_{xy}(f)$:

$$CC_{TR}(t_s) = FFT^{-1}\,[G_{xy}(f)] \qquad \text{(Eq. 2.8)}$$

The maximum $CC_{TR}(t_s)$ denotes the corresponding time shift between the signals being analysed, which is the travel time of the shear wave. The corresponding shear wave velocity is given by v_{cc}.

Cross-correlation can be a more consistent method compared with the previous two but this only holds true if the transmitted and received traces consist of sufficiently similar frequency components. An example of good correspondence between the transmitted and received signals was given by Viggiani and Atkinson (1995), as represented by the linear spectrum for both signals in Figure 2.28. The frequency distribution plots of the signals show common peaks at 5 kHz, corresponding with the input frequency as generated by the function generator in the test.

It is obvious then that analysis in the time domain can be uncertain due to the inherent characteristics of the signals. One way of analyzing the signals without such influence is to decompose the traces into their frequency spectra and carry out the analysis in the frequency domain, as described in the following sections.

2.4.4.4 Cross-spectrum

Implementation of the cross-spectrum method in analysing bender element test results was also first proposed by Viggiani and Atkinson (1995). It is essentially an extension of the procedure used in the cross-correlation method, where the frequency spectra of the signals are further manipulated to obtain the absolute cross-power spectrum. The cross-power spectrum, $G_{xy}(f)$, is a function of the frequency spectrum of the received signal and the conjugate of the transmitted signal, as given in Eq. 2.7.

An example of the cross-power spectrum for the time records of Figure 2.25 is shown in Figure 2.29, where every reversal of the phase represents a missing cycle (Arroyo 2001). Assuming that the phase increases continuously, an unwrapping algorithm can be applied to the phase data to account for points where reversal occurs.

An 'unwrapping' algorithm was applied on the cross-power spectrum phase angle in Figure 2.29 to account for the missing cycles, and the resulting graph was the monotonic plot shown in Figure 2.30. The plot is termed the absolute cross-power spectrum phase diagram. With a linear regression line fitted through the data points over a range of frequency presumed to be common to both signals, Viggiani and Atkinson (1995) took the slope of the line, α, as the group travel time, $t_{cs} = \alpha / 2\pi$ (Eq. 2.9). The subscript 'cs' denotes 'cross-spectrum'.

With a phase diagram (e.g. Figure 2.30) rotated anti-clockwise through 90°, and with the angular frequency, $\omega = 2\pi f$ (Eq. 2.10), plotted against the wave number, $k = \phi/L$ (see Eq. 4.3 in Chapter 4), the secant gradient of each data point would represent the phase velocity while the tangential gradient would give the group velocity at one particular frequency, Figure 2.31 (e.g. Brillouin 1960, Graff 1975). If there is no dispersion in the signal, the phase diagram would plot as a straight line through all the points within the common frequency range, giving the same phase and group travel times. Arroyo (2001) pointed out that the regression technique used by Viggiani and Atkinson (1995), if employed in cases where curvature of the unwrapped phase plot is present, would inevitably mask dispersion and variation of the phase travel times.

2.4.4.5 Phase and group velocities

As mentioned in the previous section, the phase and group travel times (t_{ph} and t_{gr}, respectively) can be determined from the unwrapped or absolute phase diagram by taking the secant and tangential gradients respectively (Figure 2.31). Arroyo (2001) compared the phase and group velocities (v_{ph} and v_{gr}, respectively) obtained from his BE test on Gault clay, Figure 2.32. It is clearly illustrated that both the velocities differ significantly, with the group velocities being almost always higher than the phase velocities. He attributed the average low values of phase velocity to the inadequacy of the unwrapping algorithm. Arroyo concluded that if the discrepancy lies in the unwrapping procedure, an alternative method might be the next step forward. However Shatilo (1992) has experimented with various unwrapping techniques and concluded that no single one was the best.

2.4.4.6 Comparison of time and frequency domain interpretation methods

As stated earlier in this section, in spite of the various techniques employed, a method has yet to be found as being the most reliable in defining the shear wave arrival time, either in the time or frequency domain. Arroyo (2001) made a systematic attempt to compare the effect of the different methods on G_o estimation. Using statistical analysis, it was shown that there was no clear optimum, but that consistency could be significantly improved by adopting one method in an entire test series, resulting in a coefficient of variation ranging between 10 and 20 % for the shear wave velocity, corresponding to a 20 to 40 % uncertainty in G_o. However, based on histograms of the shear wave velocity data

obtained with different methods, only the cross-spectrum method displayed a normal distribution, suggesting that the method could be the more reliable than the rest.

Greening et al. (2003) reported that there is less uncertainty when determining shear wave arrival times using the phase-frequency relationship. Greening and Nash (2004) also claimed that frequency domain interpretation methods provide more information on the relationship between the transmitted and received signals in BE tests. The authors found that the time domain methods tended to underestimate the shear wave arrival time, and hence overestimated the shear wave velocity and G_o.

2.4.5 BE test in stabilised soils

Investigation of stabilised soils with bender elements has gained more attention in recent years. This is partially driven by the development and increasing popularity of geophysical testing in the field for stabilised columns. Laboratory investigation with shear waves is recognised to be useful in validating and supplementing information gathered from the field (e.g. Hiraide et al. 1996, Nishikawa et al. 1996, Massarsch 2005, Mattsson et al. 2005).

Mattsson et al. (2005) performed bender element tests on stabilised samples of soft clay from Uppsala, Sweden in unconfined conditions. The bender elements were embedded in the top cap and pedestal of an unconfined compressive strength apparatus. Field testing with the down-hole method was also conducted to plot the shear wave velocity profiles (Section 2.3.1.2 and Figure 2.13). The samples were prepared in the laboratory with 80 kg/m^3 and 120 kg/m^3 of lime-cement binder, and tested at two different curing ages. Thin grooves were pre-made on both the ends of the firm samples, which were then filled with gypsum prior to insertion of the bender elements. The gypsum, which acted as a coupling material between the bender element and the stabilised soil, was then left to harden before the BE test was conducted. It was most probably chosen for its short setting time and compatible stiffness with the stabilised soil. Too soft a coupling medium would have absorbed the vibration of the bender element, resulting in premature attenuation of the shear waves. Too stiff a coupling material, however, would have restrained the bender element from free vibration, again leading to weak motion along the sample.

The same samples were subjected to unconfined compressive strength tests and the corresponding plot of undrained shear strength versus shear wave velocity is shown in Figure 2.33. As shown on this plot, Mattsson et al. (2005) proposed a power relationship

linking the two parameters. It was also suggested that different correlations can be expected for different clays with different stabilisers added. Note that this work was published after the research described in this thesis was completed.

Other attempts to study stabilised soil behaviour with bender elements primarily involve one-dimensional compressibility tests with instrumented oedometers, which will be discussed in the next section.

2.5 Compressibility studies

Knowledge and understanding of the compressibility of stabilised soil is essential in the deformation analysis of composite soft soil systems. The magnitude and rate of settlement significantly affect the long term performance of column-stabilised soft ground. In addition to compressibility behaviour, previous work on yield stress definition, small strain shear stiffness development during compression and the relevant correlations are also reviewed. This section also highlights the possibility of using small quantities of stabiliser (i.e. less than 10 %) to achieve the required stiffness, mainly to reduce the construction cost. Finally, literature on the change of lateral stress under a zero lateral strain condition (i.e. K_o condition) is reviewed.

2.5.1 Curing effect

One of the most difficult parameters to select when investigating the compressibility of a stabilised soil sample is the most suitable age to begin testing, i.e. the curing period. It is widely recognised that cement induces faster strength, and hence stiffness, gain over time than lime. The reason for this was clearly illustrated by Kitazume (2005), Figure 2.34. In both cases, the initial reduction of the soil water content due to hydration precedes other reactions, resulting in a small increase in strength. This is followed by the cation exchange or flocculation phase which improves the plasticity of the mix. The next stage is what separates the strength gains of cement and lime treated soil. In the cement-stabilised soil, the hydration of cement is completed rapidly and most of the strength is achieved within a few weeks. The lime formed during the hydration process then undergoes a pozzolanic reaction (i.e. gel formation and crystallisation) which increases the strength over the long term. As for lime-stabilised soil, most of the strength improvement relies solely on the pozzolanic process of the lime, and it is thus significantly slower than that of cement

treated soil. Use of a combined stabiliser of lime-cement is usually aimed at shortening the time for strength gain (Schaefer et al. 1997).

Various curing periods allowed before subjecting a treated sample to a compressibility test, and chosen to reduce the effect of the on-going pozzolanic reaction, have been reported in the literature. The variations are mainly due to different soil mineralogy and binder types, as well as the initial water content of the mix.

Uddin et al. (1997) carried out oedometer tests on cement-stablised Bangkok soft clay samples left to cure for different periods and concluded that a month was the optimum curing period, after which further cementation gave no noticeable reduction in the compressibility (Figure 2.35). The authors also claimed that curing effect was secondary to that of cement content, given a certain minimum curing period.

Figure 2.36 shows the increase of shear wave velocity and maximum shear modulus with time, measured both in situ and in the laboratory with bender elements by Massarsch (2005). The shear wave velocity and maximum shear modulus for two columns, with 99 kg/m^3 and 156 kg/m^3 of lime-cement, increased with time up to 116 days (2784 hours). However a significant improvement was observed within the first 41 days (approximately 1000 hours), after which both the shear wave velocity and the small strain shear stiffness increased at a much slower rate. It is interesting to note that only the final measurements were obtained from BE tests, while the earlier ones were conducted in situ. The risk that the two measurements might not be truly comparable did not deter the author from combining the results, and leaving the systematic difference between the two methods undefined. Due to the limited data available, it is perhaps a little speculative to apply curve-fitting to obtain a trend for the change of shear wave velocity with time.

Fam and Santamarina (1995, 1996) studied the process of cementation in an instrumented oedometer cell, Figure 2.37a. It was shown that the cement mix (water/cement ratio = 0.4) was essentially inert for the first two hours before a significant increase in shear wave velocity was registered for the next 12 hours, Figure 2.37b. The improvement rate diminished with time. The authors complemented their findings with dielectric permittivity measurements (using electromagnetic waves) during the cement hydration process, Figure 2.37b. It was claimed that the distinct decay in both real and imaginary permittivity after approximately 2 hours corresponded with the onset of hydration activity within the cement paste.

Other researchers who have carried out oedometer tests on stabilised soil samples have selected an arbitrary curing period, limited by time constraints or based on past experience. For instance, Feng (2002) started the tests when the stabilised samples were 7 days old, and Horpibulsuk et al. (2004) kept the samples for 28 days prior to testing.

2.5.2 One-dimensional compressibility behaviour

Referring to Figure 2.34, due to the long term pozzolanic reaction in stabilised soils, it might not be possible to differentiate the effect of cementation from that of increased effective stress on the improved stiffness observed during a compressibility test. Fam and Santamarina (1996) attributed the increase of shear wave velocity (i.e. stiffness) in one-dimensionally compressed stabilised soils to the increased effective stress from consolidation, the increased rigidity of the soil from cementation and the reduction of double-layer repulsion with substitution of Na^{+} and Ca^{2+} in high concentrations (as measured from the dielectric permittivity of the soil). It is generally assumed, however, that although cementation limits settlement pre-yield, the cementation effect is subsequently overwhelmed by the influence of effective stress which breaks down the cement bonds (e.g. Uddin et al. 1997, Horpibulsuk et al. 2004).

Compressibility reduces with higher stabiliser content, resulting in reduction of settlement. Bangkok soft clay treated with 5 – 25 % of cement was tested by Uddin et al. (1997) after 1 month of curing, and the compression curves are shown in Figure 2.38. It is evident that an addition of 5 % cement was sufficient to reduce the settlement substantially. The higher cement contents did not seem to produce a major benefit in terms of settlement reduction. The compression curves of all the treated clays tended to become parallel to the virgin compression curve of the unstabilised clay post-yield.

Feng (2002) was the first to suggest using small quantities of cement to achieve improved stiffness. It was argued that as bearing capacity failure is not usually an issue, small binder quantities are sufficient to keep the settlements within the acceptable range. Of course, there are also economic benefits of using small quantities of binder. Figure 2.39a depicts the compression curves from Feng's work on cement-stabilised Taipei lacustrine clay (cured for 7 days) with standard oedometers. Sample tc-b had a formation of 4 soil-cement columns within unstabilised soil, while the rest were tested as homogeneous samples. Referring to the same figure, the yield stresses (termed

preconsolidation pressures) were defined using the graphical method introduced by Casagrande (1936).

It was reported that 3 % cement (sample tc-d) was insufficient to recover the pre-consolidation pressure of the remoulded unstabilised clay (sample tc-a). However the position of the tc-d curve is slightly above that of tc-a, showing that there was a change in the soil structure even with such a small cement content. Also, the difficulty in defining the yield point on the curve of tc-d could have masked the higher yield stress. Comparing curves tc-b and tc-c, it is clear that the homogeneous stabilised sample (tc-c) had a more marked improvement than the one with columnar inclusions (tc-b). The compression curves of the cemented soil do not deviate greatly from that of the unstabilised soil. They also lie almost parallel to the virgin compression curve of the unstabilised sample in the post-yield stage. This suggests that once the cementation effect was being destroyed, with the bonds being broken down, the compression behaviour reverted to the behaviour of the original soil. It is therefore vital to utilize the improved stiffness of stabilised soils pre-yield for minimal settlement. Although a small cement content significantly increases the yield stress, it is not particularly beneficial in reducing settlement post-yield.

As one of the main focuses of Feng's study was the secondary compression of cemented soils, he presented a comparison of the compression indices of primary consolidation (C_c) and secondary compression (C_α), Figure 2.39b. The presence of small cement quantities clearly reduced the secondary compression index. The ratio of C_α/C_c is a constant for any unstabilised soil and for inorganic soils, the ratio decreases with an increase of grain size (Terzaghi et al. 1996). The above observation therefore strongly suggests the presence of larger aggregates in the altered structure of the stabilised soil.

The post-yield compression curves of a cement-stabilised clay with different initial water contents have been found to converge on a single virgin compression line (Horpibulsuk et al. 2004). Figure 2.40a shows the compression curves of cement-treated Bangkok and Ariake clays, along with the physical properties of the base clays. Both clays were mixed with a fixed quantity of cement at various initial water contents and left to cure for 28 days prior to testing. The results suggest that the compression index, C_c, is constant for a particular clay treated with cement, regardless of the amount of water present in the original soil mass. Consequently, the post-yield compression of the stabilised clay is controlled by the binder content. Combining one-dimensional compression data from various unstabilised clays with that of cement-treated Bangkok and Ariake clays, the

authors proposed a 'generalised compression line' (GCL), Figure 2.40b, for post-yield compression behaviour. The effect of clay type was accounted for by normalising the void ratio, e, at the end of each loading stage with e_{100} (void ratio at the end of the 100 kPa loading stage).

2.5.3 Correlation between compressibility and maximum shear modulus or shear wave velocity

There has not been much attention given to the evolution of shear wave velocity or maximum shear modulus with effective stress in oedometer tests on stabilised soils. However Santamarina et al. (2001) studied pore pressure diffusion in kaolin slurry with shear wave velocity in an instrumented oedometer as described in Section 2.5.1 and Figure 2.37. The increase in shear wave velocity during primary consolidation was a consequence of the increase in effective stress with the dissipation of excess pore water pressure (Figure 2.41a).

Figure 2.41b shows only the early stages of a loading increment. It can be seen that the shear wave velocity decreased slightly immediately upon loading in kaolin and bentonite samples, but not in the silica flour sample. It was suggested that the non-uniform pore pressure response within the sample immediately upon loading resulted in an uneven effective stress distribution, and that this caused a transient drop in stiffness at the early stage. The drop was expected to be more significant in soils with a lower permeability, where dissipation of the excess pore water pressure requires a longer time. Spatial differences, for instance the presence of soil particle aggregates within the sample, were also thought to be a possible factor causing non-uniform pore pressure distribution. It was further suggested that the recovery time for the shear wave velocity could be an indicator of the permeability of the sample, as shown in the longer recovery time required by bentonite than kaolin.

Other researchers have made similar observations during early stages of load application in one-dimensional compression tests. For example, Hardin and Black (1969) attributed the drop to sudden breakdown of microstructure within the sample, while Schultheiss (1981) explained the phenomenon as due to excess pore water pressure in the vicinity of the transducers which altered the drainage path and affected the shear wave velocity measurement. Interestingly, Afifi and Woods (1971) reported a significant initial drop in shear wave velocity when loading dry kaolin powder.

Santamarina et al. (2001) also plotted shear wave velocity versus vertical stress on a log-log scale to highlight the power relationship between the two parameters, Figure 2.42. The plot shows a linear relationship during virgin compression and a slight drop in shear wave velocity during unloading. The higher shear wave velocity after loading and unloading was attributed to residual lateral stress locked into the overconsolidated sample.

Due to the confined nature of the sample in an oedometer test, the stiffness modulus obtained from the compression curve is the constrained modulus, M_o. In Figure 2.43, Burns and Mayne (2002) have gathered data from various unstabilised natural clays and showed that correlations linked M_o (D' on the figure), v_s and G_o. Despite the scatter, Figure 2.43 strongly suggests that the two stiffness moduli, M_o and G_o, are inter-related. A similar relationship might be expected for artificially cemented soils. Such a correlation would enable a prediction of the compressibility behaviour of a particular stabilised soil without carrying out a time-consuming oedometer test. Measurements of shear wave velocity, either in situ or in the laboratory, would allow the estimation of M_o.

2.5.4 Correlation between yield stress and strength

Horpibulsuk et al. (2004) demonstrated that a linear relationship exists between the yield stress under one-dimensional or K_o compression, σ_y', and the unconfined compressive strength, q_u (Figure 2.44). Based on data for three types of clay, σ_y' was found to vary from 1.4 to 2.2 q_u. The correlation appeared to be dependent on the clay type.

2.5.5 Lateral stress and K_o evaluations

Often due to the large lateral extent of applied loading, lateral deformation is negligible relative to the vertical displacement. Therefore compression of the soil is considered to be one-dimensional with zero lateral strain. This is known as the K_o-condition (K_o is the coefficient of earth pressure at rest; see Eq. 4.11 and Eq. 4.12 in Chapter 4). K_o values are dependent on the soil microstructure or fabric, strength and stress history (Edil and Dhowian 1981). Also according to the same authors, in unstabilised soil, K_o is known to remain constant during virgin compression but increases during unloading. Hence, K_o values tend to decrease when a soil sample is being loaded from an overconsolidated condition.

The measurement methods of lateral stress under K_o loading conditions are categorised into two main groups (Ting et al. 1994):

- Rigid lateral boundary methods

  This method uses an oedometer type apparatus, providing the zero lateral strain condition, but usually allowing for undefined friction between the soil sample and the internal wall of the cell. In practice, very small lateral strain (e.g. microstrain) is actually allowed for the cell containing the sample to facilitate K_o measurements.

- Flexible lateral boundary methods

  This method utilises feedback systems to maintain the position of the boundaries, as in triaxial type equipment. The apparent advantage of this method is the absence of side friction, but the inherent disadvantage is that the best that can be achieved with the soil sample is zero mean lateral stress.

With a rigid lateral boundary, several methods exist for measuring K_o. A full-bridge strain gauge circuit, with strain gauges mounted on the oedometer cell wall, has perhaps been most widely adopted (e.g. Newlin 1965, Edil and Dhowian 1981, Zhu et al. 1995). Brooker and Ireland (1965) and Singh et al. (1973) developed a null strain system, regulating hydraulic pressure at the back of a thin-walled oedometer ring to measure the lateral stresses. Abdelhamid and Krizek (1976) attached flush diaphragm transducers to a rigid oedometer cell for monitoring lateral stress changes. Also, Thomann and Hryciw (1990) used a horizontal loading piston with a load cell connection for lateral stress measurements in an oedometer.

With a flexible lateral boundary, Bishop (1958), Moore (1971), Menzies et al. (1977) incorporated various local lateral strain measurement devices in conventional triaxial apparatus, while regulating the cell pressure to achieve zero lateral strain conditions.

Very little research has been reported on K_o values in stabilised soils. However Zhu et al. (1995) studied the effect of artificial cementation on the lateral stress in sands, and showed that lateral stress decreases with higher cement content. An increase in K_o with vertical stress in weakly cemented samples (low cement contents), Figure 2.45, was attributed to the breakdown of cementation bonds. K_o for the most highly cemented sample (8 % cement content) remained mostly unchanged, with the cementation appearing to be able to resist the increased vertical stress.

2.6 Concluding remarks

From the review of the literature available to date, it can be seen that stabilisation technology has come a long way since its first implementation almost half a century ago. Much has been explored in terms of the improved mechanical properties of stabilised soil and the understanding of stabilised soil behaviour, especially in terms of strength and compressibility.

Quality control and assurance methods have also made significant advances. Nevertheless a shift from conventional sampling and destructive testing to non-destructive methods using seismic waves has opened up an area of research, promising less time- and effort- consuming assessment of stabilised soil. This necessitates correlating shear wave velocity with the engineering properties of the stabilised material, but there is still an apparent lack of information and experimental data about such relationships. The gaps in the knowledge are best filled by experimental work coupled with field measurements for verification.

Table 2.1: Field tests for evaluating stabilised soils (Hosoya et al. 1996).

Method	Test methods and results	Comment of quality control method
Sounding test		
standard penetration test	Let 67.5kgf hammer fall free from 75cm height and count the number of stokes (N-value) to penetrate 30cm.	Most common method on natural soil. There is correlation with unconfined compressive strength.
Dynamic cone penetration test	Let 5kgf hammer fall from 50cm height and count the number of stokes (Nd-value) for cone to penetrate 10cm.	Easy transportation and operation. Practical for unconfined compressive strength, q_u of 200 to 500 kN/m^2.
Static cone penetration test	Let the cone penetrate at uniform speed and measure the resistance ant the end and surrounding surface and pore water pressure in sequence.	Applicable to measure the improvement of low strength stabilized soil in sequence. However, not applicable for firm stabilized soil.
Rotary penetration test	Measure the bit pressure, torque and muddy water pressure by the sensor at the end of the boring rod to observe the soil strength in sequence.	Greater mobility compared with core sampling and field strength can be measured. However, correlation with the unconfined compressive strength must be compared from site to site.
wing penetrometer test	The wing penetrometer is push down or lifted up in the center of stabilized column. The measured driving or lifting load is converted to shear strength values of the stabilized columns tested.	The tests have limited applicability to high strength columns.
Test of utilizing bore hole		
PS logging	Measure the velocity of P and S waves. Then calculate rigidity and Poisson's ratio of stabilized soil. there are two testing methods, down hole method and suspension method.	There is some correlation with unconfined compressive strength although it is not so uniform. Suspension method is better to evaluate the stabilized soil.
Electrical logging	Supply electric to stabilized soil and measure electric current and voltage through an electrode. Then calculate the specific resistance.	The correlation with unconfined compressive strength is low.
Density logging	Measure the gamma rays emitted from a probe inserted into the hole by the detector installed at a certain distance. Then convert the data into density.	Since it is influenced by hole diameter and water inside the hole, calibration is important. there is no correlation with unconfined compressive strength.
Loading test		
Bore-hole lateral load test	Press rubber tube toward the bore hole wall in stages and measure the strength and deformation modulus of stabilized soil. Measurement apparatus is Pressiometer and LLt.	Deformation modulus rather than strength is often the objective of the tests. Vertical measurement is costly so it is used as representative value of stabilized soil.
Plate loading test	Place a loading plate (round plate of 30cm in diameter) on the stabilized soil and put on load in stages. Bearing capacity and deformation characteristics can be obtained directly from the load and settlement curve.	Bearing capacity and deformation characteristics can be obtained directly. However, the evaluation of stabilized soil is possible only down to the depth of 2 to 3 times of (load) plate diameter.
Stabilized pile loading test	Load on the top of the stabilized column through the load plate of the same diameter as the stabilized column. The bearing capacity characteristics are obtained from the load and settlement curve.	Bearing capacity characteristics of a stabilized column can be directly obtained. However, testing equipment is costly and the number of tests available is limited.
Non destructive test		
Integrity test	Stroke the top of a stabilized column with a hammer and measure the reflected wave of the vibration by the accelerometer. Length and discontinuity of stabilized column is measure.	Simple method. However, evaluation standard for a stabilized column has not been established.
Elastic wave exploration	Emit P and S waves to measure the velocity distribution of stabilized soil. In the case of stabilized soil, measurement of S wave is preferred.	Stabilized condition is measured by velocity distribution of the S wave. The measurement is made in the bore hole and on the ground surface. Tomography is used to improve accuracy of the test.
Other test		
Penetration test	Use pocket type pin penetration apparatus and measure the penetration resistance of stabilized soil on the job site. Then estimate the unconfined compressive strength.	Easy and simple method. A lot of tests can be done. However, only the surface of the stabilized soil can be tested.

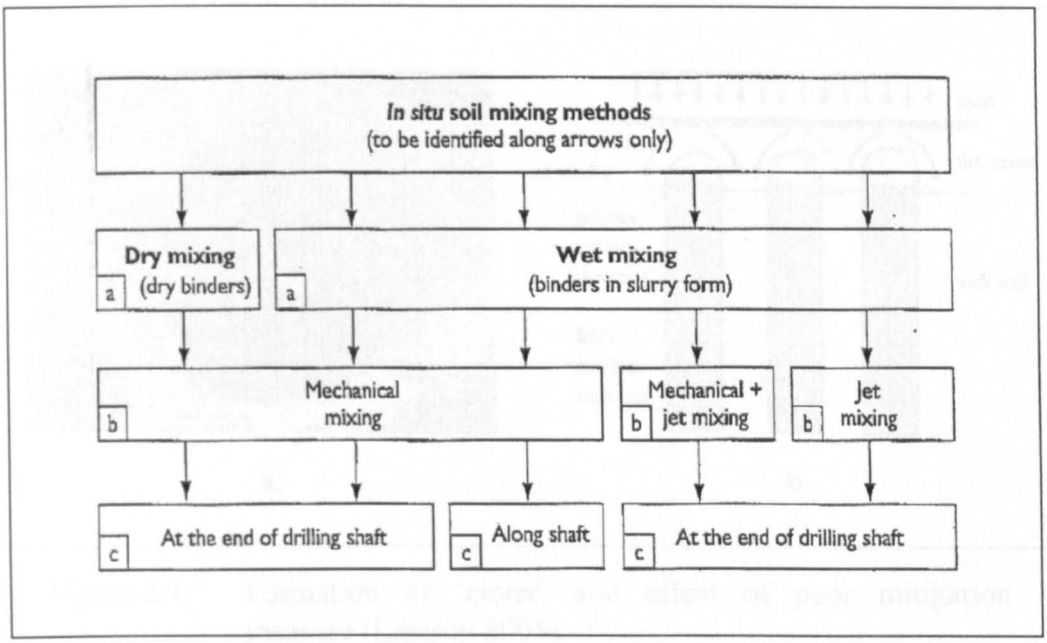

Figure 2.1: Classification of deep mixing methods (adapted from Topolnicki 2004).

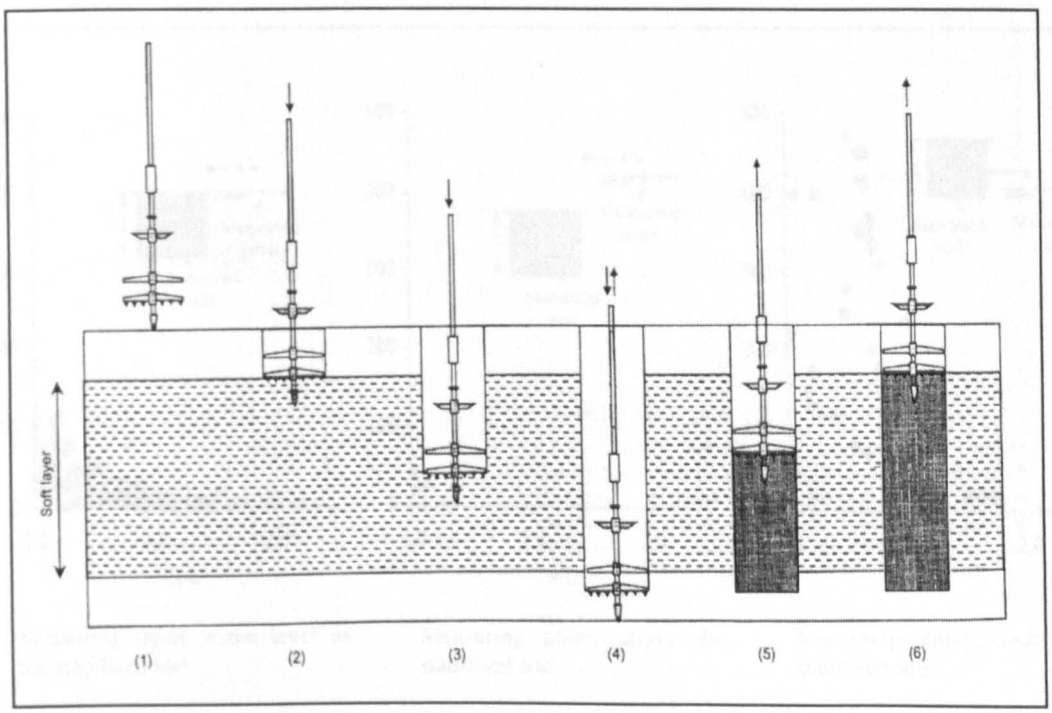

Figure 2.2: Sequence of a column installation (Porbaha et al. 2001).

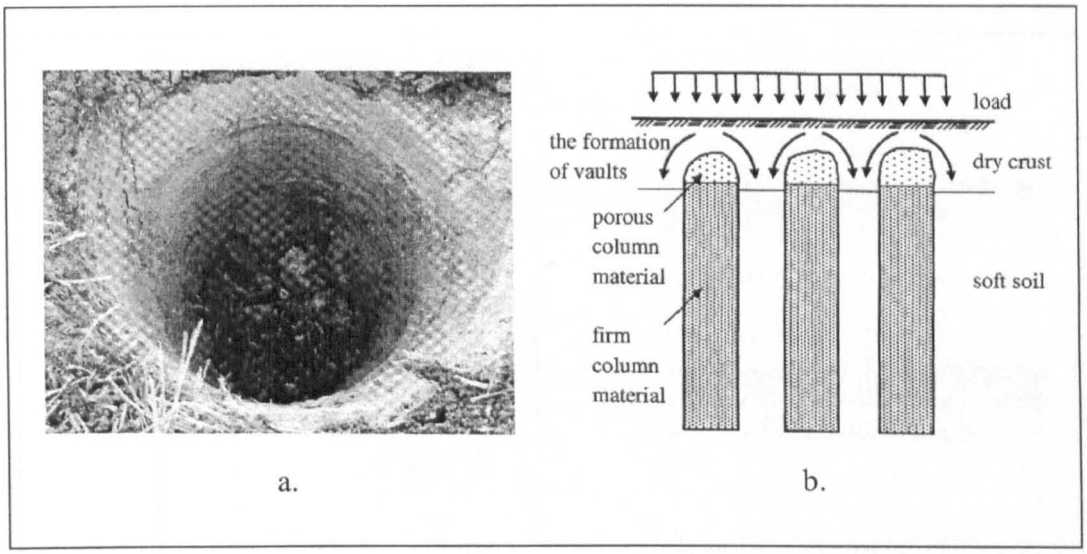

Figure 2.3: Formation of 'crater' and effect of poor mitigation measure (Larsson 2005).
a. 'Crater' at the top of a column.
b. Formation and effect of 'vaults'.

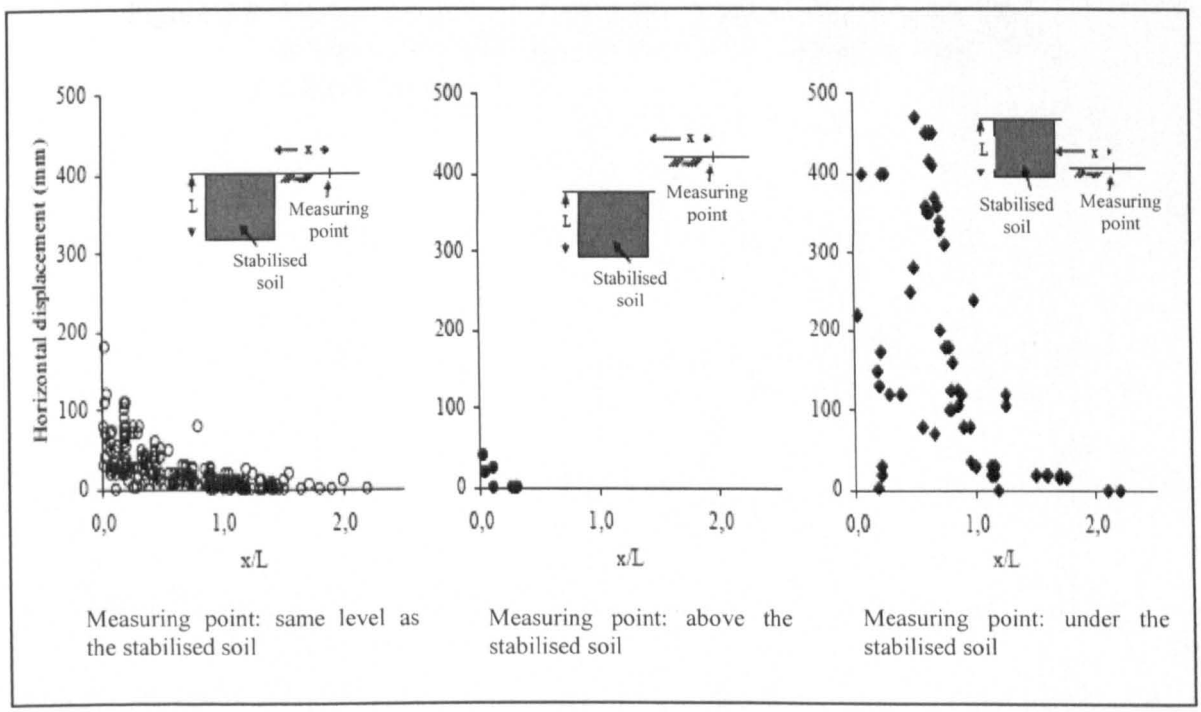

Figure 2.4: Lateral displacements during column installation (Larsson 2005).

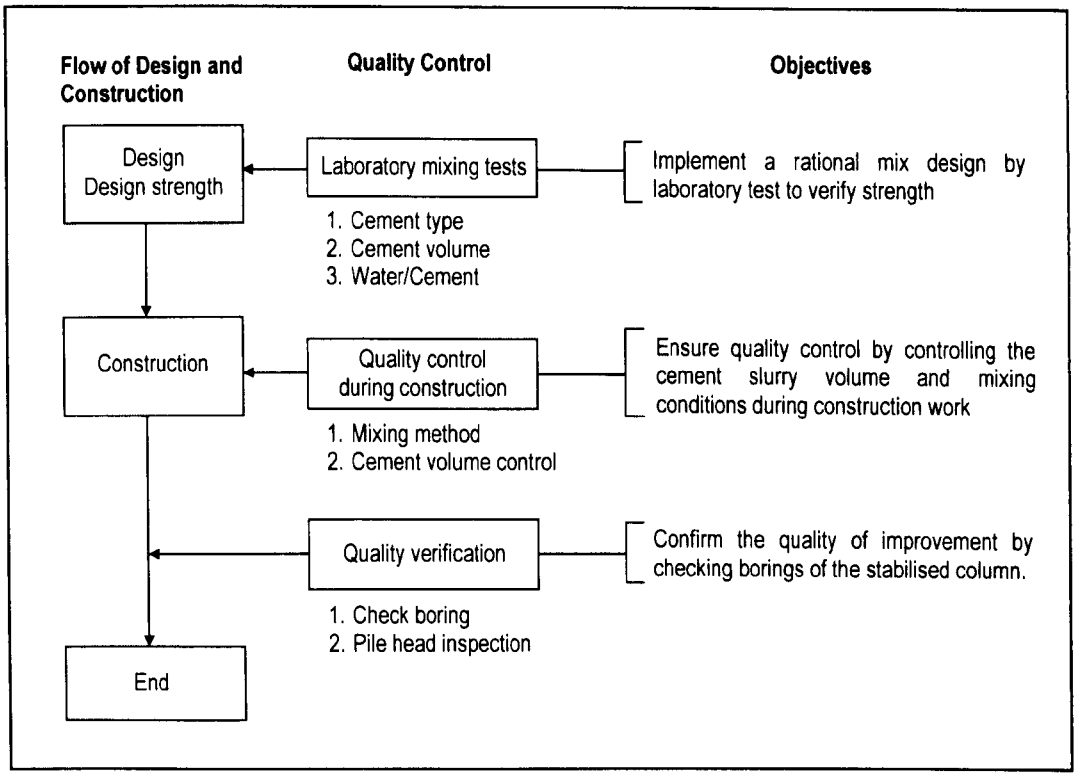

Figure 2.5: Process of quality control and assurance for deep mixing. (Coastal Development Institute of Technology, Japan 2002, after Kitazume 2005)

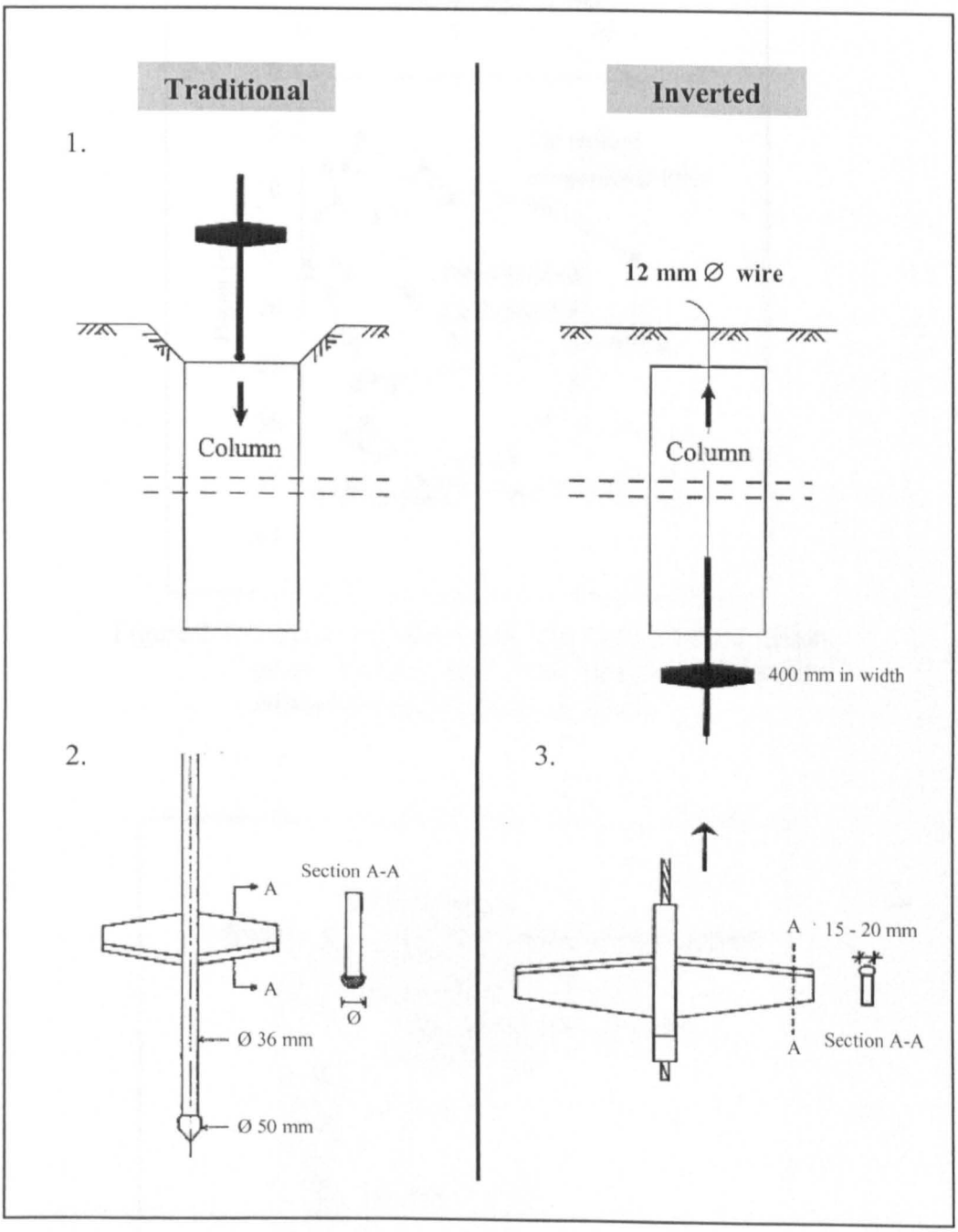

Figure 2.6: Column penetration tests ([1] Rathmayer 1996; [2] Torstensson 1980; [3] Holmqvist 1992, after Larsson 2005).

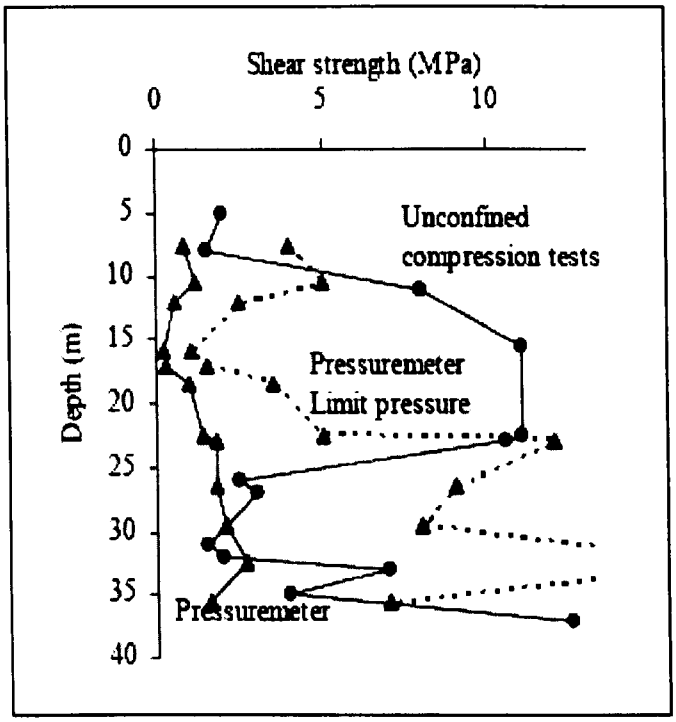

Figure 2.7: Undrained shear strength measurements from pressuremeter and unconfined compressive strength tests (Hughes et al. 2001).

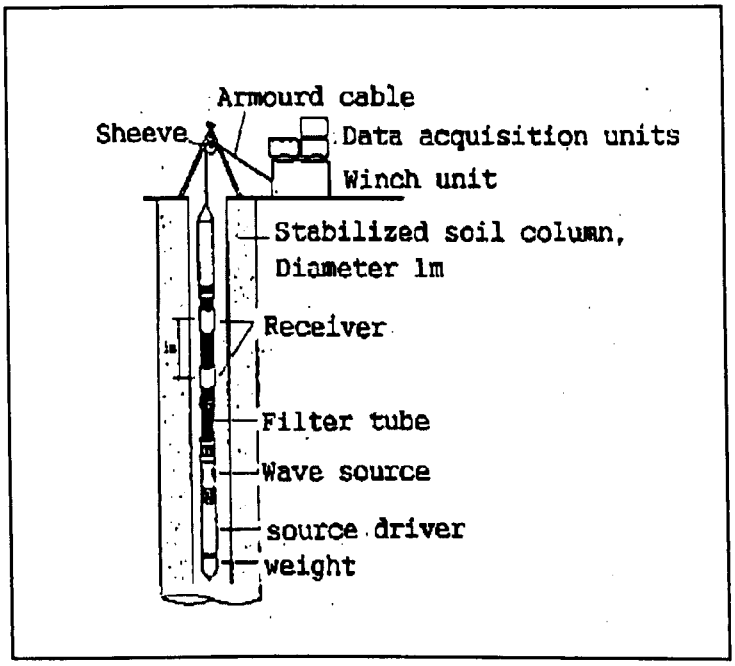

Figure 2.8: Suspension type P-S logging test set-up (Hiraide et al. 1996).

(i) Azuma

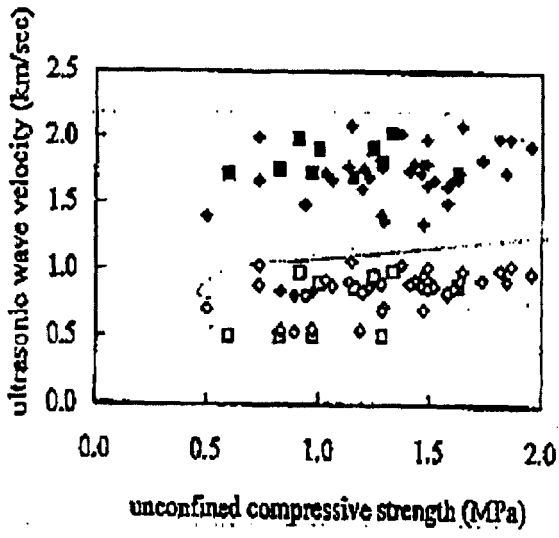

(ii) Chippubetsu

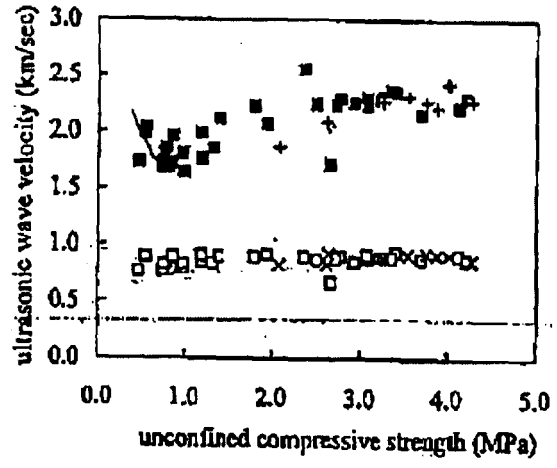

(iii) Hakodate

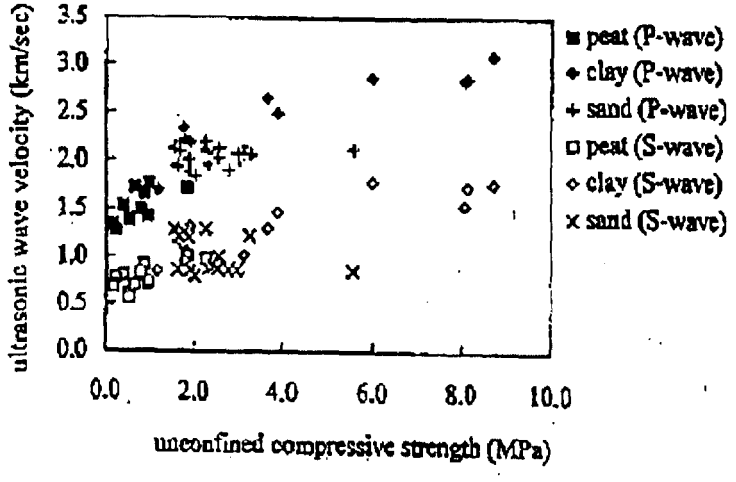

Figure 2.9: Ultrasonic wave velocities - unconfined compressive strength (Nishikawa et al. 1996).

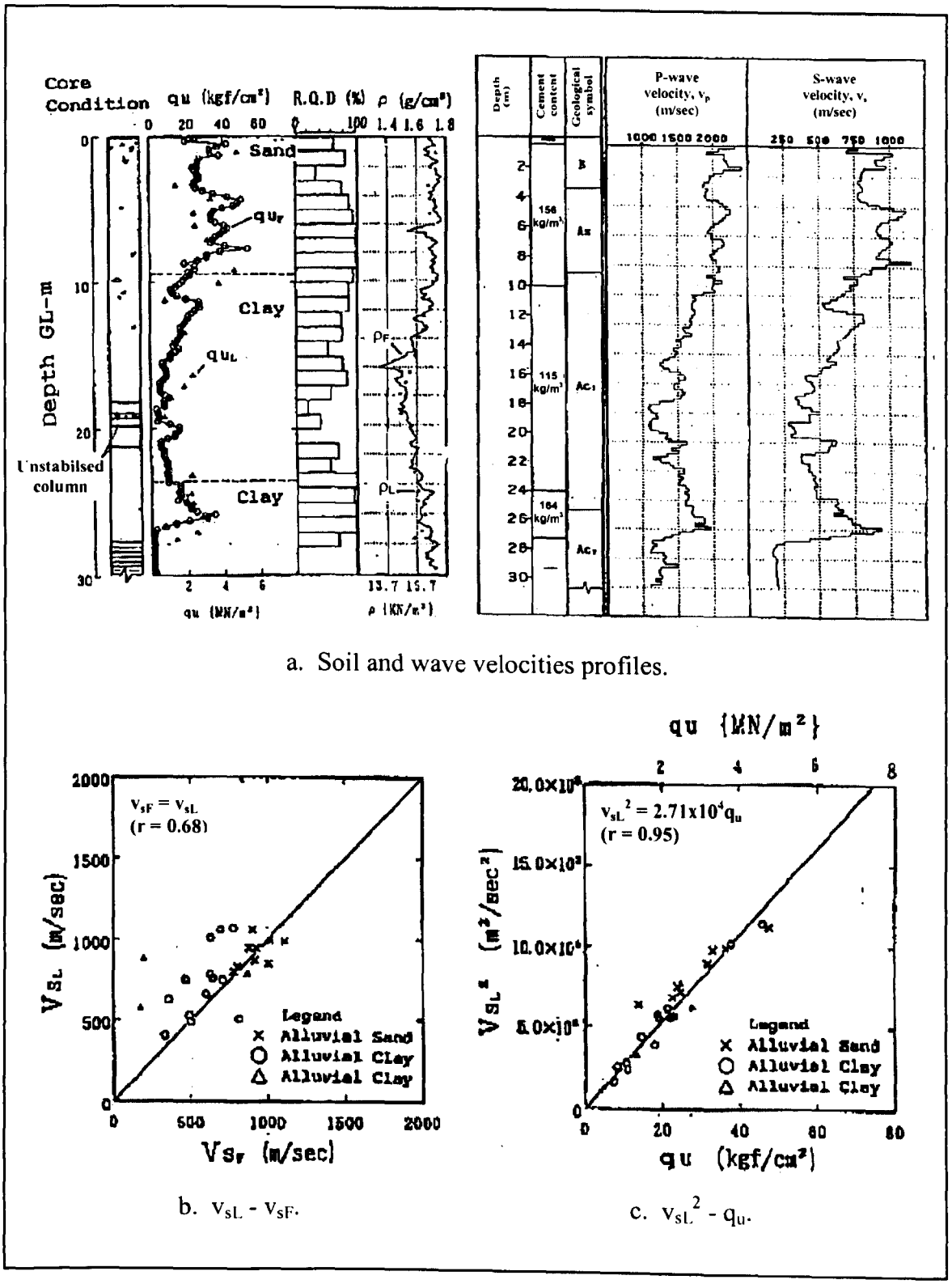

a. Soil and wave velocities profiles.

b. V_{sL} - V_{sF}.

c. V_{sL}^2 - q_u.

Figure 2.10: Suspension type P-S logging test results by Hiraide et al. 1996.

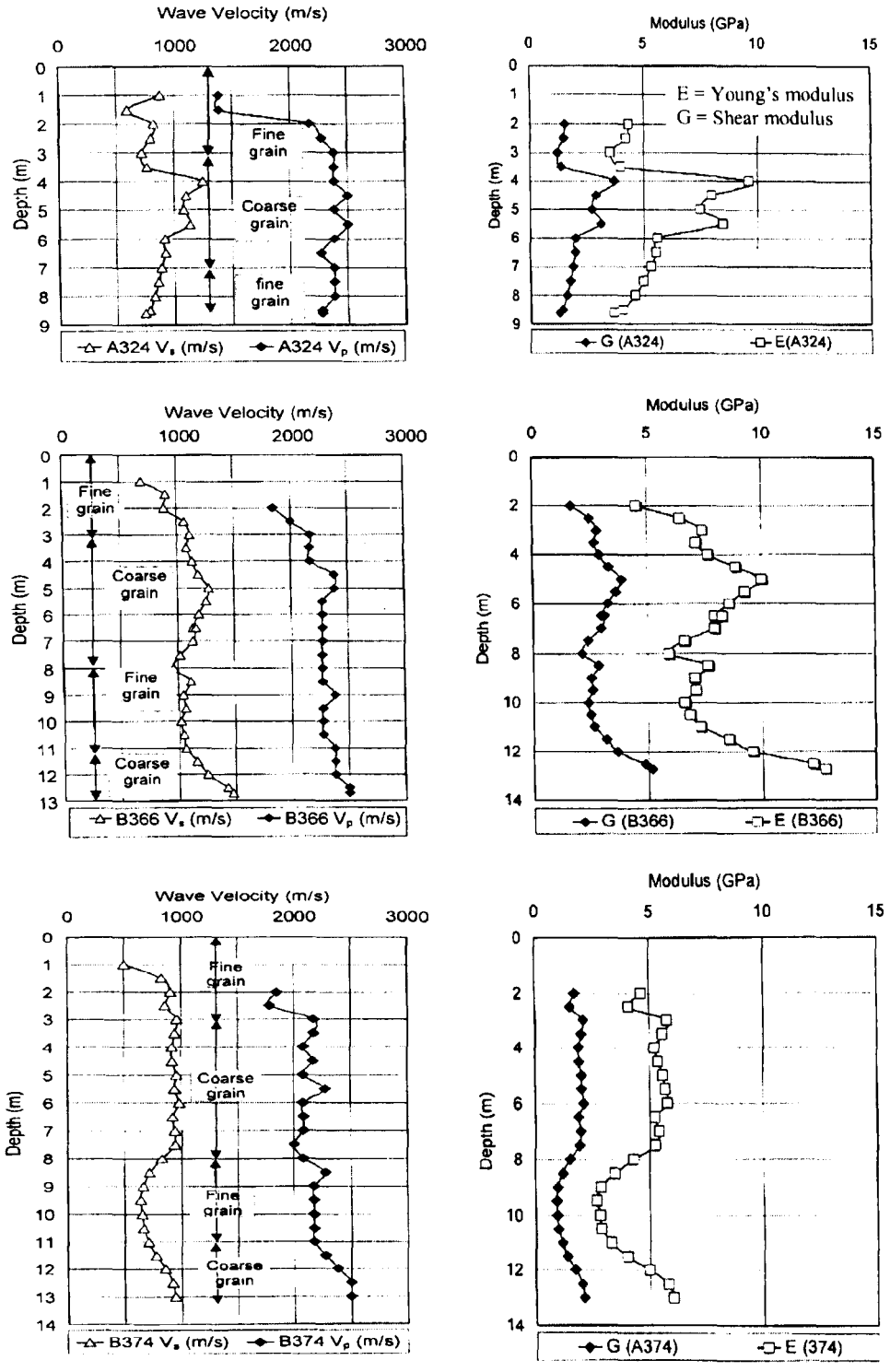

a. Profiles of wave velocities and stiffness modulus in three columns.

Figure 2.11: Suspension type P-S logging test results by Porbaha et al. 2005.

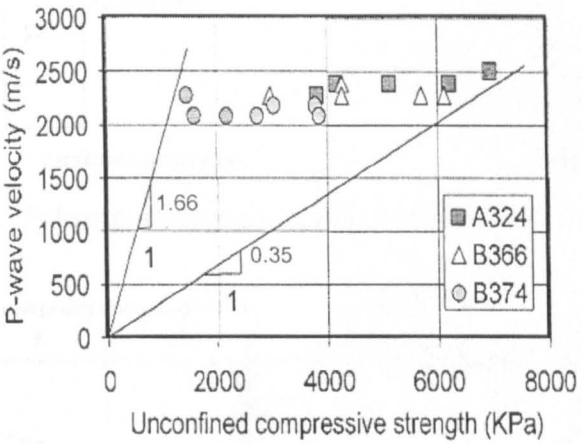

$(v_p - q_u)$

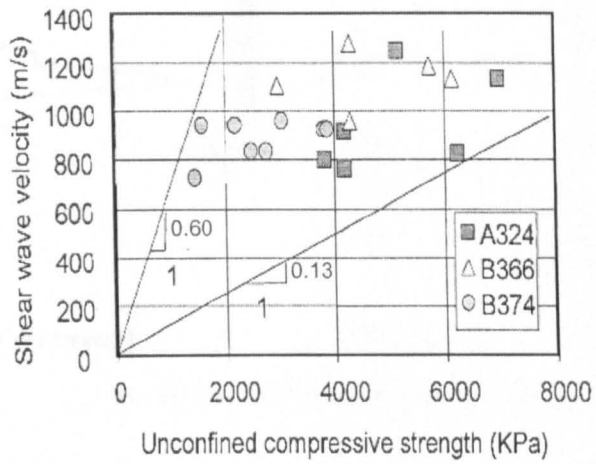

$(v_s - q_u)$

b. Wave velocities – unconfined compressive strength.

Figure 2.11: Suspension type P-S logging test results by Porbaha et al. 2005. *(continued)*

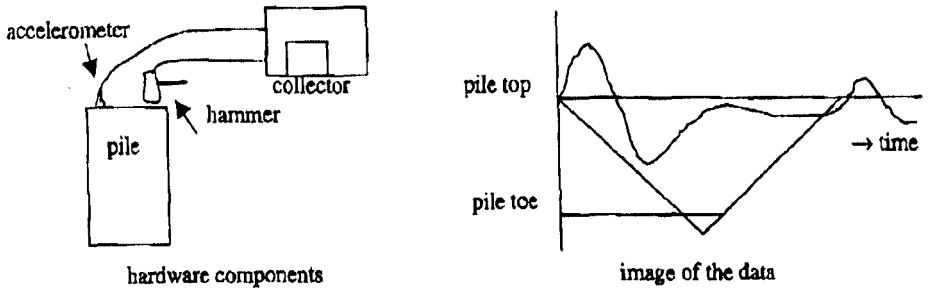

a. Schematic diagram of pile integrity tester and data image.

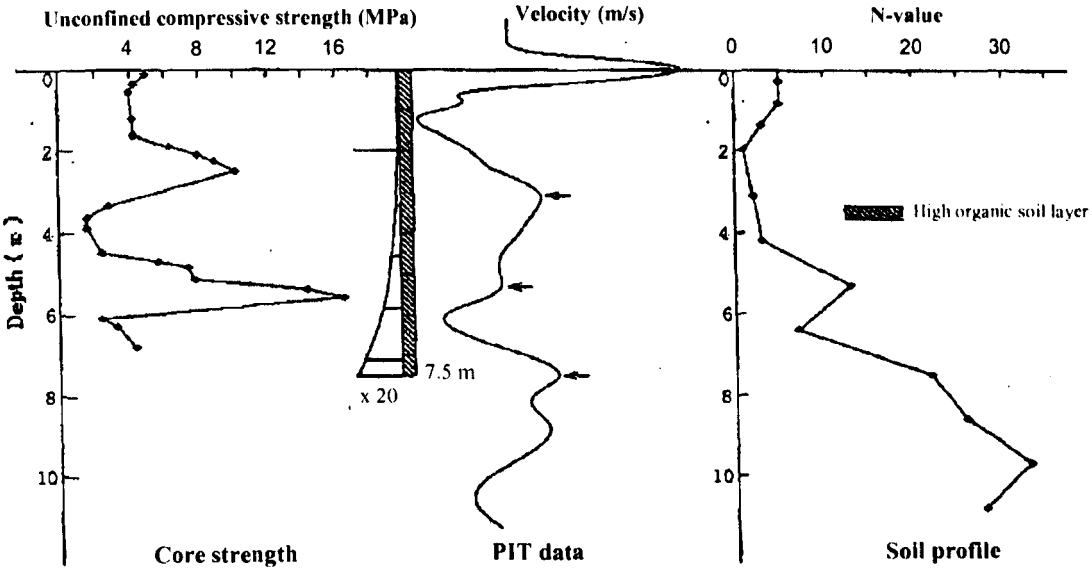

b. Profiles of strength and wave velocity.

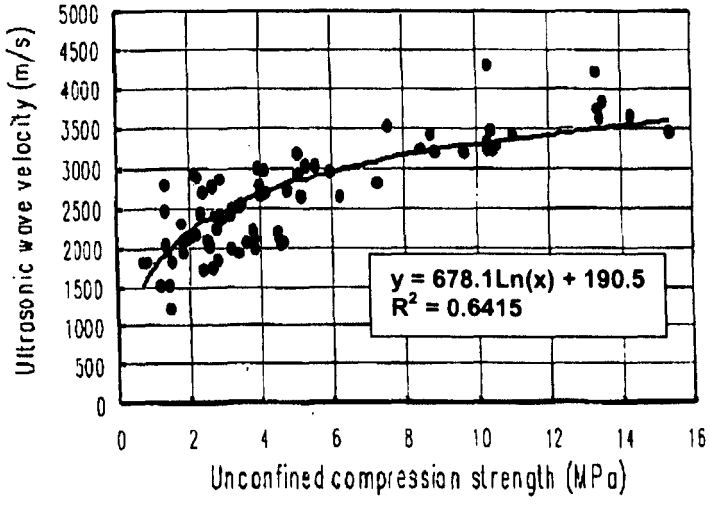

c. Ultrasonic wave velocity – unconfined compressive strength.

Figure 2.12: Pile integrity test (PIT) set-up and results (Goto et al. 2000).

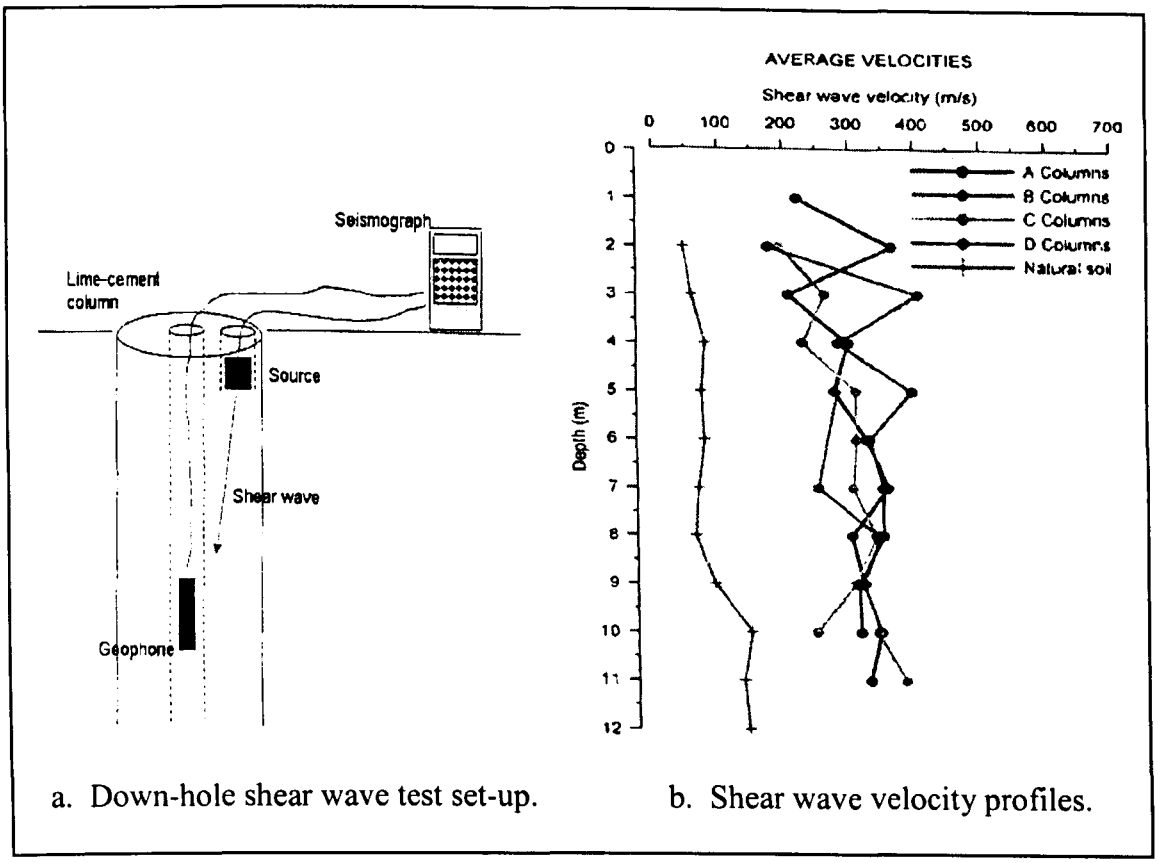

a. Down-hole shear wave test set-up. b. Shear wave velocity profiles.

Figure 2.13: Down-hole shear wave test set-up and results (Mattsson et al. 2005).

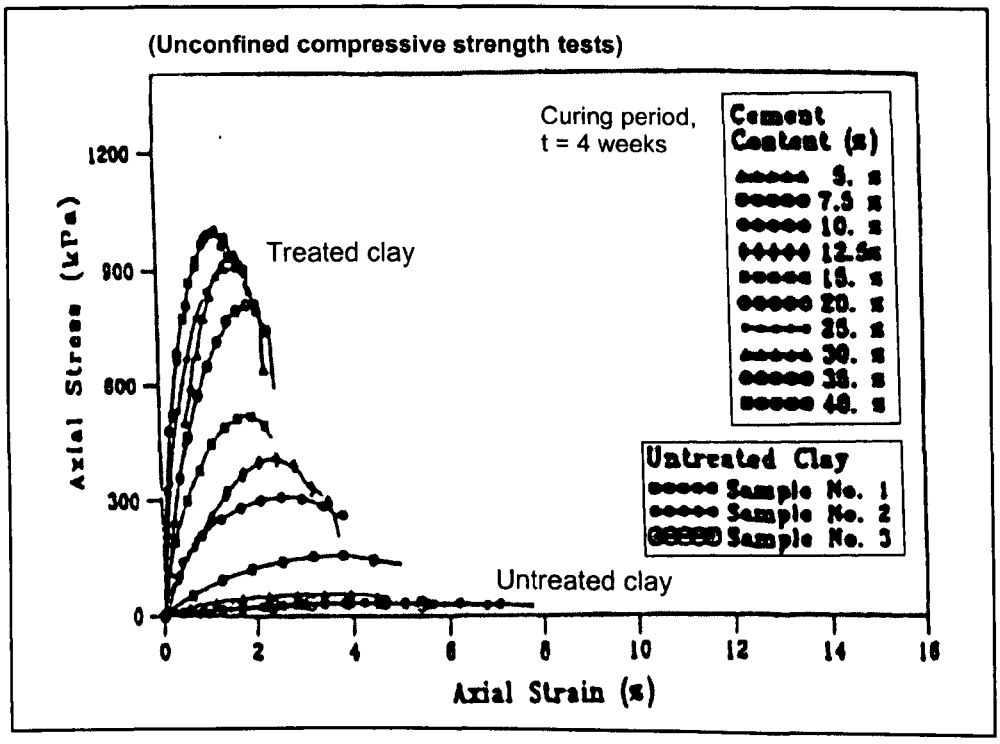

Figure 2.14: Typical stress-strain curves of untreated and cement-treated Bangkok clay (Uddin et al. 1997).

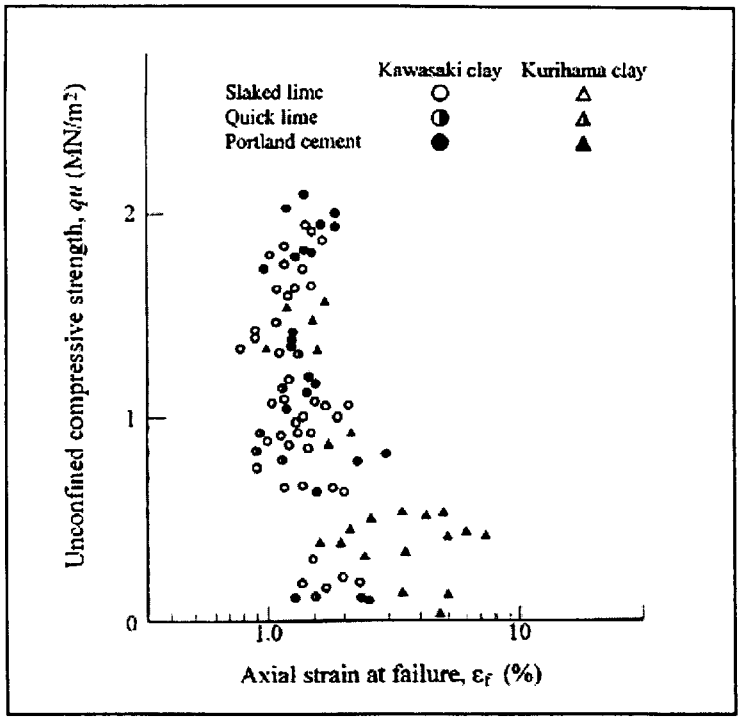

Figure 2.15: q_u - ε_f plot of stabilised clays (Terashi et al. 1980, after Kitazume 2005).

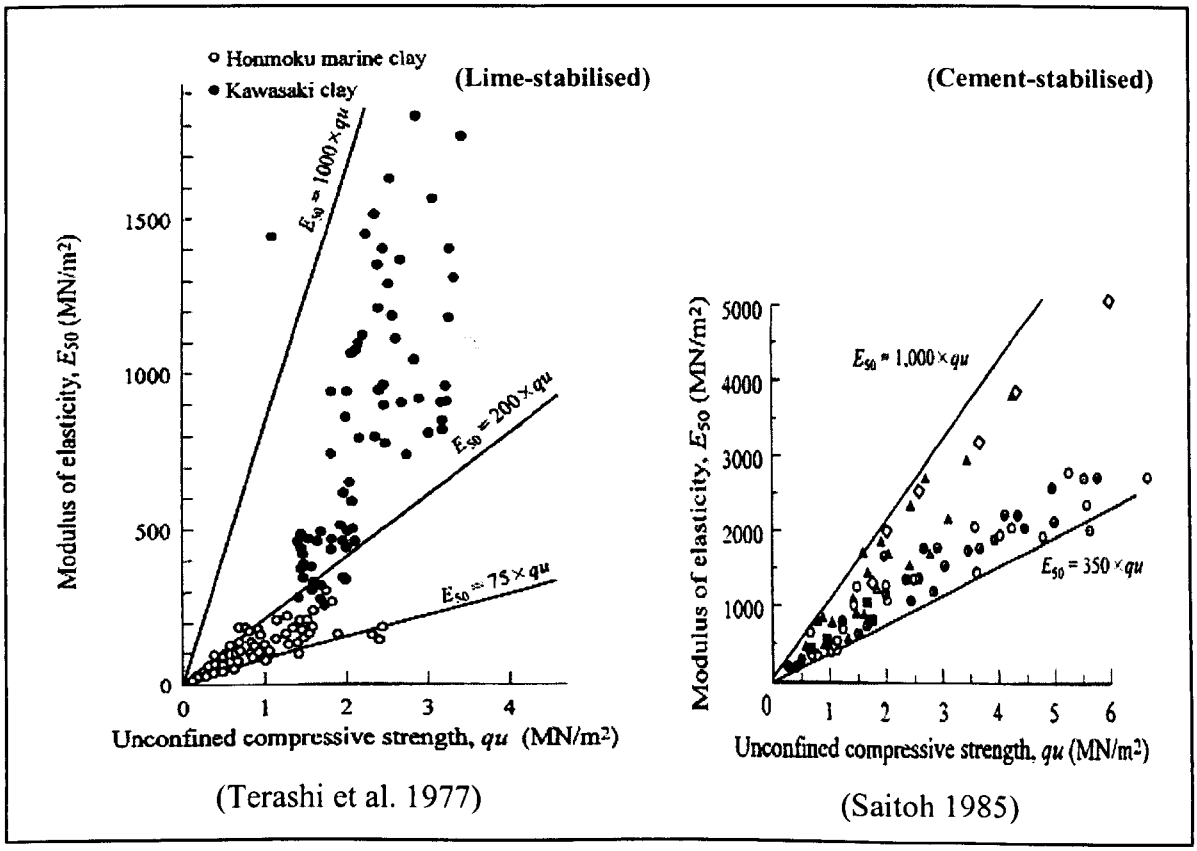

Figure 2.16: E_{50} - q_u plots of stabilised clays (after Kitazume 2005).

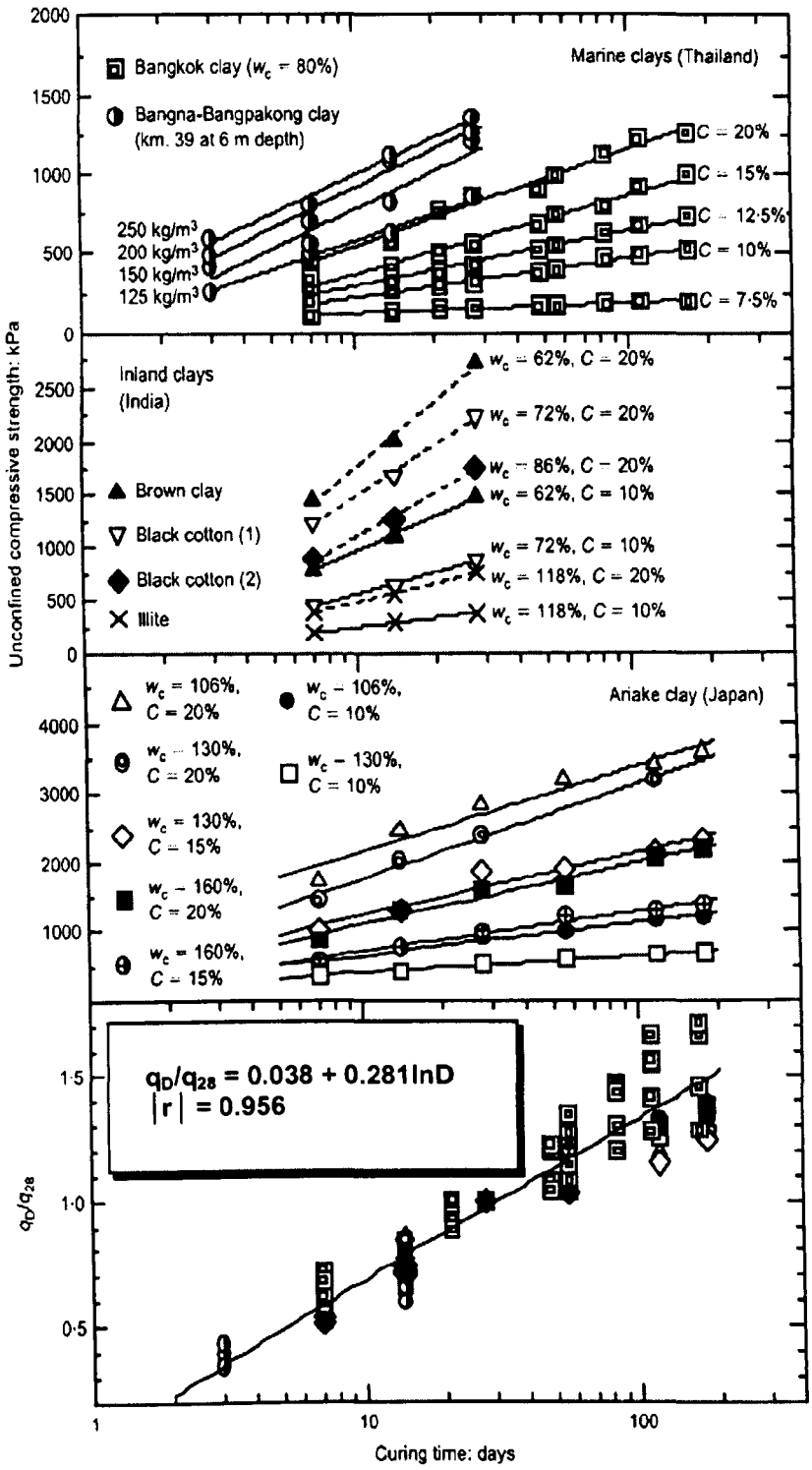

w_c = clay water content (LI = 1.0 – 2.5)
C = cement content
q_D = unconfined compressive strength after D curing period
q_{28} = 28 day unconfined compressive strength
D = curing period in days

Figure 2.17: Strength development and normalisation plots (Horpibulsuk et al. 2003).

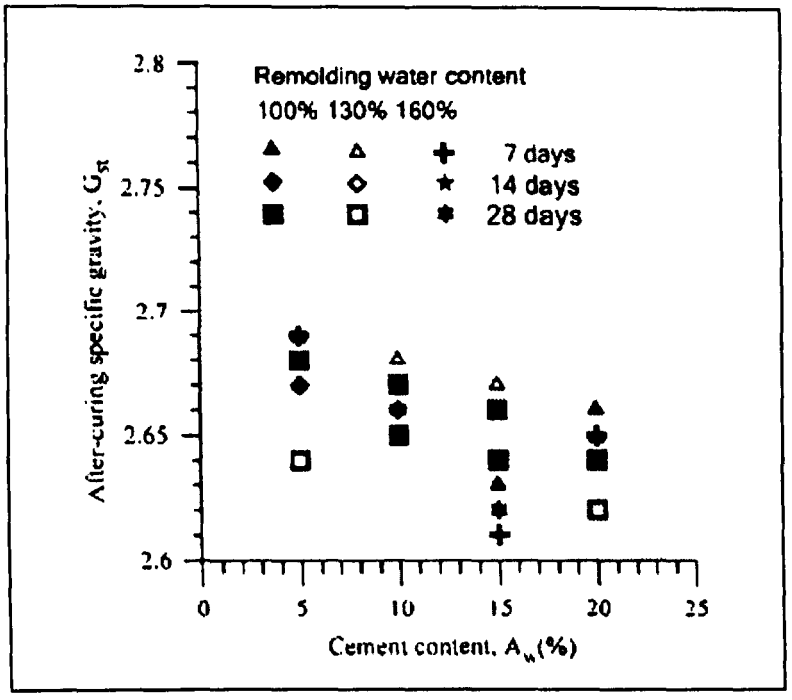

Figure 2.18: Specific gravity of cement-stabilised Bangkok clay (Lorenzo and Bergado 2004).

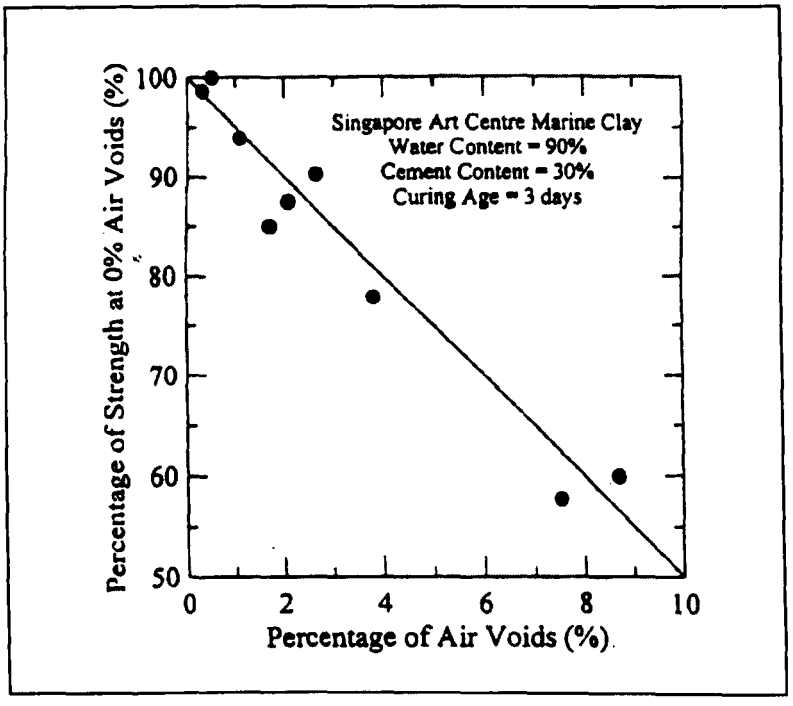

Figure 2.19: Effect of air voids in cement-stabilised Singapore marine clay (Tan et al. 2002).

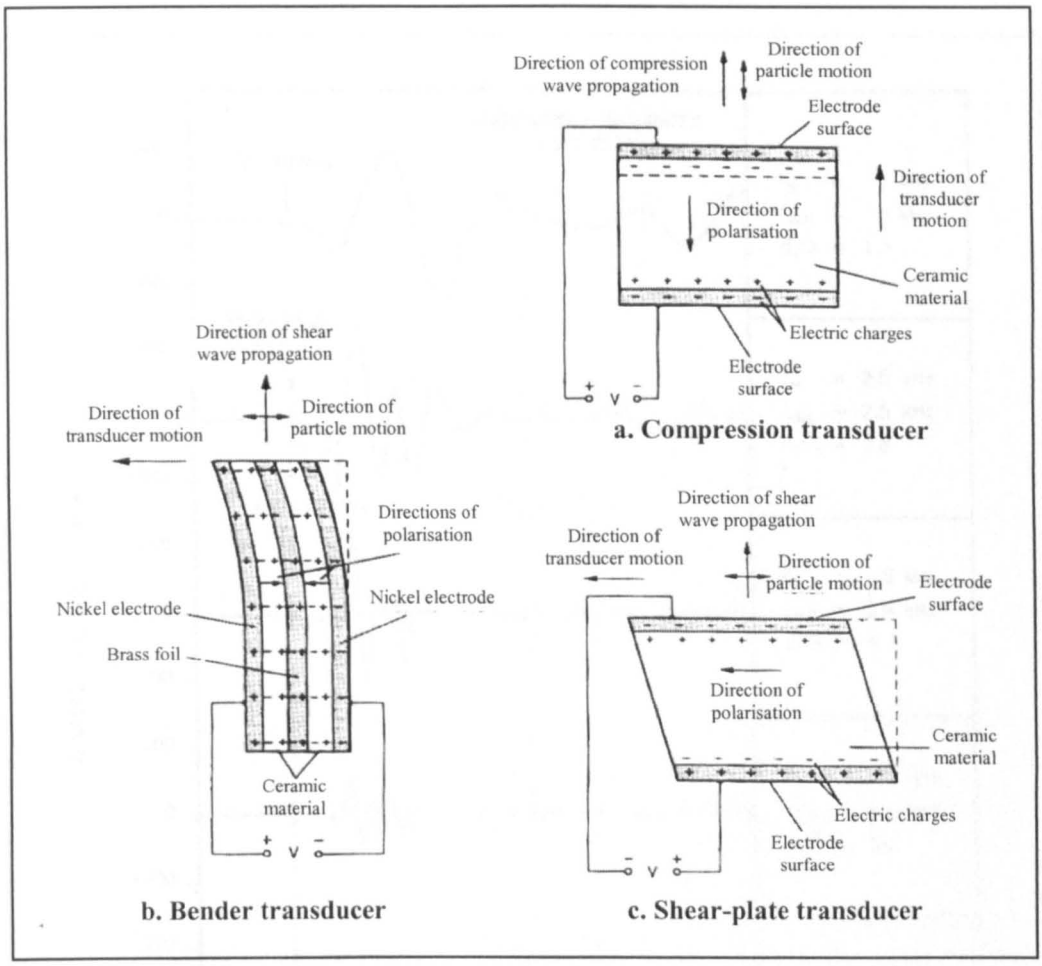

Figure 2.20: Various transducers from piezoceramic strips (Strassburger 1982).

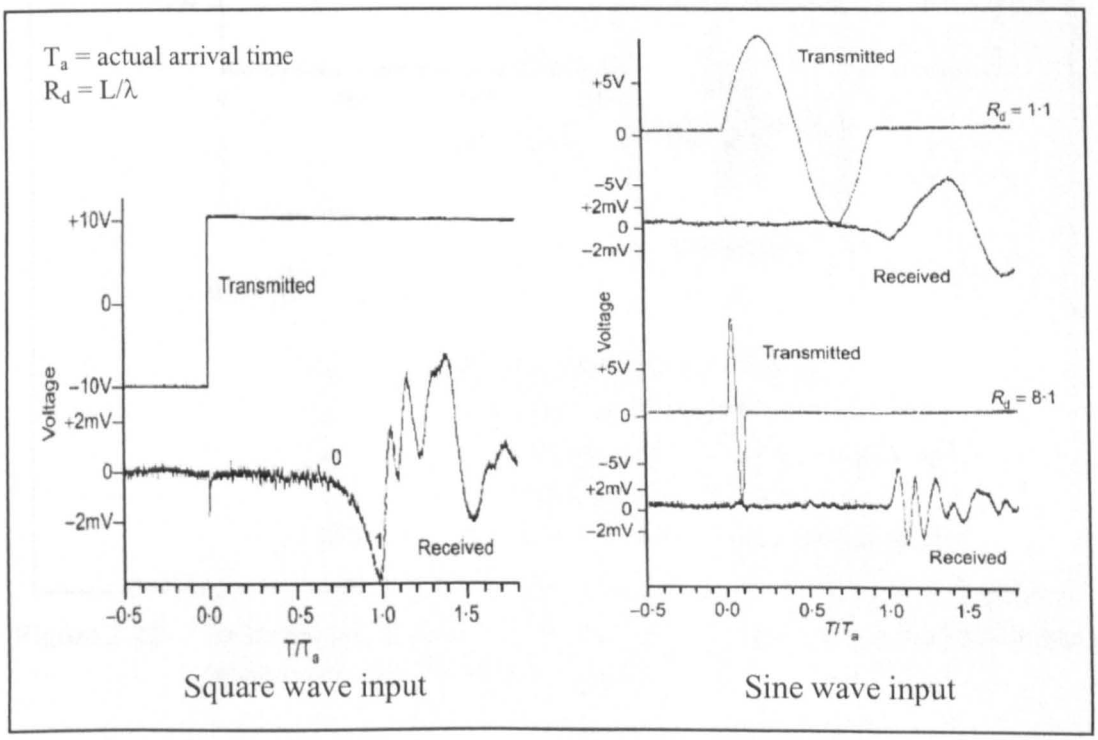

Figure 2.21: Shear waves traces for kaolin samples (Jovičić et al. 1996).

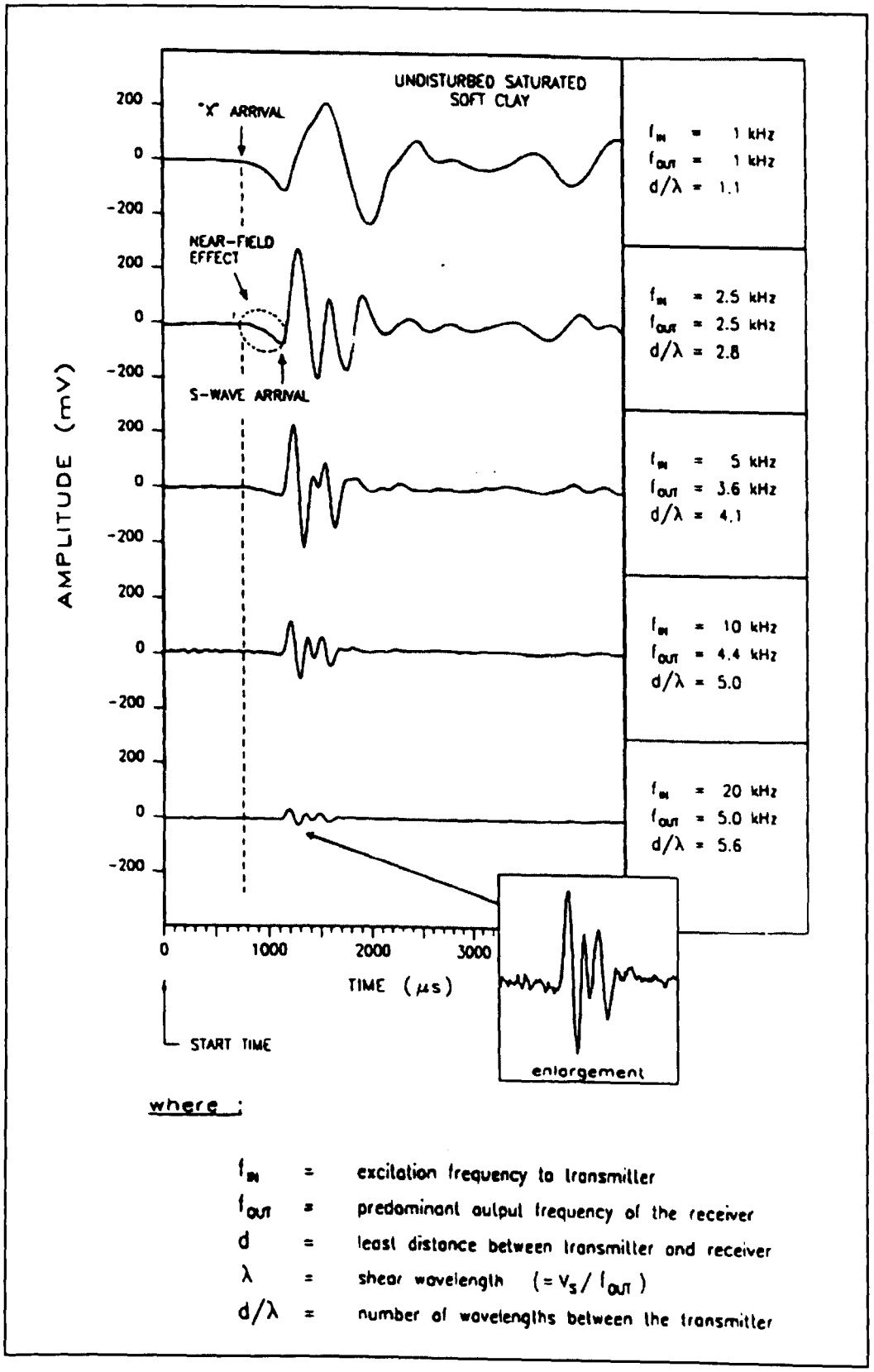

Figure 2.22: Influence of near-field effect on the waveform preceding the initial shear wave arrival (Brignoli et al. 1996).

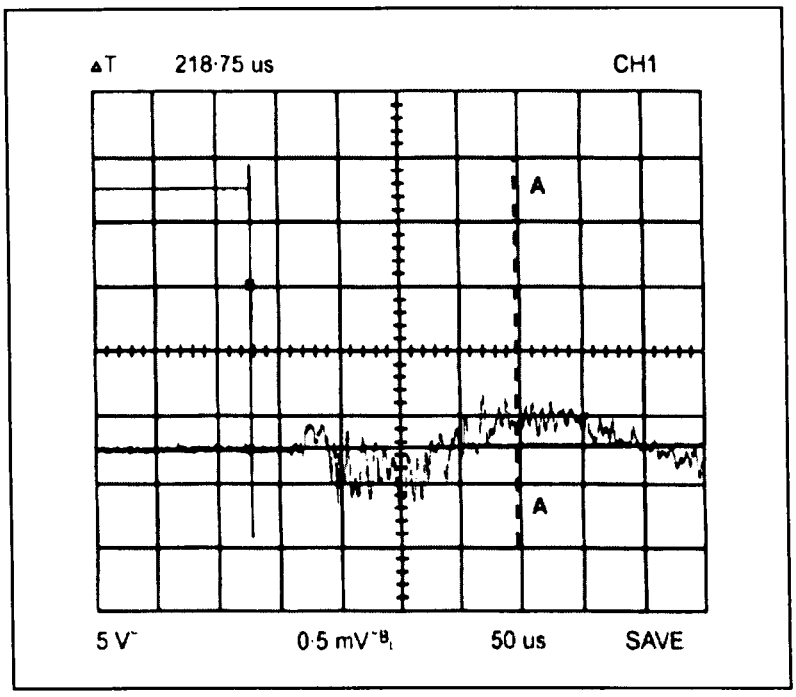

Figure 2.23: Trace showing 'overshooting' of the transmitter BE for a square wave input in a soft rock (Jovičić et al. 1996).

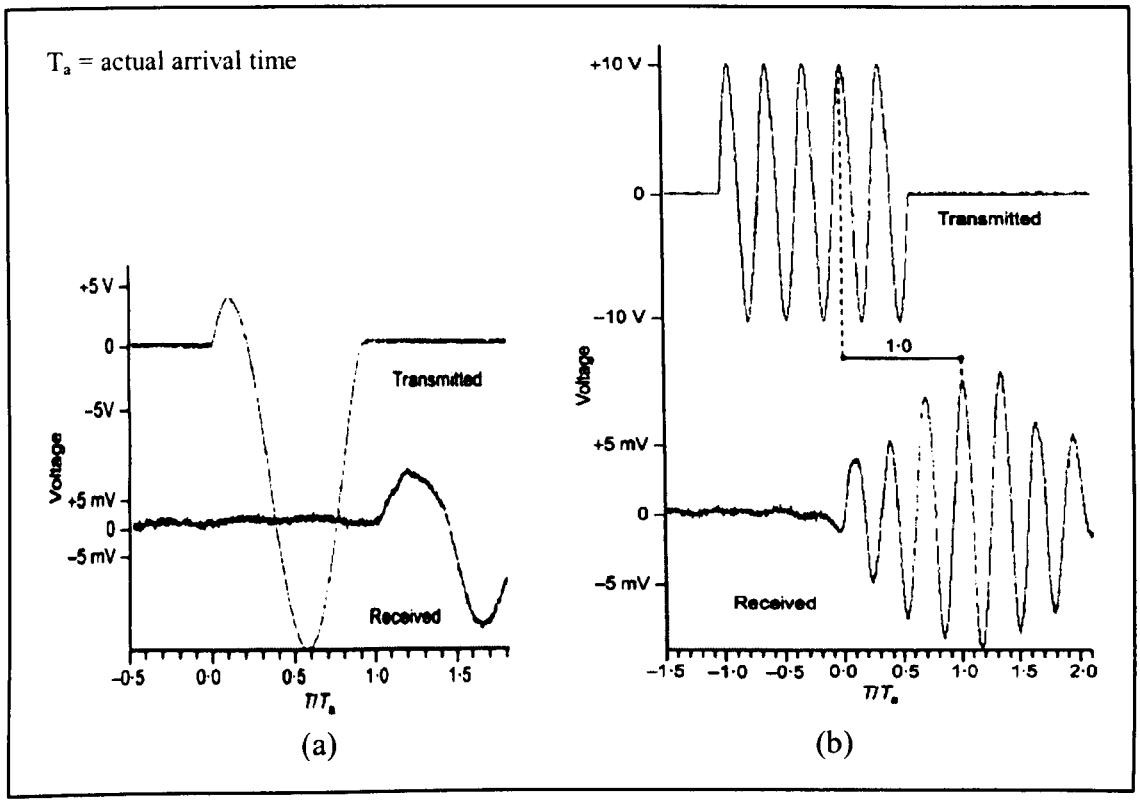

Figure 2.24: Techniques proposed to overcome the problem of 'overshooting' (Jovičić et al. 1996).

a. Distortion of input wave.
b. Resonance of received signal.

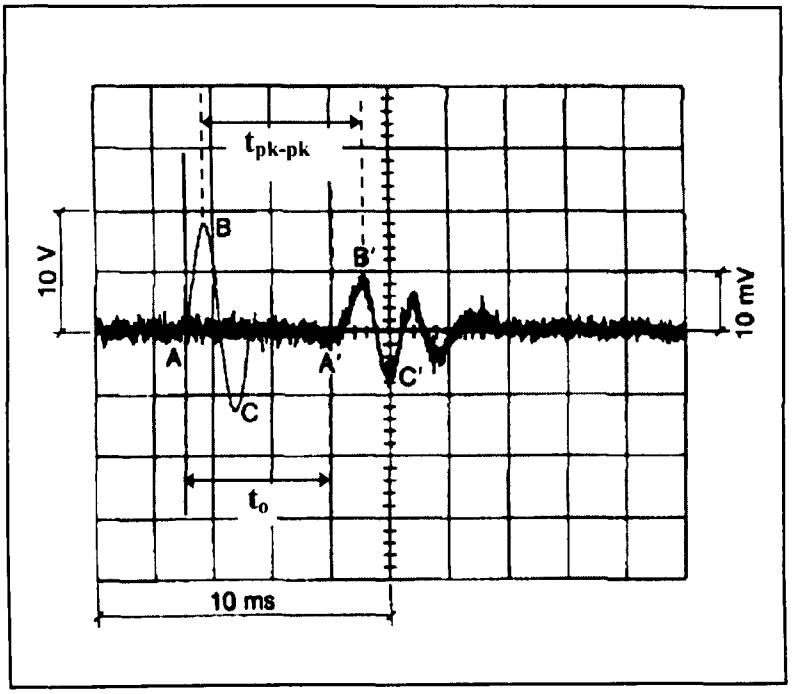

Figure 2.25: Visually picked and first major peak-to-peak shear wave arrival time (Viggiani and Atkinson 1995).

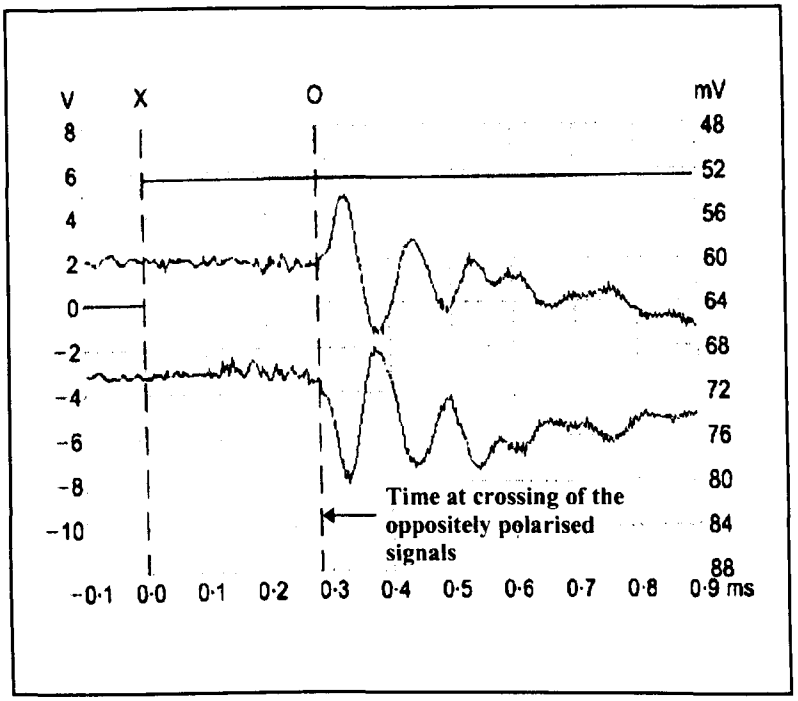

Figure 2.26: Shear wave arrival time from the crossing of two oppositely polarised received signals (Teachavorasinskun and Amornwithayalax 2002).

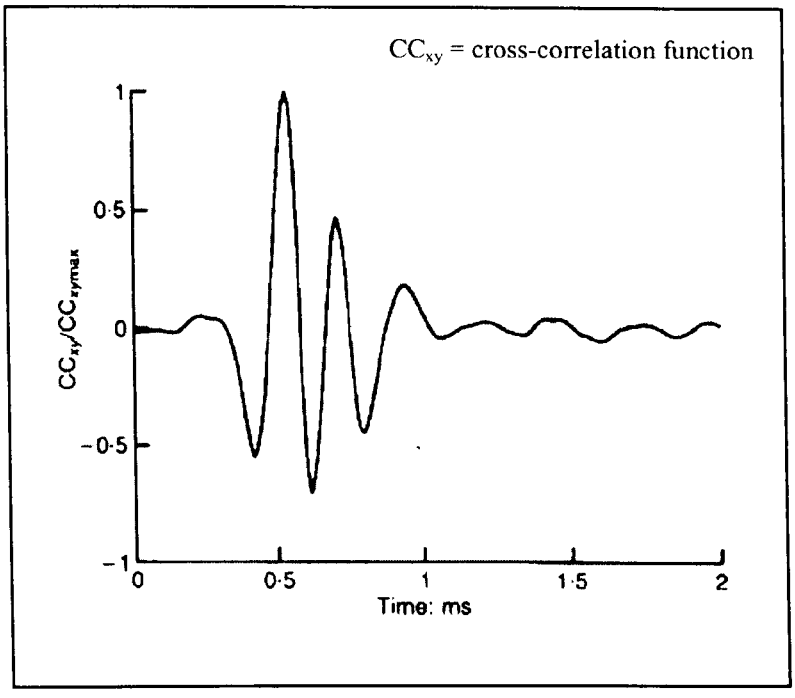

Figure 2.27: Cross-correlation function for the signals in Figure 2.25 (Viggiani and Atkinson 1995).

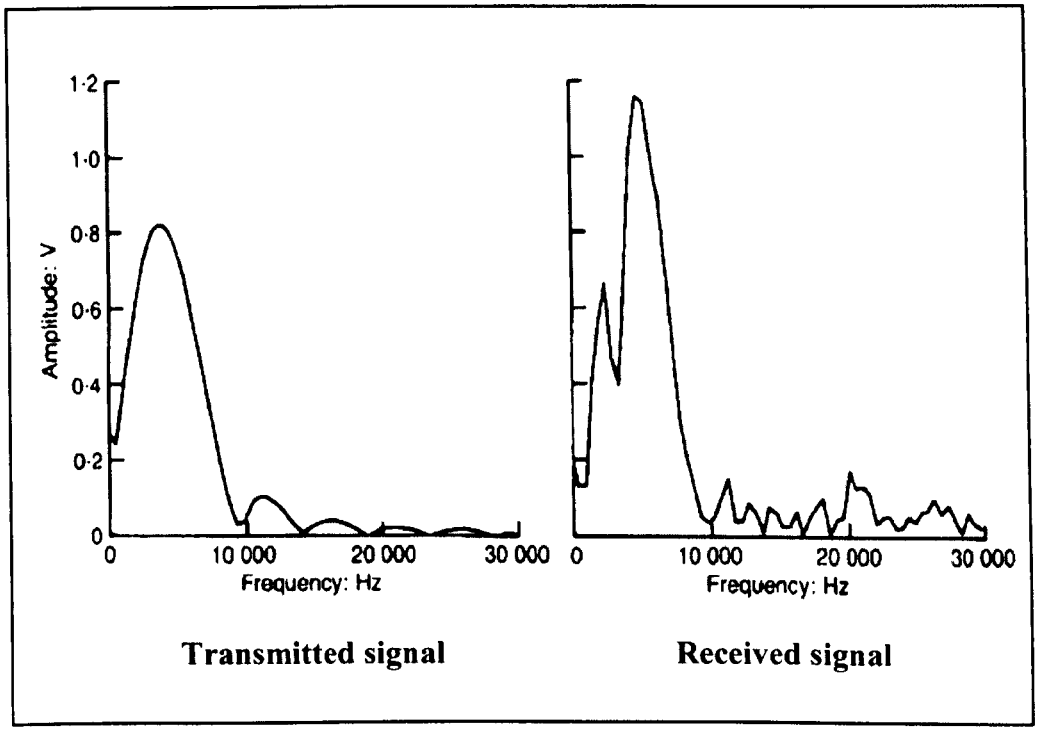

Figure 2.28: Linear spectra for the transmitted and received signals in Figure 2.25 (Viggiani and Atkinson 1995).

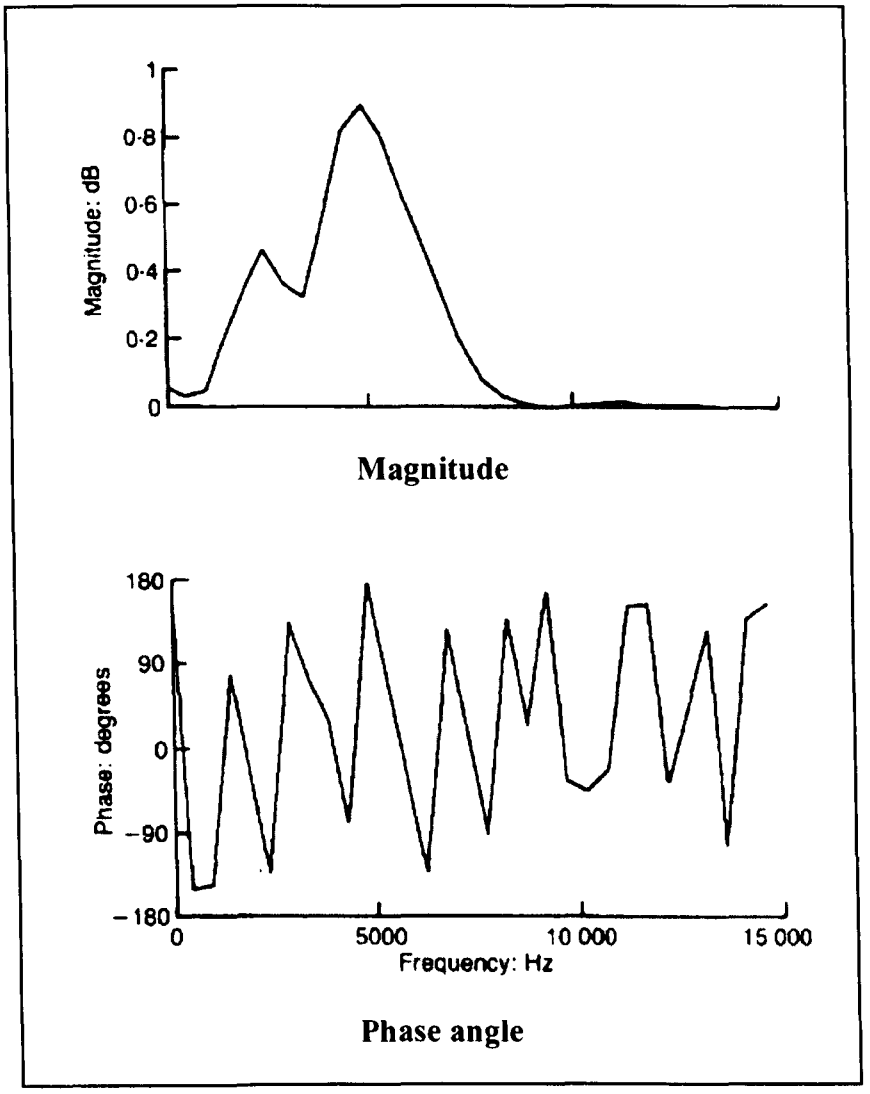

Figure 2.29: Cross-power spectra for the time records in Figure 2.25 (Viggiani and Atkinson 1995).

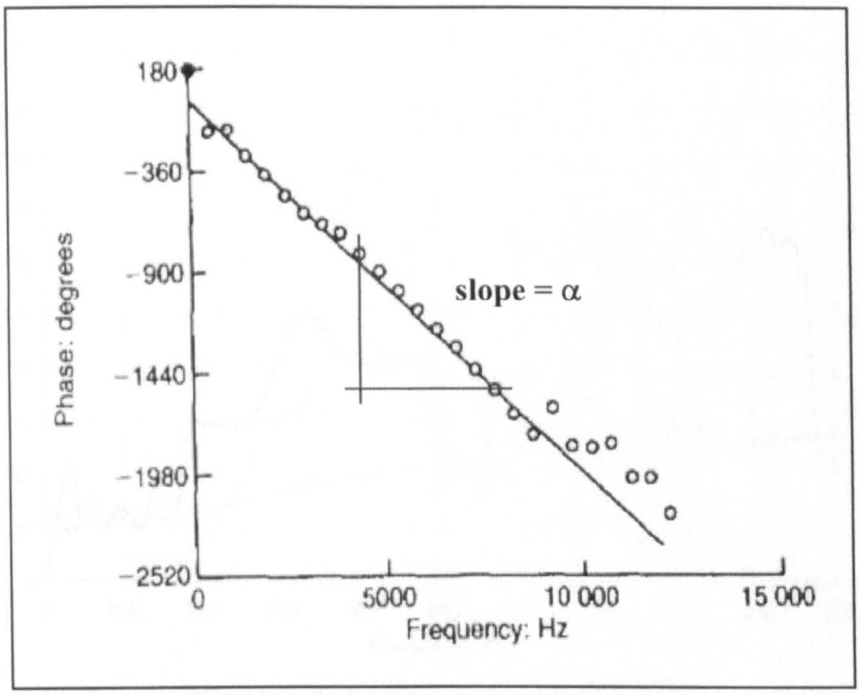

Figure 2.30: Absolute cross-power spectrum phase diagram (Viggiani and Atkinson 1995).

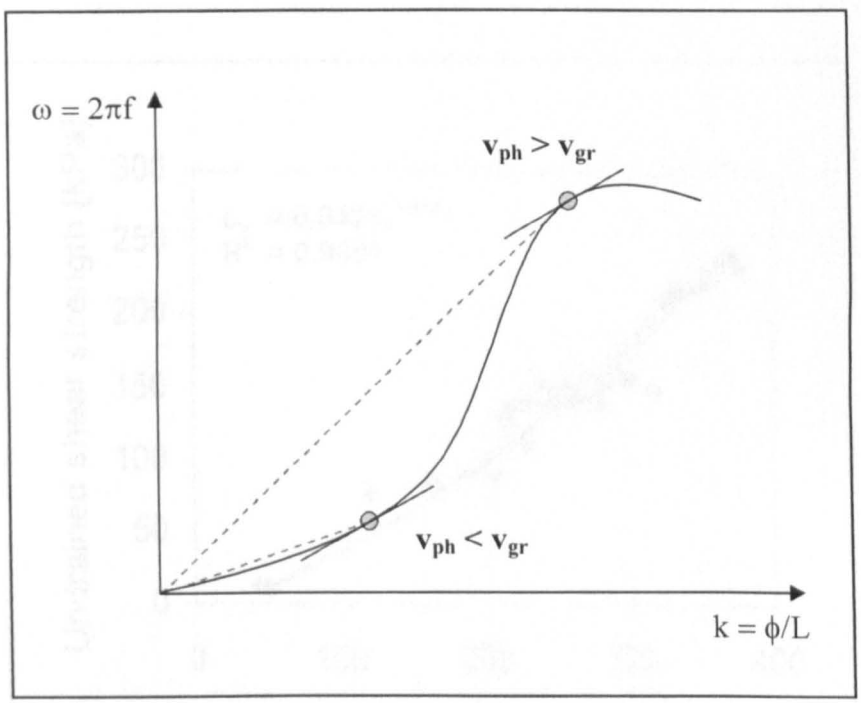

Figure 2.31: Definition of phase and group velocities (Brillouin 1960).

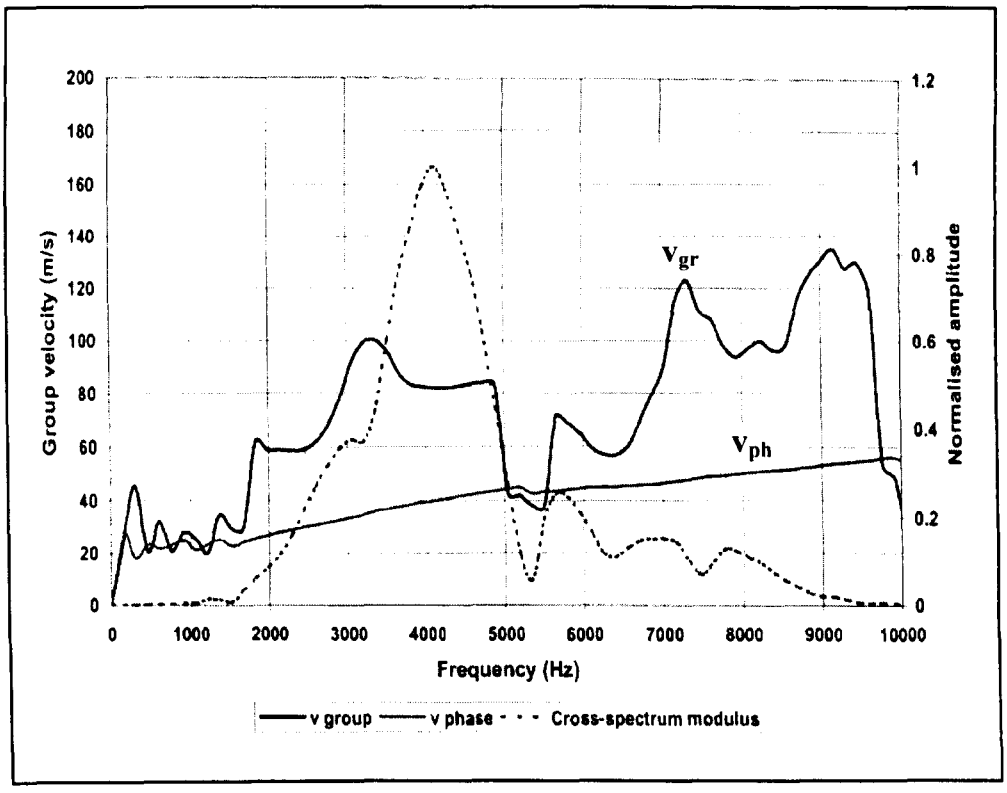

Figure 2.32: Phase and group velocities from BE test in Gault clay (Arroyo 2001).

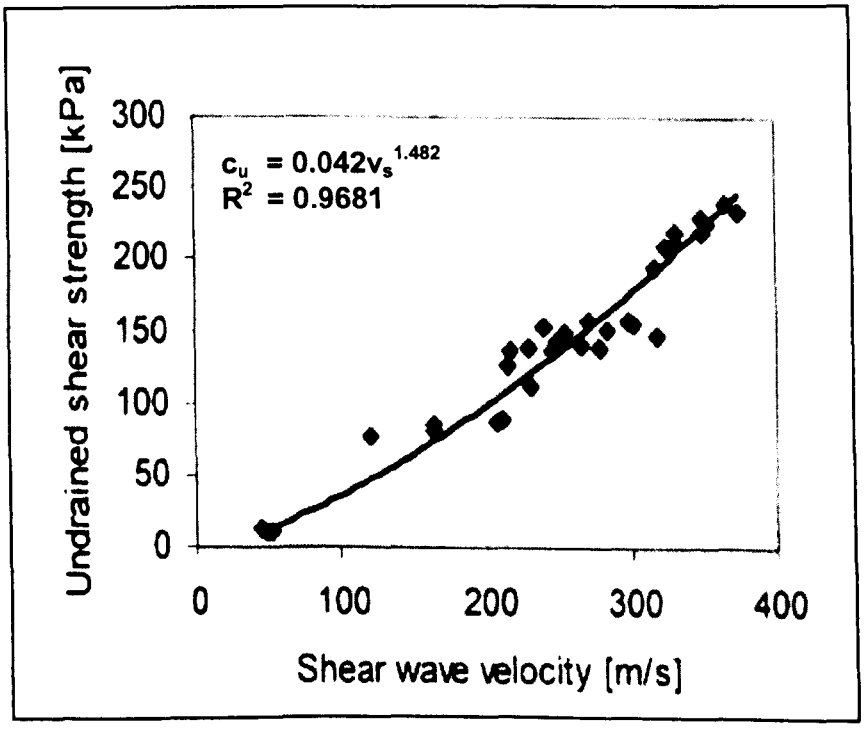

Figure 2.33: Correlation between undrained shear strength – shear wave velocity for stabilised Swedish clay (Mattsson et al. 2005).

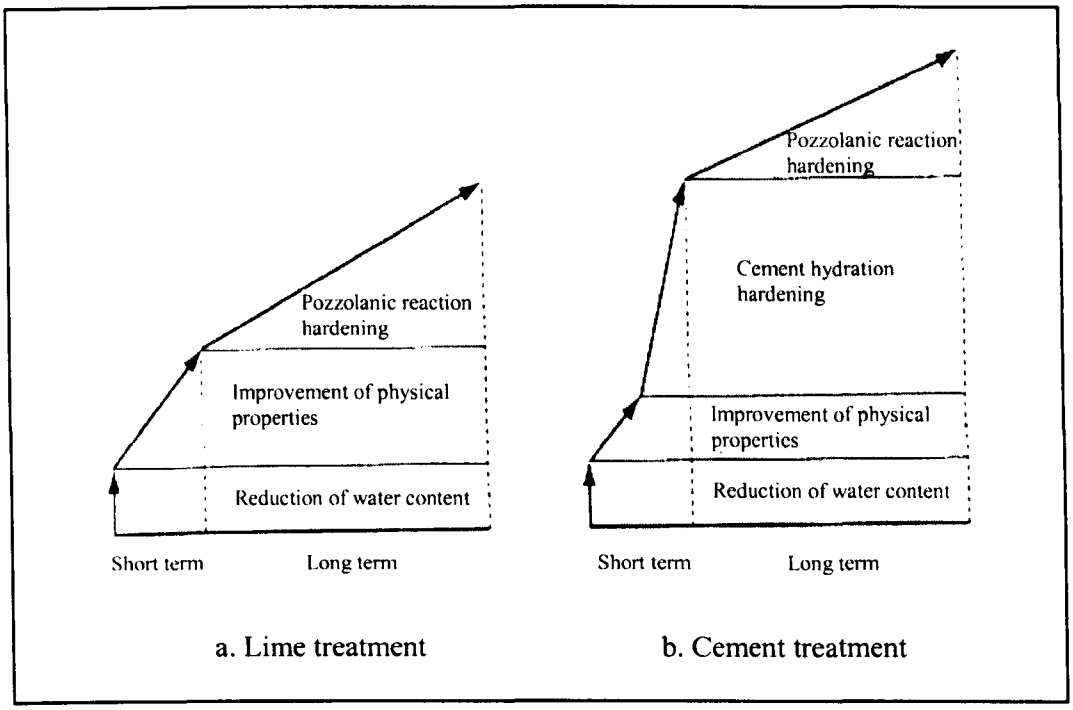

Figure 2.34: Simplified improvement process of lime and cement stabilisations (Kitazume 2005).

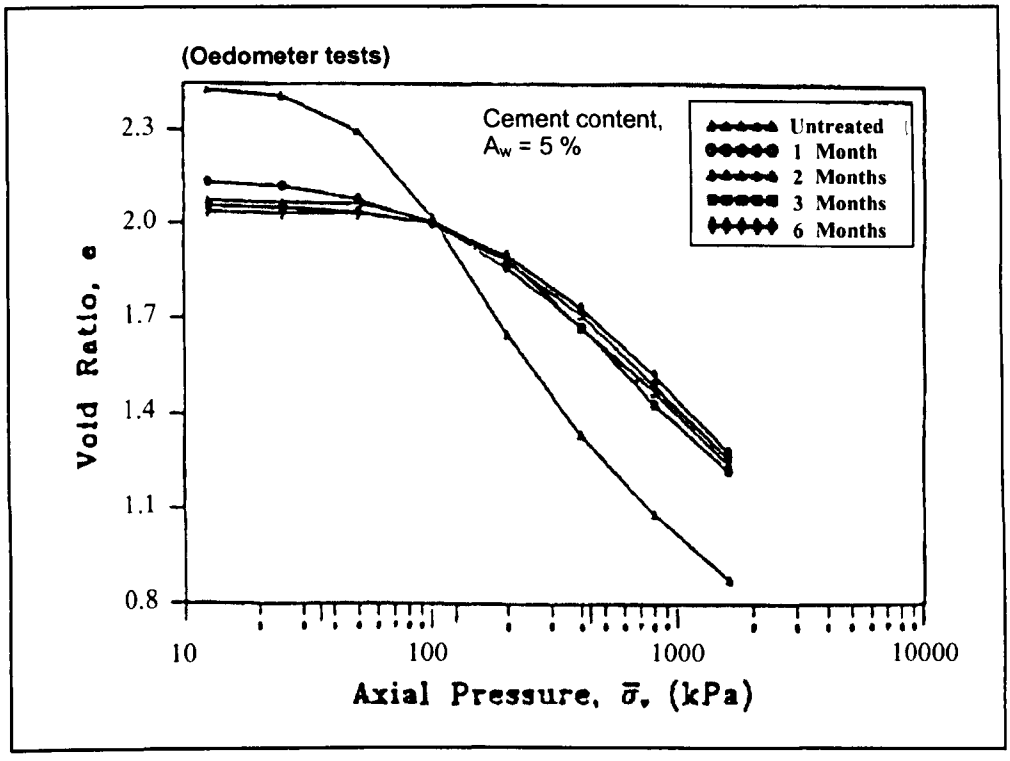

Figure 2.35: Effect of curing period on cement-stabilised Bangkok soft clay (Uddin et al. 1997).

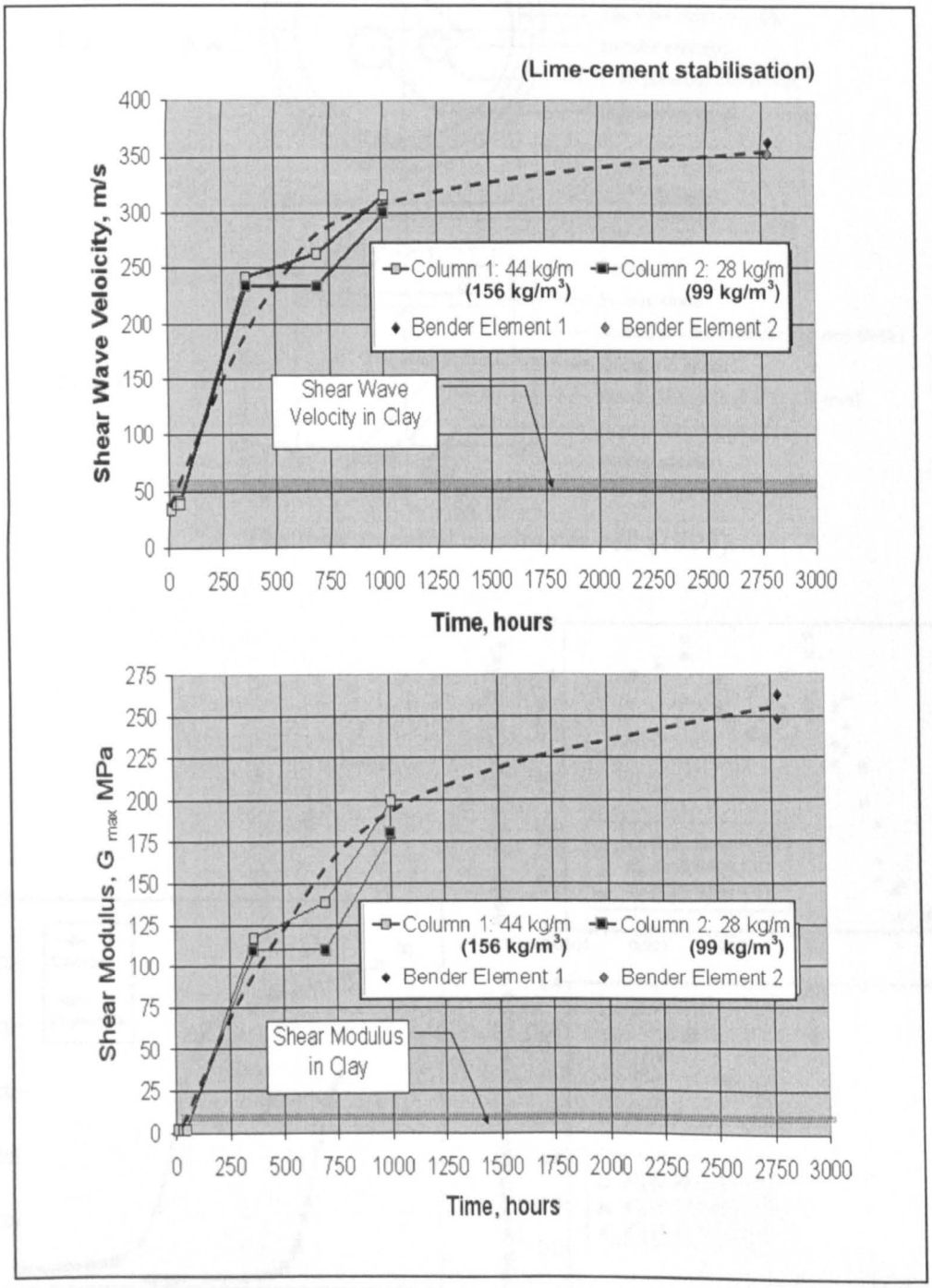

Figure 2.36: Variation of shear wave velocity and maximum shear modulus with time (Massarsch 2005).

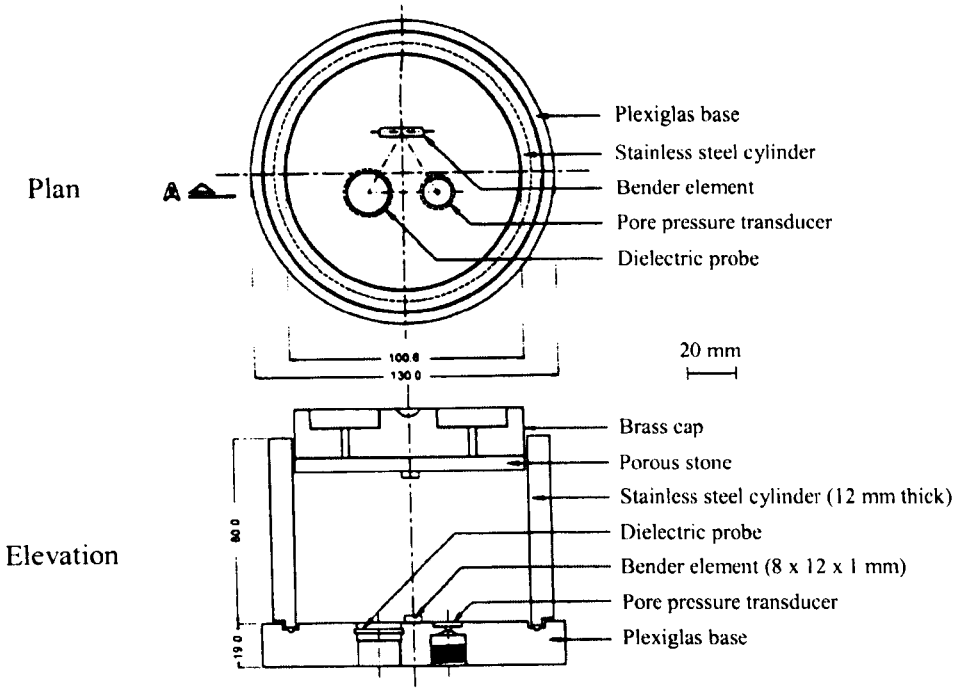

a. The instrumented oeodmeter cell (1995).

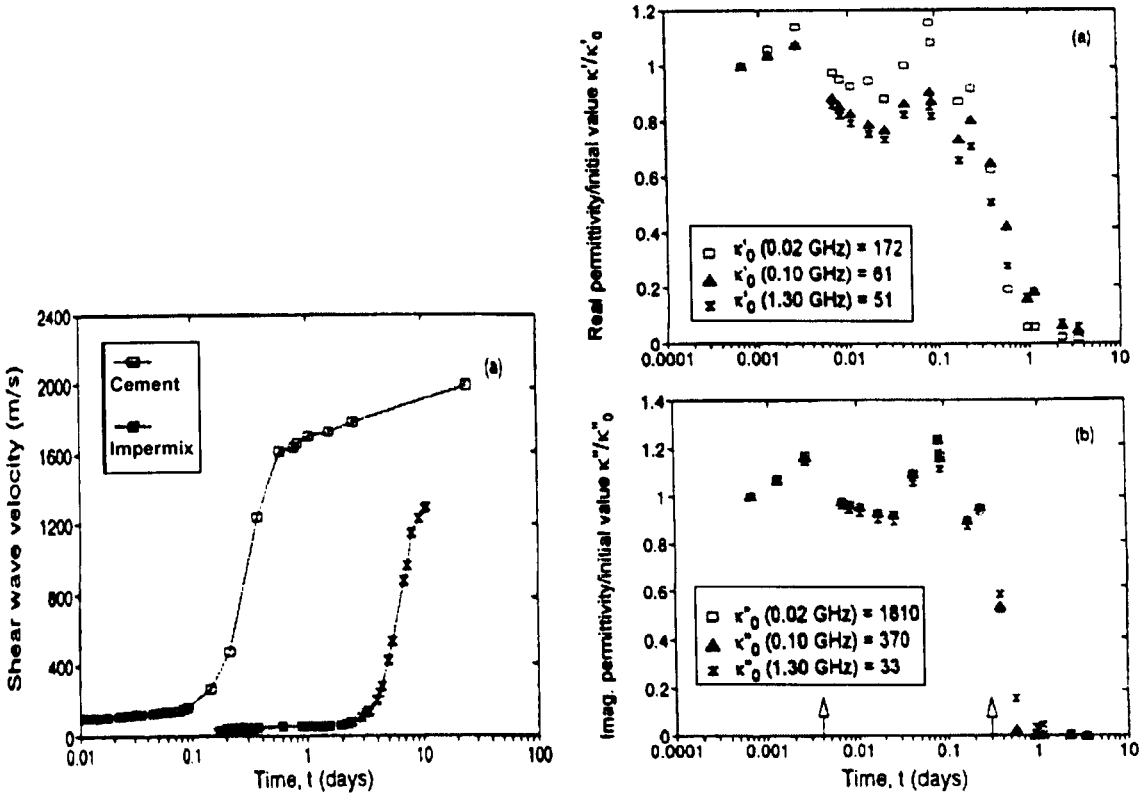

b. Variation of shear wave velocity and permittivity with time for cement (water/cement ratio, w/c = 0.4) (1996).

Figure 2.37: Shear wave velocity measurement in an instrumented oedoemeter (Fam and Santamarina 1995, 1996).

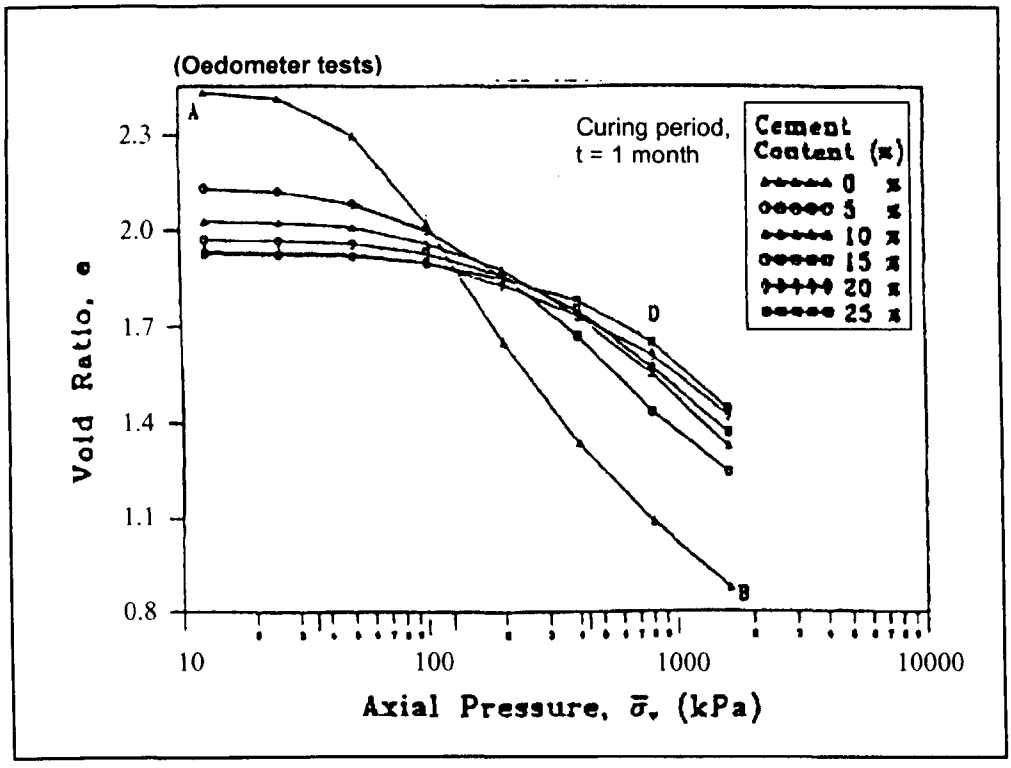

Figure 2.38: Effect of cement content on stabilised Bangkok soft clay (Uddin et al. 1997).

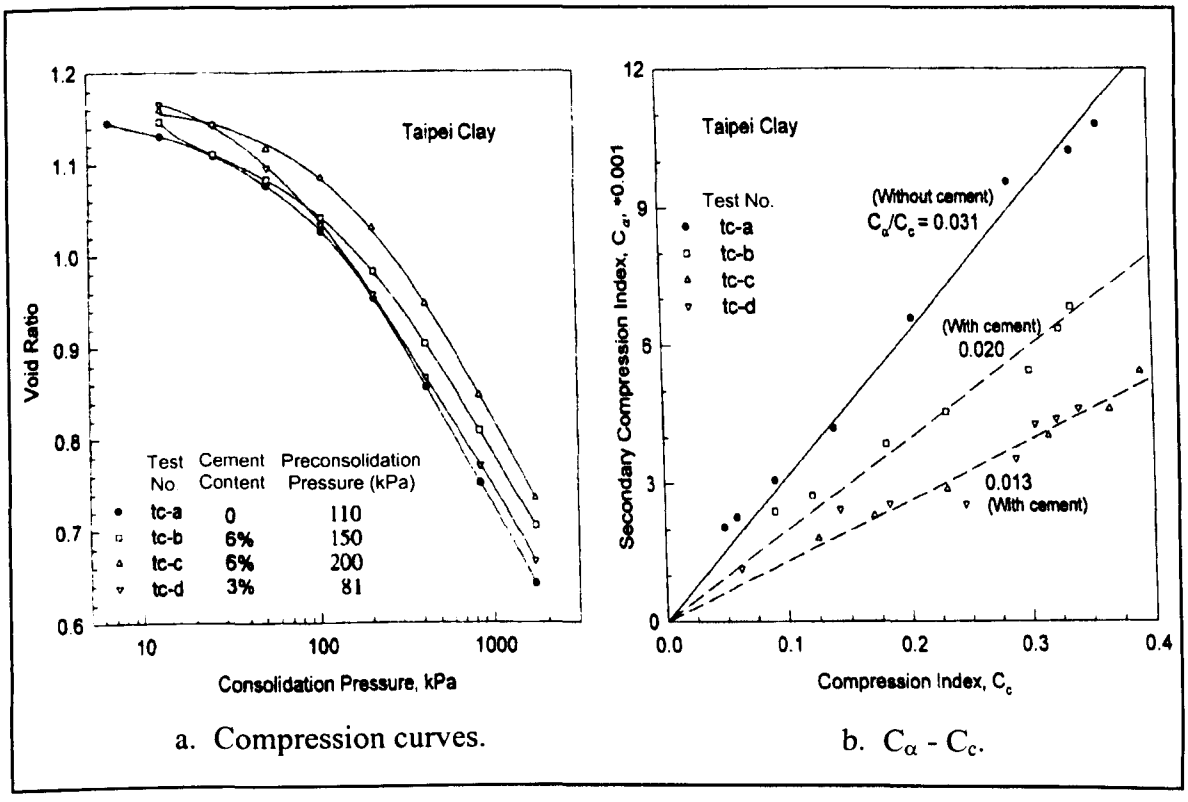

a. Compression curves. b. C_α - C_c.

Figure 2.39: One-dimensional compression test results for cement-stabilised Taipei lacustrine clay (Feng 2002).

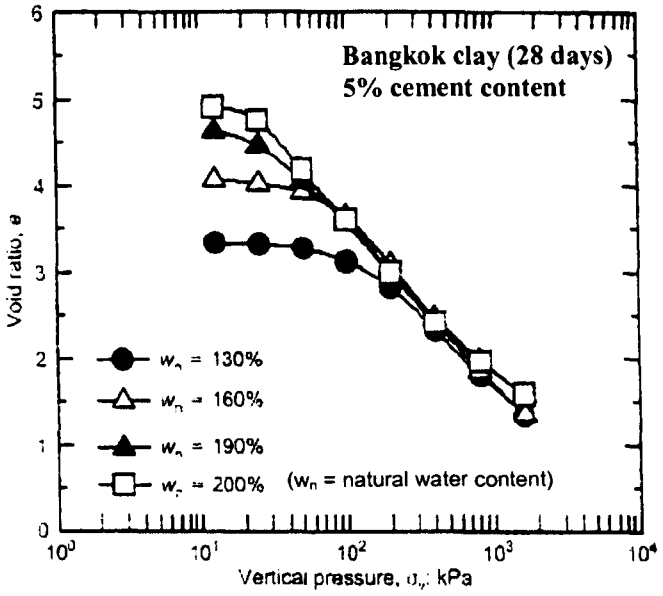

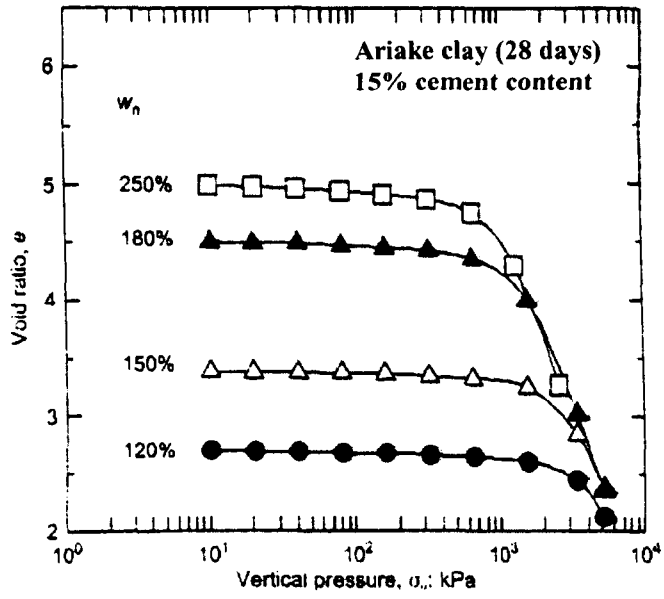

Properties	Bangkok clay	Ariake clay
Liquid limit: %	103	125
Plastic limit: %	43	60
Plasticity index	60	65
Natural water content	76–84	120–130
Grain size distribution: %		
Clay	69	55
Silt	28	44
Sand	3	1
Total unit weight: kN/m^3	14·3	14·1

Figure 2.40a: Compression curves of cement-stabilised clays at various water contents (Horpibulsuk et al. 2004).

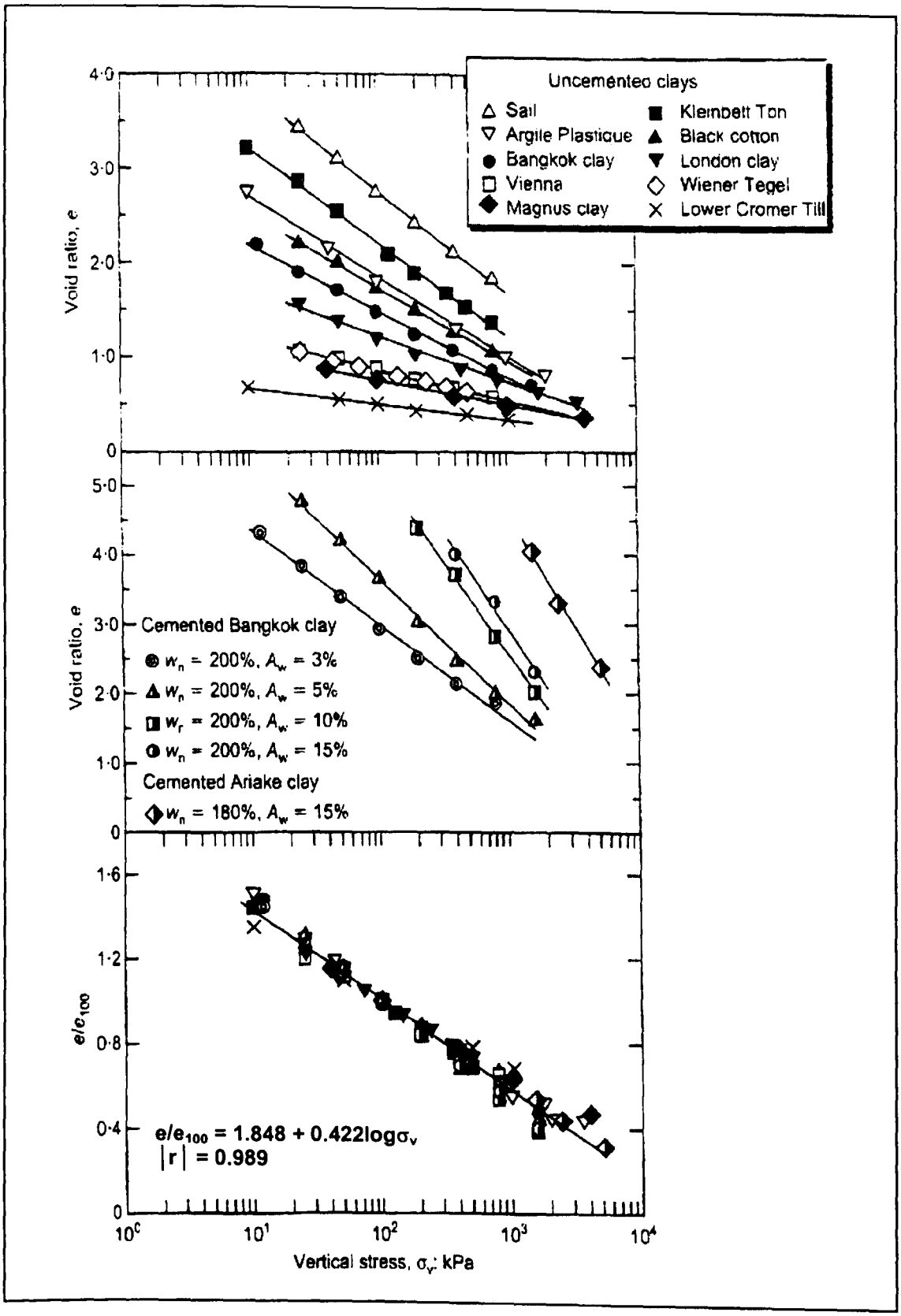

Figure 2.40b: 'Generalised compression curve' (Horpibulsuk et al. 2004).

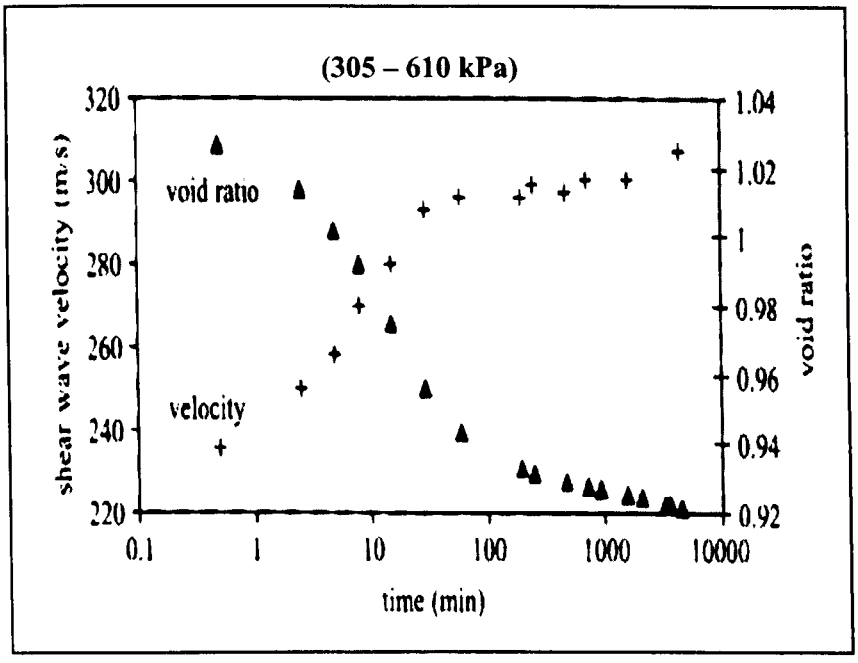

Figure 2.41a: Evolution of shear wave velocity in kaolin slurry during pore pressure diffusion (Santamarina et al. 2001).

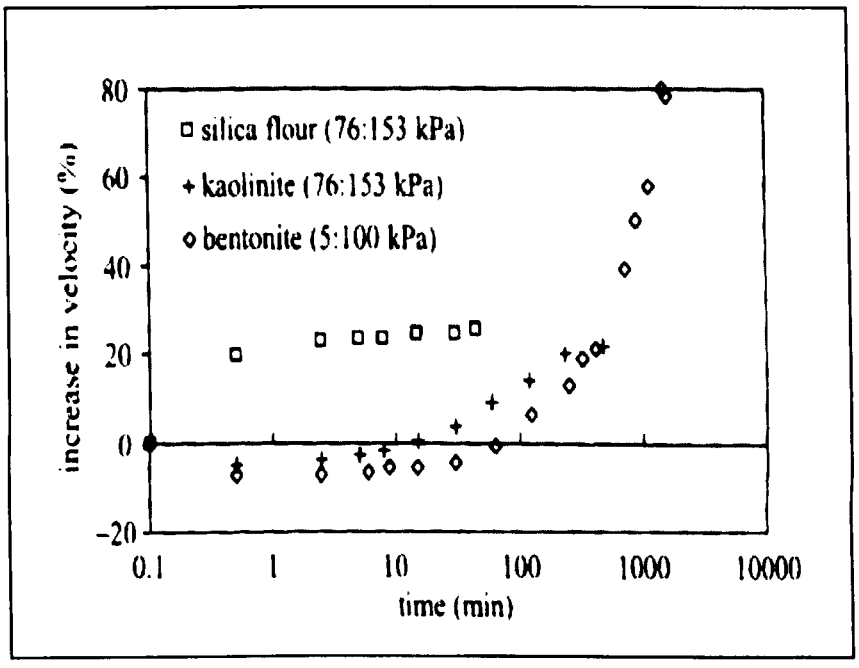

Figure 2.41b: Initial changes in shear wave velocity during a loading stage (Santamarina et al. 2001).

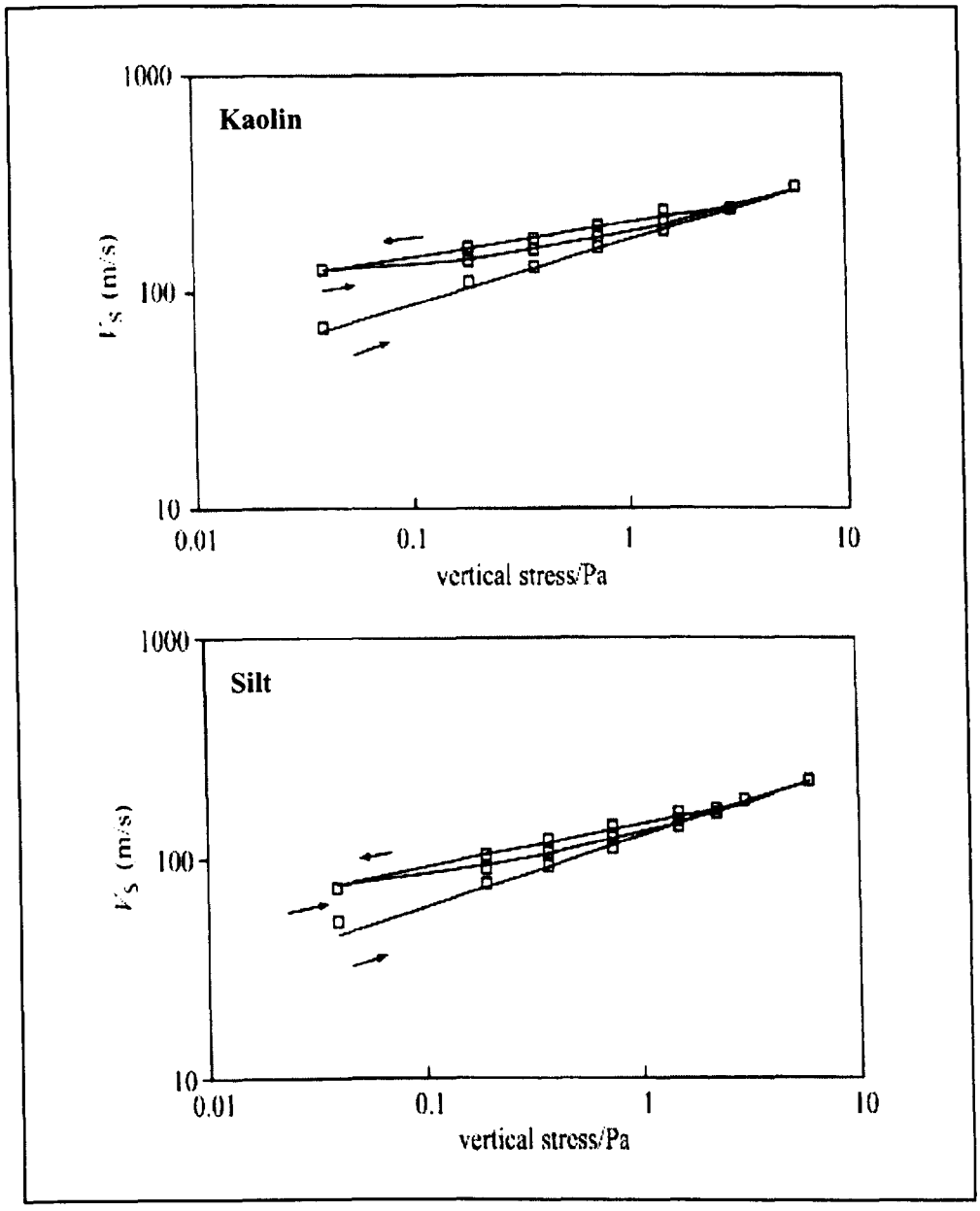

Figure 2.42: Change of shear wave velocity with vertical stress (Santamarina et al. 2001).

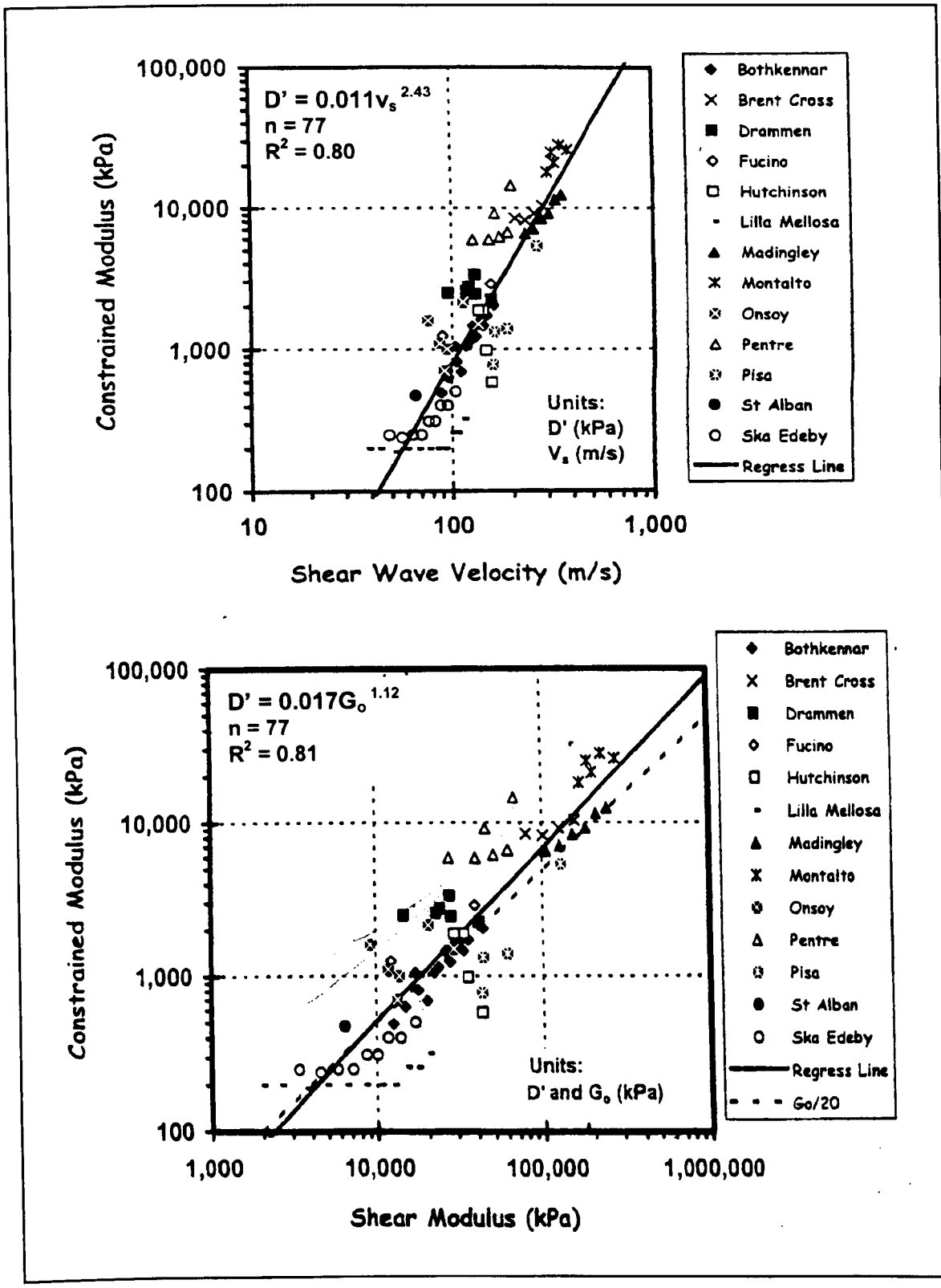

Figure 2.43: Correlations of constrained modulus with v_s and G_o for various unstabilised natural clays (Burns and Mayne 2002).

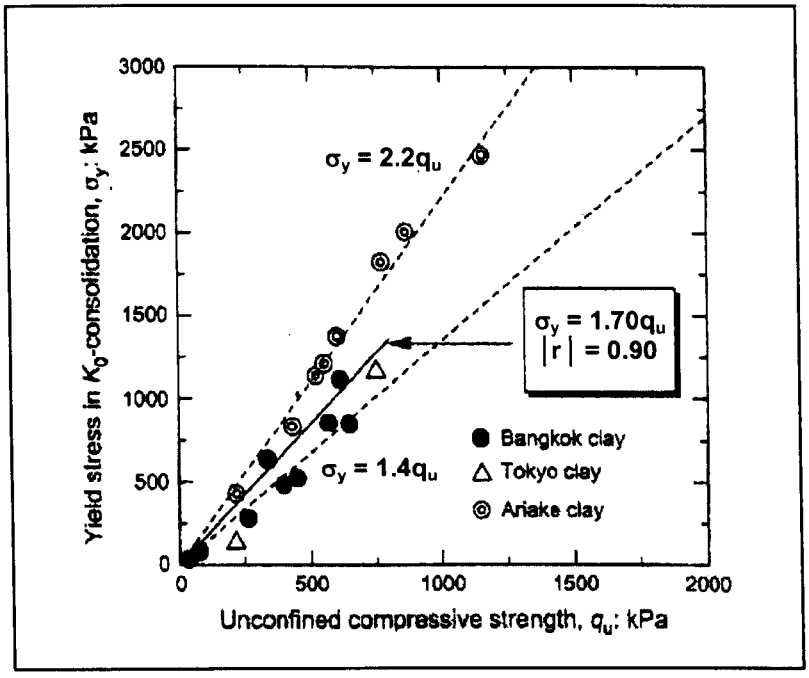

Figure 2.44: Relationship between q_u and σ_y' of stabilised clays (Horipibulsuk et al. 2004).

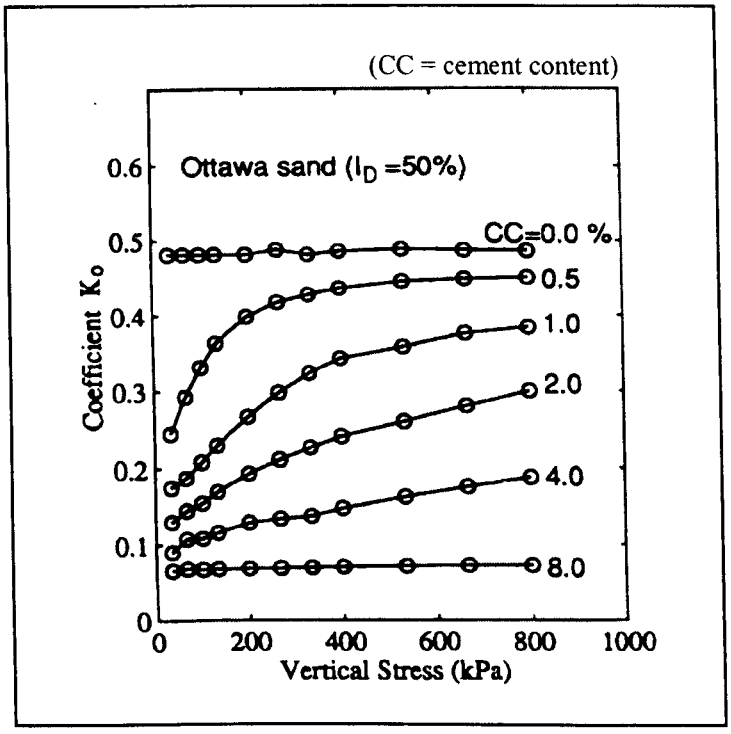

Figure 2.45: Effect of vertical stress on K_o in a cemented sand (Zhu et al. 1995).

Chapter 3
Experimental Equipment, Methods and Procedures

3.1 Introduction

Laboratory based experimental work was carried out to study the strength and stiffness of stabilised clays. The materials used for the experimental programme had two basic constituents: base clays and stabilisers. The base clays comprised one artificial clay, i.e. Speswhite kaolin and two naturally occurring clays, i.e. the Malaysian and Swedish clays. Ordinary Portland cement and unslaked lime (calcium oxide, CaO) were the only stabilisers used in the test programme. This chapter describes the materials and sample preparation procedures, and gives a detailed account of the development of special equipment as well as calibration and testing methods.

The unconfined tests involved a combination of a non-destructive bender element test for shear wave velocity and a subsequent unconfined compressive strength or laboratory vane shear test on samples of 38 mm diameter and 76 mm high. Separate studies were also conducted on samples of different dimensions to investigate the characteristics of shear wave propagation.

One-dimensional compression tests were carried out in both the specially designed oedometer-bender element (oedo-BE) cell as well as in standard oedometers. The main reasons for including the standard oedometer tests in the programme were, firstly, to study the post-yield behaviour at higher stresses and, secondly, to examine the effect of curing on the stiffness of the stabilised samples. The compression curves also served as a useful check on results from the oedo-BE tests.

In the model column test a composite material representing a stabilised system (i.e. stabilised column with surrounding base clay) was tested in place of an entirely stabilised sample in the oedo-BE cell. The test modelled the interaction between the column and the unstabilised clay in one-dimensional compression.

3.2 Materials for testing

The kaolin, supplied by IMERYS Minerals Ltd. (UK), came in powder form, with more than 80 % of particles (by weight) passing the 2 μm sieve. Properties of the material are shown in Table 3.1. The powder was oven-dried at 105°C for at least 24 hours prior to storage for making test samples to ensure control over their water content.

The Malaysian clay was retrieved from a depth of approximately 2 m at Batu Pahat, Johore in the south of Peninsular Malaysia. It was a grey silty clay with small quantities of organic matter. The Swedish clay was a uniform soft clay sampled at Uppsala, Sweden, from a depth of 2 to 3 metres beneath a 1 m thick dry crust. In both cases bulk samples were collected without caution for sample disturbance but were tightly sealed to maintain the original moisture contents and kept in a moist environment at constant room temperature of 20°C. The clays were remoulded in the laboratory for the preparation of the test samples. A comparison between water contents taken on site at the time of sampling and prior to remoulding in the laboratory showed no significant loss of moisture. Properties of the Malaysian and Swedish clays are given in Table 3.2 and Table 3.3 respectively.

It is worth remarking that the Malaysian clay took two months to reach the UK by sea, and in spite of the careful sealing and packaging of the samples, bacterial growth and oxidation on the outside of the soil were clearly visible on arrival. However the contaminated layer was superficial and could be removed by gentle scraping prior to sample preparation.

In terms of stabilisers, ordinary Portland cement with a specific gravity of 3.08 to 3.18 was purchased from Lafarge Cement UK. The unslaked lime came in the form of calcium oxide (CaO) powder, had an average specific gravity of 3.30 and was purchased from Fisher Scientific UK.

The stabilisers were sometimes used in combination at a ratio of 1:1 lime-cement; otherwise just ordinary Portland cement was used on its own. Lime-cement was only used for stabilising the Swedish clay, while pure cement was used in kaolin and Malaysian clay samples. Using lime-cement for the Swedish clay was essentially to comply with the normal practice in Sweden and to allow comparisons with other research on Swedish clays. Otherwise, pure cement was used for simplicity (in the case of the kaolin and Malaysian clay). As for the binder content, the initial consumption of lime (ICL) test, for instance, could be carried out to estimate the minimum quantity of lime required to produce long-term changes to the stabilised material (Rogers et al. 1997).

3.3 Fabrication of bender element (BE) probes

As the BEs were to be used in a rather harsh environment, i.e. cured and compressed in stabilised samples for periods up to 1 month, it was presumed at the start that risks of malfunction and frequent replacement would be high. In addition, the cost of commercially available BEs and the considerable time required for shipment further justified a need to be self-sufficient in terms of BE manufacture.

Therefore the BEs were made in-house, greatly assisted by advice received from the Geotechnics research team at Bristol University. Bimorph PZT-5A strips, 69 mm x 10 mm x 0.5 mm, supplied by Morgan Electro Ceramics, were cut into lengths of 16 mm with a diamond wheel cutter. The strips had either series or parallel polarisation. An opposite-sense polarised / series ceramic, appropriately wired, was used for the receiver and a same-sense polarised / parallel one for the transmitter (Lings and Greening 2001). A detailed step by step description of the fabrication procedure is given in Appendix A.

The electrical connections were made with a 1.8 mm diameter coaxial cable. Once made, the BEs were encapsulated in resin. A resin coating was necessary to provide waterproofing and protection to the ceramic as well as the wiring circuit. A 40 mm x 30 mm x 20 mm aluminium split potting mould was designed and manufactured in the workshop to produce an encapsulation of 0.5 to 1.0 mm thickness on all sides of the protruding ceramic (Figure 3.1 and Figure 3.2). The mould had to be able to withstand a temperature exceeding 100°C for curing of the resin in the oven. It also had to be robust and reusable.

The mould was also designed to provide a thicker resin coating for extra support and protection of the fragile wiring to the BE. After clamping the wired ceramic in the mould, the two halves were placed and fastened together with 4 counter-sunk screws. A close fit was essential to ensure that no leakage occurred during the resin curing period, which could jeopardize the proper formation of the coating around the BE. A 2-part epoxy resin (Araldite MY753 and HY951) was introduced into the mould with a syringe through the access hole on the mould. The intention was to squeeze the air out through the opening at the top of the mould as the resin filled the space in the mould from the bottom. However the problem of trapping air within the encapsulation was not entirely eradicated, resulting in a rejection rate of 20 % due to imperfect encapsulation. The mould was then kept in an oven at 105°C for 24 hours to enable the resin to cure more rapidly. In order to put the

mould to the test, numerous attempts with dummy BEs made from 0.5 mm thick brass plates were carried out for practice purposes.

Upon de-moulding, the now encapsulated BE was potted in a brass cup of 20 mm external diameter and 20 mm depth with the same resin. The final protrusion of the BE was 12 mm wide x 7 mm long (Figure 3.3a and Figure 3.3b). The substantial protrusion length was intended to ensure a good coupling between the sample and the BE, and hence give clear signals for the determination of the shear wave travel time. A BNC (Bayonet Neill Conringman) plug was fixed to the far end of the cable for connection to the relevant devices.

The same BE probes were used for the measurement of shear wave velocity in the unconfined tests and in the oedo-BE apparatus.

3.4 Development of the oedometer-bender element (oedo-BE) apparatus

The oedo-BE apparatus, illustrated schematically in Figure 3.4a, incorporated the capability to concurrently measure one-dimensional compressibility and shear wave velocity using the bender elements.

The oedometer was designed and built as a floating ring type. The stainless steel ring was machined to the dimensions of 100 mm diameter and 90 mm high with a thin-walled middle section 30 mm high (Figure 3.4b). The ASTM Standards D2435-96 (2000) required a minimum aspect ratio (diameter to height, D/H) of 2.5 for samples not less than 50 mm in diameter and 12.5 mm in height. Considering that the oedo-BE ring was a floating type, the sample height was taken as half of the total sample height (i.e. 0.5 x 70 mm = 35 mm) and the ratio obtained was 2.86. The aspect ratio was lower than that of the standard oedometer (3.75), but fulfilled the ASTM requirements and still provided sufficient travel distance for the shear wave velocity measurement.

The top cap and base were both installed with BE probes for shear wave velocity measurements (Figure 3.4b). The final protrusion length of the BE was 4 mm, taking off 3 mm for the porous plastic sheet which was mounted on each platen. The oedo-BE device was mounted on a conventional Wykeham Farrance oedometer frame with an LVDT (linear variable differential transformer) replacing the dial gauge for monitoring vertical displacement, Figure 3.4c.

Drainage was allowed from both the top and bottom of the sample via the top cap and base of the cell. Porous plastic sheets were placed at the contact of the top cap and base with the sample. The sheets were put in dry when setting up the test. This was because the sample had a tendency to absorb moisture from the sheets if they were wet during curing, and this would have changed the initial water content of the sample. A burette was connected to drainage tubes but the volume change, though recorded, was not included in the analysis of test data because of possible error in the measurements due to evaporation.

Both the top cap and base had o-rings for sealing the sample within the ring but there was concern over the significance of the frictional resistance caused. To estimate the friction incurred, a simple test was conducted by loading the top cap with small weights till it began sliding downwards. It was shown that the frictional loss was negligible under normal loading circumstances, but when added to the weight of the top cap, could potentially subject the sample to at least 2 kPa vertical stress at the final unloading stage (i.e. nominal zero vertical stress). Adjustments to the results are discussed in Section 4.3.2.

3.4.1 Lateral stress measurement

The thin-walled mid-height section of the ring was instrumented with two identical Wheatstone full-bridge strain gauge circuits, labelled as A1/A2 and A3/A4 (referring to the horizontal gauges in each circuit) to measure lateral stresses. The strain gauges were KYOWA foil gauges from Sensors UK Ltd. Details of the gauges and other relevant accessories are given in Table 3.4.

Each circuit consisted of two pairs of gauges placed on opposite sides of the ring, and the two gauges in each pair were arranged perpendicular to each other. The vertical gauges, though subjected to far less strain compared to their horizontal counterparts, were still active. Hoop strain and vertical strain induced by lateral stress on the internal ring wall were detected by the strain gauges, which in turn generated an output via the circuits. The microstrains generated a very small voltage output that was amplified 500 times via the Fylde FE-492-BBS bridge conditioner and FE-254-GA differential DC pre-amplifier prior to being logged by a Viglen Genie Professional 4Dx33 computer. With input of the corresponding calibration factors to the logging program, QuickLog PC by Strawberry Tree Inc., measurement of the lateral stress within the ring was achieved. The estimation of hoop strains and the design of the strain gauge circuits are elaborated in Appendix B.

The ring had a total length of 90 mm which varied in thickness. The 30 mm high thin-walled section 0.8 mm thick was sandwiched between the two equal heights 3 mm thick sections (Figure 3.5). The thickness of the thin-walled section was at the limit of what the milling machine available in the workshop could achieve without producing a ring with non-uniform all round thickness. The top and bottom thicker sections provided support and protection to the middle thin wall, especially for handling when the ring was fully instrumented. The ring would also have been at the risk of deformation and damage during compaction of sample if it had had a thin wall all through.

The hoop strain induced by an estimated maximum internal pressure of 462 kPa was 0.015 micro strain (Appendix B), equivalent to a change of 1.5 microns in the sample's diameter. Such a minute deviation from zero hoop strain should have a negligible effect on values of K_o, as shown by several researchers. Zhu et al. (1995), adopting a very similar fixed ring stainless steel strain-gauged oedometer cell, but with an almost doubled wall thickness of 1.5 mm, successfully measured K_o values for artificially cemented sands, even with a hoop strain in the region of 0.4 micro strain; Edil and Dhowian (1981), using a strain-gauged stainless steel test tube for peat samples, quoted a maximum hoop strain of the order of 0.2 micro strain, which was claimed to be far too small to bring K_o values down to active values as proposed by Terzaghi (1934) and Bishop (1958); Andrawes and El-Sohby (1973), by interpolation from two constant stress ratio tests on dense glass ballotini, proved that K_o was unaffected by hoop strains within the limit of 0.15 %.

The ring was re-gauged after four initial tests due to one of the circuits breaking down; comparison of the calibration factors before and after the first four tests clearly indicated a problematic circuit. Although the other circuit was unimpaired, the tight clearance between the wiring and adjoining protective coating made it impossible to strip the malfunctioning circuit off without the risk of ripping off the other. Hence it was decided to replace both circuits.

The strain gauge circuits were calibrated with a Budenberg dead weight tester using pressurized air in the range of 0 to 400 kPa, in three consecutive ascending and descending cycles. The oedo-BE cell was mounted on the loading frame as in a normal test set-up, with the lever arm clamped down to the frame body. The bottom drainage access was sealed with a plug, while the top drainage access was connected to the calibrator via a plastic tube.

The pressure in the ring, as provided by a pressurized nitrogen gas cylinder, was brought up in increments of 10 kPa from 0 to 50 kPa, followed by increments of 50 kPa for the remaining pressures and vice versa for the descending order. Voltage outputs of the circuits were automatically amplified and logged by a computer. A calibration chart was produced by plotting the intended lateral pressure (σ_h) against the voltage output (V_{out}), where the gradient of the best fit line was taken as the calibration factor, e.g. Figure 3.7. Note that the calibration factors for the original circuits were seemingly half of those for the new circuits simply because of the different amplification factors used in both cases, 1000 for the original circuits and 500 for the 'new' ones (Appendix B).

The estimation of the lateral or hoop strain, and hence the output voltage, was based on the assumption of internal pressure acting on a thin-walled cylinder. A detailed account of the estimations and predicted calibration factors (i.e. for both the 'original' and 'new' circuits) are given in Appendix B. However the predicted calibration factors were lower than the actual values by 4.5 to 11.0 %. This difference could be attributed to several factors:

- There were changes in thickness (from 0.8 mm to 3.0 mm) over the length of the ring, i.e. the ring was not uniform as assumed in the estimations.
- The connecting wires probably increased resistances within the circuit, hence lowering the outputs and increasing the calibration factors.
- The thin layer of cement between the gauge and the ring wall might have affected the sensitivity of the gauges.
- Material properties (i.e. Young's modulus and Poisson's ratio) for the stainless steel were assumed, as no test information was available.

Only two calibrations were carried out for the original circuits, before and after the four initial tests. Following the problem that developed, as a precautionary measure with the new circuits, calibrations were carried out before and after almost every test to ensure the integrity of both circuits. A compilation of all the calibrations is given in Table 3.5. From the small differences in the successive calibration factors (the largest difference being approximately 4.5 % for both circuits), it is apparent that errors caused by changes in the calibration factors would have been relatively small.

3.4.2 Shear wave velocity measurement

For measurements of shear wave velocity within the sample, BE probes were inserted in the pre-drilled cylindrical recesses in the top cap and base, with o-rings in each recess to ensure proper sealing (Figure 3.4a and Figure 3.4b).

Connected to a function generator, Thandor TG503 (triggered by a separate function generator, Continental Specialities Corporation Type 4001), the transmitting bender element was excited with ±10 V single cycle sine pulses of 7 kHz, 9 kHz, 12 kHz and 15 kHz (Figure 3.4c and Figure 3.6). This was the optimal range based on results of preliminary studies on the input frequency dependence of shear wave arrival time (Section 4.2.1.1). The received signal, as detected by the receiving bender element, was amplified through a battery-powered amplifier which inadvertently reversed the polarisation of the signal. The transmitted and received signals were both captured on a digital phosphor oscilloscope (Tektronix TDS3012B, 100 MHz, 1.25 GS/s) and the digitised data were subsequently processed in spreadsheets for different methods of shear wave arrival time determination (see Section 4.2.2). However, the main interpretation method employed to define shear wave arrival time for the present work was the visual picking method, for reasons that are explained in Section 4.2.2.5.

3.5 Unconfined tests

3.5.1 Sample preparation

The same compaction method was adopted for both the artificial and natural clay samples. However, the material preparation methods differed slightly. Note that the untreated clay samples were prepared in the same way, but without the addition of stabilisers.

For the artificial clay (i.e. Speswhite kaolin) samples, the required amount of oven-dried kaolin powder and ordinary Portland cement (OPC) were poured into the mixing bowl of a food mixer. The powders were gently mixed with a spatula before water was added. For the wet natural clays, the required dosage of stabiliser (OPC for Malaysian clay and lime-cement for Swedish clay) was added to the base clay and the mixture was hand-kneaded prior to mixing with the machine. The small quantities of organic material present in the Malaysian clay were removed to improve homogeneity of the samples.

The food mixer was initially run at a low speed to avoid spillage, followed by high speed mixing for 1 minute. The mixer was then stopped and the material was scraped off the paddle and sides of the bowl before resuming mixing for another full minute. In total the mixing process took approximately 3 minutes. A thoroughly blended and sufficiently homogeneous mix was achieved this way even without mixing for the recommended 10 minutes (EuroSoilStab 2002). This could be due to the small amounts being mixed in each batch as well as the stoppage and scraping process, which helped to homogenize the paste.

The compaction equipment and tools are shown in Figure 3.8. The mixed material was transferred to a standard brass split mould of 38 mm diameter and 76 mm height, in 4 layers of 40 g each. It was tamped and compacted with the compaction tools in the following order: each layer was first tamped with Tool A to obtain a level surface, followed by an even tamping with Tool B for 50 times, simultaneously rotating the tool. The top of each compacted layer was scarified before compacting the following layer to improve bonding between the layers. The weight of the sample was recorded so that the bulk density could be calculated and used for maximum shear modulus (G_o) computation in the tests.

Note that the samples were compacted well above the optimum water content and therefore the final bulk density would not have been highly sensitive to the compactive effort adopted. Standard Proctor tests carried out on several stabilised kaolin samples showed that the initial water contents of the samples in this research were substantially higher than the optimum water content (29 – 32 % depending on cement content), with a low air voids content and a high degree of saturation (see Table 4.6a).

A slot 12 mm long x 3 mm wide x 7 mm deep was formed by pushing in a Perspex block at each end of the sample. This was later used for insertion of the BEs, as curing significantly stiffened the sample and made it impossible to penetrate the clay without damaging the BEs.

The samples were finally extruded from the split mould, wrapped in cling film and kept in tightly closed buckets with raised Styrofoam platforms at a room temperature of 20°C. The buckets were partially filled with a bleach solution to prevent fungal growth during the curing period.

In addition, cement-stabilised kaolin samples of different diameters, namely 38 mm and 114 mm (with 70 mm height), were prepared to investigate the influence of sample geometry and input frequency on shear wave propagation characteristics. The samples

were compacted in a separate mould with interchangeable rings of different diameters lined with PTFE (polytetrafluoroethlene) sheet, Figure 3.9. The compaction effort was scaled up for the large sample, as done for the oedo-BE samples (see Section 3.6.1).

3.5.2 Bender element (BE) tests

BE tests were carried out to measure the shear wave velocity in the stabilised samples and hence determine the maximum shear modulus, G_0. The pre-made slots on the samples were filled with plasticine as a coupling material before inserting the BE, Figure 3.10. A short length of wire was attached to the base of the sample to earth it, in addition to wires attached to each of the brass cups of the BE probes. All the wires were connected to one common earth point to avoid any potential differences. The experimental set-up is shown in Figures 3.11 and 3.6, with the electronics as described in Section 3.4.2. The procedure was also as described in Section 3.4.2.

A separate series of tests involving 70 mm high samples of different diameters, 38 mm and 114 mm, was carried out to investigate the effects of sample geometry and input frequency on shear wave propagation through the stabilised media. Additional frequencies of 1 kHz, 3 kHz, 5 kHz and 20 kHz were added to the original frequency range of sine pulse input mentioned in Section 3.4.2.

3.5.3 Unconfined compressive strength (UCS) tests

After the BE tests had been completed, the unconfined compressive strengths of the same samples were measured with a conventional triaxial testing machine at a strain rate of 1.5 mm per minute. The test procedure was as prescribed in Part 7 of BS 1377 (1990).

Care was taken to ensure that both ends of the sample were as flat as possible to minimize bedding error. It is worth noting that the pre-made slots on both ends of the test samples were unlikely to have significantly affected the UCS test, considering the small surface area of the slot relative to the total surface area of the sample (i.e. 3.2 %). Also, there was no visual evidence of the samples' failure mechanisms being influenced by the slots (see Figure 4.16).

Calibration of the proving ring was carried out with a Budenberg dead weight tester and a standard load cell frame at the beginning and end of all tests (Section 4.2.3), to ensure consistency of the measurement.

3.5.4 Vane shear tests

Laboratory vane shear tests were conducted only on the Malaysian clay samples to obtain the undrained shear strength. This represented a deviation from the original plan of estimating the undrained shear strength from the UCS test and was due to the exceptionally soft nature of the samples, mainly those stabilised with low cement contents.

A conventional laboratory vane shear test apparatus, with a vane 12.7 mm wide and 12.7 mm long, was used for the tests, following the procedure laid out in Part 7 of BS 1377 (1990). However the sample was tightly held by hand on the base during shearing instead of being contained in a mould. The torque was applied by turning the handle at a rate of 6^{o} to 12^{o} per minute.

Due to the absence of a satisfactory means of calibrating the vane shear apparatus, it was instead calibrated against two hand vanes, using homogeneous samples of pottery clay from a single batch (Section 4.2.3).

3.6 One-dimensional compression tests

3.6.1 Sample preparation

Samples were mixed and compacted in the rings using similar methods to those used for unconfined samples (Section 3.5.1) and left to cure without drainage, water access or pre-loading before the test. The oedo-BE samples were compacted in 3 layers (100 times of tamping per layer with Tool B, Figure 3.8) while the standard oedometer samples were prepared in only 1 layer (50 times of tamping with the same compaction tool). The compaction effort was based on volume of the material being compacted in each layer. The moisture content of each sample was also determined using material from the fresh mix.

The sample stabiliser contents were relatively small, i.e. 1.5 and 3.0 % for kaolin and Malaysian clay, 5 and 10 % for Swedish clay. The low stabiliser contents were primarily due to limitations of the experimental set-up and devices (Section 1.3).

3.6.2 Oedo-BE tests

The tests were conducted, with several modifications but generally in accordance with the Part 5 of BS 1377 (1990), in the cell described in Section 3.4.

The sample was first compacted in the ring in a specially designed rig to a uniform height of 70 mm. The ring containing the sample was then transferred to the cell base that

was seated on the pedestal of the loading frame. Care was taken to ensure that the bender elements were properly lined up when the top cap was put on the sample. As the bender elements were pushed into the sample, there was invariably good contact and coupling between the bender elements and the sample.

Prior to the tests, the samples were cured for 7 days in the cell without drainage. The designated curing period of one week was long enough to achieve sufficient hydration of the stabiliser, which could not be too short but not too long so as to constrain the test programme as a whole. Further justifications for the 7-day curing period are given in Section 4.3.1.

The cured samples were subjected to the sequence of stresses listed in Table 3.6. Each loading or unloading stage was maintained for 24 hours, and in most cases secondary compression was well underway by then. As the vertical displacement and lateral stress were automatically logged by the computer, only the shear wave velocity required manual measurement and recording at pre-determined intervals of 0 second, 30 seconds, 1 minute, 2 minutes, 4 minutes, 8 minutes, 15 minutes, 30 minutes, 1 hour, 2 hours, 4 hours, 8 hours and 24 hours. The settlements were subsequently corrected with the frame stiffness data determined prior to the test.

Also, a representative moisture content was taken at the end of each test.

Datums for the lateral stresses measured by both the strain gauge circuits were taken with an empty cell before and after each test, as summarised in Table 3.7.

3.6.3 Standard oedometer tests

The standard oedometer tests were carried out based on the recommended procedure in Part 5 of BS 1377 (1990). A series of five standard oedometer tests were run at any one time for each clay, with one sample of base clay and two samples each with a different stabiliser content but cured for 7 and 28 days respectively. The stresses applied were the same as in the oedo-BE tests, but with two modifications:

1. In the unloading stages, instead of unloading back to zero, a minimum of 12.5 kPa was maintained at the end of unloading (mainly to allow plotting of the results on a logarithmic scale).
2. An additional loading increment 800 - 1600 kPa was introduced, before finally unloading back to 12.5 kPa in two steps, 800 kPa followed by 400 kPa.

Table 3.8 gives a summary of the sequence of stresses applied in all the standard oedometer tests.

3.7 Model column tests

3.7.1 Sample preparation

Preparation of the composite test material required additional accessories apart from the original compaction rig for making the oedo-BE samples, as shown in Figure 3.12. First, the base clay was remoulded thoroughly and compacted in the oedo-BE ring in the usual way (see Section 3.6.1). Without trimming the top of the base clay sample, the top plate with a hole in the centre which served as a guide was then placed on the sample. A tube was pushed through the centralized hole, and after sealing the top of the tube, a column of clay was extracted, leaving a cylindrical void of 38 mm diameter throughout the height of the clay sample.

Next the stabilised portion was prepared and compacted in the void in a similar manner as for an unconfined sample (see Section 3.5.1). This was done within a thin-walled tube, inserted into the sample to keep disturbance of the surrounding clay to a minimum. Finally, with the tube removed, the top of the composite sample was trimmed off and the sample was ready for curing in the oedo-BE cell.

3.7.2 One-dimensional compression of composite system

The ring containing the composite sample was then assembled with the top cap and base in similar way as for the normal oedo-BE test. The stresses applied are shown in Table 3.6. The test was carried out essentially in the same manner as described in Section 3.6.2.

Table 3.1 Properties of Speswhite kaolin

Mineralogy	*Kaolinite with minor amounts of mica, quartz and feldspar or illuminite.	
Particle shape	*Platy, with typical aspect ratio of 20:1.	
Specific gravity, G_s	2.61 *(2.60)	
Liquid limit, LL	%	61
Plastic limit, PL	%	34
Plasticity Index, PI	%	27
Clay fraction (percentage by weight passing 2 μm sieve)	%	82
Activity, A = PI / Clay fraction	0.33	

*Particle size distribution plot:

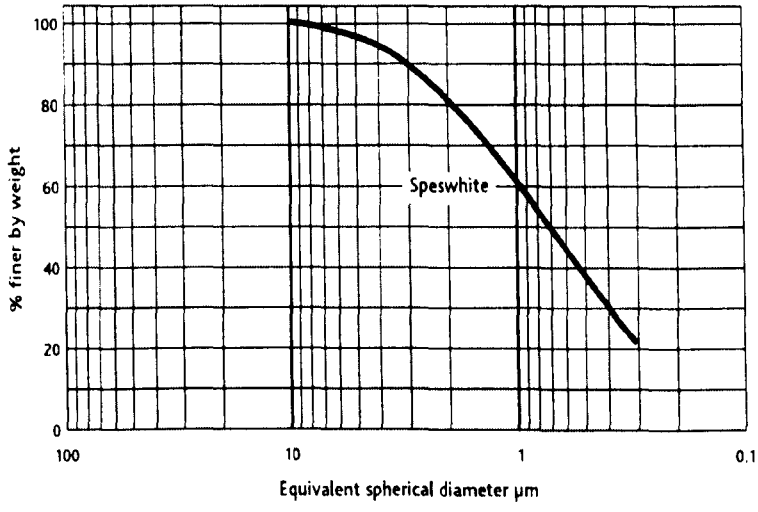

* and *( )- extracted from the data sheet by IMERYS Minerals Ltd. (UK)

Table 3.2 Properties of Malaysian clay

Soil description	Grey silty clay at 2 m depth with small amount of organic content (grass blades, roots, fragments of wood).	
Natural water content	%	74
Average water content before remoulding in the laboratory	%	74
Bulk density, ρ_b	Mg/m^3	1.36
Specific gravity, G_s	2.66 *(2.60)	
Liquid limit, LL	%	77 *(88)
Plastic limit, PL	%	31 *(24)
Plasticity Index, PI	%	46 *(64)
Liquidity Index, LI	0.94 *(0.78)	
Clay fraction (percentage by weight passing 2 μm sieve)	%	28
Activity, A = PI / Clay fraction	1.64	

*Particle size distribution plot:

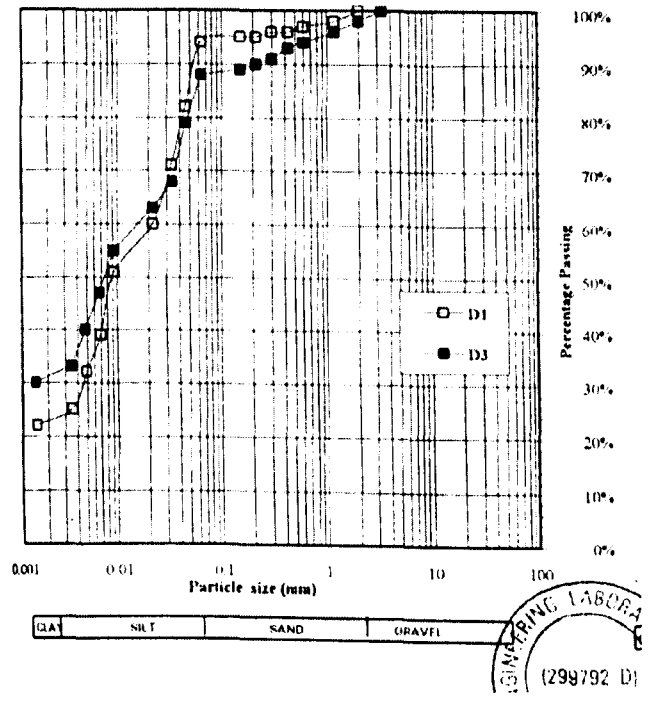

* and *( )- extracted from the site investigation report by Ideal Engineering Laboratory Ltd. (Malaysia)

Table 3.3 Properties of Swedish clay

Soil description	Grey soft clay.	
Natural water content	%	*(65 to 85)
Average water content before remoulding in the laboratory	%	67
Bulk density, ρ_b	Mg/m^3	*(1.50 to 1.60)
Specific gravity, G_s	2.73	
Liquid limit, LL	%	60 *[66]
Plastic limit, PL	%	24 *[32]
Plasticity Index, PI	%	36 *(34)
Liquidity Index, LI	1.19 *(1.12)	
Clay fraction (percentage by weight passing 2 μm sieve)	%	49
Activity, A = PI / Clay fraction	0.73	

Particle size distribution plot:

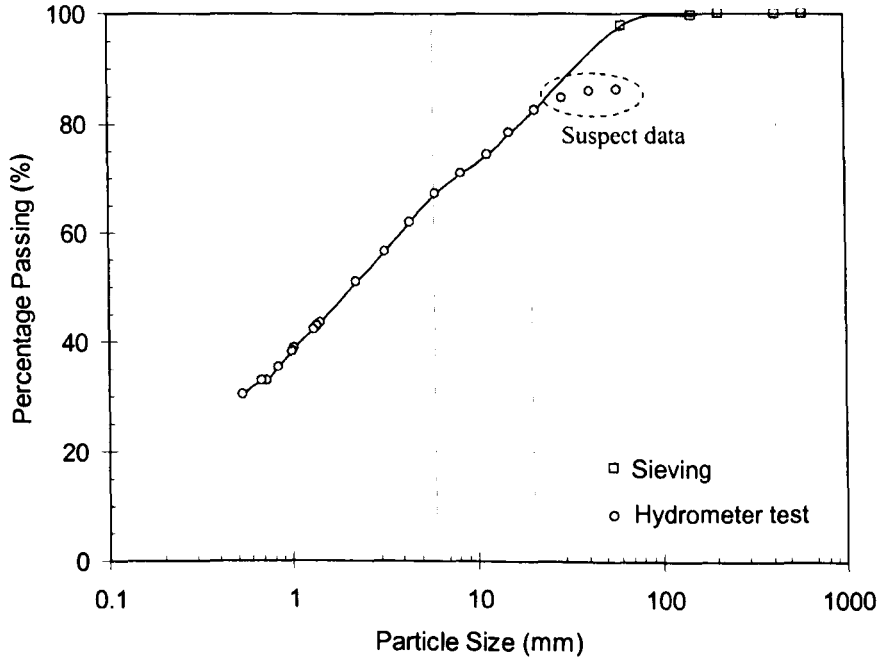

*( )- extracted from Mattsson et al. (2005)

*[ ]- personal communication with Mattsson (2005)

Table 3.4 Properties of strain gauge and relevant accessories

Type	KYOWA KFG-5-120-C1-16	
Temperature compensation for	Stainless steel	
Gauge length	mm	5 mm
Gauge resistance (24°C, 50 % RH)	Ω	119.8 ± 0.2
Gauge factor	%	2.14 ± 1.0
Adoptable thermal expansion	PPM/°C	16.2
Transverse sensitivity (24°C, 50 % RH)	%	0.40
*Gauge cement	CC-33A (operating temperature: -196°C to +120°C)	
*Bondable terminals	CEG-75c (with 0.13 mm thick epoxy-glass laminate backing)	
**Connecting wire	Insulated copper wire 0.315 mm ∅ (RS 357-722)	
*Protective coating	M-Coat A Air-drying solvent-thinned (xylene) polyurethane	

Sources: KYOWA Electronic Instruments Co. Ltd. (Japan)
* Vishay Intertechnology (USA)
** RS Components Ltd. (UK)

Table 3.5 Calibration factors for strain gauge circuits

Circuits	Sample	Calibration Factors ($kN/m^2/V$)	
		Circuit A1/A2	Circuit A3/A4
ORIGINAL	K0	494.18	467.80
	K1.5		
	K3		
	MC0	473.12	474.55
NEW	MC1.5	933.78	971.07
	MC3		
	SC0	943.85	942.62
	SC10	969.95	943.83
	COL1	929.55	985.92
	COL2	942.66	959.02
	COL3	937.83	961.23

Note:

K0	Kaolin with 50% water content and 0% cement
K1.5	Kaolin with 50% water content and 1.5% cement
K3	Kaolin with 50% water content and 3% cement
MC0	Malaysian clay with 0% cement
MC1.5	Malaysian clay with 1.5% cement
MC3	Malaysian clay with 3% cement
SC0	Swedish clay with 0% lime-cement
SC10	Swedish clay with 10% lime-cement
COL1	Base clay: kaolin with 50% water content Column: kaolin with 50% water content and 3% cement
COL2	Base clay: kaolin with 50% water content Column: kaolin with 50% water content and 3% cement
COL3	Base clay: Swedish clay Column: Swedish clay with 10% lime-cement

Table 3.6 Sequence of stress application in oedo-BE tests

Loading / Unloading (kPa)	**Sample**	**Loading / Unloading (kPa)**	**Sample**
0 - 12.5		0 - 12.5	
12.5 - 25		12.5 - 25	
25 - 0		25 - 0	
0 - 25	K0	0 - 25	
25 - 50	K1.5	25 - 50	
50 - 100	K3	50 - 100	MC1.5
100 - 50	MC0	100 - 50	MC3
50 - 0	COL1	50 - 0	SC0
0 - 50	COL2	0 - 50	SC10
50 - 100	COL3	50 - 100	
100 - 200		100 - 200	
200 - 400		200 – 400 (aged for 10 days)	
400 - 200		400 - 800	
200 - 0		800 - 400	
		400 - 0	

Note:

Nominal '0 kPa' was at least 2 kPa (see Section 4.3.2)

Refer to Table 3.5 for sample descriptions.

Table 3.7 Datum for lateral stresses in oedo-BE tests

Sample	Lateral Stress, σ_h (kPa)					
	A1/A2			A3/A4		
	Before Test	After Test	Average	Before Test	After Test	Average
K0	11.1	18.3	14.7	66.4	70.7	68.6
K1.5	48.0	10.6	29.3	48.0	71.0	59.5
K3	14.6	16.1	15.4	71.1	78.5	74.8
MC0	-1.8	6.1	2.2	-7.5	-26.2	-16.9
MC1.5	-24.4	-21.6	-23.0	15.8	25.3	20.6
MC3	-21.6	-19.5	-20.6	28.0	31.1	29.6
SC0	-9.0	2.4	-3.3	4.5	7.3	5.9
SC10	-26.9	-29.5	-28.2	33.4	36.9	35.2
COL1	-12.9	-12.5	-12.7	4.8	4.8	4.8
COL2	-0.9	2.7	0.9	2.4	-3.2	-0.4
COL3	-9.5	-14.8	-12.2	18.7	15.2	17.0

Table 3.8 Sequence of stress application in standard oedometer tests

Loading / Unloading (kPa)	**Sample**
0 - 12.5	
12.5 - 25	
25 – 12.5	K0_*7d
12.5 - 25	K1.5_7d
25 - 50	K1.5_28d
50 - 100	K3_7d
100 - 50	K3_28d
50 – 12.5	
12.5 - 50	MC0_7d
50 - 100	MC1.5_7d
100 - 200	MC1.5_28d
200 - 400	MC3_7d
400 - 200	MC3_28d
200 – 12.5	
12.5 - 200	SC0_7d
200 - 400	SC5_7d
400 - 800	SC5_28d
800 - 1600	SC10_7d
1600 - 800	SC10_28d
800 - 400	
400 – 12.5	

* curing period in days

Refer to Table 3.5 for sample descriptions.

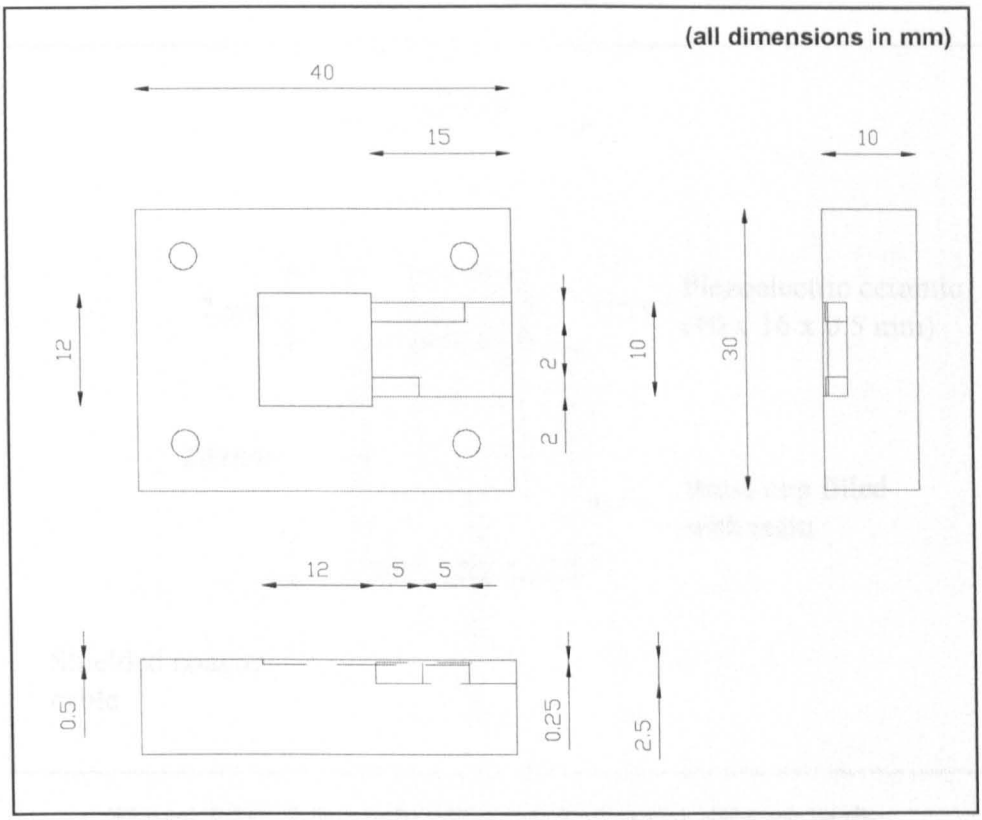

Figure 3.1: Schematic drawing of the BE potting mould.

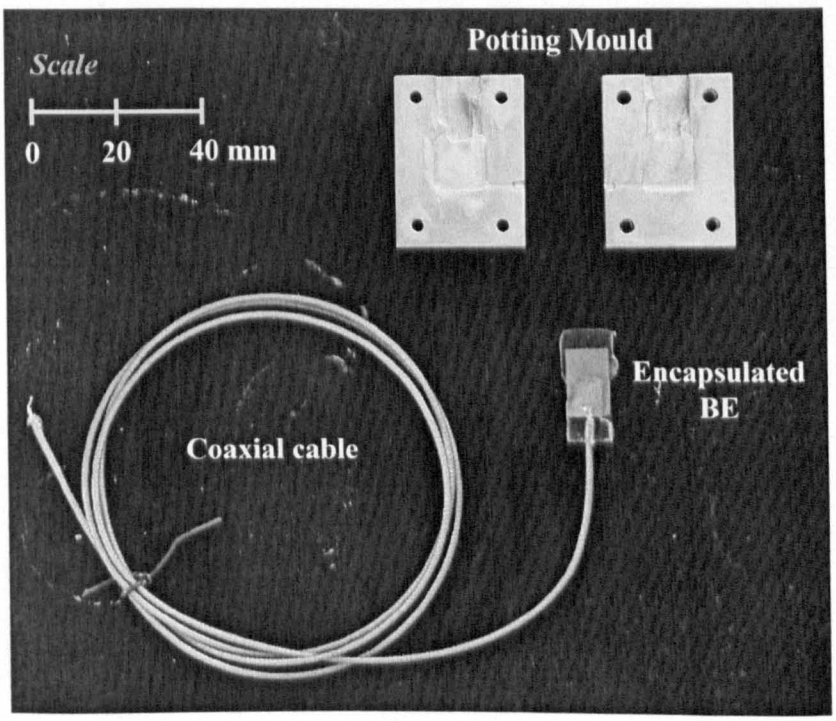

Figure 3.2: The BE potting mould and an encapsulated BE.

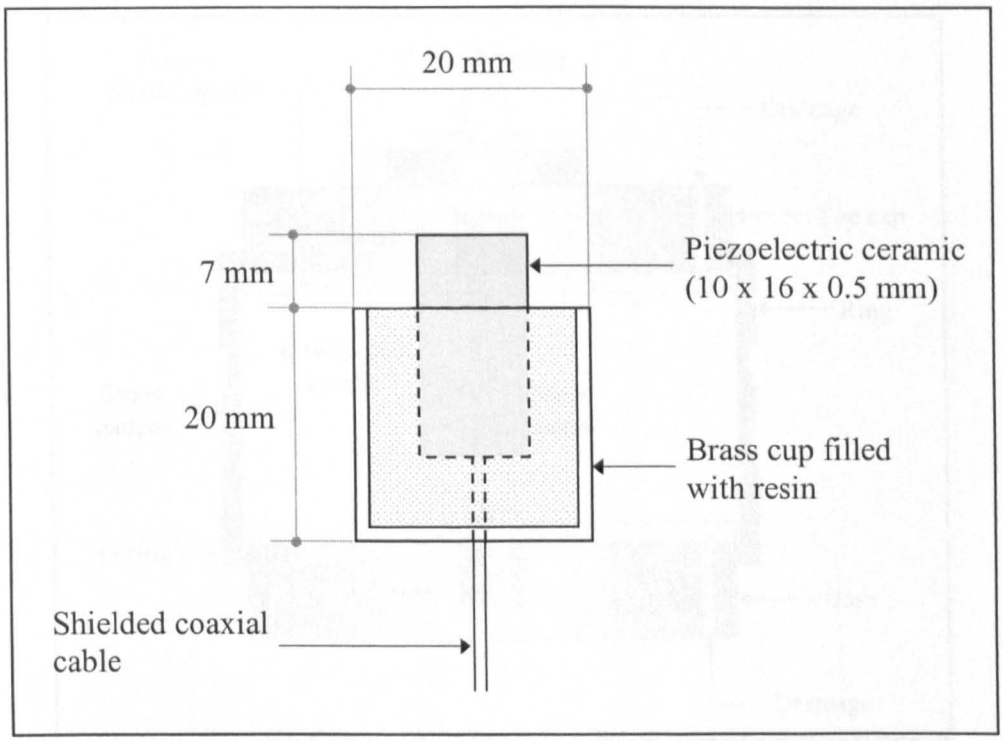

Figure 3.3a: Schematic diagram of a bender element probe.

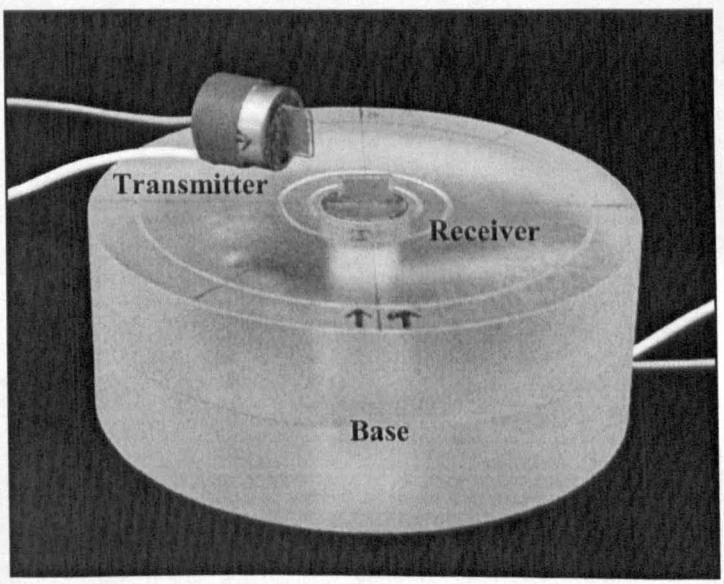

Figure 3.3b: Bender element probes for the unconfined test.

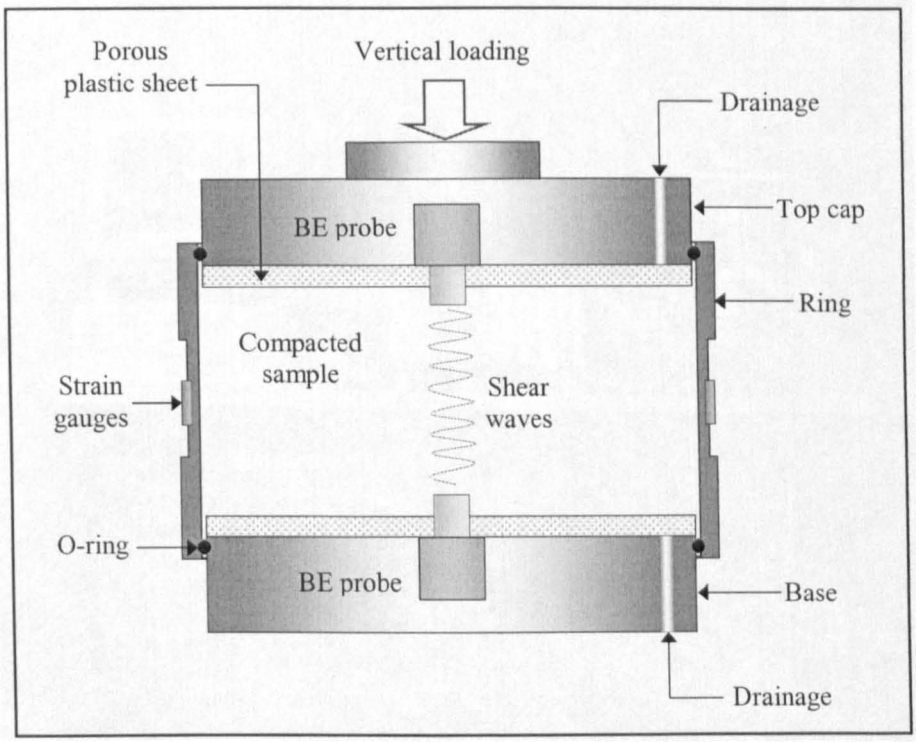

Figure 3.4a: Schematic diagram of the oedo-BE cell.

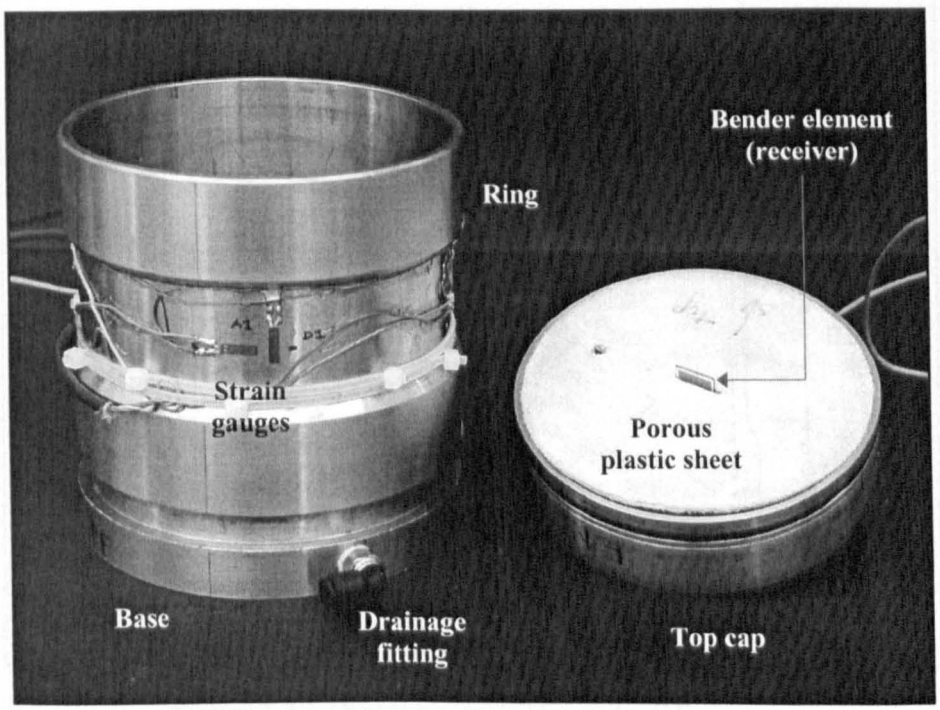

Figure 3.4b: Oedo-BE cell- ring, top cap and base.

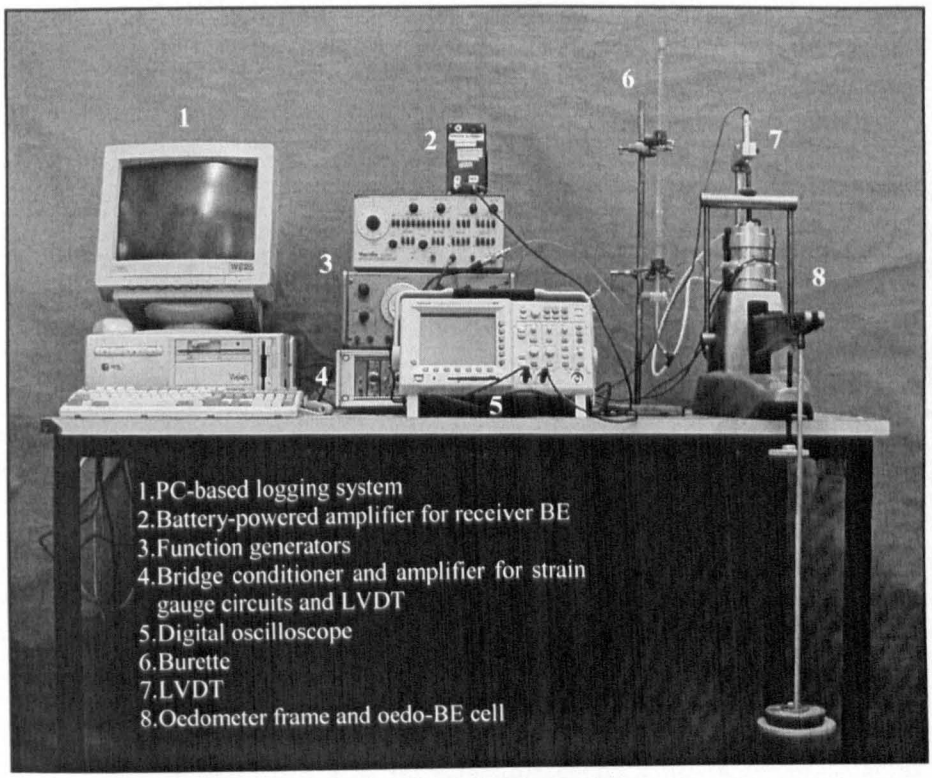

Figure 3.4c: Oedo-BE test set-up.

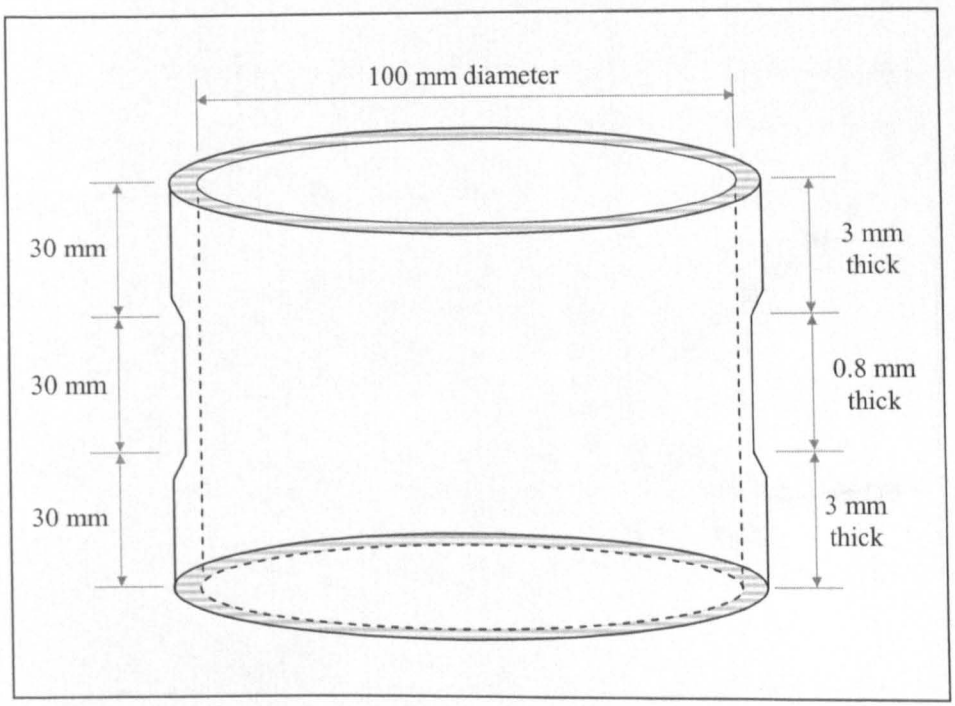

Figure 3.5: Dimensions of the oedo-BE ring.

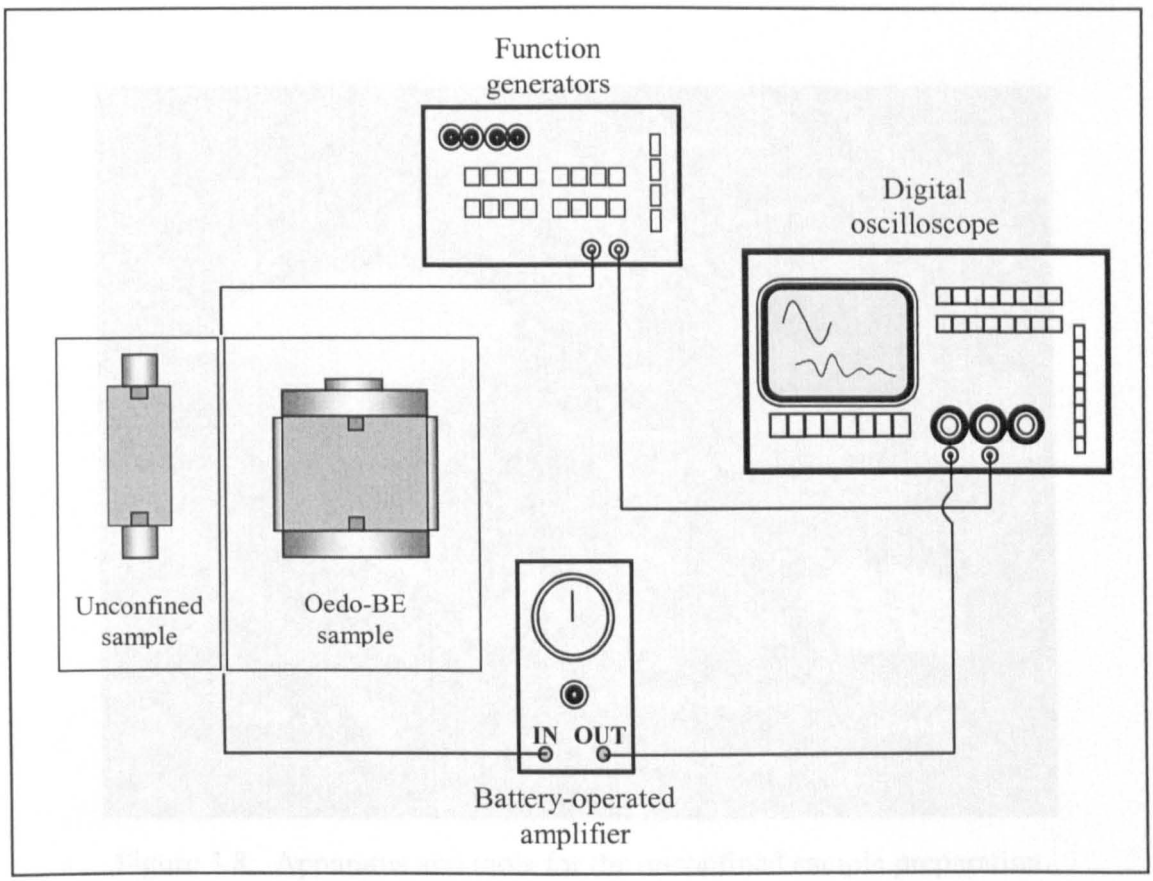

Figure 3.6: Schematic diagram of the BE test set-up.

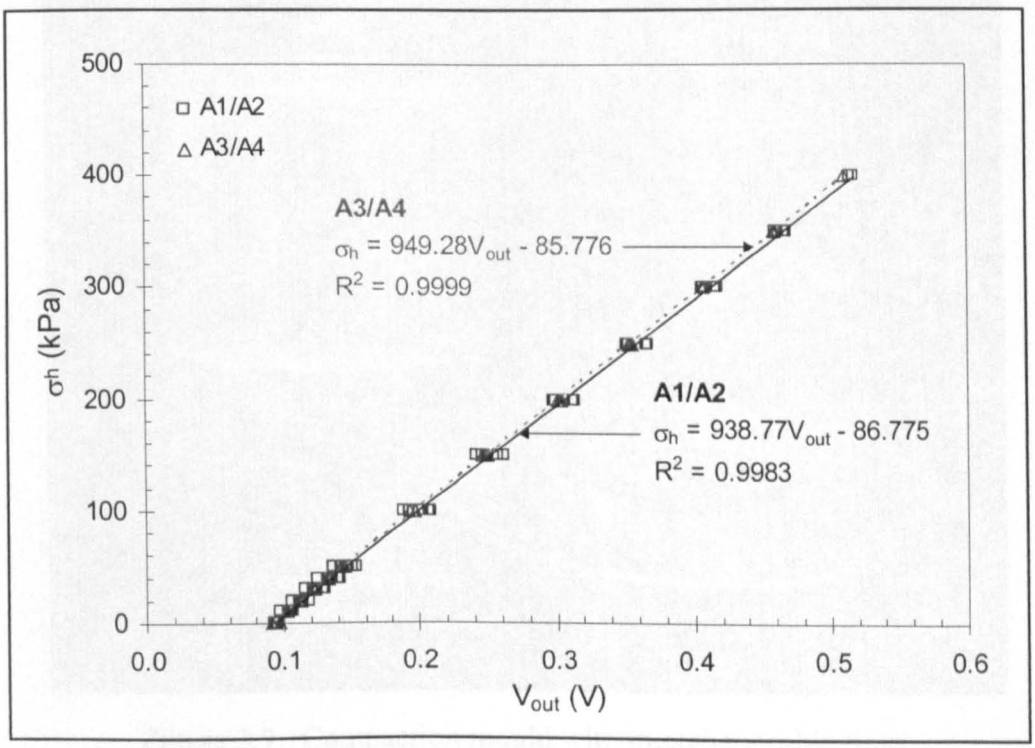

Figure 3.7: Typical calibration chart for the strain gauge circuits.

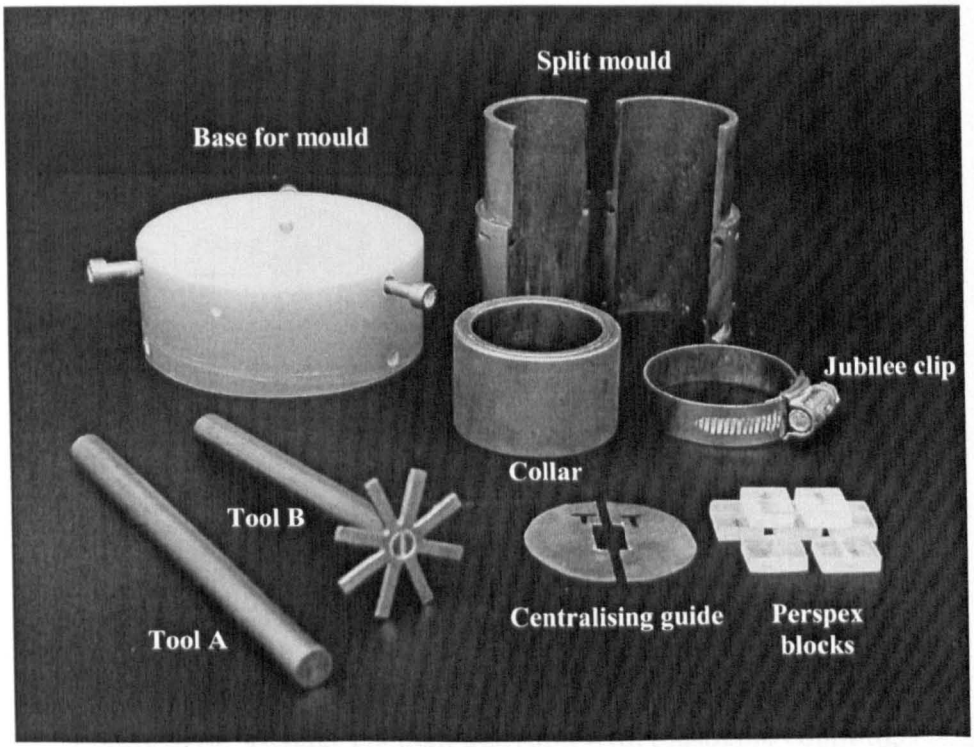

Figure 3.8: Apparatus and tools for the unconfined sample preparation.

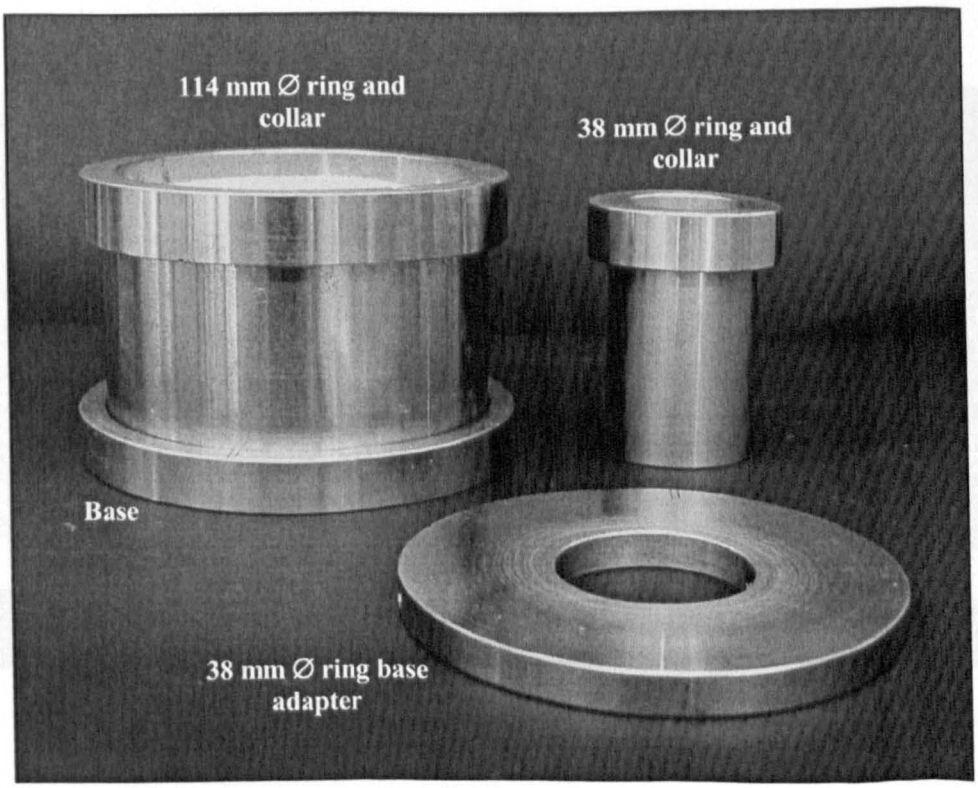

Figure 3.9: Compaction mould with interchangeable rings.

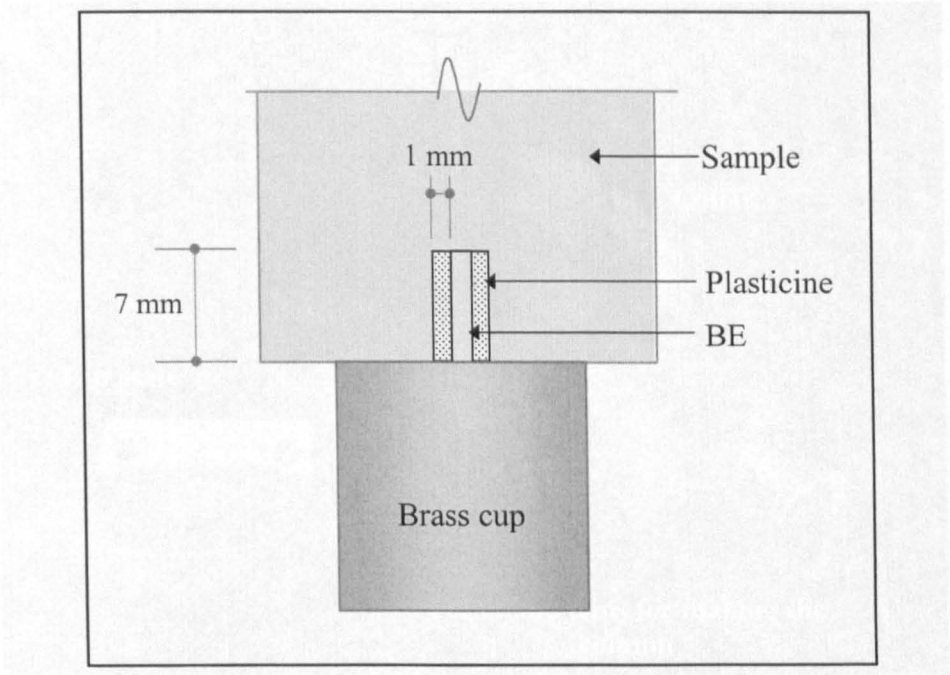

Figure 3.10: Bender element insertion with plasticine coupling.

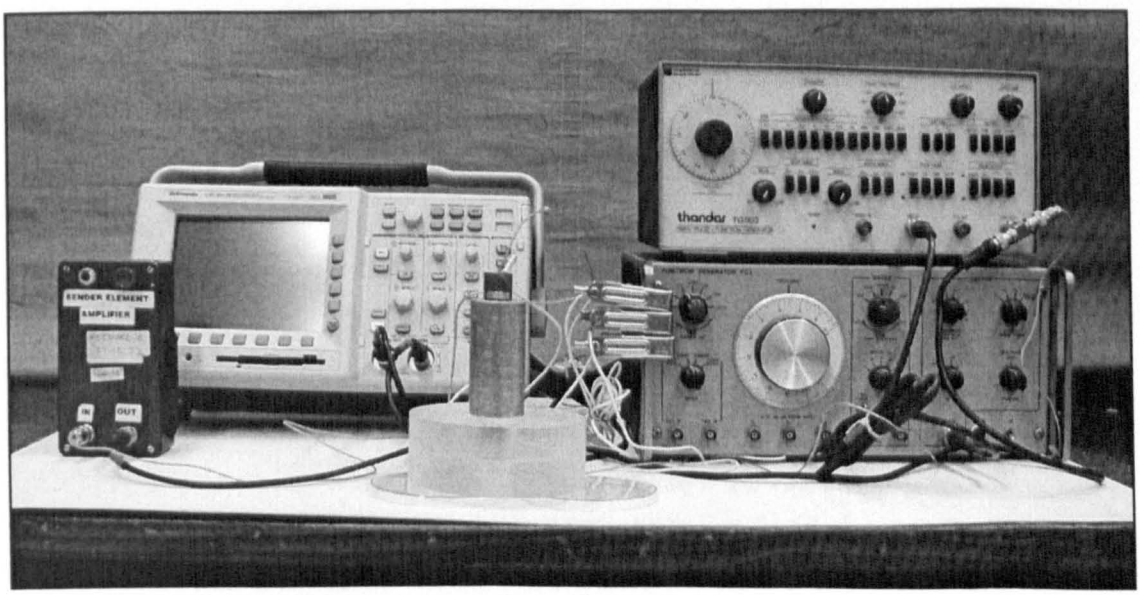

Figure 3.11: Unconfined BE test set-up.

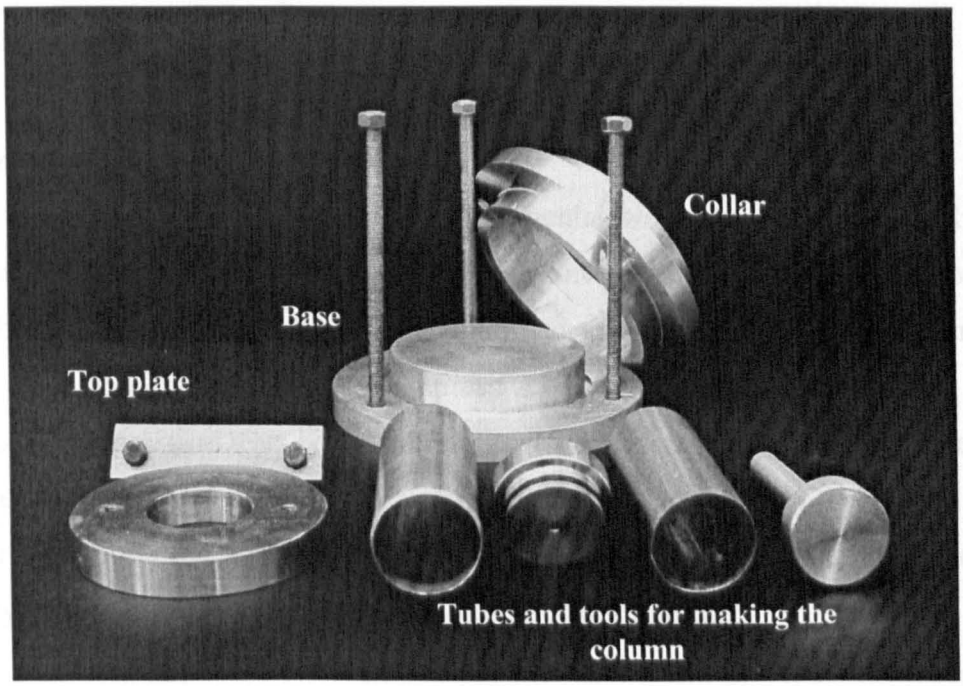

Figure 3.12: Additional apparatus for the model column test sample preparation.

Chapter 4
Results: Interpretations, Analysis and Discussions

4.1 Introduction

In this chapter, the results of the experimental work are presented, analysed and discussed. Correlations established between relevant parameters are also developed. The chapter begins with findings from the unconfined tests, which include both the bender element tests and the unconfined compressive strength tests. Results from the one-dimensional compression tests come next, followed by a final section on the model column tests. The plots presented are those of typical results, representative of the general trends or characteristics observed in the other similar tests. Separate plots are included where necessary to better illustrate extraordinary or interesting findings.

4.2 Unconfined tests

The unconfined tests were conducted as described in Section 3.5. The present section begins with the measurements of shear wave velocity, including various influencing factors and shear wave arrival time determination techniques. This is followed by an account of the variation in strength measurements, the correlations derived for the parameters investigated, and the trends of strength and stiffness development with time.

4.2.1 Factors affecting shear wave velocity measurement

The measurement of shear wave velocity depends very much on the accuracy of the shear wave arrival time determination. The accuracy of the arrival time interpretation in turn depends on the quality of the signal captured. That accounts for the usually fervent attempts in BE tests to obtain clear signals, which bear as much resemblance to the transmitted signals as possible.

Unfortunately, this is not always achievable under the actual test conditions and circumstances. Firstly, the geometry of test samples is often constrained by the test equipment where bender elements are incorporated. Secondly, soil, as a composition of solids and pore fluids, is by itself a dispersive and energy-absorbing medium for shear

waves to propagate through, thus causing distortion to the received signals. Effects of these two factors are elaborated in the following sections.

A series of unconfined tests was carried out to investigate the effect of input frequencies and sample geometry, in terms of the lateral dimension (diameter), on shear wave velocity measurements. The test samples consisted of two pairs of samples, each with the same composition and curing period (kaolin with 50 % water content and 3 % cement), and the same length, 76 mm. The diameters of each pair were 38 mm (samples S1 and S2) and 114 mm (samples L1 and L2). The input frequencies covered a range from 1 kHz to 20 kHz. Details of the sample preparation and test methods can be found in Sections 3.5.1 and 3.5.2.

4.2.1.1 Influence of input frequency

The input frequency was used to compute the wavelength, $\lambda = v_s/f_{in}$ (see Eq. 2.2), where v_s is the shear wave velocity determined using the visually picked arrival time, and f_{in} is the input frequency. The wavelength is therefore dependent on the frequency with which the transmitting BE was excited with during the test, assuming that it was also the dominant frequency in the received signal.

Lutsch (1959) and Thill and Peng (1969) (as reviewed by Leong et al. 2004) highlighted the obscuring of the first major deflection in the received signal if the wavelength is equal to the average grain size, taken as D_{50} (grain diameter with 50 % material passing on the particle size distribution curve). Also, the ratio of λ/D_{50} is suggested to be more than 3 to avoid dispersion in ASTM Standard 2845-95 (2000). The wavelengths in the present tests are approximately 13 mm to 300 mm for S1 and S2, 14 mm to 100 mm for L1 and L2 (Table 4.1). Considering that the samples were essentially composed of clay particles with small quantities of cement, D_{50} could be assumed to be sufficiently low, satisfying the criteria recommended in both sets of test samples. This contributes to the clearly discernible shear wave arrival time on the received traces, Figure 4.1.

4.2.1.2 Influence of sample geometry

As soil is an attenuating medium, an excessive travel distance for a low energy shear wave would significantly reduce its amplitude and mask the time of arrival at the receiver. Therefore attenuation ultimately limits the length or height of test samples. However, the

length of the samples in the present test series was fixed at 76 mm to correspond with the normal unconfined test sample height, leaving the diameter, D, as the variable in terms of sample geometry. The shear wave travel distance, L, was taken from tip to tip of the bender elements (Dyvik and Madshus 1985, Viggiani and Atkinson 1995).

The ASTM Standard 2845-95 (2000) recommends the minimum sample length or height to be at least 10 times D_{50} to accurately define the average propagation velocity. Referring to Section 4.2.1.1, it can be seen that this criterion was readily satisfied in the present work.

Distortion of a signal (dispersion) can occur due to interference of reflected waves from the medium boundaries, resulting in a composite wave with various frequency components (Section 2.4.3). Such an occurrence could easily obscure the arrival of the transmitted shear wave. According to Wasley (1973), and as mentioned in the ASTM Standard 2845-95 (2000), the lateral dimension, i.e. D, should exceed the wavelength, λ, by at least 5 times ($D/\lambda \geq 5$) in order to avoid such dispersion.

From Table 4.1, it is shown that S1 and S2 barely meet the requirements even with high frequencies, whereas L1 and L2 do, but only at frequencies higher than 12 kHz. In the corresponding dispersion plots, Figure 4.2, the linearity of the plots improves at higher frequencies, indicating a reduction of dispersion effects. However, with closer inspection, it can be seen that Figure 4.2a depicts a non-linear trend, indicating varying v_{ph} and v_{gr} with frequency, while Figure 4.2b shows better linearity and hence less dispersion.

Based on the analysis and discussion above, it is clear that lateral boundaries have a significant effect on how well the received signal represents the transmitted signal, in terms of the frequency content. When the diameter of a cylindrical sample is restricting the free propagation of waves through the sample, a phenomenon that is comparable to a 'waveguide effect' is observed (Section 2.4.3). The further the distance of the boundaries is in the direction of polarisation (perpendicular to the direction of propagation) of the shear wave, the less prominent is the effect of lateral rebounds and distortion of the propagating wave. That explains why dispersion plots from the larger samples display better linearity than those from the smaller samples.

4.2.1.3 Near-field effects

Most of the traces showed the presence of near-field effects in varying degrees, Figure 4.1. This is not uncommon in past experience with bender element tests on

unstabilised soils, among which were tests conducted by Mancuso and Vinale (1988), Brignoli et al. (1996) and Jovičić et al. (1996). Elaboration on the subject based on previous work was given in Section 2.4.3.

Sánchez-Salinero et al. (1986) suggested keeping the ratio of L/λ between 2 and 4, where the lower limit was meant to avoid near-field effects, and the upper limit was to cater for attenuation via damping (Section 2.4.3). In Table 4.1 it is shown that the L/λ values for both sets of samples only fall within the above range when frequencies are higher than 9 kHz, where the near-field effects of the corresponding signals were found to be less significant. Jovičić et al. (1996) recommended mechanical remediation which involved manipulating the shape and frequency of the input shear wave (Section 2.4.3). However it was thought that such manipulations could not only be inconveniently time-consuming, but could also adversely increase the subjectivity of the interpretation method.

4.2.1.4 Attenuation

Although higher frequencies are sometimes preferred to avoid near-field effects, the guideline recommended by Sánchez-Salinero et al. (1986), as discussed in the previous section (Section 4.2.1.3), ought to be used with caution. At higher frequencies the energy-absorbing nature of soil makes it ineffective in sustaining prolonged and effective dynamic interaction between the bender element and the soil, hence resulting in attenuation.

According to Brignoli et al. (1996), input waves with $f_{in} \geq 5$ kHz tend to generate received signals of considerably lower frequencies than the sent ones. This was however not observed in the present work, where the input frequencies employed in the tests generally ranged from 7 to 15 kHz. From the frequency decomposition of both the input and output signals (via Fast Fourier transform, FFT), it was shown that the dominant frequency component in the output signal strongly represented that of the input signal. Nevertheless, the amplitude of the output signal was observed to reduce with increased input frequency, which obviously indicated the effect of attenuation.

4.2.2 Determination of shear wave arrival time

As mentioned in Section 2.4.4, in spite of the various techniques explored to date, no one method seems to stand out as being superior to the others. The different techniques were therefore explored by the Author. The first three methods discussed below are those in the time domain category, while the last two are based on frequency domain analysis.

The results are based on signals from tests on the samples of two different sizes (Section 4.2.1) and are presented in Table 4.2 as well as in Figure 4.3.

4.2.2.1 Visual picking

This method is perhaps the simplest and most straightforward method of all, as elaborated in Section 2.4.4.1. The method depends on a visual determination of the first major positive departure of the received signal from zero amplitude, where the shear wave arrival time and velocity defined are denoted by t_o and v_o respectively. There is no complication if the received signal remains flat before a clear cut deflection on the plot (Figure 4.4), but due to the effects of background noise, near-field effects or dispersion, the first sign of the trace rising can be difficult to identify.

4.2.2.2 First major peak-to-peak

The shear wave travel time is defined as the time interval between the positive peak of the transmitted signal and the first major peak on the received signal, $t_{pk\text{-}pk}$, and the shear wave velocity is represented by $v_{pk\text{-}pk}$ (Section 2.4.4.2). An example is shown in Figure 4.5 with the same signals as used in Section 4.2.2.1. It may seem to be a better method than the visual picking of the first deflection point as it is not affected by distortion of the received signal or by near-field effects, but again this method relies on the quality of the signals. A received signal with little distortion, hence minimal dispersion, makes the definition of the first major peak more reliable. Also, it may be noticed in Figure 4.5 that the first major peak in the received signal is not of the highest amplitude, which indicates the influence of dispersion.

4.2.2.3 Cross-correlation

Cross-correlation essentially measures the level of correspondence between the transmitted and received signals (Section 2.4.4.3). Using the same signals as before, an example of the method is illustrated in Figure 4.6, where the cross-correlation function is plotted alongside the transmitted and received signals.

Ideally, in the present work, the maximum cross-correlation function was supposed to correspond with the first major positive peak in the received signal. However, the first positive peak rarely had the highest magnitude, and thus did not produce the maximum

cross-correlation function. This resulted in a misleading interpretation of the travel time, which was determined by a subsequent peak in the received trace.

4.2.2.4 Cross-spectrum

The cross-spectrum method works in the frequency domain of the signals, where the shear wave arrival time or velocity is derived from the phase diagram (Section 2.4.4.4). An example of a 'wrapped' phase plot is shown in Figure 4.7a. Every major reversal (negative slope) of the plot represents a missing cycle. By subjecting the phase data to an 'unwrapping' process, the missing cycles are accounted for and a monotonic phase plot is obtained, Figure 4.7b. Referring to Viggiani and Atkinson (1995) in Section 2.4.4.4, the slope of a linear regression line (α) fitted through data points over a range of frequency, presumed to be common to both signals, gives the so-called 'group travel time', $t_{cs} = \alpha / 2\pi$ (Eq.2.9).

As pointed out in Section 2.4.4.4, the line-fitting performed on the phase plot to obtain t_{cs} is an average of the actual varying group velocity (tangential slope of the plot). The non-linearity of the plot depicting change of phase velocity with frequency clearly shows dispersion, resulting in a mismatch of the phase and group velocities (see Table 4.3 and Figure 4.8).

4.2.2.5 Comparison of shear wave arrival time determination methods

Referring back to Table 4.2 and Figure 4.3, summarising the shear wave velocities obtained from the four methods, it appears that v_o, v_{pk-pk} and v_{cc} tend to converge at higher frequencies, whereas the v_{cs} values were consistently lower than the other three velocities. This observation agrees with the comment by Arroyo (2001) that t_{cs} tends to be significantly larger than the arrival times defined in the time domain. On the other hand, Arroyo (2001) also reported that t_o was always lower than t_{cc} but that was not observed in this test series.

In general, the visually picked t_o is perhaps most influenced by subjectivity, depending on both signal quality as well as the judgement exercised to determine the arrival time. Determination of t_{pk-pk} may escape the near-field effects, but still affected by the criterion set for the first major peak (e.g. when the first peak is not of the largest magnitude). The t_{cc} method, despite the laborious data manipulation procedure, is still fundamentally influenced by the signal quality, seeing how closely the cross-correlation

function (labelled as 'CC' in the plot) follows that of the received signal, Figure 4.6. The differences between the shear wave velocities defined with the three methods therefore clearly reflect the uncertainty of the time domain interpretation methods, due to various influencing factors as described in Section 2.4.3.

Nevertheless, the shear wave arrival time in the present work was determined using the visual picking method (see Section 3.4.2). This was mainly due to the fact that the method was simple, direct and less time-consuming. Also, based on comparison of the results from the various methods in Table 4.2 and Figure 4.3, there was no evidence that the other methods were more superior than the visual picking method. In Figure 4.3, the scatter of the shear wave velocity data defined with the other methods (i.e. v_{cc}, $v_{pk\text{-}pk}$ and v_{cs}) does not appear to be less significant than that observed in the visually picked ones (i.e. v_o).

Referring to Section 2.4.4.6, there is still uncertainty regarding the best shear wave arrival time definition method, be it in the time or frequency domain. However, based on the literature review, there seems to be more confidence in the potential of the frequency domain methods (e.g. Arroyo 2001, Greening et al. 2003, Greening and Nash 2004). Although assessment in the frequency domain could reveal more information about the soil-wave interaction, the extra data processing involved could inadvertently eclipse the primary advantage of the BE test- its simplicity.

4.2.2.6 Phase and group velocities

As mentioned in Section 4.2.2.4, non-linearity of the unwrapped phase diagram indicates dispersion (see Figure 4.7b). By plotting the angular frequency, $\omega = 2\pi f$ (Eq. 2.10), against the wave number, $k = \phi/L$ (ϕ = unwrapped phase), the phase and group travel velocities (v_{ph} and v_{gr}) are defined directly from the secant and tangential gradients respectively (Section 2.4.4.5). The plot is simply a -90° rotation of the original unwrapped phase, ϕ, against the frequency, f, plot. Conversion of the unwrapped phase, ϕ, to wave number, k, is based on conventional wave theory as follows:

$$\text{Wave number, } k = 2\pi/\lambda \quad \text{(Eq. 4.1)}$$

$$\text{Wavelength, } \lambda = 2\pi L/\phi, \quad \text{(Eq. 4.2)}$$

where L = travel distance and ϕ = phase in radians (Theron et al. 2003).

Hence, $k = \phi/L$ (Eq. 4.3)

The plots for a frequency range of 0 – 20 kHz as obtained from samples S1 and L1 (f_{in} = 7 kHz) are shown in Figure 4.2 as examples. By compiling the phase and group velocities from the two plots (see Table 4.3 and Figure 4.8), it becomes clear that the phase velocities increase slightly with frequency and are generally more uniform above 6 kHz. On the other hand, the group velocities fluctuate throughout the frequency range with intermittent surges, having only a small number of points which correspond with the phase velocities. This mismatch between the two velocities is attributed to a significant influence of dispersion in the signal. Similar evidence was also presented by Arroyo (2001), as discussed in Section 2.4.4.5.

It should be noted too that reversal trends in the unwrapped phase (Figure 4.2) are depicted as negative velocities on the plots in Figure 4.8. The corresponding v_{ph} and v_{gr} at various frequencies can be found in Table 4.3. For instance, point 'X' in Figure 4.2a shows a marked decrease in phase by the reversed trend at 19 kHz. The tangential gradient at point 'X' automatically gives an absurd negative v_{gr} ($\approx$ -8152 ms^{-1}), as shown in Figure 4.8a. It is unclear as to why reversal of the unwrapped phase occurred, but inefficiency of the unwrapping process could be a possible cause.

The extremely high positive v_{gr} in Figure 4.8b (corresponding to the marked circle, 'Y', in Figure 4.2b) is another example of the effect of the unwrapping procedure applied to the phase data. In Figure 4.2b, there were actually intermediate data points between the two points within circle 'Y' (at 10 kHz and 10.5 kHz), and those points had reversed phases. Due to the frequency resolution chosen for the plot (0.5 kHz), the phase reversal was missed, resulting in the seemingly unchanged angular frequency, ω, between the two points. It can be seen from this example that the consequence of an inadequate unwrapping process is very significant for the definition of v_{gr}, as the local gradients are involved.

The study of the dispersive nature of shear waves propagating through cemented soils and the refinement of arrival time interpretation were not the major objectives of this thesis. However, the conclusion was reached, that because of dispersion, the determination of shear wave arrival time remains difficult, depending on judgement and the method applied. It is therefore important to employ a consistent interpretation method and to exercise consistent judgement in any test series.

4.2.3 Influence of strength measurement method

As mentioned in Section 3.5, two methods were employed to measure the undrained shear strength of the stabilised materials, i.e. unconfined compressive strength and vane shear tests. The unconfined compressive strength test was carried out on the kaolin and Swedish clay samples, while the vane shear test was conducted on the Malaysian clay samples. The undrained shear strength, c_u, was measured directly in the vane shear test, whereas the unconfined compressive strength, q_u, was halved to obtain the corresponding value.

Several pairs of nominally identical samples were tested using both methods to examine the consistency of the measurements, Figure 4.9. This was initially aimed at determining a correction factor linking the strengths from the two measurement methods. Unexpectedly, it was found that the vane strengths were consistently about twice the strengths from the unconfined compressive strength tests. This was considered unusual as the measured vane strength is commonly lower than that of the unconfined test (e.g. Skempton 1948, Wroth 1984).

To ensure that the equipment was not faulty or wrongly calibrated, the proving ring of the unconfined compressive strength apparatus was recalibrated but the calibration factor was almost unchanged compared with the one made at the beginning of tests on the stabilised samples. The calibration factor for the proving ring was 1.458 N/div prior to the tests and 1.443 N/div at the end of all tests (Section 3.5.3). Following that, the proving ring was manually loaded with dead weights of known values to further confirm the calibration.

The vane shear apparatus was unfortunately not able to be calibrated with the means available in-house. Nevertheless by testing a ready-mixed pottery clay, comparisons were made between measurements from the laboratory vane shear (with 12.7 mm diameter vanes) and two hand vanes (with 19.0 mm diameter vanes). The laboratory vane shear tests were conducted on 100 mm diameter and 76 mm high samples, while the hand vane tests were carried out on a bulk sample to avoid the confining effect. The results are presented in Table 4.4. Firstly, it can be seen that both the hand vanes (Hand Vanes 1 and 2) produced very similar results. Secondly, measurements with the laboratory vane shear apparatus gave slightly lower values than those from the hand vanes. Based on these observations, it is believed that performance of the laboratory vane shear apparatus was satisfactory.

The axial strain at failure, ε_f, in the unconfined compressive strength tests for kaolin and Swedish clay samples is shown in Figure 4.10. For kaolin, except at low strengths, the failure strain generally ranged between 0.5 % and 2.5 % (Figure 4.10a). The Swedish clay samples had failure strains between about 2.5 % and 5.5 % (Figure 4.10b). This is consistent with the observation made by other researchers on stabilised soils (e.g. Sugiyama et al. 1980, Uddin et al. 1997, Lee et al. 2005), where the samples showed high peak or failure strengths at very low strains (Section 2.3.2 and Figure 2.14).

Overall, the failure strains do not appear to have a strong relationship with strength, although some high values were associated with relatively low strengths ($q_u < 100$ kPa), as seen in the kaolin data.

4.2.4 Correlations of strength with shear wave velocity and small strain shear stiffness

The relationships between undrained shear strength (c_u), shear wave velocity (v_s) and maximum shear modulus (G_o) for the three stabilised clays are presented in Figure 4.11. The correlations between c_u and v_s in Figure 4.11a were established by taking the average bulk densities of the stabilised clays: 1.70 Mg/m^3 for stabilised kaolin samples, 1.56 Mg/m^3 for stabilised Malaysian clay samples and 1.68 Mg/m^3 for stabilised Swedish clay samples. The corresponding relationships between c_u and G_o for the three stabilised clays are presented in Figure 4.11b. Both linear and non-linear correlations between c_u, v_s and G_o were established as follows.

Linear correlations:

Stabilised kaolin

$c_u = 0.644 \times 10^{-3} G_o$; $c_u = 1.095 \times 10^{-3} v_s^2$ (Eq. 4.4)

Stabilised Malaysian clay

$c_u = 1.473 \times 10^{-3} G_o$; $c_u = 2.254 \times 10^{-3} v_s^2$ (Eq. 4.5)

Stabilised Swedish clay

$c_u = 1.105 \times 10^{-3} G_o$; $c_u = 1.856 \times 10^{-3} v_s^2$ (Eq. 4.6)

Non-linear correlations:

Stabilised kaolin

$c_u = 0.003x10^{-7}G_o^2 + 0.492x10^{-3}G_o$; $c_u = 8.670x10^{-10}v_s^4 + 0.836x10^{-3}v_s^2$ (Eq. 4.7)

Stabilised Malaysian clay

$c_u = -0.026x10^{-6}G_o^2 + 1.927x10^{-3}G_o$; $c_u = -0.064x10^{-6}v_s^4 + 3.005x10^{-3}v_s^2$ (Eq. 4.8)

Stabilised Swedish clay

$c_u = -0.003x10^{-6}G_o^2 + 1.433x10^{-3}G_o$; $c_u = -8.467x10^{-9}v_s^4 + 2.407x10^{-3}v_s^2$ (Eq. 4.9)

Similar correlations with unconfined compressive strength, q_u, can be obtained by simply doubling the coefficients on the right hand side of the above equations.

It is evident from the plots in Figure 4.11 that the undrained shear strength is strongly related to v_s, and hence G_o, and that this relationship can be expressed using either a linear or polynomial correlation. However, the polynomial regression gives a slightly better fit.

The present samples were prepared in the laboratory under better controlled conditions than would occur on site; in situ samples of the same composition and curing period would not necessarily have yielded such high strengths and stiffnesses. Also, the different correlations established for the three clays show that the relationship is at least dependent on the base clay mineralogy. Therefore such correlations are site specific, regardless of the binders used for stabilisation. Nevertheless they could be useful as a guide to the undrained shear strength of any particular stabilised clay based on the shear wave velocity measured with a seismic test, without having to perform actual strength evaluation on site or on retrieved samples in the laboratory.

These strong correlations give further support to relationships found by other researchers (Sections 2.3 and 2.4.5). For instance, an alternative power law relationship fitted to the Swedish clay data from the present work, $c_u = 0.0382v_s^{1.437}$ (Eq. 4.10), compares well with the correlation proposed by Mattsson et al. (2005), as shown in Figure 4.12. However, curvature of the plot by Mattsson et al (2005) was significantly influenced

by data points in the strength range above 100 kPa, as there were relatively few data in the lower range (Figure 2.33).

The v_s versus q_u plot for cement-stabilised clay by Porbaha et al. (2005) shows very high strength and stiffness characteristics, Figure 2.11b. In Figure 4.13, data from the present work with the stabilised kaolin and Swedish clay are combined with data by Porbaha et al. (2005), and plotted as q_u versus v_s. Interestingly, although not comparing like with like in terms of clay type, the present data seem to occupy the lower stiffness and strength range in a compatible manner. The combined plot indicates a non-linear relationship between q_u and v_s, where the improvement in small strain shear stiffness is more significant in the lower strength range. Porbaha et al. (2005) fitted linear regression lines on the individual data sets (i.e. columns A324, B366 and B374; see Figure 2.11b), which could be misleading and potentially overestimate the column's mechanical properties and performance.

In Figures 4.14 a and b, comparisons between the sample pairs of kaolin and Swedish clay are shown in terms of unconfined compressive strength and maximum shear modulus. Each pair of samples had the same composition and curing period. Results from the BE tests appear to have been repeatable to within about 20 % while the unconfined compressive strength tests produced results with repeatability to within about 25 % for both clays. Figures 4.15 a and b show similar plots for the Malaysian clay but with undrained shear strength values as measured using the vane apparatus. Here the results were repeatable to within approximately 30 % for the BE tests and 13 % for the vane shear tests. These variations could explain the scatter observed in the correlation plots shown in Figures 4.11, as well as in the forthcoming Section 4.2.5.3 (Figure 4.19).

The scatter in both Figures 4.14a and 4.15a highlights the error in strength measurement, be it with the unconfined compressive strength apparatus or the vane. Strength testing using the compression machine was based on uniaxial loading principles, but there were inevitably errors from bedding at the ends of the samples and non-symmetrical distortion of the samples during the tests. Also the sample pairs would not have been truly identical. Preparation of the samples in compacted layers could have contributed to the failure modes of the cemented samples. The lower layers were unavoidably more compacted, and hence stronger than the upper layers. Therefore, instead of failing along a diagonal shear plane as normally observed in unstabilised clay samples, the top layer sometimes deformed in a mushroom shape, leaving the lower layers quite

intact. Failure with vertical splits along the length of the sample was also observed in the tests, indicating non-uniform stress distribution within the sample. Some examples of the failure modes are illustrated in Figure 4.16, where the photographs were taken immediately after the unconfined compressive strength tests.

Measurement of strength using the vane shear apparatus encountered problems with the stiffer samples. Initial penetration of the vane sometimes formed deep cracks in the sample, which then affected the accuracy of the measurement as the vane was rotated to shear the soil.

4.2.5 Contributing factors to the improved properties

Apart from the mineralogy and plasticity of the base clays, the factors governing the properties of the stabilised materials are the water content, stabiliser content and curing period. Studies of these factors are quite prolific, recent work having been carried out by Uddin et al. (1997), Horpibulsuk et al. (2003) and Lee et al. (2005), as described in the various sections in Chapter 2.

The individual effects for stabilised kaolin are described in the following sections to show the significance of each. This is possible due to the availability of data on the kaolin samples prepared with various water and cement contents from dry mixes. The proportions of constituents in kaolin samples were probably more reliable than those of the natural clays (Malaysian and Swedish clays), which were remoulded at the natural water content.

4.2.5.1 Water content effect

The plots of c_u and G_o against curing period (grouped according to the initial water contents) for kaolin samples are shown in Figures 4.17 a and b. Each figure contains data from samples of various initial water contents but the same cement content (zero cement content included). As easily perceived, samples with the least water content (42 %) have the highest c_u and G_o values. Taking the 42 % water content data for example, the addition of 9 % cement increased c_u and G_o by factors of 37 and 42 (after 28 days) respectively, as compared to the unstabilised base clay.

In terms of the rate of increase of c_u and G_o with time, there was no significant difference between the samples with various water contents. This is very likely due to the small quantities of cement present in the samples, which require equally small amounts of water to form the chemical bonds with hydration. In fact, the amount of water needed to

chemically bond with the cement is merely 25 % of the weight of the cement to achieve at least 95 % hydration (Neville 1995). So regardless of the initial clay water content, the cementation skeleton would have been the same for all the samples. With higher water contents, the cementation effect was offset by the presence of "excess" water in the samples, therefore resulting in lower strength and stiffness values in comparison with samples with lower water contents.

The uncemented samples showed only a very slight increase in c_u and G_o with time. This is clearly illustrated in c_u and G_o versus curing period plots for samples with 0 % cement content, Figures 4.17a and b. This observation is attributed to the ageing effect which is commonly observed in unstabilised clay samples (Bjerrum and Lo 1963, Schmertmann 1991).

4.2.5.2 Stabiliser content effect

Figures 4.18 a and b depict c_u and G_o plotted against curing period, but the data are grouped according to the binder contents. As can be readily perceived, for any given initial water content, the most significant improvement in c_u and G_o is observed in the samples with the highest cement content. This is similar to observations reported by other researchers, an example of which was shown in Figure 2.14 (in terms of strength increase).

In general, for a given curing period (i.e. 28 days) and cement content (i.e. 9 %), the improvement in c_u ranged between a factor of 37 and 69, with samples having higher water contents showing a more significant proportional increase. The stiffness, G_o, was seen to increase by a factor of 42 to 99, similarly with more significant proportional increases for samples with higher water contents. Both increases were based on comparisons with c_u and G_o of the uncemented samples, which were taken as datum values to assess the improvement.

4.2.5.3 Curing period effect

In Figures 4.19 a and b, c_u and G_o were both normalized with the seventh day values, and were plotted against curing period (C) normalised with 7 days (7d) for the different stabilised clays. It can be seen from the plots that the rate of strength improvement during the first week is higher than that during the following three weeks. This observation indicates that the hydration process was more active in the first 7 days, after which the chemical reaction slowed down as the small amounts of binders were mostly hydrated.

Errors incurred in the measurements were compounded with normalisation, as can be observed in the scatter of the data in Figure 4.19, especially so with the strength measurements. Referring back to Figures 4.14 and 4.15, in spite of the acceptable differences between measurements from the pairs of samples, the compounded error was evident in the normalised comparisons. Nevertheless the normalised plots do show that the improvement of c_u and G_o with time exhibit a trend which is seemingly unaffected by the clay type, initial water content, binder type and quantity. By comparing the power law expression for each clay type (given in Figure 4.19), it can be seen that the variation is not significantly large, particularly for the two natural clays (i.e. Malaysian and Swedish clays).

From a compilation of normalised strength data (normalised with the 28-day strength) of several Asian clays, Horpibulsuk et al. (2003) reported that strength gain over time follow a single pattern, regardless of the property differences between them (Figure 2.17). The proposed correlation, along with the upper and lower boundaries, are plotted with data from the present tests in Figure 4.20. Note that the Malaysian clay was excluded from the comparison as the strength was measured with the vane shear apparatus; hence no q_u data are available. It is obvious that the data scatter mainly above the proposed expression, and that the gradient for both the clays would have been much gentler. Notwithstanding the measurement errors significantly obscuring the normalised expressions, this raises the question of whether or not the generalised expression proposed by Horpibulsuk et al. (2003) is substantially valid for all stabilised clays.

4.3 One-dimensional compressibility tests

The one-dimensional compressibility tests consisted of tests conducted in the oedo-BE cell and the standard oedometers, following procedures detailed in Section 3.6. The data presented in this section are from both types of test, analysed and discussed separately but occasionally compared and discussed collectively. A summary of all the oedometer tests conducted can be found in Tables 4.6 and 4.7, which will be further elaborated in this section.

4.3.1 Duration of curing process

The 7-day curing period for all samples in the oedo-BE tests (Section 3.6.2) was initially decided upon for two reasons: firstly, the time constraint on the number of tests to

be carried out with the single oedo-BE cell and, secondly, the trends of strength and small strain shear stiffness gain over time from the unconfined tests. Referring to Figures 4.17 and 4.18, the relative plateaus of G_o with time after 7 days suggest that prolonged curing would not have significantly reduced the compressibility. Nevertheless this is undeniably a much shorter time compared to the 1 month curing period recommended by Uddin et al. (1997) based on oedometer tests on cement-stabilised Bangkok clay (Section 2.5.2 and Figure 2.35).

The justification for the 7-day curing period is further illustrated in Figure 4.21, where the increases of G_o over the 7-day curing period in the oedo-BE cell are plotted alongside the unconfined test data. An extrapolated line for G_o in the oedo-BE cell is also included, derived from the normalised unconfined test results (see Figure 4.19b) for the corresponding sample. The seventh day oedo-BE G_o value was used in the normalised equation (i.e. G_{o7d}) to predict the evolution of G_o for up to 28 days. The reasonable match between the G_o values measured in both tests up to 7 days shows the consistency of the sample preparation methods. In general, the trend of G_o gradually flattened after a week as mentioned earlier. However some mismatches are seen in samples MC3 and SC10. These are probably due to inconsistent initial water contents of the base clays, as different bulk samples of the clays were used to prepare the test samples.

Figure 4.22 shows an example (Sample MC1.5) of the change in shear wave signals throughout the 7-day curing period, starting from the time when the test was first set up (within an hour after the sample was prepared in the cell). Apart from the obvious shorter travel time (first major deflection), the amplitude of the signal improves over time too. These two observations reflect the increased stiffness of the material as hydration of the cement proceeded with time. The improvement was most significant during the first 24 hours, after which the rate gradually reduced, but still kept rising. This can be seen in the corresponding trend of G_o-time plot for MC1.5 in Figure 4.21.

Subsequently standard oedometer tests were conducted with comparable 28-day old and 7-day old samples, as will be further discussed in Section 4.3.3. The compression curves of samples with the same stabiliser content but different curing periods (i.e. 7 and 28 days) fold into one from a very early stage in the tests, Figure 4.23. There was very little improvement in settlement reduction, if any, arising from extending the curing period, and this implies that the extra cementation networks formed within the older samples were probably destroyed at the beginning of the tests.

4.3.2 Nominal 'zero' vertical stress

As samples were subjected to unloading-reloading loops, where the unloading steps ended with no weights on the hanger, the vertical stress, σ_v, was then nominally 'zero'. However, the nominal 'zero' vertical stress when a sample was fully unloaded was really greater than zero due to the mass of the top or loading caps in either oedometer.

The oedo-BE had a top cap that weighed 1.6 kg, which was conveniently compensated in the loading process by friction from the o-ring used to seal the top cap, but was imposing a vertical stress on the sample upon full unloading (when the friction force reversed). Since the true friction of the o-ring during unloading was not quantifiable, it was logical to assume that the mass of the top cap, at least, was acting down on the sample at 'zero' vertical stress. By dividing the corresponding force by the surface area of the sample, an equivalent vertical stress of about 2 kPa was obtained. Therefore, all final unloading steps in the unloading-reloading loops of the oedo-BE samples were assumed to end at 2 kPa instead of 0 kPa.

The standard oedometers did not have complications from o-ring friction. Also, with the intention of avoiding difficulties of plotting data on a logarithmic stress scale (abscissa), the samples were unloaded to 12.5 kPa instead of 'zero'. However the mass of the loading caps corresponded to about 2 kPa of vertical stress and that was the nominal 'zero' vertical stress used for the initial stresses at the beginning of these tests.

4.3.3 Compressibility of the stabilised clays

Compression curves of the three stabilised clays are presented in Figure 4.23, combining loading data only from both types of oedometer test. The discrepancy at low stresses for unstabilised samples, between Swedish clay samples SC0 (standard oedometer test) and SC0_7d (oedo-BE test) for example, is probably attributed to bedding errors and friction losses at the o-ring and along the cell wall. Note that all settlement data were corrected for the stiffness of the oedometer frames only, as the bedding errors were impossible to ascertain with confidence.

It is also immediately obvious that cementation had major positive effect on the compressibility behaviour, though there was no evidence that the effect was more pronounced in the 28-day samples compared to the 7-day ones. This lends further support to the justification of 7-day curing period as discussed in Section 4.3.1.

With the induced cementation, final settlements were effectively reduced by 67 % and 79 % respectively for kaolin and Swedish clay with the highest stabiliser contents (i.e. 3 % and 10 %). The Malaysian clay was evidently 'under-stabilised' even at the highest cement content, with compressibility reduced by a mere 5 % for the standard oedometer tests, and 42 % for the oedo-BE tests.

Overall, the kaolin samples were the most controlled in terms of initial water content. Not surprisingly, therefore, kaolin has the best agreement between the results of the two types of test. The two natural clays, unfortunately, do not always display similarly good matches. The Malaysian clay results, especially, show poor agreement between results of the 3 % cement content samples, where the MC3 curve (oedo-BE) lies well above the MC3_7d (standard oedometer) one.

The comparison between the water contents of the samples, initial (w_i) and final (w_f), from both tests is given in Figure 4.24. Note that w_i was taken from sub-samples of the fresh mix of base clay and binder. There was fairly good agreement between values of w_i from samples for both tests (Figure 4.24a). However, values of w_f do not compare as well, with the oedo-BE samples showing higher moisture contents at the end of the tests, especially with the Malaysian clay samples (Figure 4.24b). This is consistent with the lower compressibility exhibited by the oedo-BE samples (e.g. MC3 and SC0).

One hypothesis is that o-ring friction loss varied from one sample to the next in the oedo-BE cell. The o-rings sealing the top cap and base of the oedo-BE cell occasionally suffered from adhesion of the sample material, which was squeezed out of the cell during loading. This increased friction loss could have reduced the total vertical load transferred to the sample, hence diminishing the compression under the given (or assumed) vertical stress. In retrospect, the 'under-stabilised' nature of the Malaysian clay samples (as mentioned above) could have caused the initially (relatively) soft material to squeeze into the gap between the o-ring and the cell wall. The possible effect of the friction losses will be discussed in detail in Section 4.3.8.

A second hypothesis is that the small differences in the initial water content of the natural clay samples could have contributed to the discrepancy observed in the two oedometer test results. To illustrate this point, an example with the Malaysian clay samples, MC3 and MC3_7d, is given as follows:

MC3

Taking the initial weight of the sample, W, as 831.8 g, and the initial water content, w_i, as 72.3 %, the dry weight of the sample, W_s, is 482.9 g. The amount of cement, W_c, required to produce the 3.0 % cement stabilisation as intended would be 14.5 g. Comparing this value with the 13.0 g (equivalent to 2.4 %) that was actually added to the mix (based on an average initial water content for the Malaysian clay of 74.0 %), the sample was apparently stabilised with 0.6 % less cement than it was intended to be.

MC3_7d

With the same calculation as above, W = 128.6 g, w_i = 70.2 %, and hence W_s = 75.6 g. The amount of cement required, W_c, would be 2.3 g. The actual amount added to the sample was 2.0 g (equivalent to 2.6 %), again based on an average initial water content of 74.0 %. The sample was also under-stabilised, short of 0.4 % cement to achieve the 3.0 % as intended.

From the above calculations, it can be seen that the two samples were not identical in terms of cement content. Therefore a mismatch between the two compression plots is only to be expected. However the samples were both stabilised with less binder than intended, with the oedo-BE sample having the lower binder content of the two, and this is in conflict with the observation, in Figure 4.23, that the compression line of MC3 lies above that of MC3_7d, clearly indicating MC3 to be a stiffer material. Therefore, it does not appear that the second hypothesis explains the observation.

The complete oedo-BE test results, depicting all the loading, unloading and reloading paths, are presented in Figure 4.25. Insets are included, where necessary, for clarity of presentation at small stress levels. From the unloading-reloading loops, it is apparent that the stabilised soils behave very similarly to normal clays, with an almost complete recovery upon reloading. The ratio of compression index to recompression index, C_c/C_r, for the base clay and stabilised clay samples ranges from 11.3 to 17.1 and from 16.7 to 126.9 respectively, indicating that the settlement incurred in the pre-yield range is very small for the stabilised samples. This explains the importance and advantages of utilizing deep-mixed columns within the pre-yield zone, beyond which settlements can be significant.

Finally, some limitations of the experimental set up affecting the compressibility assessment should be mentioned here. The vertical displacement measurements were registered by either a dial gauge (for the standard oedometers) or an LVDT (for the oedo-BE cell). Both devices made external measurements with a resolution of 0.001 mm at the top of the loading cap. As the settlements of the cemented samples pre-yield were very small, accuracy of the measurements at this stage was inevitably compromised by the compression of the porous media as well as bedding errors. Compression of the porous plastic sheets at the top and bottom of the oedo-BE samples could have masked the actual vertical strains. Attempts to account for the compressibility of the porous media were futile due to excessive creep of the material, making any correction factor difficult to determine with confidence. Therefore no corrections were made to the final settlement readings of the oedo-BE tests with regard to the stiffness of the porous media. Also, bedding errors in the initial and subsequent loading stages could not be accounted for accurately to obtain the actual settlements of the samples, both in the oedo-BE and standard oedometer tests.

4.3.4 Void ratio and degree of saturation of stabilised samples

The void ratio (e) and degree of saturation (S_r) of the oedometer samples were determined at the beginning and end of the tests (Tables 4.6a and 4.7a). However, the calculations were subject to complications.

Firstly, due to hydration and pozzolanic reactions within the sample, the specific gravity, G_s, of the composite material evolved from its initial value. Initially, G_s of the clay and cement mixture could be estimated from the proportions of solid materials present. The G_s value of the mixture was higher than that of the base clay due to the presence of stabilisers (i.e. cement or lime-cement) which have higher G_s values than the clay particles. However, the process of hydration chemically bonded the cement or lime-cement with water, therefore changing the G_s of the (transformed) solid material. From specific gravity tests conducted on both the base clays and the stabilised samples, it was found that the final G_s values of the cemented clay remained almost unchanged from the base clay values, Table 4.5. The final measured values were used in the calculations for Table 4.6 and 4.7.

For comparison, Lorenzo and Bergado (2004) reported that the G_s value of cemented clay reduces slightly with increasing cement content (Section 2.3.2 and Figure 2.18). Although non-hydrated cement has a much higher G_s value than the base clay (for Bangkok clay $G_s = 2.68$), the G_s of the hydrated material must be comparable.

The second factor that complicated the calculations of S_r and e, at the end of the tests, was the inaccuracy of the measured settlement sustained by the sample. This was predominantly due to the difficulties of separating bedding error from the actual settlements recorded. Upon the first application of a given load, the immediate change in the sample height was almost certainly the combination of "real" immediate settlement of the sample (e.g. squeezing of air pockets within the sample) and bedding settlement. The bedding errors could be attributed to several causes, such as readjustment of the top cap and base due to uneven upper and lower surface contacts, as well as compression of the unsaturated porous plastic sheets or porous discs. Also, the loss of water in a cemented sample is a combined effect of soil consolidation and binder hydration. Therefore the amount of water drained from the sample does not represent the volume change as normally assumed in a normal oedometer test on a "fully saturated" sample. Recognising these difficulties, the final settlements recorded for each sample were used to calculate the final volume. Two different assumptions were made to calculate the final e and S_r values. The first assumption was that the sample was fully saturated at the end of the test, S_{rf}= 1.0, while the second assumption was S_{rf} = S_{ro} (S_{ro} = initial degree of saturation, S_{rf} = final degree of saturation).

The first assumption was initially thought to be logical as any air in the sample would have been compressed under the stresses applied during the test; hence the probability of achieving full saturation would have been high. Table 4.6a gives a summary of the results for each sample in both the oedo-BE and standard oedometer tests. Corresponding back calculations for the final settlements based on either e_o or e_f were attempted, but only those based on e_o are shown in Table 4.6b. This is due to the uncertainty of the final sample height and G_s at the end of the tests, as mentioned above.

Similar tabulations are included in Tables 4.7a and b for the second assumption (S_{rf} = S_{ro}). This assumption implies that any entrapped air in the voids within the sample did not compress, even under high stresses.

The higher average e_o, and hence lower S_{ro} values, of the oedo-BE samples compared with those of the standard oedometer samples (Table 4.6a) suggest that the compaction effort in the oedo-BE cell was less effective, in spite of the fact that it was scaled up from the effort applied to the standard oedometer samples (see Section 3.6.1).

Close examination of Tables 4.6 and 4.7 indicates that not all anomalies are eliminated with either of the two assumptions regarding saturation. The bedding errors can

be deduced from the final void ratio by performing back calculations, as shown in the right most column, (ΔH_m - ΔH_c), of Tables 4.6b and 4.7b. Negative values are attributed to errors since the actual measured settlements, ΔH_m, which include the bedding errors cannot be lower than the back calculated settlements, ΔH_c. Because the assumption of $S_{rf} = S_{ro}$ produces fewer anomalies, it is perhaps a better representation of the state of the samples after the tests.

4.3.4.1 $e/e_{100} - \sigma_v'$

Normalising the void ratio of the sample at the end of each loading stage with the void ratio at 100 kPa (e_{100}), the post-yield values of e/e_{100} are plotted against σ_v' on a logarithmic scale in Figure 4.26. Note that for the data sets with yield stresses above 100 kPa, extrapolation of the virgin compression curves was carried out to estimate e_{100}. In Figure 4.26a, the e values were obtained by using e_o and working forward with the settlement data. In this method, the effect of hydration on the initial water content was not accounted for. In Figure 4.26b, the e values were obtained by working backwards on the settlement data with e_f, from the assumption of $S_{rf} = S_{ro}$ (see Section 4.3.4). Horpibulsuk et al. (2004) suggested that there could be a universal trend to fit uncemented and cemented clays on such a normalized plot.

It is apparent in both Figures 4.26 a and b that results from both the oedo-BE and standard oedometer tests are in agreement. Also, the normalised correlations from both calculation methods are not significantly different. However, the trend for each clay type does vary and the gradients are all lower than that proposed by Horpibulsuk et al. (2004) to different degrees (see Section 2.5.2 and Figure 2.40b). The gradient for Malaysian clay agrees more closely with the proposed relationship compared to those of kaolin and Swedish clay, suggesting that properties of the base clay, such as the plasticity characteristics, could be influential. The Malaysian clay is classified as a high plasticity clay (see plasticity indices for Malaysian clay in Table 3.2), and so are the Bangkok clay (LL= 103 %, PI = 60) and the Ariake clay (LL = 125 %, PI = 65), which were included as stabilised clays in the proposed generalised plot by Horpibulsuk et al.

4.3.5 Relationship between compressibility and small strain shear stiffness

It was shown in the oedo-BE experiments that G_o increased while the sample compressed during a single loading stage, an example of which is shown in Figure 4.27a.

Note that steps in the G_o trend were due to the limited resolution of the shear wave arrival time, t_o, which was rounded off to the nearest 10 μs. Some of the stiffness increase was gained during consolidation when water was expelled from the sample. However even with the decrease of settlement rate (at the onset of secondary compression), G_o clearly maintains an upward trend. This particular loading increment was held for an extended period of 10 days to study the stabilised material's creep behaviour. As the plot shows, it was not possible to distinguish the end of primary consolidation from the trend of G_o alone.

A slight initial dip in G_o with loading during normal consolidation was sometimes observed in the test series with the oedo-BE cell. The same observation was reported by Santamarina and Fam (2001), who tried to validate the cause as the collapse of cementation bonds with loading. However, the same phenomenon was present in dry kaolin sample, as reported by Afifi and Woods (1971), showing that it is not unique to cemented material. There is a possibility that the dip is due to the breakage of cementation bonds in stabilised soils, whereas in unbonded soil interlocking particles, under stress from the previous loading, are disturbed and rearranged, causing the initial slight decrease in G_o.

During an unloading stage, G_o remained almost unchanged, as can be seen in Figure 4.27b. This indicated that much of the stiffness gained with previous loading was locked in even when σ_v and σ_h were substantially removed.

An example of the variation of v_s and G_o during an entire test is illustrated in Figures 4.28 a and b respectively. Also marked on the two plots is the yield stress as defined using the reloading line fitting method (to be described in Section 4.3.6.3). Prior to yield, G_o was nearly constant, indicating a strong cementation maintaining the structure even under stress (see insets). Following yield, the significant increase of G_o is mainly attributed to the influence of effective stress, where any loss of stiffness due to the breakdown of cementation bonds was outweighed by consolidation of the sample. A comparison of the overall test results showed that, during final unloading, a less significant decrease in G_o occurred in samples with higher binder content. This could further suggest that cementation has a major contributory effect on the overconsolidated behaviour of stabilised soils.

The constrained modulus, M_o, was obtained using two methods:

- Derivation from tangents to the compression curve at stress levels where the shear wave velocity was measured at the end of a loading stage, M_{otan}.

- Derivation from the line joining two consecutive points on the compression curve, M_{omid}. It is denoted such as to represent the approximate value of M_o midway between two stress levels.

Plots of both M_{otan} and M_{omid} against σ_v' are shown in Figure 4.29. Generally there was good agreement between the two, though M_{omid} was usually higher than M_{otan}. The plots follow a similar trend, corresponding with the characteristics of the respective compression curves in Figure 4.23. M_o gradually decreased with loading as the sample approached yield. Once yield had occurred, the increase of effective stress resulted in a steady rise in M_o. Note that the unusually sharp increase of M_o pre-yield in some of the samples with higher binder contents was attributed to bedding errors, which resulted in overestimation of the initial settlement and underestimation of the initial M_o.

The correlations of M_{otan} with v_s and G_o for all the stabilised samples are shown next in Figure 4.30, together with regression lines derived by Burns and Mayne (2002) for natural clays. Only post-yield values are included in the plot; v_s and hence G_o remained largely constant prior to yield and did not correlate well with M_o. It is perhaps worth mentioning that Burns and Mayne (2002) obtained the regression lines from various sources of natural soil data without making a distinction between normally and overconsolidated clays. Although the present data fit the relationships fairly well, especially the M_o - G_o correlation, for practical purposes with stabilised soils, it is perhaps essential to differentiate the pre- and post-yield condition.

Such correlations (i.e. both M_o - v_s and $M_o - G_o$) could be very useful for predicting the compressibility of stabilised soils post-yield, provided v_s and hence G_o is known, without conducting time-consuming oedometer tests. However, it is appreciated that the stiffness pre-yield is equally, if not more important (Section 4.3.3), from both the design and practical points of view. It is unfortunate that the experimental set-up was unable to measure pre-yield compressibility accurately enough to establish complementary correlations (Section 4.3.3).

4.3.6 Definition of effective yield stress (σ_y')

Various methods for determining the effective yield stress (σ_y') for natural soils have been developed over the years, the earliest being the graphical procedure developed by Casagrande (1936), which is still widely adopted today. Later methods were published by

Schmertmann (1953), specifically for heavily overconsolidated clay, and Butterfield (1979), whose method involves plotting the compression curve on natural logarithmic scales.

As part this research, three methods were used to determine σ_y'. The first two methods were conventional means for yield stress definition in consolidation tests, while the third one was an adaptation by the Author.

4.3.6.1 Casagrande's method

On a plot of vertical strain (ε_v) or void ratio (e) against log σ_v', horizontal and tangential lines were drawn through the point of maximum curvature. The angle formed by the two lines was bisected equally. The post-yield or normal consolidation line (NCL) was extended to intersect the bisecting line and σ_y' was defined at the intersection, as illustrated in Figure 4.31.

4.3.6.2 Butterfield's method

With both the specific volume (v) and σ_v' plotted on logarithmic scales, the pre-yield and NCL data points were fitted with best fit lines respectively. The intersection of the two lines indicated σ_y', an example of which is shown in Figure 4.32.

4.3.6.3 Reloading line (RL) fitting method

After fitting a linear regression line (RL) through the reloading data points of the first unloading-reloading cycle post-yield, a parallel line was then drawn to represent the initial loading, with an intercept of the σ_v' axis at 2 kPa. The 2 kPa datum was coincidentally the same for both the oedo-BE and standard oedometer tests as explained in Section 4.3.2. σ_y' was then determined by extending the NCL and finding the intersection with the initial loading line (Figure 4.33).

4.3.7 Correlations of yield stress with small strain shear stiffness and strength

Yield stresses, σ_y', obtained using the RL fitting method (Section 4.3.6.3) are plotted against G_o in Figure 4.34, with tentative linear trend lines drawn. The Malaysian and Swedish clays seem to share the same correlation, and a common best fit line and equation for both sets of data are shown on the plot. It is undeniably a rather sparsely populated plot

with an appreciable amount of scatter, so any definitive conclusions cannot be reached. However, it is likely that a correlation exists for a given clay type. Horpibulsuk et al. (2004), for instance, established a correlation between σ_y' and q_u for three stabilised clays, namely Bangkok, Tokyo and Ariake clays. As q_u has been proven to be related to v_s, and hence G_o (e.g. Hird and Chan 2005, Mattsson et al. 2005), it follows that σ_y' and G_o must be linked in some way.

In Figure 4.35 σ_y' is plotted against q_u, where the strength values were extracted from corresponding unconfined test results for samples with the same initial water and stabiliser contents, as well as matching curing time. Only data points from kaolin and Swedish clay are presented because the strengths of the Malaysian clay samples were measured with a laboratory vane instead of the unconfined compressive strength apparatus. Also included in the plot are correlations established by Horpibulsuk et al. (2004) for stabilised Bangkok and Ariake clays, $\sigma_y' = 1.4q_u$ and $2.2q_u$ respectively. In spite of the appreciable scatter, kaolin does show a reasonably linear correlation, though the ratio of σ_y' to q_u is lower than expected. A relevant factor here may be the way yield stresses were determined, as the variations can be significant with different methods of definition. Yield stresses obtained with different methods for the oedo-BE and standard oedometer tests are presented in Table 4.8.

4.3.8 Lateral stress and K_o values

Lateral stresses, σ_h, were measured throughout each load increment or decrement. Figures 4.36 a and b illustrate the typical evolution of σ_h during a loading and an unloading stage, with the settlements also included. Measurements from both strain gauge circuits (i.e. A1/A2 and A3/A4) are shown on the same plot. Note that readings at the end of the previous loading stage could not be represented on the log time scale.

The mismatch between the results from the two circuits could be due to a differential stress distribution along the circumference of the cell. This could be due to test material being squeezed out into the gap between the o-ring and the cell wall (see Section 4.3.3). Also, it could be due to tendency of the circuits to drift, as shown in Table 3.7, whereby the lateral stress reading with the cell empty varied slightly before and after a test. However, despite this lack of stability in the circuits at zero lateral stress, both circuits almost always gave the same pattern of results as the test progressed.

Figure 4.36a shows an immediate surge in σ_h with immediate settlement upon loading, attributable to the sudden build-up of pore pressure within the sample. This is followed by the primary consolidation phase, where σ_h gradually decreased as the excess pore water drained and effective stresses increased. With the onset of secondary compression, the reduction in σ_h was eventually replaced by a plateau as creep progressed.

Figure 4.36b shows the unloading sequential to the loading increment referred to above. Initial steps in the graphs of both settlement and σ_h were due to the lifting of individual weights from the hanger at the beginning of the test stage. It is interesting to note that σ_h stabilised relatively quickly as swelling continued. Cementation is thought to be partially responsible for limiting the swelling.

From measurements of σ_h at the end of each increment or decrement, plots of σ_h against σ_v were derived, an example of which is given in Figure 4.37. Negative σ_h values on the plot indicate suction (i.e. negative total lateral stress) between the sample and the cell wall, which was not uncommon at lower stresses.

Values of K_o were obtained assuming zero pore pressure ($\sigma_h = \sigma_h'$):

$$K_o = \sigma_h / \sigma_v' \qquad \text{(Eq. 4.11)}$$

The K_o values are plotted against σ_v' for each loading stage, as shown in Figure 4.38. Note that negative values (resulting from suction) were considered erroneous and omitted from the plot. K_o increased steadily with σ_v' until the sample yielded (σ_y' = 138 kPa), where the value dipped slightly and then remained constant with the remaining load increments. This pattern of behaviour is not exclusive to stabilised clays but was also observed in cemented sand samples, as reported by Zhu et al. (1995) (see Section 2.5.5 and Figure 2.45). The increase of K_o with loading is attributed to the breakdown of cementation bonds. However, the relatively constant K_o trend post-yield is not unlike the behaviour of unstabilised soils during normal consolidation (e.g. Edil and Dhowian 1981).

Based on the widely used empirical relationship for predicting K_o during normal consolidation (Jaky 1944):

$$K_o = 1 - \sin\phi' \qquad \text{(Eq. 4.12)}$$

where ϕ' = angle of shearing resistance, K_o values for the unstabilised samples may be estimated. The K_o values for unstabilised kaolin, Malaysian clay and Swedish clay are 0.64, 0.59 and 0.53, giving ϕ' values of 21°, 24° and 28° respectively. These ϕ' values are within the range expected from their plasticity indices (Wood 1990 and Rossato et al. 1992), with the value for kaolin being comparable to the value that Rossato et al. (1992) obtained from a triaxial compression test, i.e. 20°.

The cemented clays, being stiffer materials, produced K_o values that were, on the whole, slightly lower than the uncemented samples, Table 4.9. This is consistent with observations on cemented sands as reported by Zhu et al. (1995), where the K_o values reduced with higher cement contents (Section 2.5.5). However, there could be a suspicion that the values are a little too low because of friction losses at the o-ring and the ring wall. Potential friction losses from the o-ring sealing the top cap of the oedo-BE cell have been mentioned and discussed in Sections 3.4 and 4.3.3 respectively. It was assumed that the friction loss was entirely countered by the self weight of the cap, but if the friction loss was greater than this, then the vertical stresses applied to the samples would be less than presumed. The true K_o values would consequently be higher than those presented in Table 4.9.

As mentioned earlier (Section 3.4), the aspect ratio of the oedo-BE ring was lower than that of the standard oedometer. This could adversely increase the friction loss between the sample and the ring wall (Shibuya et al 2004). In order to evaluate the significance of the friction losses, a check on the immediate lateral stress responses upon loading (first 3 – 5 seconds), expressed in terms of the ratio $(\Delta\sigma_h/\Delta\sigma_v)_{immediate}$, was carried out for each individual test. This was based on the same principles as a 'B-value' check routinely performed in triaxial tests to ascertain the saturation of samples, as given in Part 8 of BS 1377 (1990).

The ratio of $(\Delta\sigma_h/\Delta\sigma_v)_{immediate}$ can be seen to be comparable to the 'B-value' by considering an undrained loading condition immediately after a load was applied to the sample. The sudden surge in pore pressure should ideally, in saturated soil, equal the total applied vertical stress and result in an equal change of total lateral stress acting on the ring. However, the measured $(\Delta\sigma_h/\Delta\sigma_v)_{immediate}$ ratio was 0.76 on average (all tests), corresponding to a possible wall friction loss of 24 %. A hypothetical friction losses correction factor, F_r, was then defined based on the average $(\Delta\sigma_h/\Delta\sigma_v)_{immediate}$ ratio in each individual test (Table 4.10). By applying F_r to the experimentally obtained K_o values,

corrected values, termed K_o', were calculated, as shown in the last three columns of the same table. This correction resulted in K_o values (i.e. K_o') which far exceeded the reasonable range.

Based on the discussion above, it is recognised that friction losses at the o-rings and along the cell wall were present in the oedo-BE tests. Unfortunately, they were not quantifiable accurately enough to justify any appropriate corrections to the test results.

In view of the fact that friction losses alone were unlikely to account for the $(\Delta\sigma_h/\Delta\sigma_v)_{immediate}$ values that are lower than expected, a second hypothesis put forward is the lack of saturation of the samples. Tables 4.6a and 4.7a list the values of void ratio (e) and degree of saturation (S_r) for all the samples in both types of oedometer test. It is apparent that the samples were not fully saturated, especially in the instrumented cell. The scaled up compaction effort did not produce samples of as high a degree of saturation as those in the standard oedometers, particularly with high stabiliser contents. This seems to be a plausible explanation for the low $(\Delta\sigma_h/\Delta\sigma_v)_{immediate}$ values obtained.

4.4 Model column tests

The model column tests were conducted as described in Section 3.7, but only with kaolin and Swedish clay samples. The Malaysian clay could not be tested due to a shortage of material.

The tests were primarily intended to investigate the one-dimensional compression behaviour of the columnar inclusion system and to make comparisons with predicted behaviour based on information from the individual sample tests, i.e. the test results reported in Section 4.3. Changes in small strain shear stiffness (G_o), as well as lateral stresses (σ_h), were also made to widen the scope of study.

4.4.1 Curing of samples

Figure 4.39 illustrates the gain in v_s measured over the 7-day curing period in the centre of the composite samples. Data from the individual stabilised sample tests are included for comparison. Although the shear wave velocity increased over time and eventually reached a plateau, as normally seen in the oedo-BE tests (Section 4.3.1), the columns did not have as significant an increase as the individual cemented samples. The reason could have been the migration of additional water from the base clay around the

column, leading to a cured cemented column that contained a higher water content, and hence had lower stiffness, than its whole sample counterpart. It could also be due to difference in compaction effort. The whole samples may have been more effectively compacted than the columns in the composite samples.

The tendency of cemented soils to shrink with curing might have contributed to the decrease in lateral stresses during curing, Figure 4.40. However, the effect of shrinkage was much less prominent compared with the homogeneous test samples (i.e. Samples K3 and SC10). This is simply due to the modest proportion of the column diameter, which is 38 % of the cell diameter. Measurements from both circuits are shown in the plots. Note that for Sample K3, there is a significant dip in the reading from circuit A3/A4 at 7 days, deviating significantly from the previous trend. The reason for this is unknown, but an electrical anomaly is thought to be the most plausible explanation.

4.4.2 Compressibility of the composite systems

Figure 4.41a shows the compression curves from the column tests for kaolin (i.e. COL1 and COL2), while Figure 4.41b presents results from the Swedish clay column test (i.e. COL3). Both plots include compression curves of the base and cemented clays tested as whole samples for comparison. Note that for the cemented samples (i.e. K3_7d and SC10_7d), compression curves from the standard oedometer tests are shown, due to the availability of data at higher stresses (for making predictions). In Figure 4.41a, there are two compression curves for the same type of composite sample, serving as a check on the consistency of the sample preparation method.

As to be expected, settlements of the composite system fall between those of the uncemented and cemented clays. Predicted curves are also included in the plots, using the actual average effective vertical stress acting on the surface of the composite sample, $\sigma_v'_{AVG}$, as tabulated in Table 4.11. Taking an equal strain assumption (Baker 2000), and based on the surface areas of column and surrounding unstabilised clay, values of force on each component (i.e. P_{COL} and P_{SOIL}) were calculated by multiplying the appropriate effective vertical stress, $\sigma_v'_{COL}$ or $\sigma_v'_{SOIL}$, with the respective surface area. Note that σ_v' for the column and soil at a common strain are significantly different. The values of $\sigma_v'_{AVG}$ was next obtained by dividing the total load, ($P_{COL} + P_{SOIL}$), by the total surface area of the composite sample. By comparing the last two columns of the table, the difference between $\sigma_v'_{AVG}$ and $\sigma_v'_{TEST}$ can be assessed.

The predicted curves on Figures 4.41 a and b were in fairly good agreement with the model column tests. It appears that a reasonable prediction of the compression curve of a composite system can be obtained based on the oedometer test data of both the base clay and cemented samples. However, as it was unlikely that the soft base clay surrounding the column could have completely prevented radial expansion of the column in the centre, the column probably did expand radially with loading instead of deforming only in the vertical direction.

Compression curves for the composite samples are comparable to the one shown by Feng (2000), where a composite sample of stabilised Taipei lacustrine clay was tested in a standard oedometer (Figure 2.39). Feng's work enables good comparisons, partly because of the low cement contents (maximum 6 %) in his samples. The compression curve of his composite system displayed no distinct yield point. As for the present work, the average effective yield stress, $\sigma_y'_{AVG}$, was identified using the Casagrande and RL fitting methods, Table 4.12. $\sigma_y'_{AVG}$ can be reasonably defined from the compression curves of COL1 and COL2 (Figure 4.41a), but the definition is less certain for COL3 (Figure 4.41b), due to the unusually shaped virgin compression curve. Also, Feng's compression curve lay parallel to that of the unstabilised base clay, a feature which is only pronounced in the COL1 and COL2 tests. The initial virgin compression curve of COL3 is almost parallel to that of SC0, but the curve eventually deviates in an unexpected fashion, though the reason for that was unknown. This could be attributable to experimental errors (e.g. jamming of the o-rings).

4.4.3 Change in small strain shear stiffness

Figure 4.42 shows the change of the small strain shear stiffness, G_o, with increased effective stress. As v_s (and hence G_o) measurements were made in the column and not in the surrounding soil, the corresponding $\sigma_v'_{COL}$ values (from the compression curves of the homogeneous cemented samples, i.e. K3_7d and SC10_7d) were used for the plot. The effective yield stress of the column, $\sigma_y'_{COL}$, was defined from the compression curve of the homogeneous sample. The G_o curves of both the homogeneous sample and the column appear to follow a similar trend, but there is a consistent difference between the two measurements. This difference in G_o was registered right from the beginning and persisted through the rest of the tests. The differences in sample preparation method (i.e. compaction of the column) and curing environment were considered as possible causes of this mismatch. Also, the test conditions which the samples were subjected to were not exactly

similar; lateral expansion could have occurred in the column during compression, whereas no expansion was permitted for the homogeneous samples.

In Figure 4.43, G_o and vertical strain, ε_v, are plotted against the average effective vertical stress, $\sigma_v'_{TEST}$. The average effective yield stresses ($\sigma_y'_{AVG}$) of both the composite systems, as shown on the plots, were defined using the RL fitting method. Data of COL1 and COL2 show excellent agreement for both parameters, incidentally demonstrating the repeatability of the composite system tests (Figure 4.43a). In the COL1 and COL2 tests, G_o was observed to remain almost constant even after the composite system yielded. A significant rise in G_o did not occur until well into the higher stress range, suggesting that yielding of the composite system did not affect G_o of the column within. As for COL3 (Figure 4.43b), G_o showed a marked rise immediately post-yield, similar to the observations made in the other oedo-BE tests (see Section 4.3.5 and Figure 4.28).

4.4.4 Lateral stress and K_o values

The information on the average K_o values from both circuits for all the column tests is compiled in Table 4.13. Note that the K_o value from circuit A3/A4 for test COL3 is far lower than expected, and this is attributed to an electrical anomaly. Examples of the changes of lateral stress, σ_h', and K_o (from COL1) are presented in Figures 4.44 and 4.45, but for clarity only data from one circuit is included. The development of both σ_h and K_o follows a similar pattern as in the oedo-BE samples under loading (Section 4.3.8). By comparing the average K_o values in Tables 4.9 and 4.13 (but excluding the result of A3/A4 for COL3), it can be concluded that the overall average K_o values of the composite samples were not much different from those of the homogeneous ones.

The stresses on the column and base clay were not separately measured. However, as pointed out in Section 4.4.2 and evident in Table 4.11, the transfer of the vertical load to the composite sample was non-uniform between the column and the base clay, with the column taking a higher proportion of the load. Therefore the so called average K_o values shown in Table 4.13 are really not representative of the column behaviour.

By taking the measured lateral stresses in the tests ($\sigma_h'_{TEST}$) as average values applicable to both the column and soil components, separate coefficient of earth pressure, K values, for the components (i.e. K_{COL} and K_{SOIL}) were calculated, Table 4.14. Due to the higher stresses in the columns, K_{COL} is always significantly lower than K_{SOIL}. This is consistent with some lateral expansion of the column, as mentioned earlier in Section 4.4.3.

No visual observation of the column's deformation was available as no attempts were made to extrude and dissect the sample after the test. However, it would have been very difficult to remove the sample from the ring with minimal disturbance or damage. If the column did expand laterally under load, the radial displacement in the surrounding clay would have diminished gradually towards the ring wall. Therefore, the term K_o, as given to the values in Table 4.13, was perhaps misused. The values can at best be taken as a global representation of the response of the composite system under loading.

Table 4.1 Influence of input frequency on dispersion and attenuation

Sample: S1

f_{in}	t_o	v_o	λ	L/λ L = 61 mm	L/D	D/λ	G_o
kHz	ms	ms^{-1}	m				MPa
1	0.260	235	0.235	0.260	1.605	0.162	94
3	0.250	244	0.081	0.750		0.467	102
5	0.240	254	0.051	1.200		0.748	110
7	0.240	254	0.036	1.680		1.047	110
9	0.240	254	0.028	2.160		1.346	110
12	0.230	265	0.022	2.760		1.719	120
15	0.230	265	0.018	3.450		2.149	120
20	0.230	265	0.013	4.600		2.866	120

Sample: S2

f_{in}	t_o	v_o	λ	L/λ L = 61 mm	L/D	D/λ	G_o
kHz	ms	ms^{-1}	m				MPa
1	0.200	305	0.305	0.200	1.605	0.125	160
3	0.220	277	0.092	0.660		0.411	132
5	0.225	271	0.054	1.125		0.701	126
7	0.225	271	0.039	1.575		0.981	126
9	0.230	265	0.029	2.070		1.290	121
12	0.230	265	0.022	2.760		1.719	121
15	0.220	277	0.018	3.300		2.056	132
20	0.240	254	0.013	4.800		2.990	111

f_{in} = input frequency (kHz)

t_o = shear wave arrival time (visually picked) (ms)

v_o = shear wave velocity (based on visually picked arrival time) (ms^{-1})

λ = wavelength (m)

L = shear wave travel distance (tip-to-tip of BEs) (m)

D = diameter of sample (m)

Table 4.1 Influence of input frequency on dispersion and attenuation *(continued)*

Sample: L1

f_{in}	t_o	v_o	λ	L/λ L = 63 mm	L/D	D/λ	G_o
kHz	ms	ms^{-1}	m				MPa
1	-	-	-	-	0.553	-	-
3	0.200	315	0.105	0.600		1.086	166
5	0.230	274	0.055	1.150		2.081	125
7	0.230	274	0.039	1.610		2.913	125
9	0.220	286	0.032	1.980		3.583	137
12	0.230	274	0.023	2.760		4.994	125
15	0.230	274	0.018	3.450		6.243	125
20	0.230	274	0.014	4.600		8.324	125

Sample: L2

f_{in}	t_o	v_o	λ	L/λ L = 62 mm	L/D	D/λ	G_o
kHz	ms	ms^{-1}	m				MPa
1	-	-	-	-	0.544	-	-
3	0.215	288	0.096	0.645		1.186	139
5	0.220	282	0.056	1.100		2.023	132
7	0.220	282	0.040	1.540		2.832	132
9	0.220	282	0.031	1.980		3.641	132
12	0.210	295	0.025	2.520		4.634	145
15	0.200	310	0.021	3.000		5.516	160
20	0.200	310	0.016	4.000		7.355	160

f_{in} = input frequency (kHz)

t_o = shear wave arrival time (visually picked) (ms)

v_o = shear wave velocity (based on visually picked arrival time) (ms^{-1})

λ = wavelength (m)

L = shear wave travel distance (tip-to-tip of BEs) (m)

D = diameter of sample (m)

Table 4.2 Shear wave velocities from various arrival time definition methods

a. Sample S1 and S2

Sample	Diameter	Input Frequency	Shear Wave Velocity			
	D	f_{in}	ms^{-1}			
	mm	kHz	v_o	v_{pk-pk}	v_{cc}	v_{cs}
S1	38	1	235	555	254	52
		3	244	169	179	74
		5	254	161	226	57
		7	254	156	226	219
		9	254	218	277	195
		12	265	277	265	229
		15	265	277	277	223
		20	265	265	277	150
S2	38	1	305	1220	381	52
		3	277	218	254	55
		5	271	244	244	139
		7	271	244	290	162
		9	265	290	277	174
		12	265	290	277	164
		15	277	277	265	225
		20	254	277	277	232

v_o = shear wave velocity based on visually picked travel time (t_o)

v_{pk-pk} = shear wave velocity based on peak-to-peak travel time (t_{pk-pk})

v_{cc} = shear wave velocity based on cross-correlation function (t_{cc})

v_{cs} = shear wave velocity based on cross-spectrum method (t_{cs})

Table 4.2 Shear wave velocities from various arrival time definition methods *(continued)*

b. Sample L1 and L2

Sample	Diameter	Input Frequency	Shear Wave Velocity			
	D	f_{in}	ms^{-1}			
	mm	kHz	v_o	v_{pk-pk}	v_{cc}	v_{cs}
L1	114	1	-	-	-	24
		3	315	420	300	42
		5	274	315	332	45
		7	274	300	315	138
		9	277	305	290	138
		12	265	305	290	141
		15	265	298	290	137
		20	265	290	290	146
L2	114	1	-	-	-	31
		3	288	388	295	43
		5	282	295	270	212
		7	295	282	310	143
		9	282	326	295	102
		12	295	310	310	139
		15	310	310	295	141
		20	310	295	295	142

Table 4.3 Phase and group velocities

Sample S1

Frequency	**Shear Wave Velocity**		**Frequency**	**Shear Wave Velocity**	
f	**ms^{-1}**		**f**	**ms^{-1}**	
kHz	**v_{ph}**	**v_{gr}**	**kHz**	**v_{ph}**	**v_{gr}**
0.0	-	-	**10.5**	105	288
0.5	37	99	**11.0**	108	318
1.0	50	99	**11.5**	110	345
1.5	59	807	**12.0**	112	693
2.0	69	776	**12.5**	112	-427
2.5	77	29	**13.0**	114	-827
3.0	76	-320	**13.5**	118	364
3.5	84	952	**14.0**	120	373
4.0	99	256	**14.5**	123	276
4.5	103	92	**15.0**	125	252
5.0	101	67	**15.5**	127	293
5.5	91	41	**16.0**	129	302
6.0	83	788	**16.5**	131	216
6.5	84	-182	**17.0**	132	205
7.0	88	453	**17.5**	134	185
7.5	91	712	**18.0**	135	223
8.0	96	71	**18.5**	136	408
8.5	99	143	**19.0**	142	-8152
9.0	100	123	**19.5**	145	128
9.5	101	129	**20.0**	144	139
10.0	103	57			

Table 4.3 Phase and group velocities *(continued)*

Sample L1

Frequency	Shear Wave Velocity		Frequency	Shear Wave Velocity	
f	ms^{-1}		f	ms^{-1}	
kHz	v_{ph}	v_{gr}	kHz	v_{ph}	v_{gr}
0.0	-	-	**10.5**	105	160388
0.5	76	720	**11.0**	107	386
1.0	91	196	**11.5**	111	166
1.5	102	294	**12.0**	113	159
2.0	124	-368	**12.5**	114	-718
2.5	155	47	**13.0**	115	116
3.0	131	57	**13.5**	116	96
3.5	99	49	**14.0**	115	366
4.0	86	-343	**14.5**	114	-132
4.5	93	-2031	**15.0**	120	-964
5.0	103	201	**15.5**	130	157
5.5	107	205	**16.0**	134	169
6.0	107	309	**16.5**	134	138
6.5	108	299	**17.0**	135	157
7.0	113	174	**17.5**	135	154
7.5	115	127	**18.0**	135	125
8.0	115	164	**18.5**	136	105
8.5	115	179	**19.0**	135	153
9.0	117	131	**19.5**	131	159
9.5	117	71	**20.0**	134	156
10.0	109	2689876			

Table 4.4 c_u from hand vane and laboratory vane shear tests

	Laboratory vane shear test	Hand vane tests	
		Hand vane 1	Hand vane 2
Average c_u (kPa)	38.09	39.84	39.03

Table 4.5 Specific gravity (G_s) of oedo-BE and standard oedometer samples

Sample	Specific gravity (G_s)
K0	2.61
K1.5	2.63
K3	2.63
MC0	2.66
MC1.5	Not measured. Interpolated as 2.66.
MC3	2.66
SC0	2.73
SC5	Not measured. Interpolated as 2.74.
SC10	2.74

Table 4.6a S_r and e values for oedo-BE and standard oedometer samples **(S_{rf} = 1.0)**

		Initial Values					Final Values				
Sample	**G_s**	**w_i**	**ρ_{bo}**	**ρ_{do}**	**e_o**	**S_{ro}**	**w_f**	**ρ_{bf}**	**ρ_{df}**	**e_f**	**S_{rf}**
		%	**g/cm^3**	**g/cm^3**			**%**	**g/cm^3**	**g/cm^3**		
K0	2.61	49.23	1.63	1.09	1.38	0.93	39.97	1.79	1.28	1.04	**1.00**
K1.5	2.63	47.96	1.65	1.11	1.34	0.93	42.16	1.77	1.25	1.11	**1.00**
K3	2.63	47.18	1.65	1.12	1.34	0.93	45.08	1.75	1.20	1.19	**1.00**
MC0	2.66	72.26	1.53	0.89	1.99	0.96	43.18	1.77	1.24	1.15	**1.00**
MC1.5	2.66	72.51	1.50	0.87	2.05	0.94	40.89	1.80	1.27	1.09	**1.00**
MC3	2.66	70.17	1.51	0.89	1.99	0.94	48.77	1.72	1.16	1.30	**1.00**
SC0	2.73	62.14	1.60	0.98	1.77	0.96	30.79	1.94	1.48	0.84	**1.00**
SC10	2.74	54.21	1.55	1.01	1.76	0.86	43.79	1.79	1.25	1.20	**1.00**
K0_7d	2.61	49.57	1.68	1.12	1.33	0.97	37.43	1.81	1.32	0.98	**1.00**
K1.5_7d	2.63	48.72	1.69	1.13	1.32	0.97	40.03	1.79	1.28	1.05	**1.00**
K1.5_28d	2.63	48.72	1.69	1.14	1.31	0.98	40.10	1.79	1.28	1.05	**1.00**
K3_7d	2.63	47.80	1.69	1.15	1.30	0.97	40.67	1.79	1.27	1.07	**1.00**
K3_28d	2.63	47.80	1.69	1.14	1.30	0.97	40.25	1.79	1.28	1.06	**1.00**
MC0_7d	2.66	70.24	1.62	0.95	1.80	1.04	39.35	1.81	1.30	1.05	**1.00**
MC1.5_7d	2.66	69.09	1.58	0.93	1.85	1.00	34.61	1.86	1.39	0.92	**1.00**
MC1.5_28d	2.66	69.09	1.59	0.94	1.83	1.00	36.39	1.84	1.35	0.97	**1.00**
MC3_7d	2.66	68.41	1.58	0.94	1.84	0.99	34.81	1.86	1.38	0.93	**1.00**
MC3_28d	2.66	68.41	1.59	0.94	1.82	1.00	36.79	1.84	1.34	0.98	**1.00**
SC0_7d	2.73	64.98	1.63	0.99	1.76	1.01	29.69	1.96	1.51	0.81	**1.00**
SC5_7d	2.74	58.35	1.64	1.03	1.65	0.97	40.08	1.83	1.31	1.10	**1.00**
SC5_28d	2.74	57.46	1.68	1.07	1.57	1.01	38.89	1.84	1.33	1.07	**1.00**
SC10_7d	2.74	56.03	1.67	1.07	1.56	0.98	42.07	1.81	1.27	1.15	**1.00**
SC10_28d	2.74	55.93	1.67	1.07	1.56	0.98	40.80	1.82	1.29	1.12	**1.00**

Table 4.6b Back calculations of final settlements based on e_o **(S_{rf} = 1.0)**

Sample	H_o	H_f	e_o	e_f	$\Delta H_c = (\Delta e/1+e_o)(H_o)$	ΔH_m	$(\Delta H_m - \Delta H_c)$
	mm	mm			mm	mm	mm
K0	70.00	60.14	1.38	1.04	9.99	9.86	-0.13
K1.5	70.00	63.41	1.36	1.11	7.48	6.59	-0.90
K3	70.00	67.33	1.34	1.19	4.75	2.67	-2.08
MC0	70.00	48.24	1.99	1.15	19.75	21.76	2.01
MC1.5	70.00	46.02	2.05	1.09	22.11	23.98	1.87
MC3	70.00	53.02	1.99	1.30	16.28	16.98	0.70
SC0	70.00	47.87	1.77	0.84	23.54	22.13	-1.42
SC10	70.00	62.96	1.72	1.20	13.40	7.04	-6.36
K0_7d	18.78	15.37	1.33	0.98	2.84	3.41	0.57
K1.5_7d	19.10	16.40	1.32	1.05	2.20	2.70	0.50
K1.5_28d	18.60	15.68	1.31	1.05	2.06	2.92	0.86
K3_7d	18.97	16.51	1.30	1.07	1.87	2.46	0.59
K3_28d	19.05	16.55	1.30	1.06	1.99	2.51	0.52
MC0_7d	18.78	12.85	1.80	1.05	5.05	5.93	0.88
MC1.5_7d	19.83	13.51	1.85	0.92	6.45	6.32	-0.13
MC1.5_28d	19.87	13.02	1.83	0.97	6.07	6.85	0.78
MC3_7d	19.87	13.46	1.84	0.93	6.40	6.41	0.01
MC3_28d	19.75	13.39	1.82	0.98	5.88	6.36	0.48
SC0_7d	18.97	12.23	1.76	0.81	6.51	6.75	0.23
SC5_7d	19.87	14.99	1.65	1.10	4.13	4.88	0.75
SC5_28d	19.05	14.75	1.57	1.07	3.72	4.30	0.58
SC10_7d	19.83	16.34	1.56	1.15	3.18	3.49	0.31
SC10_28d	18.78	15.15	1.56	1.12	3.24	3.63	0.39

ΔH_c = back calculated final settlement

ΔH_m = measured final settlement

Table 4.7a S_r and e values for oedo-BE and standard oedometer samples ($S_{rf} = S_{ro}$)

Sample	G_s	Initial Values					Final Values				
		w_i	ρ_{bo}	ρ_{do}	e_o	S_{ro}	w_f	ρ_{bf}	ρ_{df}	e_f	S_{rf}
		%	g/cm^3	g/cm^3			%	g/cm^3	g/cm^3		
K0	2.61	49.23	1.63	1.09	1.38	0.93	39.97	1.72	1.23	1.12	**0.93**
K1.5	2.63	47.96	1.65	1.11	1.36	0.93	42.16	1.70	1.20	1.20	**0.93**
K3	2.63	47.18	1.65	1.12	1.34	0.92	45.08	1.67	1.15	1.28	**0.92**
MC0	2.66	72.26	1.53	0.89	1.99	0.96	43.18	1.74	1.21	1.19	**0.96**
MC1.5	2.66	72.51	1.50	0.87	2.05	0.94	40.89	1.74	1.23	1.16	**0.94**
MC3	2.66	70.17	1.51	0.89	1.99	0.94	48.77	1.66	1.11	1.39	**0.94**
SC0	2.73	62.14	1.60	0.98	1.77	0.96	30.79	1.90	1.45	0.88	**0.96**
SC10	2.74	54.21	1.55	1.01	1.72	0.86	43.79	1.65	1.15	1.39	**0.86**
K0_7d	2.61	49.57	1.68	1.12	1.33	0.97	37.43	1.79	1.30	1.00	**0.97**
K1.5_7d	2.63	48.72	1.69	1.13	1.32	0.97	40.03	1.77	1.26	1.08	**0.97**
K1.5_28d	2.63	48.72	1.69	1.14	1.31	0.98	40.10	1.77	1.27	1.08	**0.98**
K3_7d	2.63	47.80	1.69	1.15	1.30	0.97	40.67	1.76	1.25	1.10	**0.97**
K3_28d	2.63	47.80	1.69	1.14	1.30	0.97	40.25	1.76	1.26	1.09	**0.97**
MC0_7d	2.66	70.24	1.62	0.95	1.80	1.04	39.35	1.85	1.32	1.01	**1.04**
MC1.5_7d	2.66	69.09	1.58	0.93	1.85	1.00	34.61	1.86	1.38	0.93	**1.00**
MC1.5_28d	2.66	69.09	1.59	0.94	1.83	1.00	36.39	1.85	1.35	0.97	**1.00**
MC3_7d	2.66	68.41	1.58	0.94	1.84	0.99	34.81	1.85	1.37	0.94	**0.99**
MC3_28d	2.66	68.41	1.59	0.94	1.82	1.00	36.79	1.84	1.35	0.98	**1.00**
SC0_7d	2.73	64.98	1.63	0.99	1.76	1.01	29.69	1.96	1.51	0.80	**1.01**
SC5_7d	2.74	58.35	1.64	1.03	1.65	0.97	40.08	1.80	1.28	1.13	**0.97**
SC5_28d	2.74	57.46	1.68	1.07	1.57	1.01	38.89	1.85	1.33	1.06	**1.00**
SC10_7d	2.74	56.03	1.67	1.07	1.56	0.98	42.07	1.79	1.26	1.17	**0.98**
SC10_28d	2.74	55.93	1.67	1.07	1.56	0.98	40.80	1.80	1.28	1.14	**0.98**

Table 4.7b Back calculations of final settlements based on e_o ($S_{rf} = S_{ro}$)

Sample	H_o	H_f	e_o	e_f	$\Delta H_c = (\Delta e/1+e_o)(H_o)$	ΔH_m	$(\Delta H_m - \Delta H_c)$
	mm	mm			mm	mm	mm
K0	70.00	60.14	1.38	1.12	7.64	9.86	2.23
K1.5	70.00	63.41	1.36	1.20	4.88	6.59	1.71
K3	70.00	67.33	1.34	1.28	1.79	2.67	0.88
MC0	70.00	48.24	1.99	1.19	18.76	21.76	3.00
MC1.5	70.00	46.02	2.05	1.16	20.52	23.98	3.45
MC3	70.00	53.02	1.99	1.39	14.21	16.98	2.76
SC0	70.00	47.87	1.77	0.88	22.58	22.13	-0.45
SC10	70.00	62.96	1.72	1.39	8.51	7.04	-1.47
K0_7d	18.78	15.37	1.33	1.00	2.62	3.41	0.78
K1.5_7d	19.10	16.40	1.32	1.08	1.94	2.70	0.76
K1.5_28d	18.60	15.68	1.31	1.08	1.87	2.92	1.05
K3_7d	18.97	16.51	1.30	1.10	1.60	2.46	0.86
K3_28d	19.05	16.55	1.30	1.09	1.70	2.51	0.81
MC0_7d	18.78	12.85	1.80	1.01	5.31	5.93	0.62
MC1.5_7d	19.83	13.51	1.85	0.93	6.42	6.32	-0.10
MC1.5_28d	19.87	13.02	1.83	0.97	6.09	6.85	0.77
MC3_7d	19.87	13.46	1.84	0.94	6.32	6.41	0.09
MC3_28d	19.75	13.39	1.82	0.98	5.89	6.36	0.47
SC0_7d	18.97	12.23	1.76	0.80	6.57	6.75	0.18
SC5_7d	19.87	14.99	1.65	1.13	3.87	4.88	1.01
SC5_28d	19.05	14.75	1.57	1.06	3.76	4.30	0.54
SC10_7d	19.83	16.34	1.56	1.17	3.01	3.49	0.48
SC10_28d	18.78	15.15	1.56	1.14	3.10	3.63	0.54

ΔH_m = measured settlement,

ΔH_c = back calculated settlement

Table 4.8 Effective yield stresses (σ_y') defined with various methods

Sample	Effective yield stress, σ_y' (kPa)		
	Casagrande's method	Butterfield's method	Reloading line (RL) fitting method
K0	20	18	10
K1.5	67	65	63
K3	200	184	176
MC0	24	20	14
MC1.5	20	23	13
MC3	40	58	25
SC0	12.	5	3
SC10	155	145	138
K0_7d	29	24	12
K1.5_7d	68	65	57
K1.5_28d	80	68	54
K3_7d	265	247	217
K3_28d	300	270	232
MC0_7d	22	22	11
MC1.5_7d	22	19	13
MC1.5_28d	20	18	11
MC3_7d	28	19	18
MC3_28d	25	21	18
SC0_7d	Not interpretable.	Not interpretable.	1
SC5_7d	115	86	87
SC5_28d	120	84	87
SC10_7d	215	163	171
SC10_28d	215	152	147

Table 4.9 Average K_o values for the oedo-BE samples during normal consolidation

Sample	K_o		
	A1/A2	A3/A4	Average
K0	0.62	0.66	0.64
K1.5	0.64	0.54	0.59
K3	0.60	0.57	0.58
MC0	0.55	0.62	0.59
MC1.5	0.67	0.60	0.63
MC3	0.46	0.36	0.41
SC0	0.56	0.51	0.53
SC10	0.54	0.44	0.49

Table 4.10 Friction losses correction factors (F_r) and corrected K_o values (K_o') for oedo-BE samples

Sample	K_o (from tests)			Friction Losses Correction Factor, F_r		$K_o' = K_o/F_r$		
	A1/A2	A3/A4	AVG	A1/A2	A3/A4	A1/A2	A3/A4	AVG
K0	0.62	0.66	0.64	0.966	1.007	0.64	0.66	0.65
K1.5	0.64	0.54	0.59	0.869	0.860	0.73	0.62	0.68
K3	0.60	0.57	0.58	0.779	0.653	0.77	0.87	0.82
MC0	0.55	0.62	0.59	0.697	0.878	0.79	0.71	0.75
MC1.5	0.67	0.60	0.63	0.720	0.805	0.92	0.74	0.83
MC3	0.46	0.36	0.41	0.734	0.651	0.63	0.55	0.59
SC0	0.56	0.51	0.53	0.794	0.744	0.70	0.68	0.69
SC10	0.54	0.44	0.49	0.578	0.541	0.93	0.82	0.87

Table 4.11 Effective vertical stresses for the column and soil components in the column tests (see Figure 4.41)

COL1 and COL2

ε_v	$\sigma_v'_{SOIL}$	P_{SOIL}	$\sigma_v'_{COL}$	P_{COL}	$\sigma_v'_{AVG}$ (PREDICTION)	$\sigma_v'_{TEST}$
%	kPa	kN	kPa	kPa	kPa	kPa
0.5	2.9	0.02	75.0	0.09	13.3	18.0
1.0	3.8	0.03	100.0	0.11	17.7	27.0
1.5	5.1	0.03	150.0	0.17	26.0	28.0
2.0	7.6	0.05	210.0	0.24	36.8	32.0
4.0	18.0	0.12	300.0	0.34	58.7	50.0
6.0	32.0	0.22	420.0	0.48	88.0	76.0
8.0	50.0	0.34	550.0	0.62	122.2	117.0
10.0	76.0	0.51	700.0	0.79	166.1	176.0
12.0	117.0	0.79	880.0	1.00	227.2	255.0
14.0	165.0	1.11	1100.0	1.25	300.0	370.0

COL3

ε_v	$\sigma_v'_{SOIL}$	P_{SOIL}	$\sigma_v'_{COL}$	P_{COL}	$\sigma_v'_{AVG}$ (PREDICTION)	$\sigma_v'_{TEST}$
%	kPa	kN	kPa	kPa	kPa	kPa
0.5	2.2	0.01	62.0	0.07	10.8	5.4
1.0	2.5	0.02	100.0	0.11	16.6	14.0
1.5	2.8	0.02	120.0	0.14	19.7	16.0
2.0	3.1	0.02	150.0	0.17	24.3	19.0
4.0	5.3	0.04	245.0	0.28	39.9	31.0
6.0	9.5	0.06	360.0	0.41	60.1	44.0
8.0	14.0	0.09	480.0	0.54	81.3	62.0
10.0	17.5	0.12	635.0	0.72	106.7	100.0
12.0	22.0	0.15	820.0	0.93	137.2	200.0
14.0	29.0	0.19	1050.0	1.19	176.4	355.0

Table 4.12 Average effective yield stresses ($\sigma_y'_{AVG}$) for the column test samples

Sample	$\sigma_y'_{AVG}$ (kPa)	
	Casagrande's method	**RL fitting method**
COL1	25	24
COL2	28	27
COL3	22	17

Table 4.13 Average K_o values for the column test samples during normal consolidation

Sample	K_o		
	A1/A2	**A3/A4**	**Average**
COL1	0.58	0.57	0.58
COL2	0.58	0.56	0.57
COL3	0.53	0.25	0.39

Table 4.14 Effective lateral stresses (σ_h') and K values for the column and soil components in the column tests during normal consolidation

COL1

σ_v'$_{TEST}$	σ_h'$_{TEST}$		σ_v'$_{COL}$	K_{COL}		σ_v'$_{SOIL}$	K_{SOIL}	
	A1/A2	A3/A4						
kPa	kPa	kPa	kPa	A1/A2	A3/A4	kPa	A1/A2	A3/A4
50	23	20	325	0.07	0.06	21	1.08	0.96
100	50	51	500	0.10	0.10	38	1.32	1.34
200	111	109	780	0.14	0.14	92	1.21	1.19
400	236	235	1200	0.20	0.20	185	1.27	1.27

COL2

σ_v'$_{TEST}$	σ_h'$_{TEST}$		σ_v'$_{COL}$	K_{COL}		σ_v'$_{SOIL}$	K_{SOIL}	
	A1/A2	A3/A4						
kPa	kPa	kPa	kPa	A1/A2	A3/A4	kPa	A1/A2	A3/A4
50	21	11	290	0.07	0.04	17	1.24	0.65
100	51	38	490	0.10	0.08	39	1.31	0.98
200	109	103	740	0.15	0.14	80	1.36	1.29
400	234	243	1100	0.21	0.22	175	1.34	1.39

COL3

σ_v'$_{TEST}$	σ_h'$_{TEST}$		σ_v'$_{COL}$	K_{COL}		σ_v'$_{SOIL}$	K_{SOIL}	
	A1/A2	A3/A4						
kPa	kPa	kPa	kPa	A1/A2	A3/A4	kPa	A1/A2	A3/A4
50	4	15	430	0.01	0.03	11.5	0.35	1.30
100	37	28	640	0.06	0.04	17	2.15	1.64
200	106	45	830	0.13	0.05	21	5.05	2.14
400	225	103	1120	0.20	0.09	31	7.26	3.33

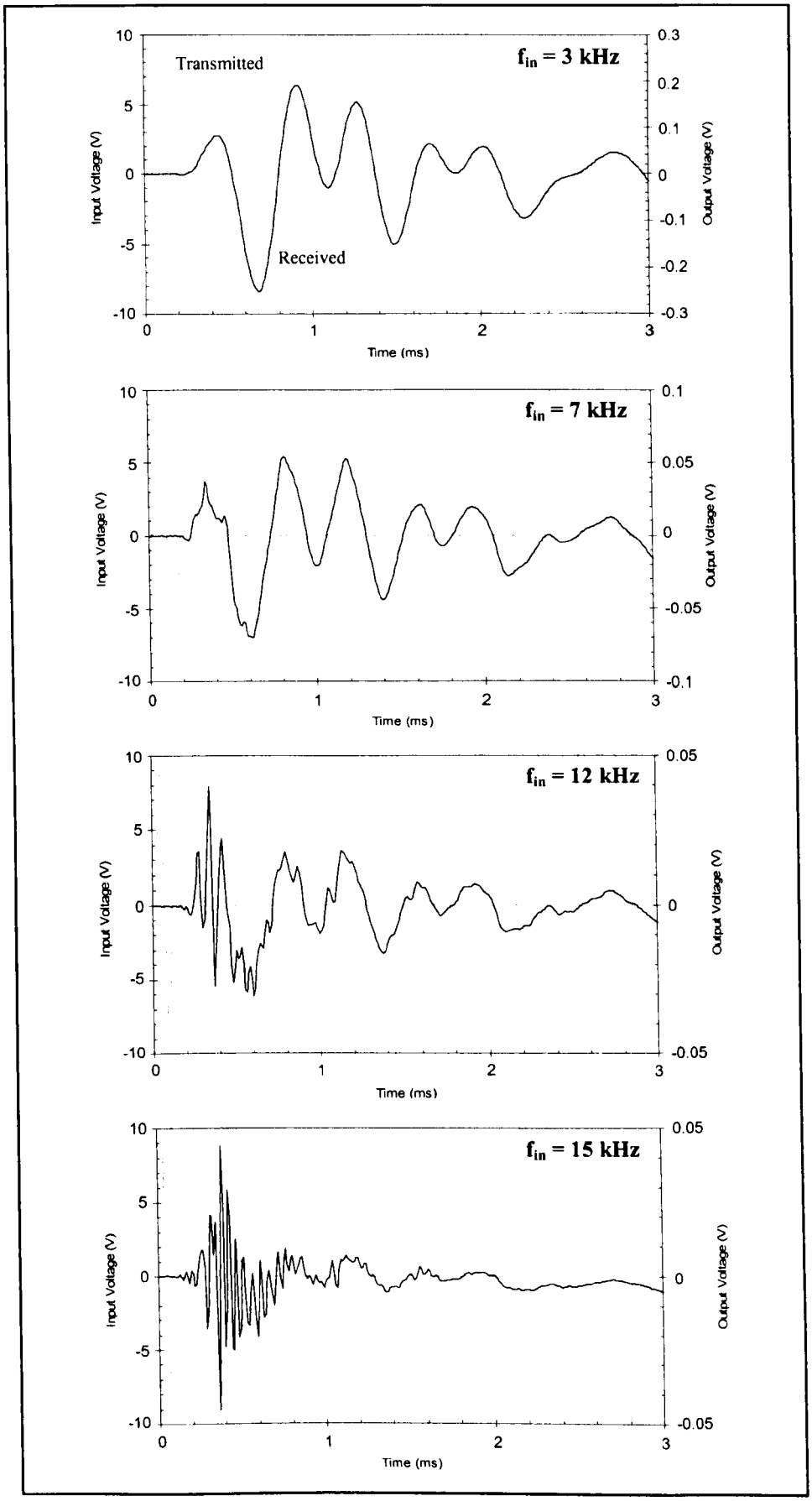

Figure 4.1a: Examples of transmitted and received signals- Sample S1.

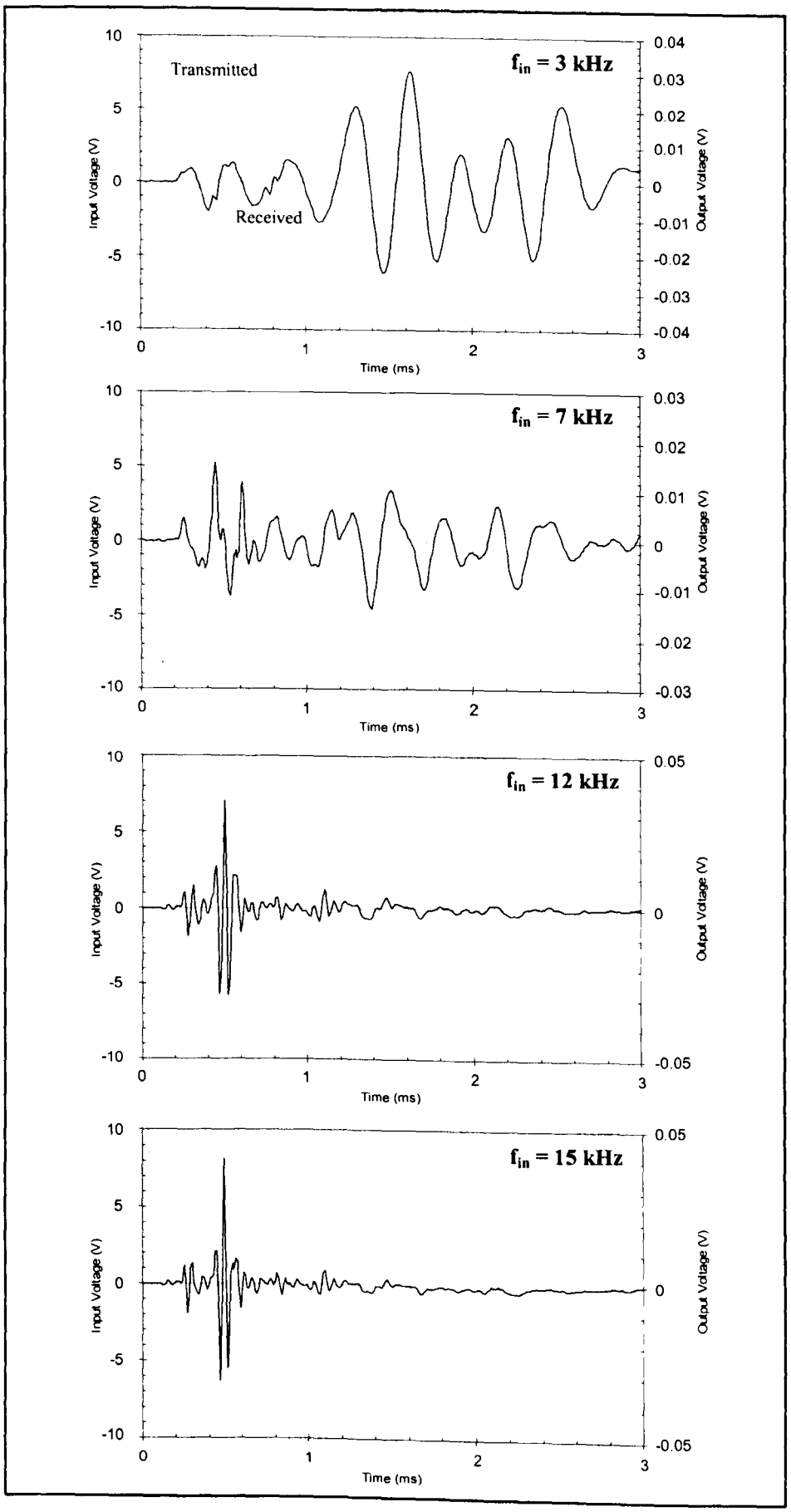

Figure 4.1b: Examples of transmitted and received signals- Sample L1.

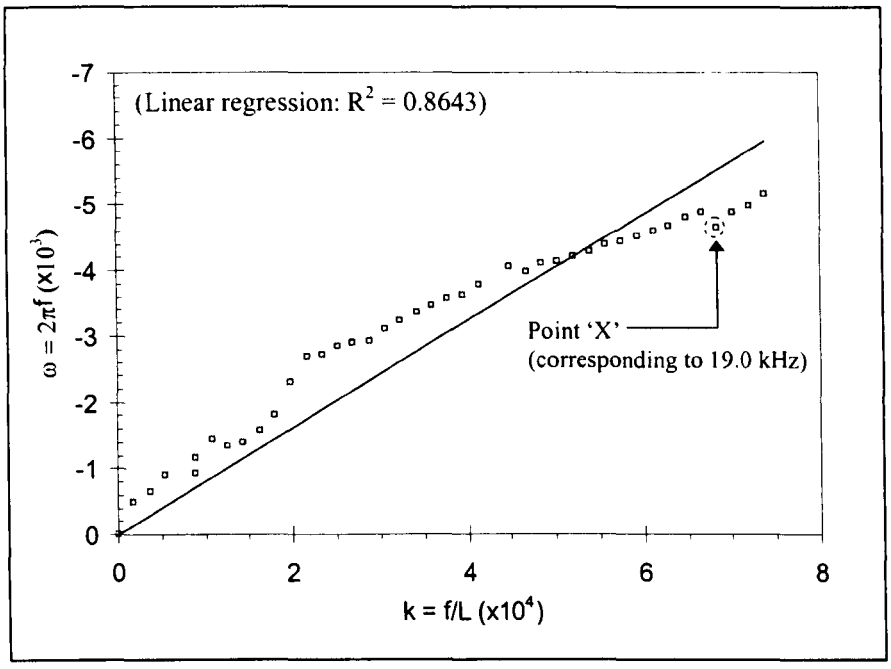

a. Sample S1 (f_{in} = 7 kHz).

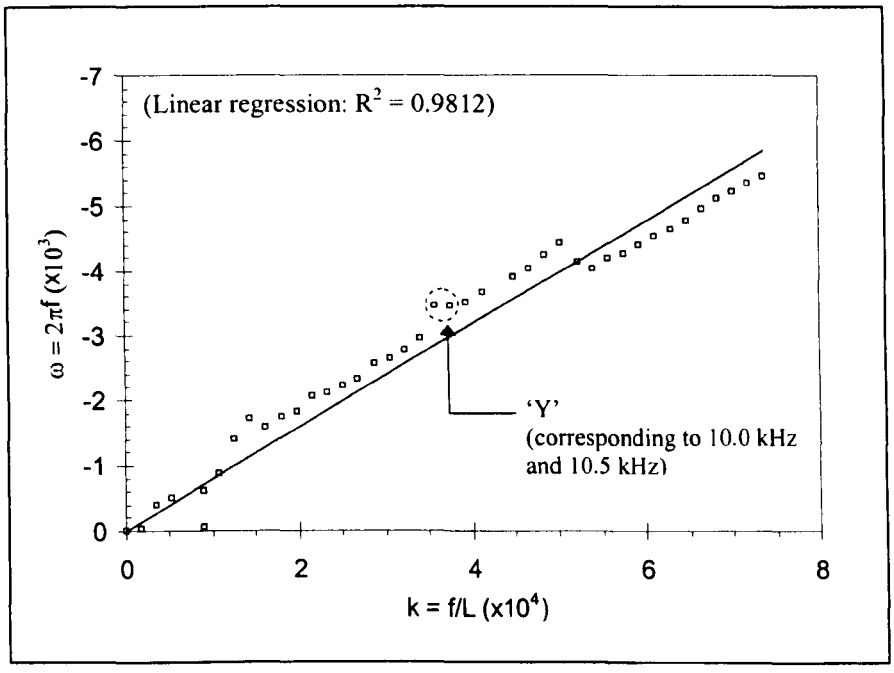

b. Sample L1 (f_{in} = 7 kHz).

Figure 4.2: Examples of dispersion plots.

Sample S1

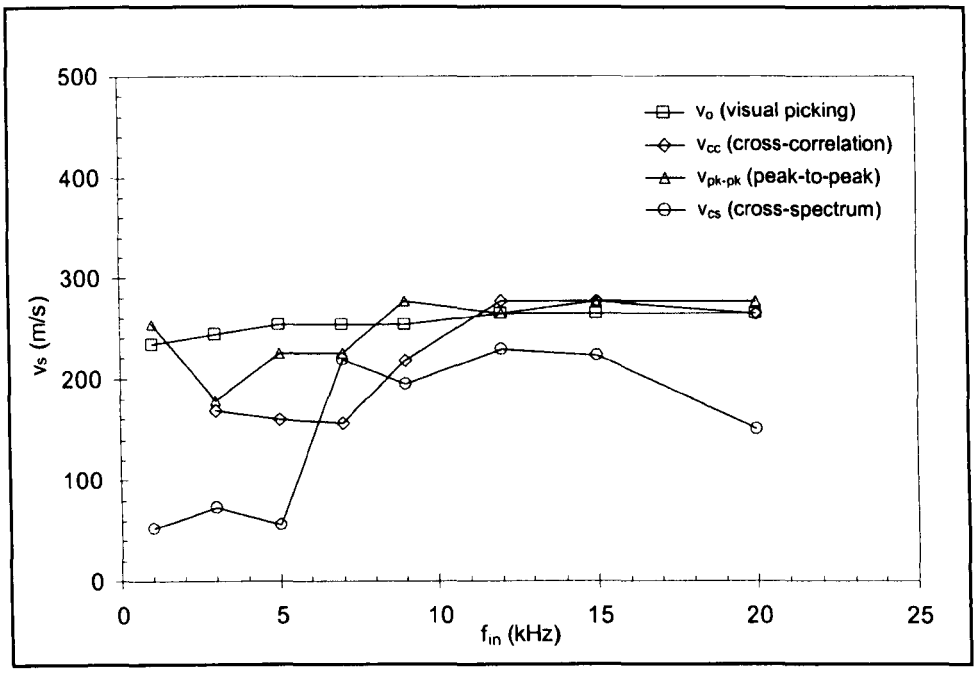

Sample S2

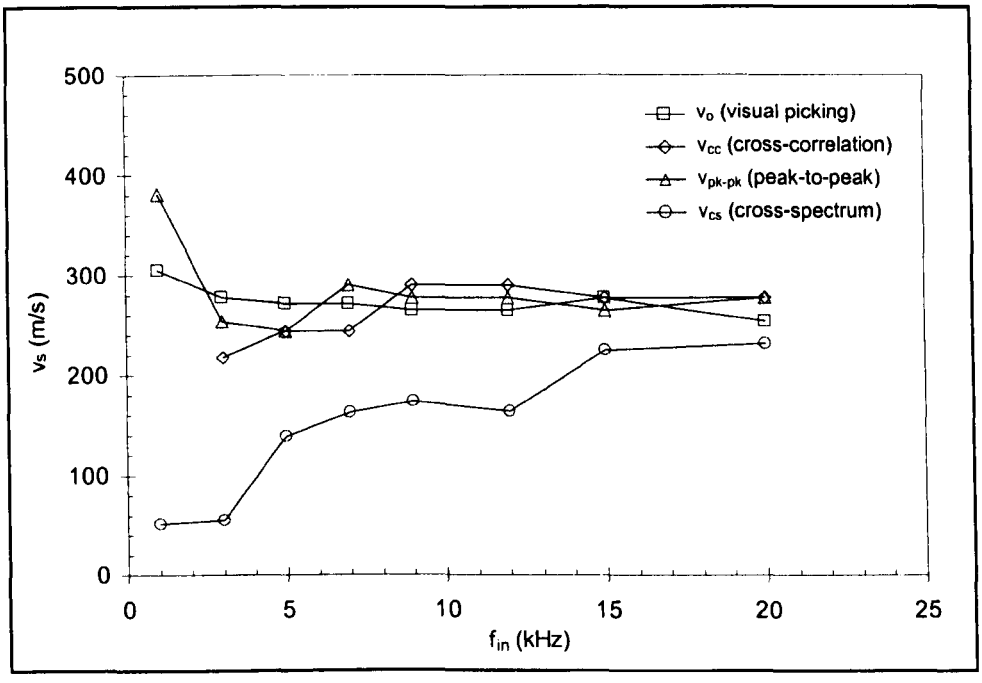

a. Samples S1 and S2 (f_{in} = 7 kHz).

Figure 4.3: Shear wave velocities obtained with various arrival time definition methods.

Sample L1

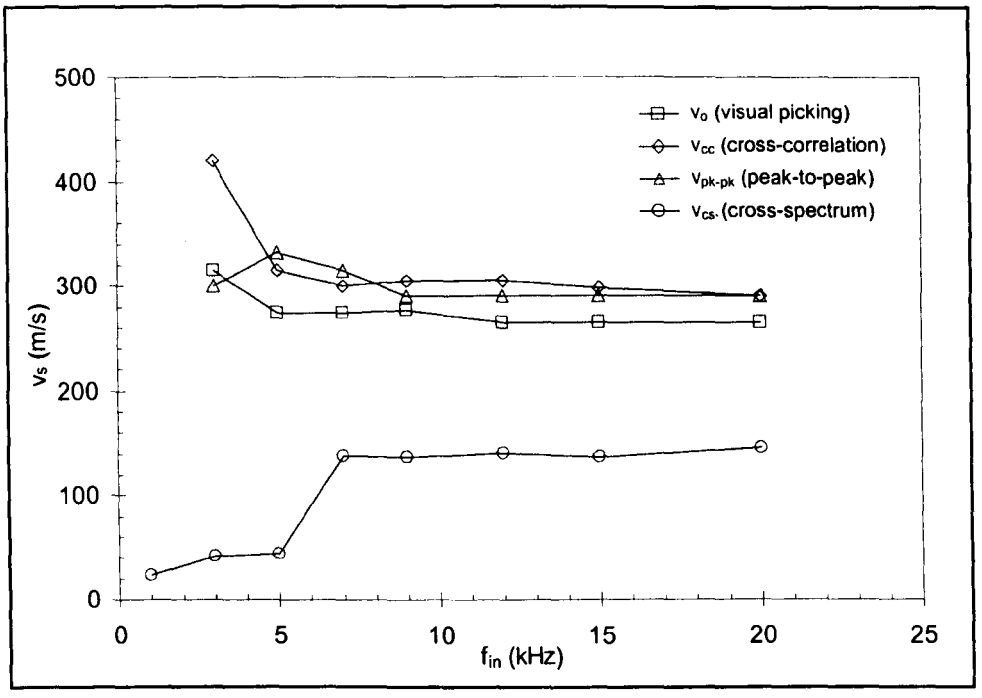

Sample L2

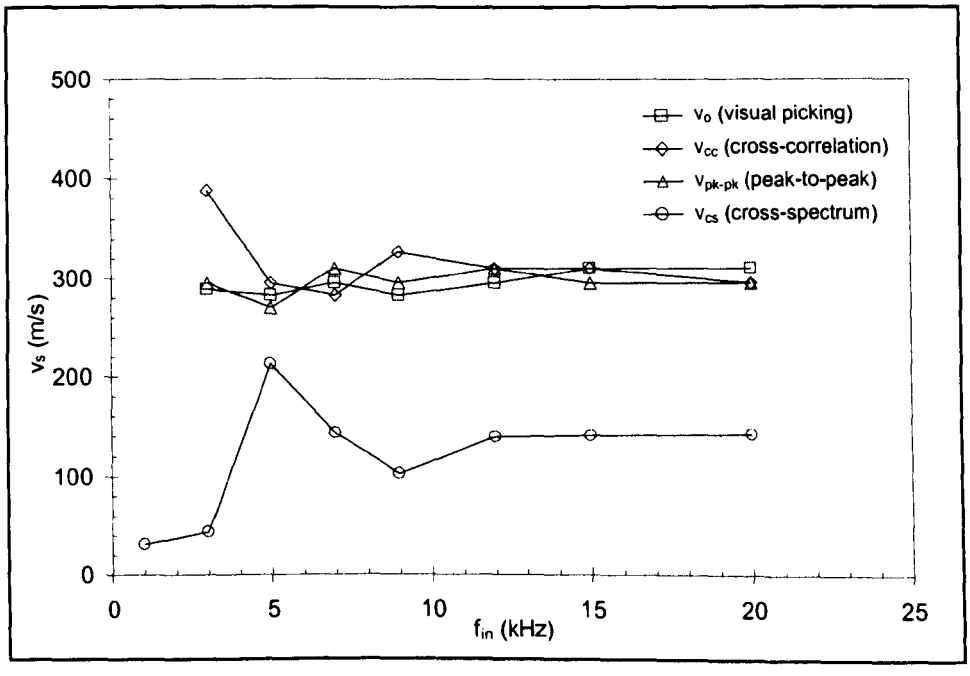

b. Samples L1 and L2 (f_{in} = 7 kHz).

Figure 4.3: Shear wave velocities obtained with various arrival time definition methods. *(continued)*

Sample S1 (f_{in} = 7 kHz)

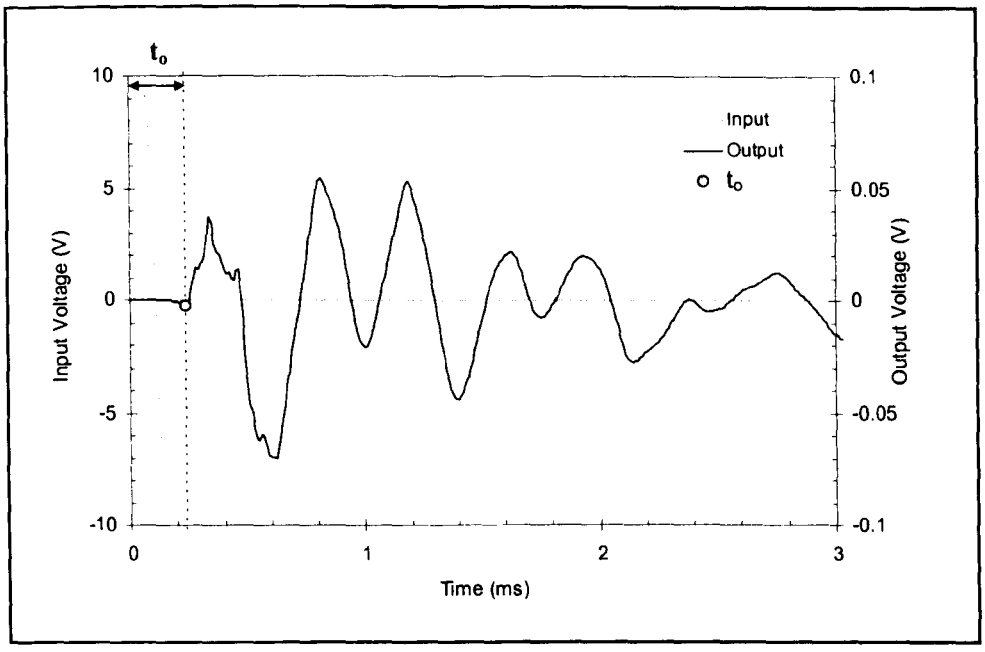

Figure 4.4: Visually picked shear wave arrival time (t_o).

Sample S1 (f_{in} = 7 kHz)

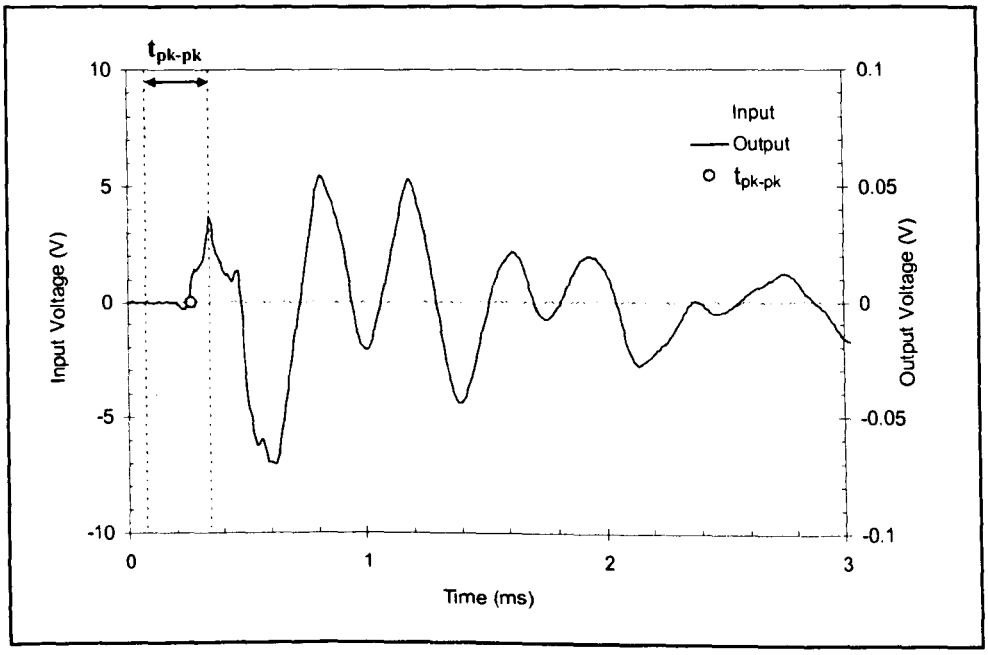

Figure 4.5: First major peak-to-peak shear wave arrival time (t_{pk-pk}).

Sample S1 (f_{in} = 7 kHz)

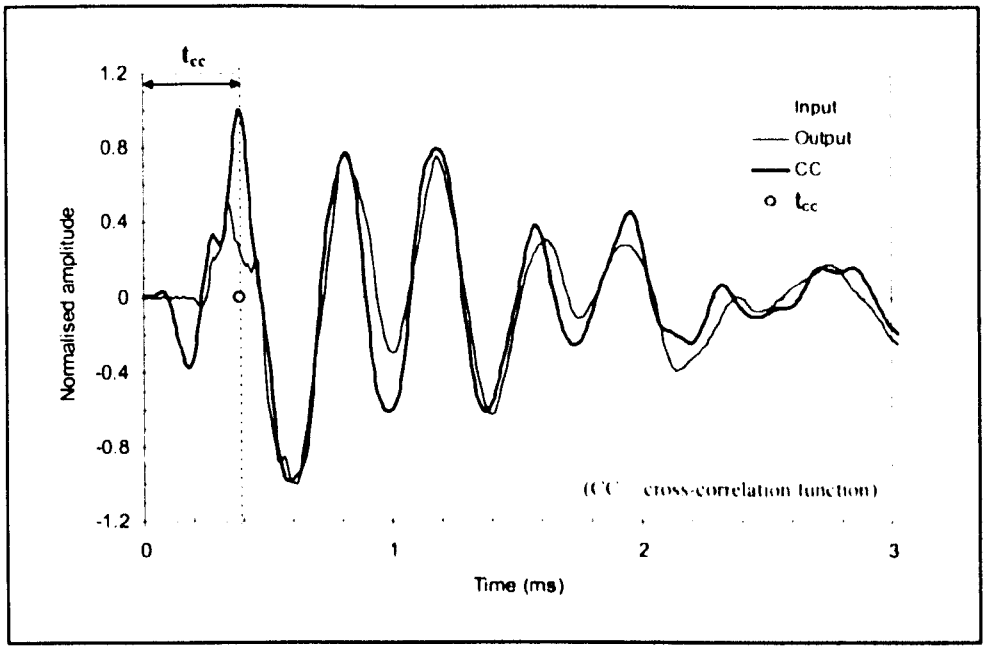

Figure 4.6: Shear wave arrival time from cross-correlation method (t_{cc}).

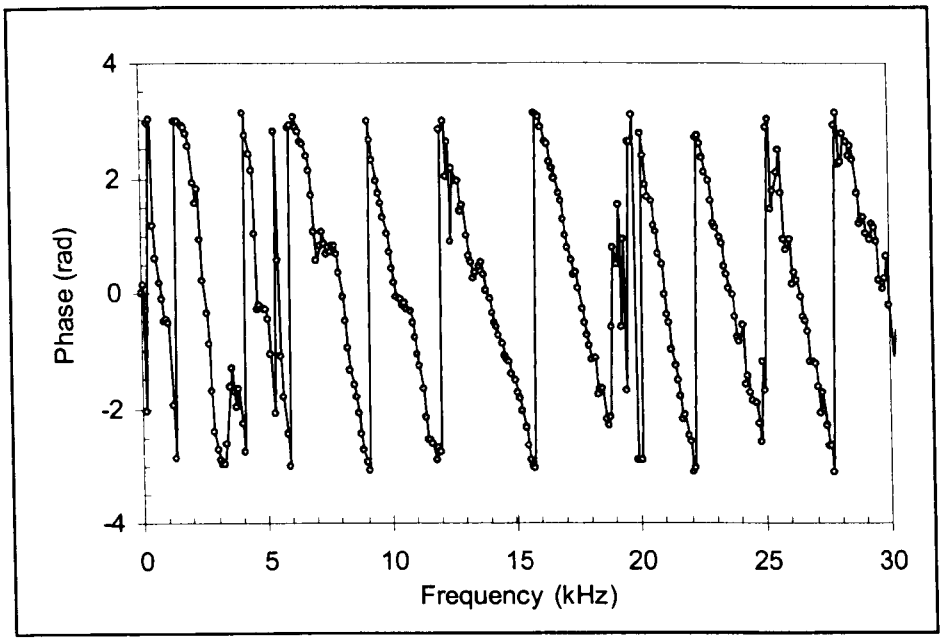

a. Wrapped phase.

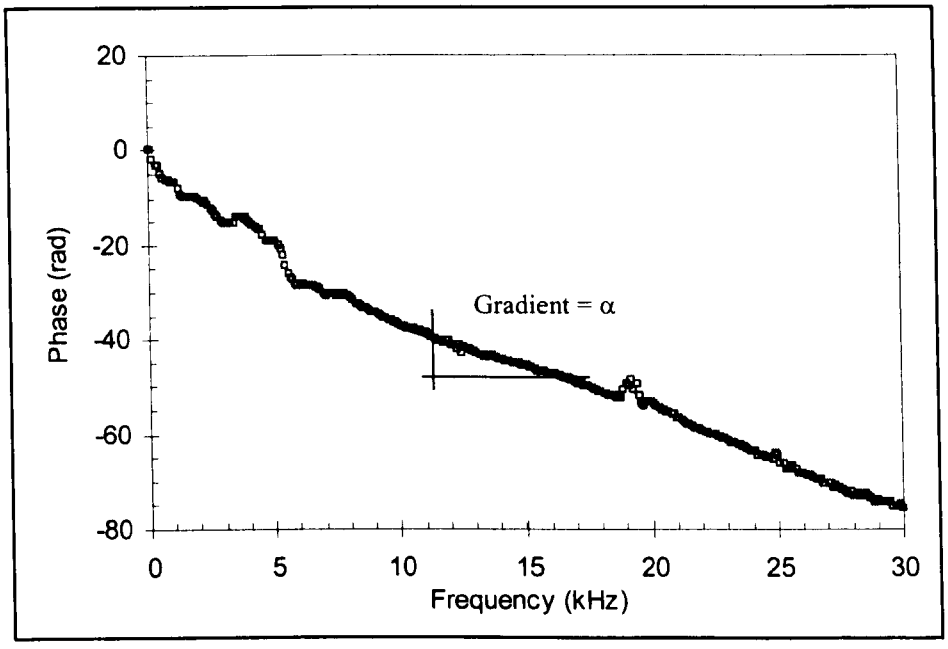

b. Unwrapped phase.

Figure 4.7: Phase diagrams of Sample S1 at f_{in} = 7 kHz.

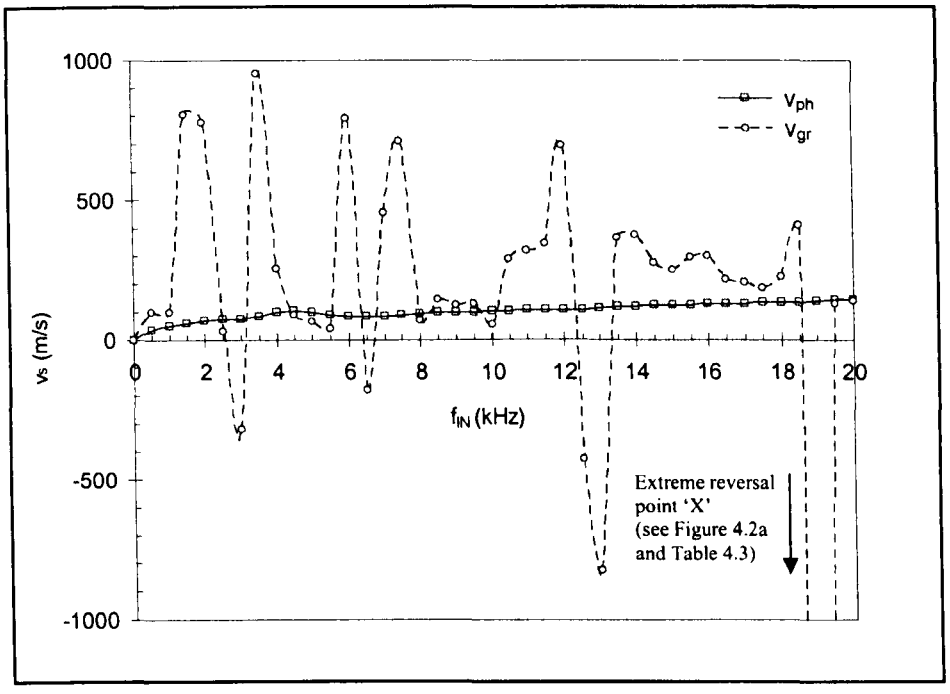

a. Sample S1 (f_{in} = 7 kHz)

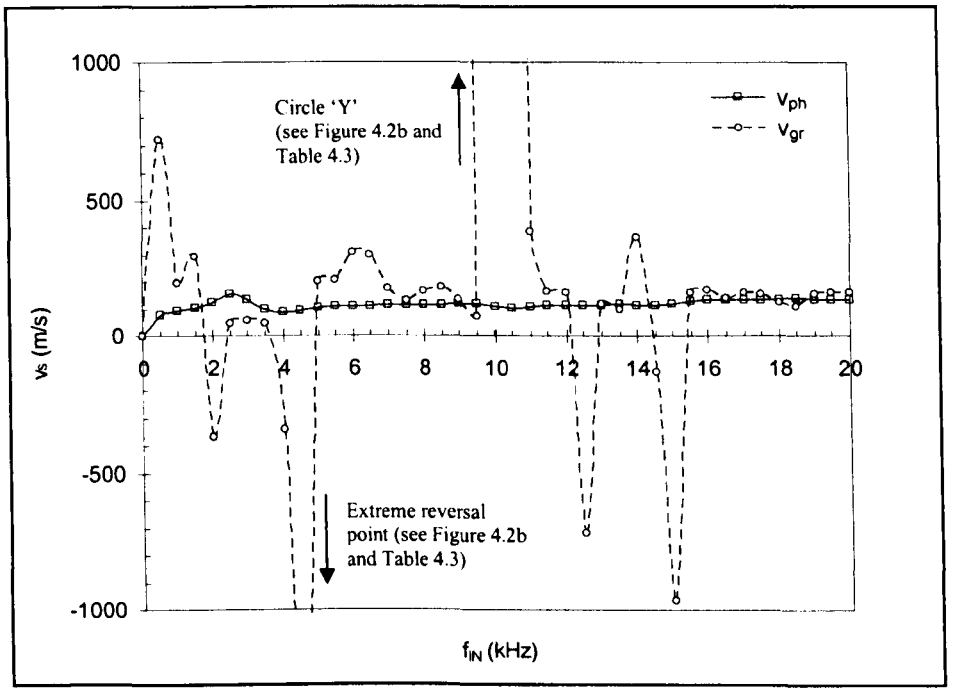

b. Sample L1 (f_{in} = 7 kHz)

Figure 4.8: Phase and group velocities against frequency plots.

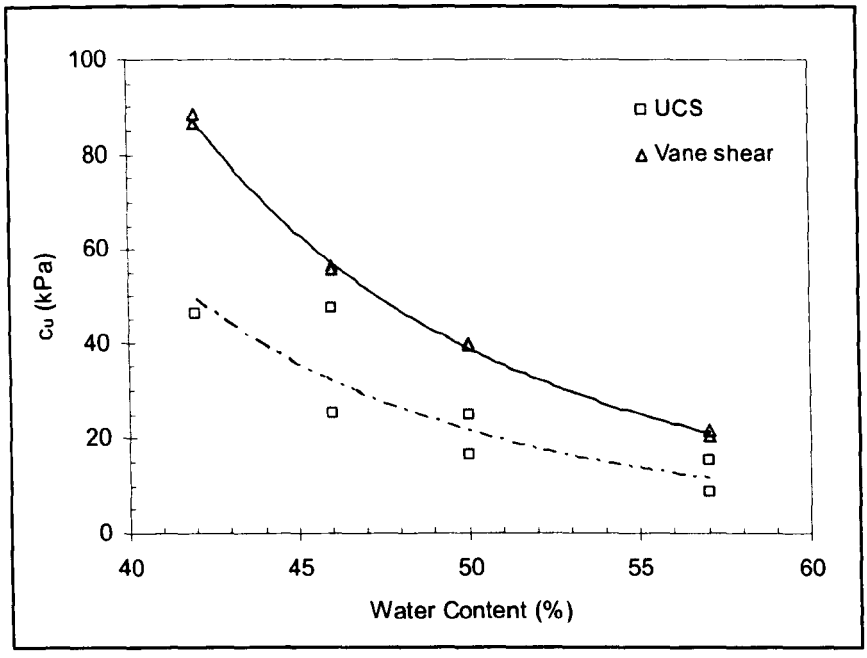

a. Kaolin: 1.5 % cement at various water contents .

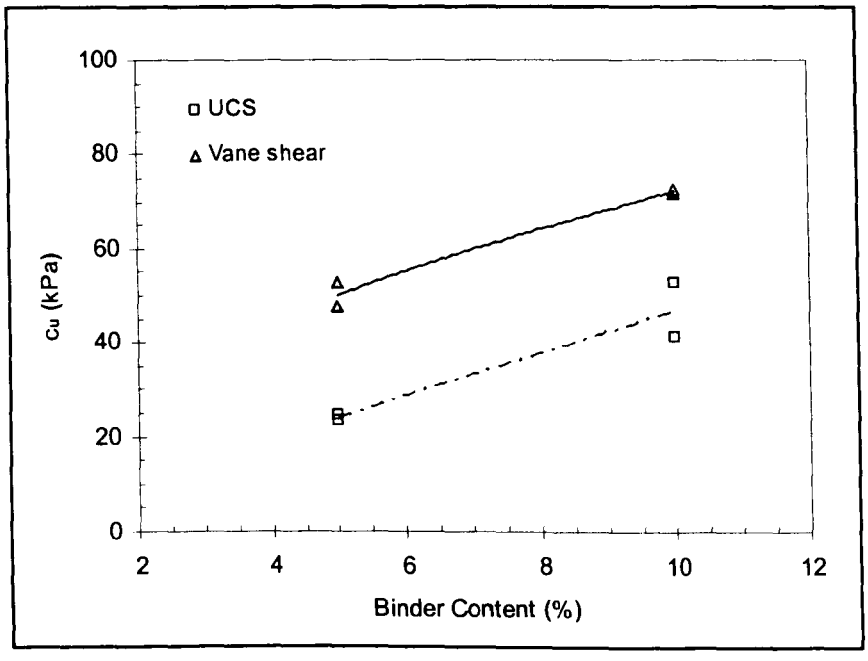

b. Swedish clay: 5 % and 10 % lime-cement.

Figure 4.9: Variation in undrained shear strength measurements.

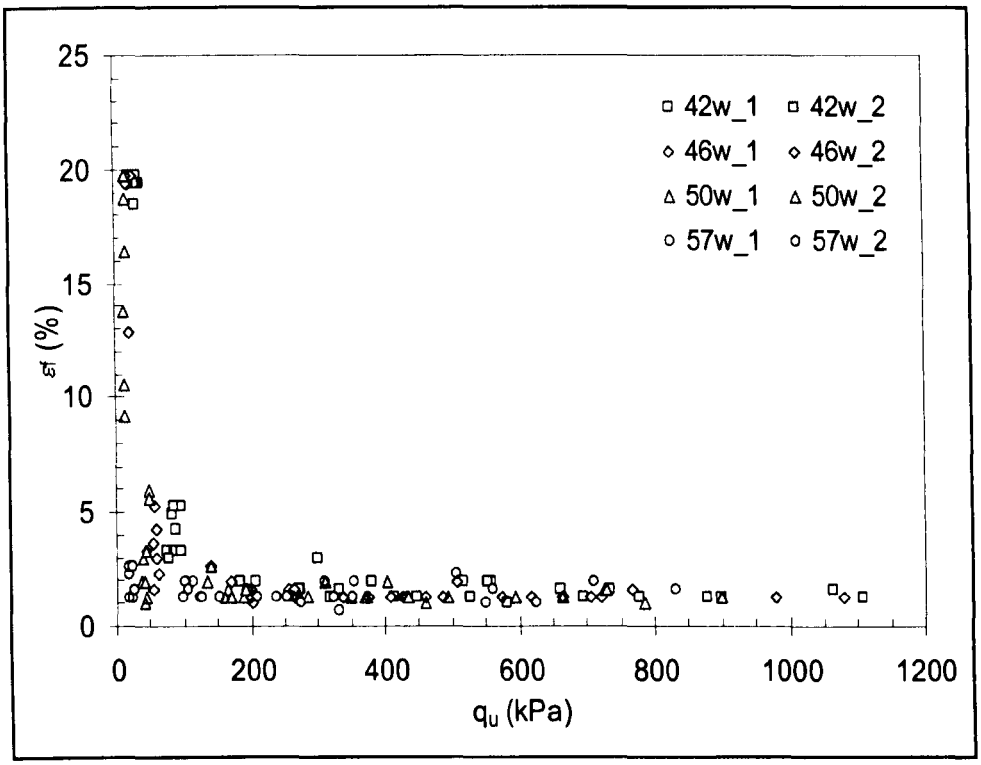

a. Kaolin samples.

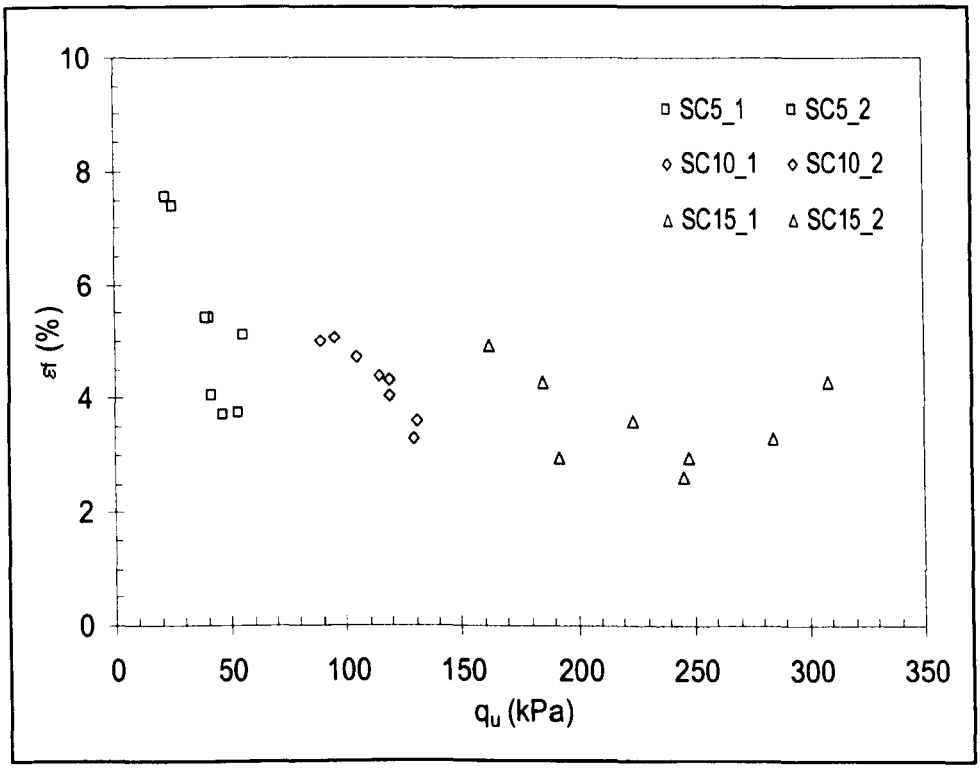

b. Swedish clay samples.

Figure 4.10: Axial failure strains of UCS tests.

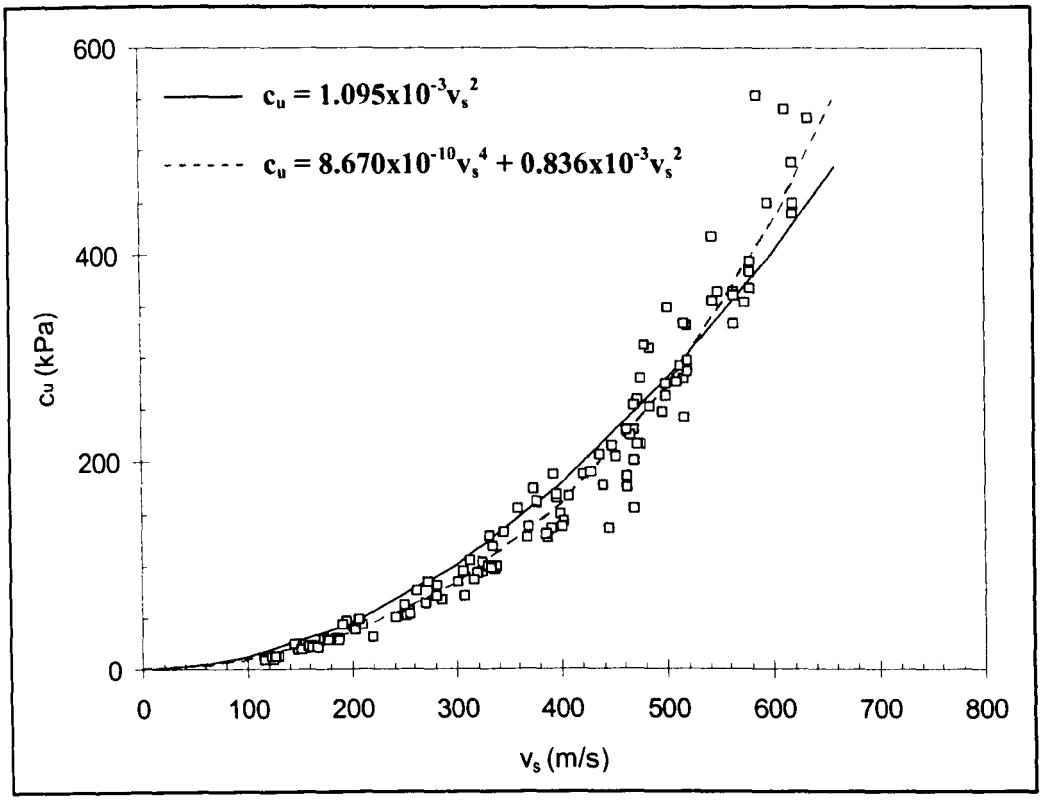

Stabilised kaolin samples.

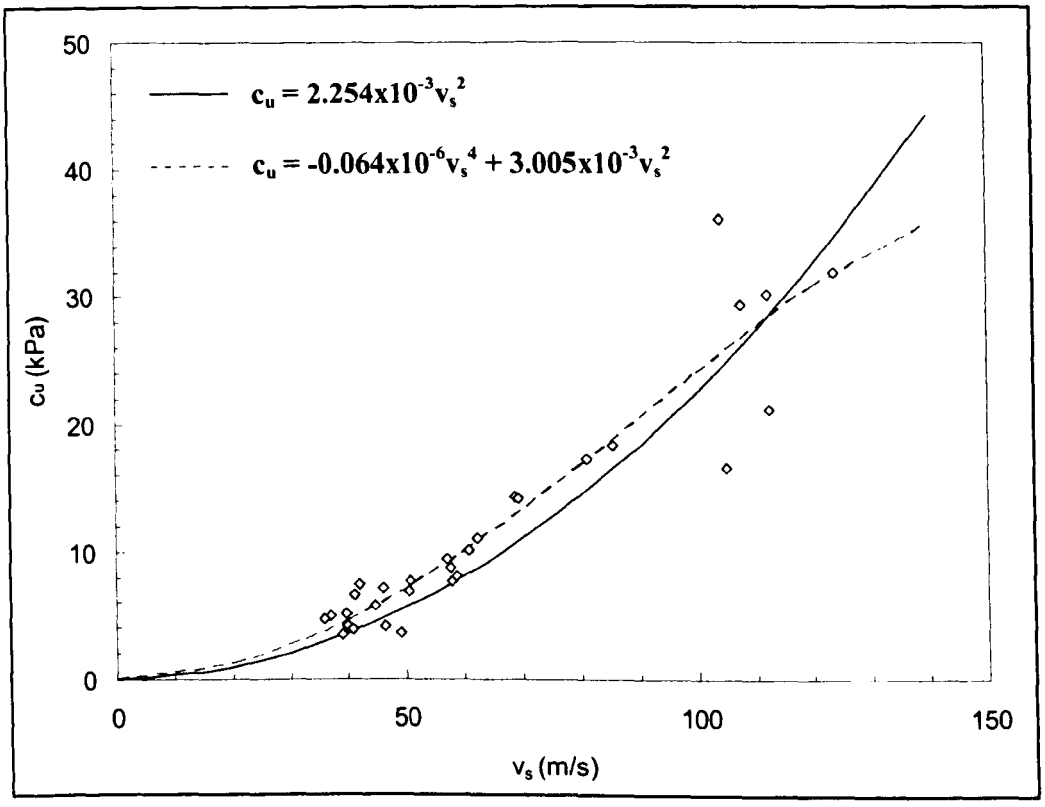

Stabilised Malaysian clay samples.

Figure 4.11a: Relationship between undrained shear strength (c_u) and shear wave velocity (v_s).

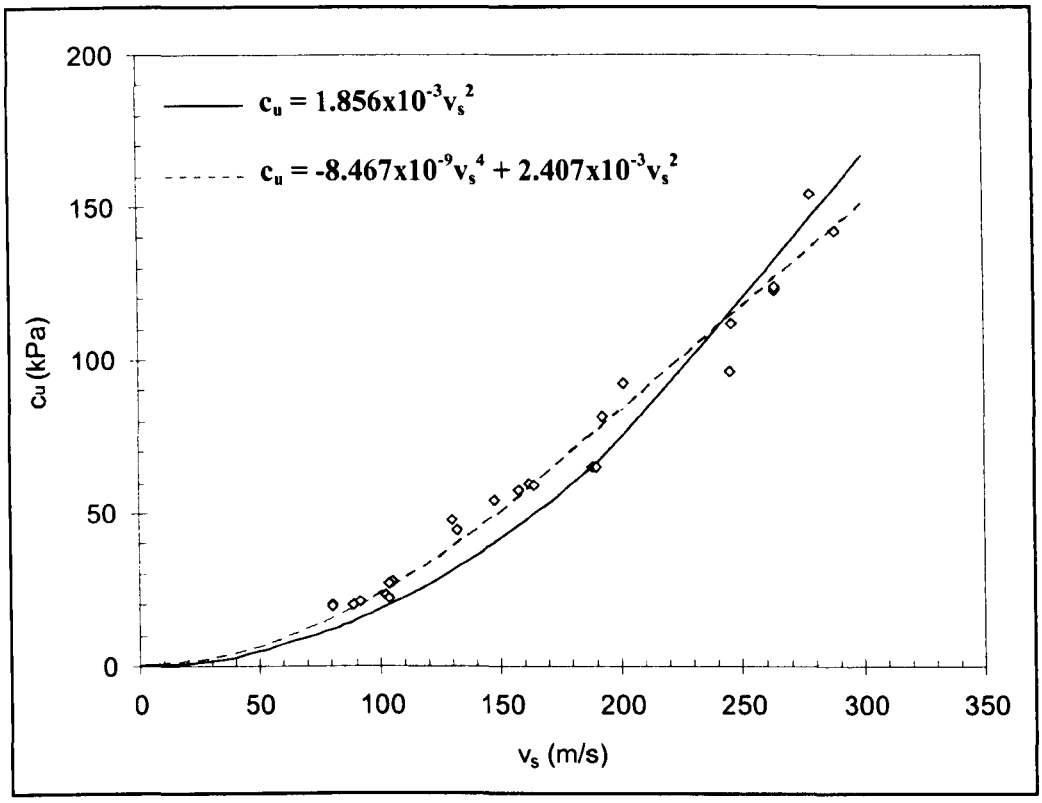

Stabilised Swedish clay samples.

Figure 4.11a: Relationship between undrained shear strength (c_u) and shear wave velocity (v_s). *(continued)*

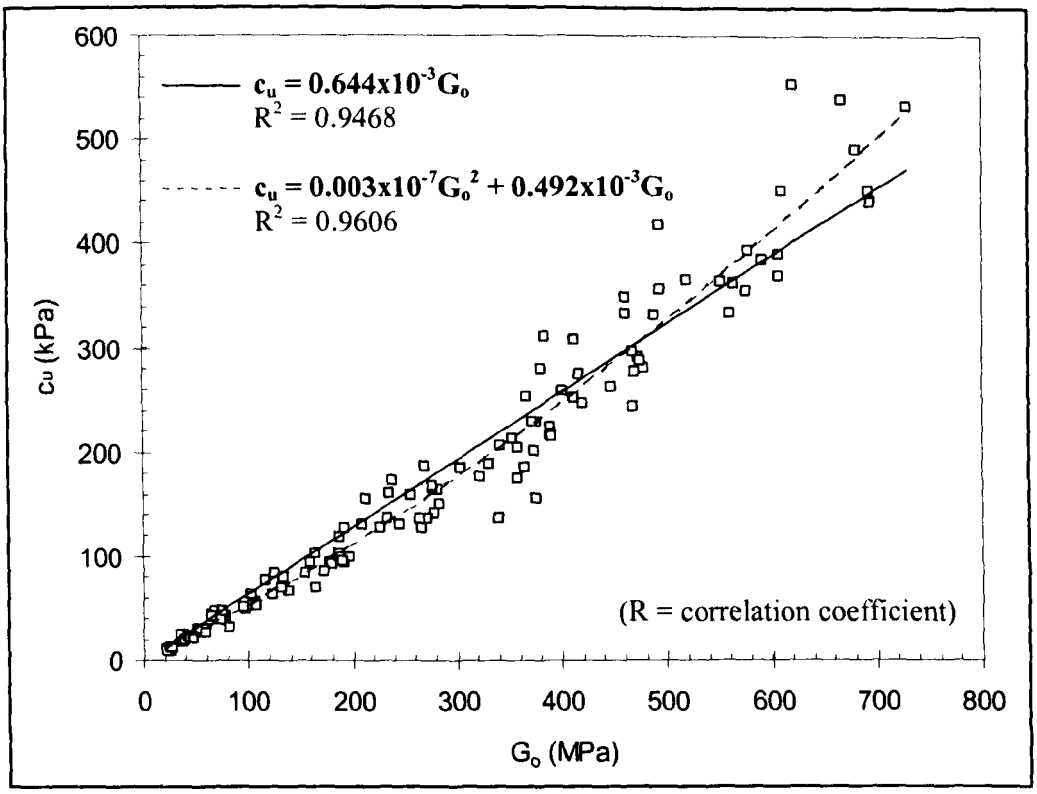

Stabilised kaolin samples.

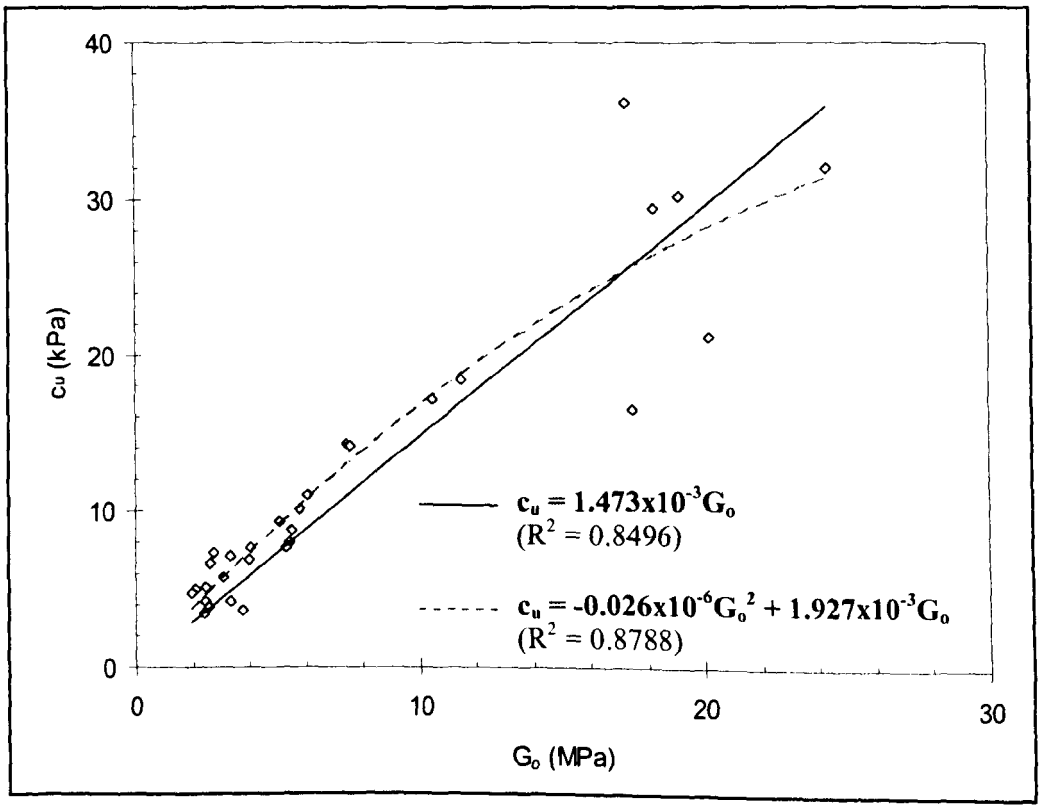

Stabilised Malaysian clay samples.

Figure 4.11b: Relationship between undrained shear strength (c_u) and maximum shear modulus (G_o).

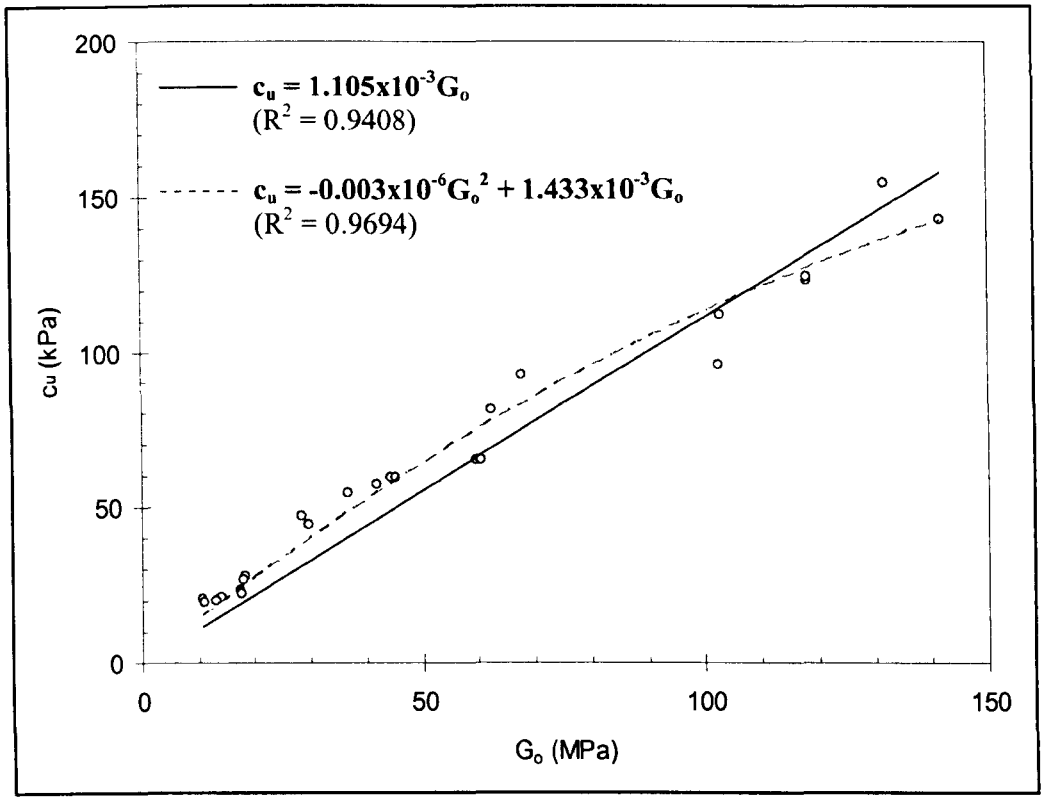

Stabilised Swedish clay samples.

Figure 4.11b: Relationship between undrained shear strength (c_u) and maximum shear modulus (G_o). *(continued)*

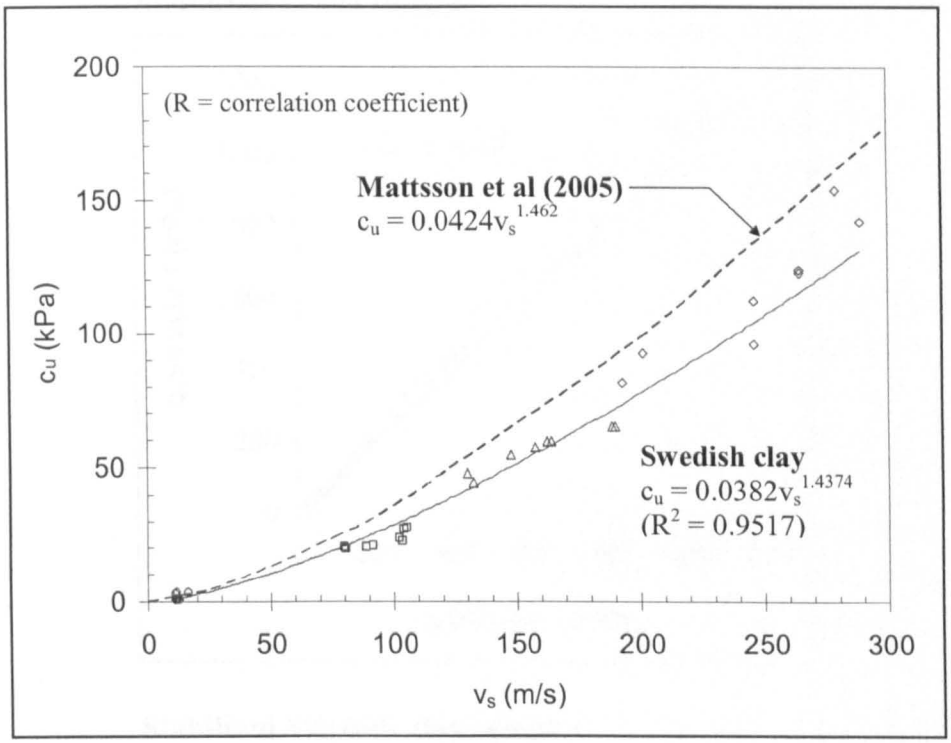

Figure 4.12: c_u - v_s, comparison with the correlation by Mattsson et al. (2005).

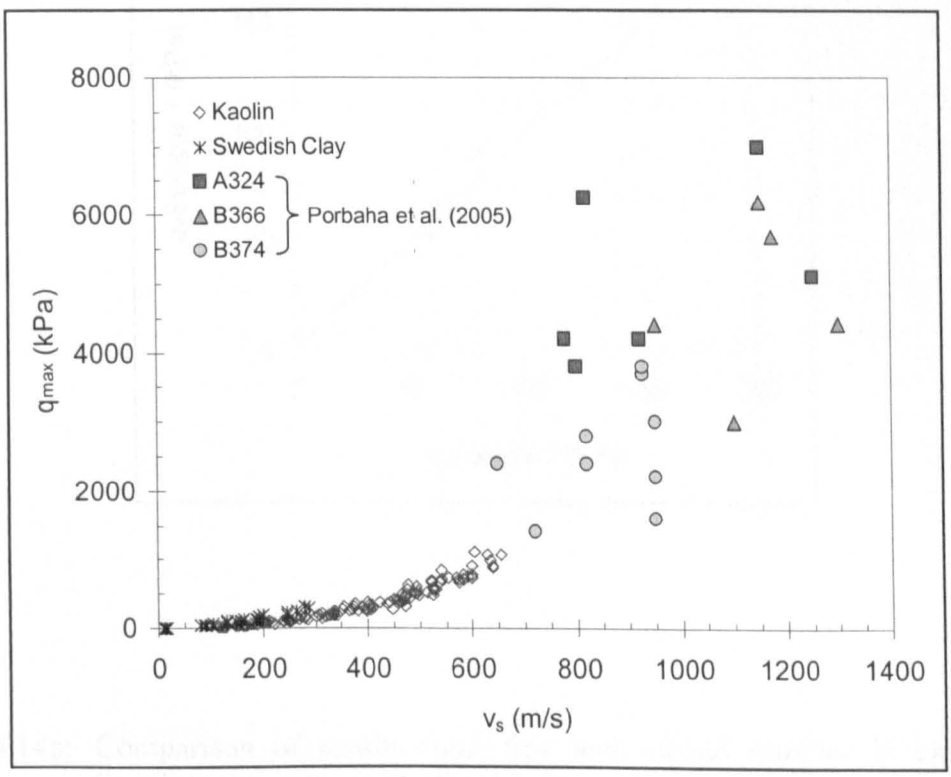

Figure 4.13: q_u - v_s, comparison with the data of Porbaha et al. (2005).

Stabilised kaolin samples

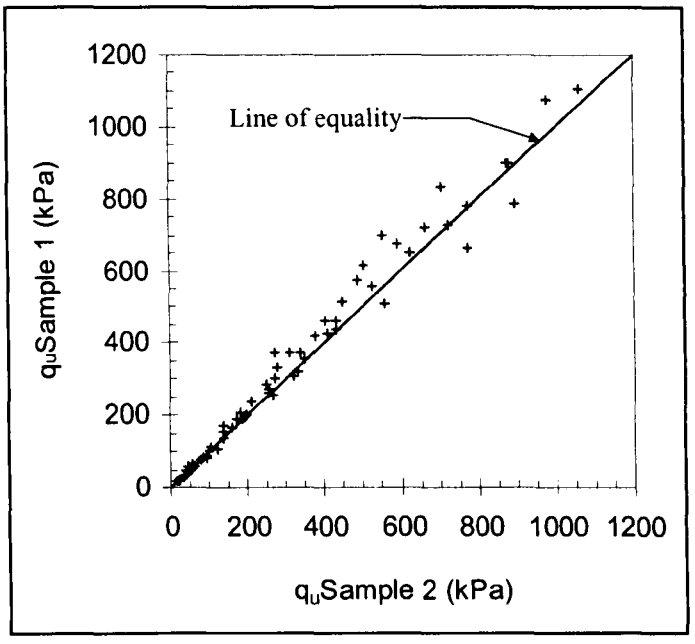

Stabilised Swedish clay samples

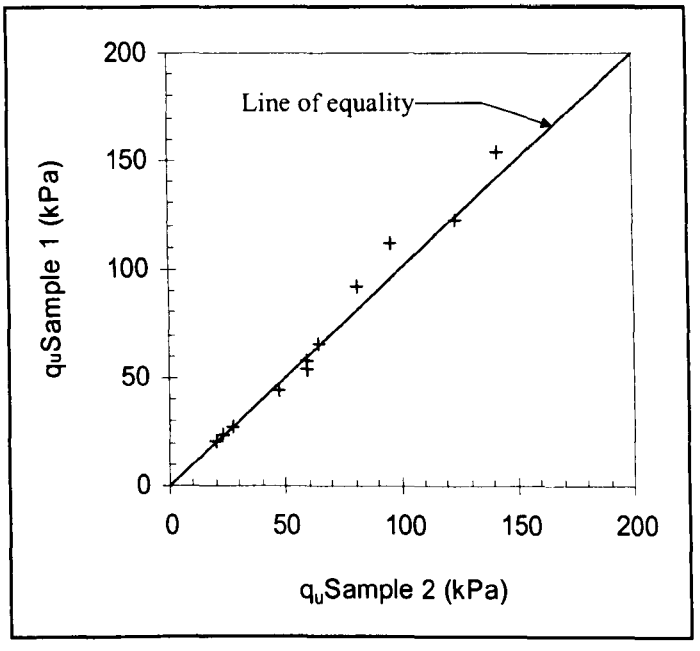

Figure 4.14a: Comparison of results from first and second samples in kaolin and Swedish clay tests- unconfined compressive strength (q_u).

Stabilised kaolin samples

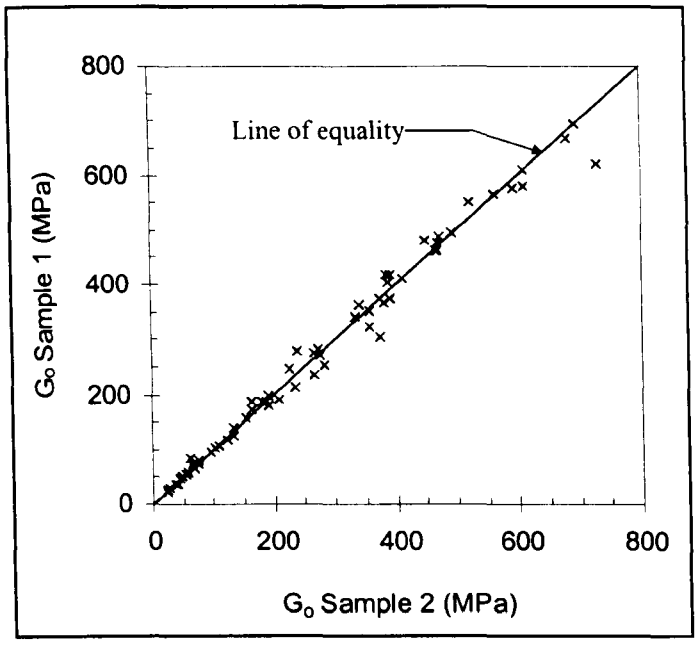

Stabilised Swedish clay samples

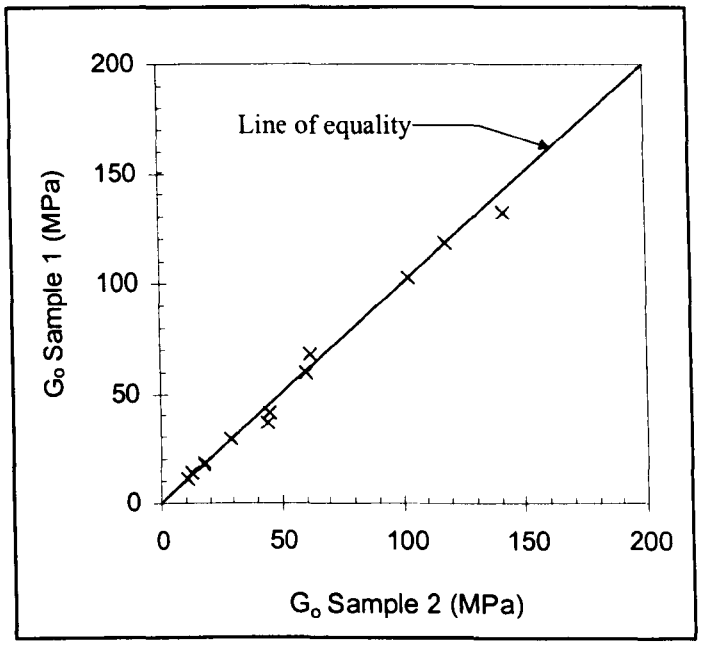

Figure 4.14b: Comparison of results from first and second samples in kaolin and Swedish clay tests- maximum shear modulus (G_0).

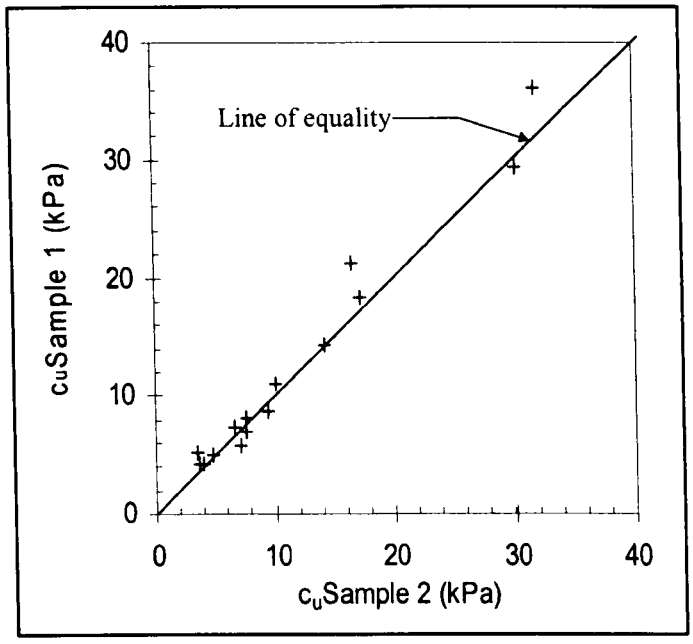

a. Undrained shear strength (c_u)

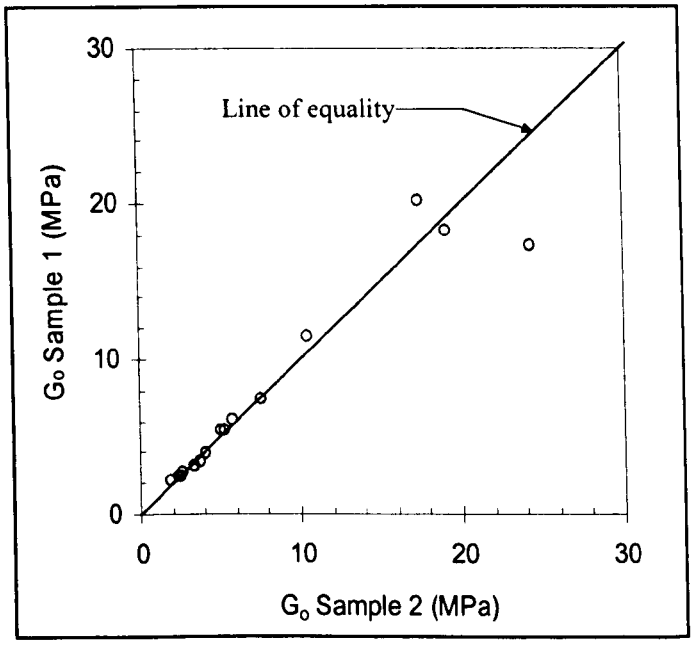

b. Maximum shear modulus (G_o)

Figure 4.15: Comparison of results from first and second samples in Malaysian clay tests- undrained shear strength (c_u) and maximum shear modulus (G_o).

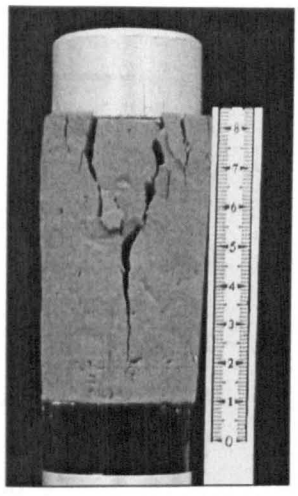

SC5_14d (C2)

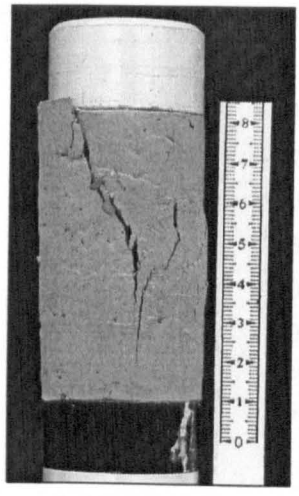

SC5_28d (D2)

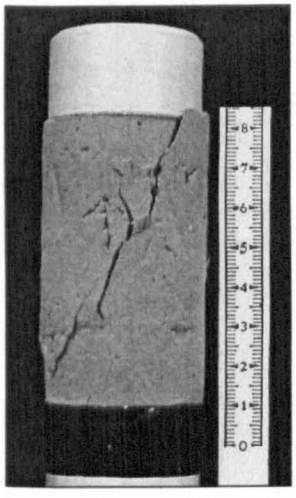

SC10_3d (A1)

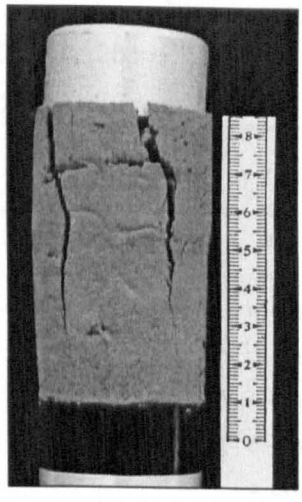

SC10_7d (B2)

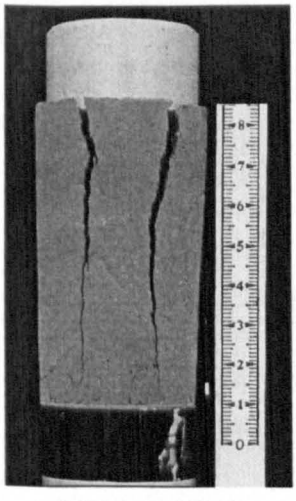

SC15_7d (B1)

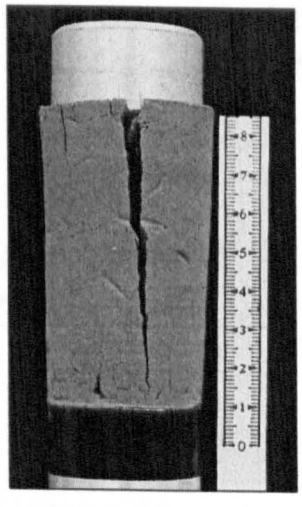

SC15_14d (C2)

Figure 4.16: Examples of failure modes observed in UCS tests of stabilised Swedish clay samples.

0 % cement content

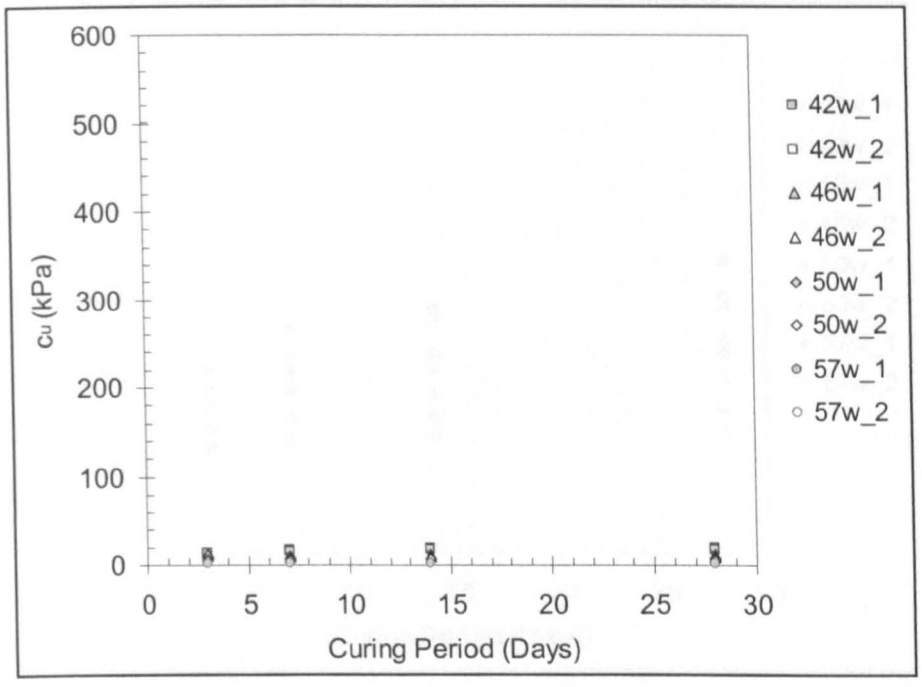

3 % cement content

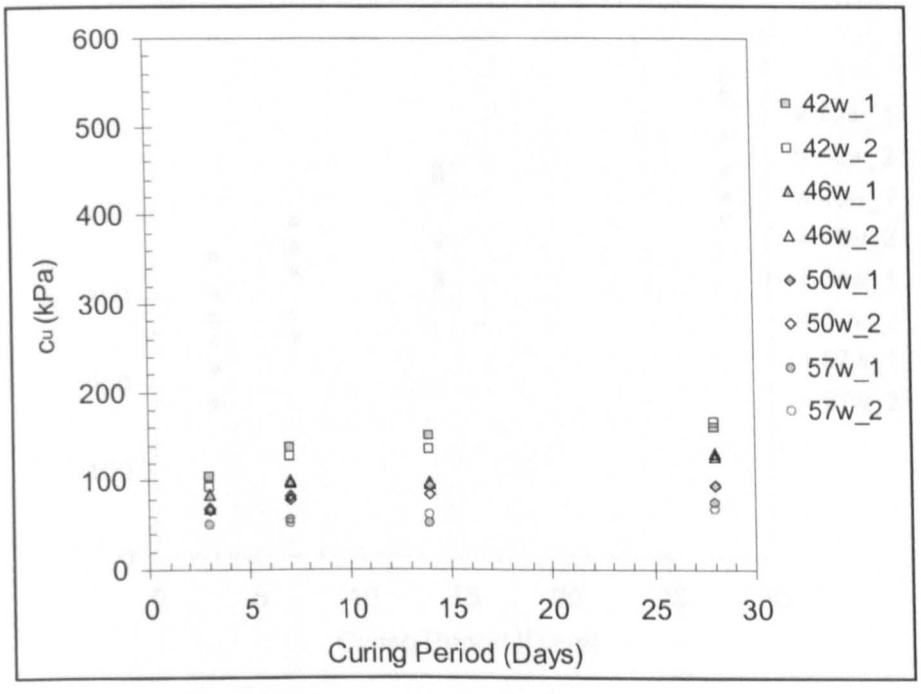

Figure 4.17a: Curing effect on kaolin samples- undrained shear strength (c_u) - curing period (grouped according to initial water contents).

6 % cement content

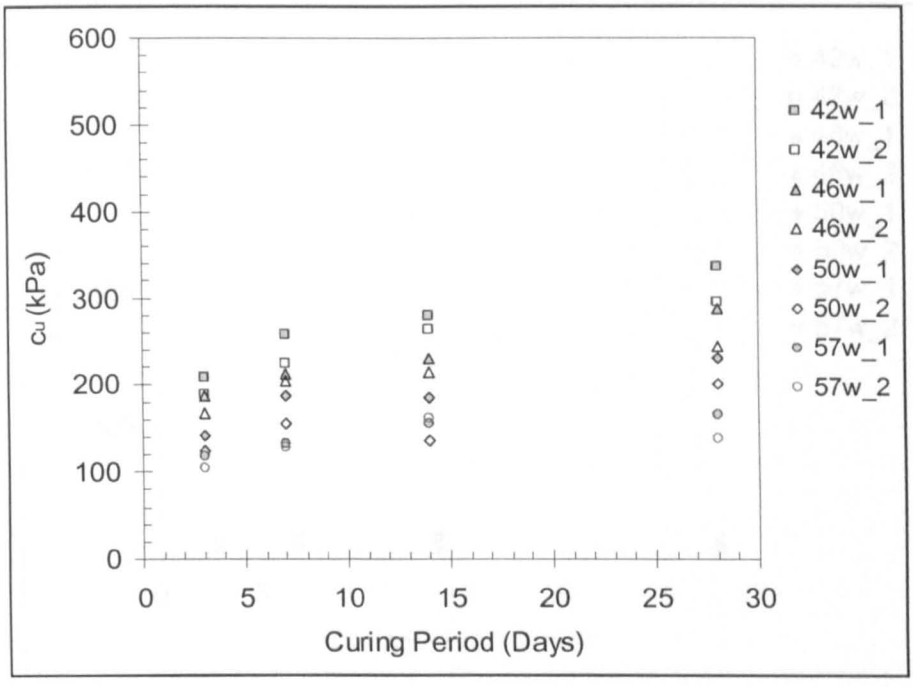

9 % cement content

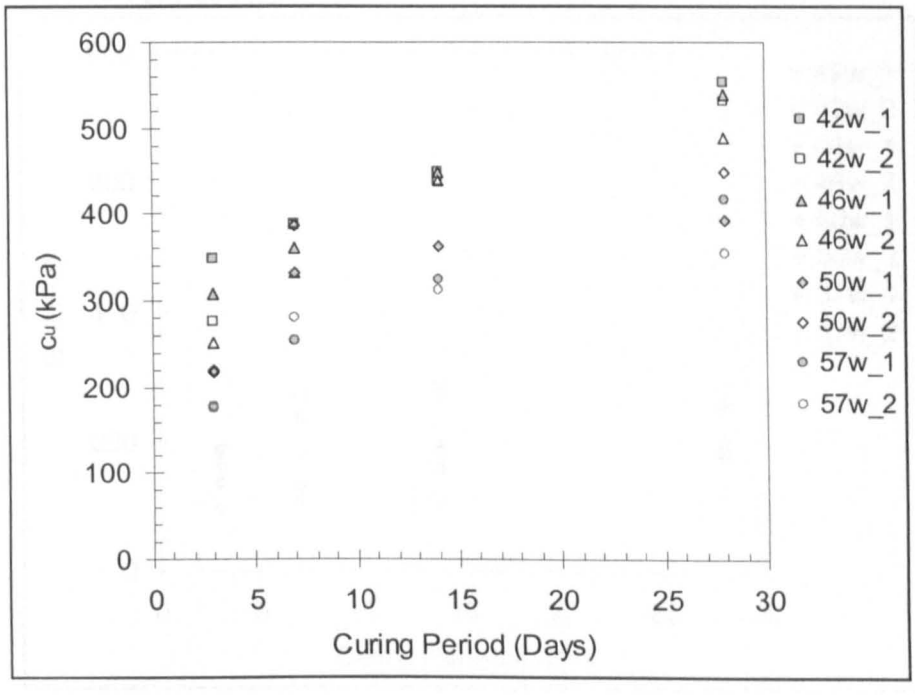

Figure 4.17a: Curing effect on kaolin samples- undrained shear strength (c_u) - curing period (grouped according to initial water contents). *(continued)*

0 % cement content

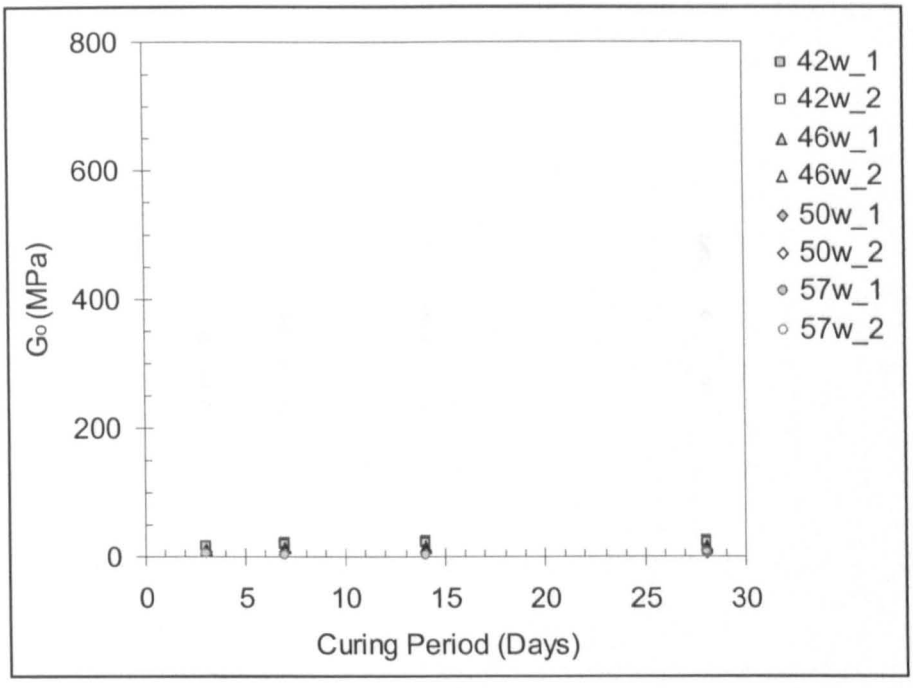

3 % cement content

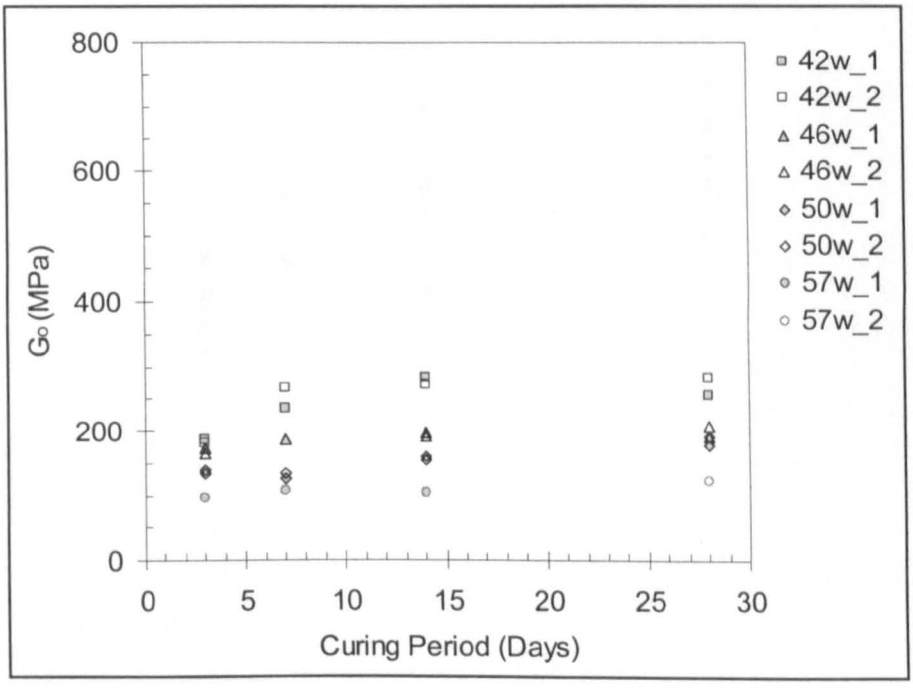

Figure 4.17b: Curing effect on kaolin samples- maximum shear modulus (G_o) - curing period (grouped according to initial water contents).

6 % cement content

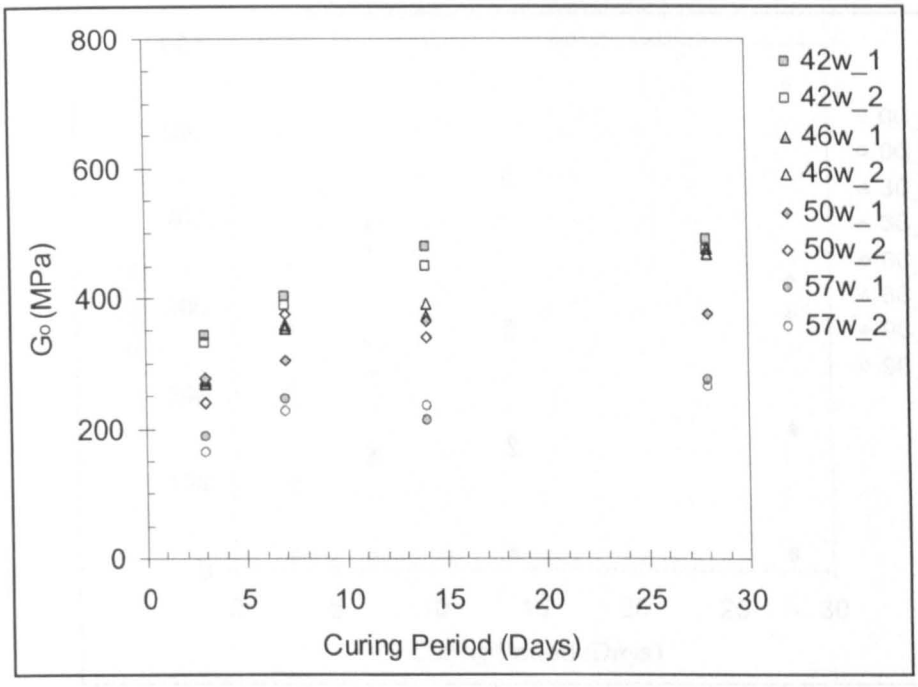

9 % cement content

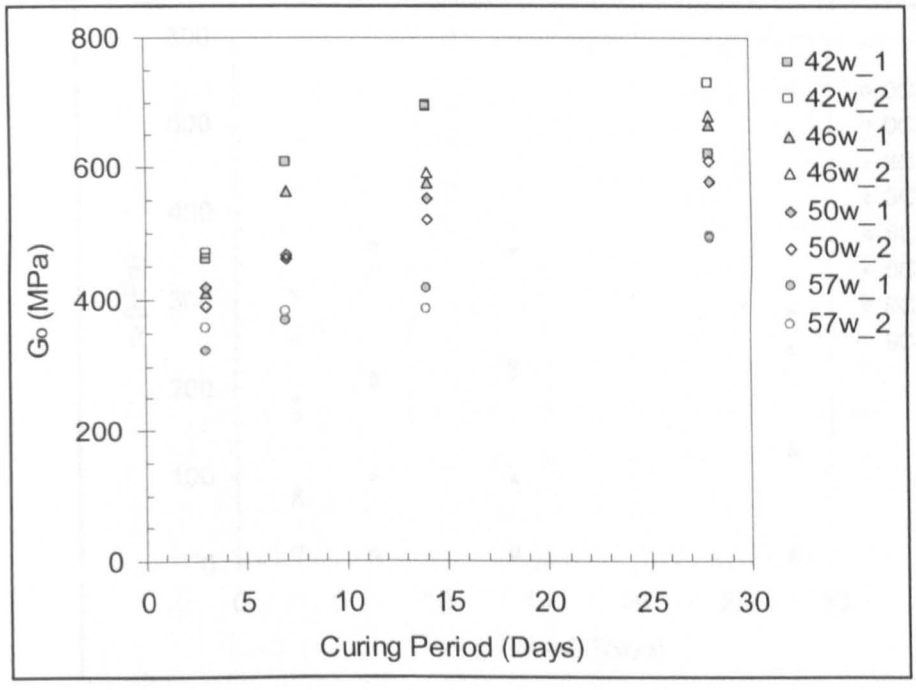

Figure 4.17b: Curing effect on kaolin samples- maximum shear modulus (G_o) - curing period (grouped according to initial water contents). *(continued)*

Kaolin 42 % water content

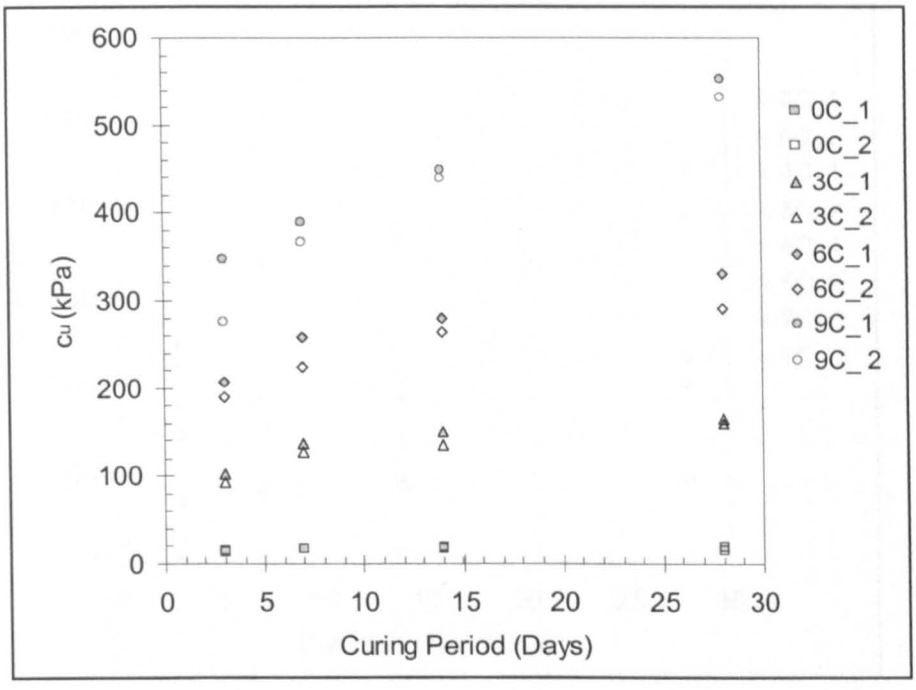

Kaolin 46 % water content

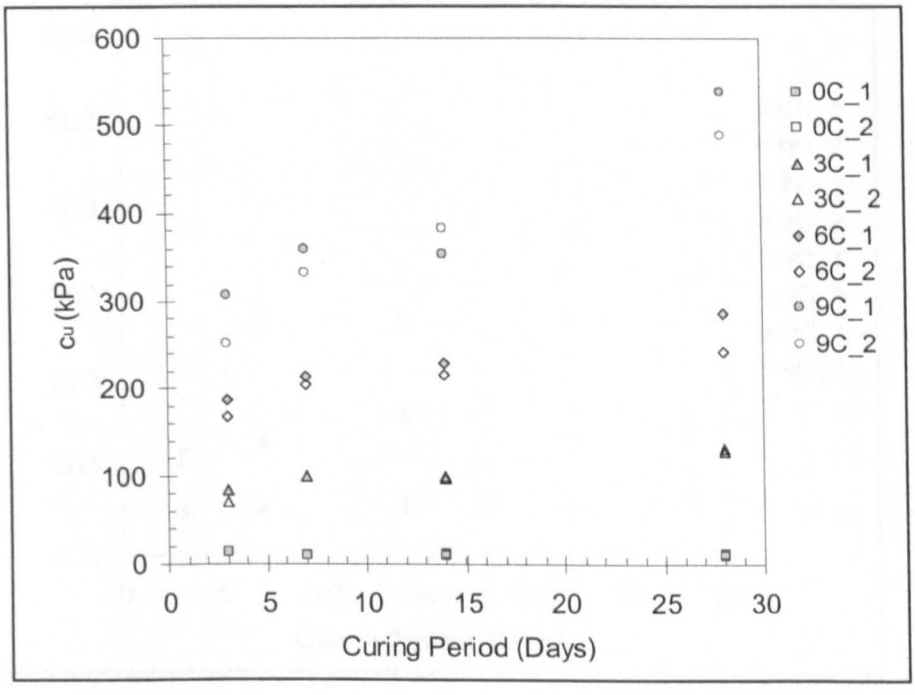

Figure 4.18a: Curing effect on kaolin samples- undrained shear strength (c_u) - curing period (grouped according to cement contents).

Kaolin 50 % water content

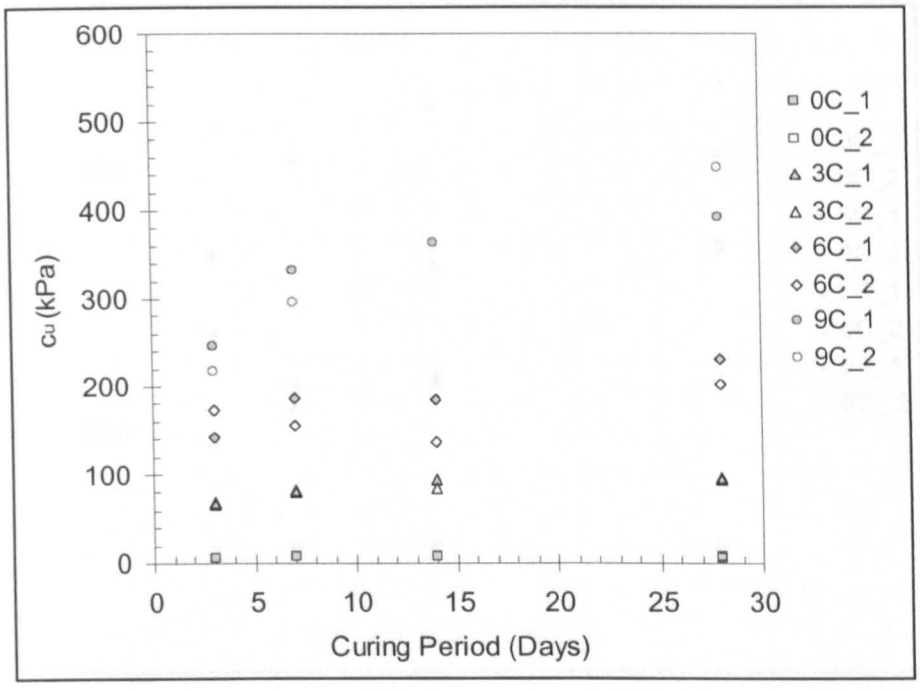

Kaolin 57 % water content

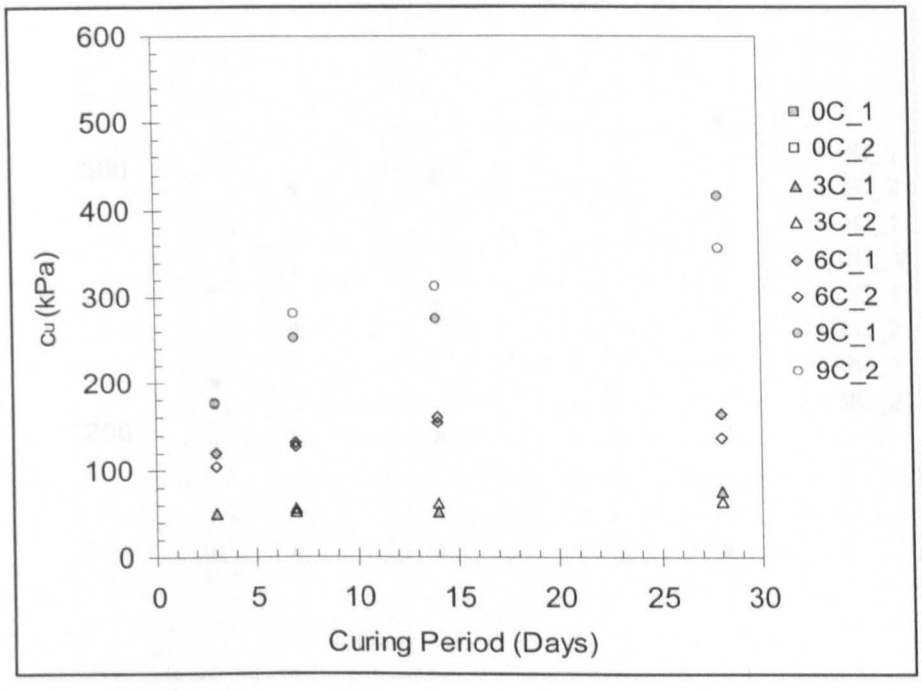

Figure 4.18a: Curing effect on kaolin samples- undrained shear strength (c_u) - curing period (grouped according to cement contents). *(continued)*

Kaolin 42 % water content

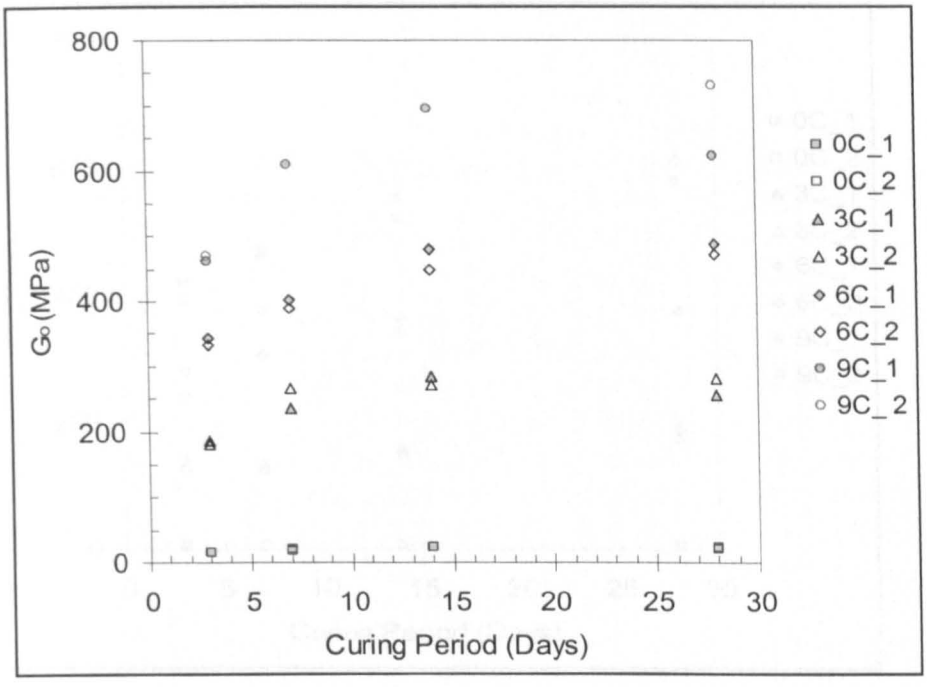

Kaolin 46 % water content

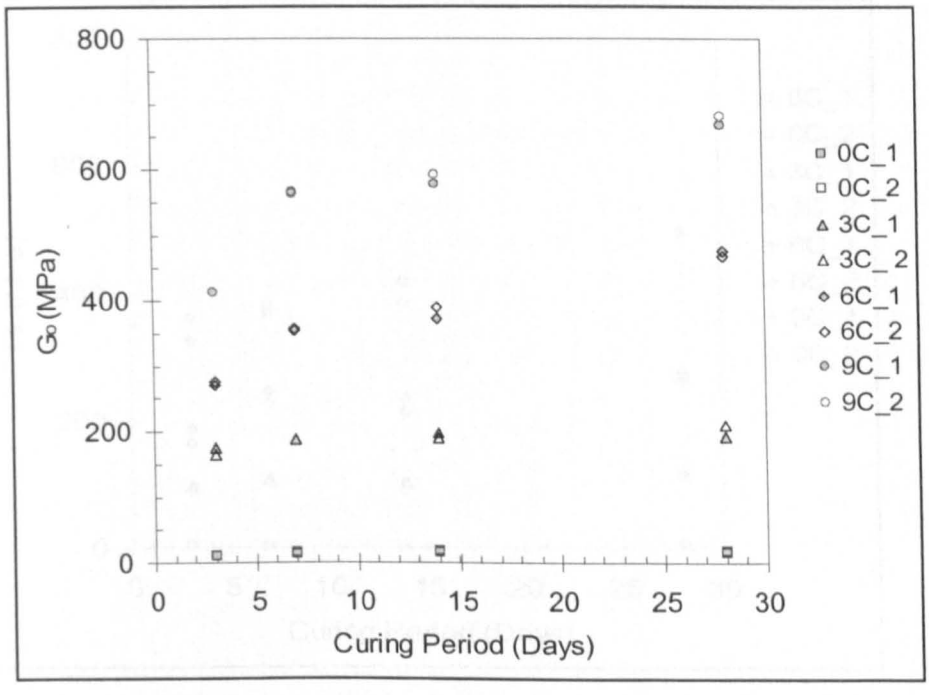

Figure 4.18b: Curing effect on kaolin samples- maximum shear modulus (G_o) - curing period (grouped according to cement contents).

Kaolin 50 % water content

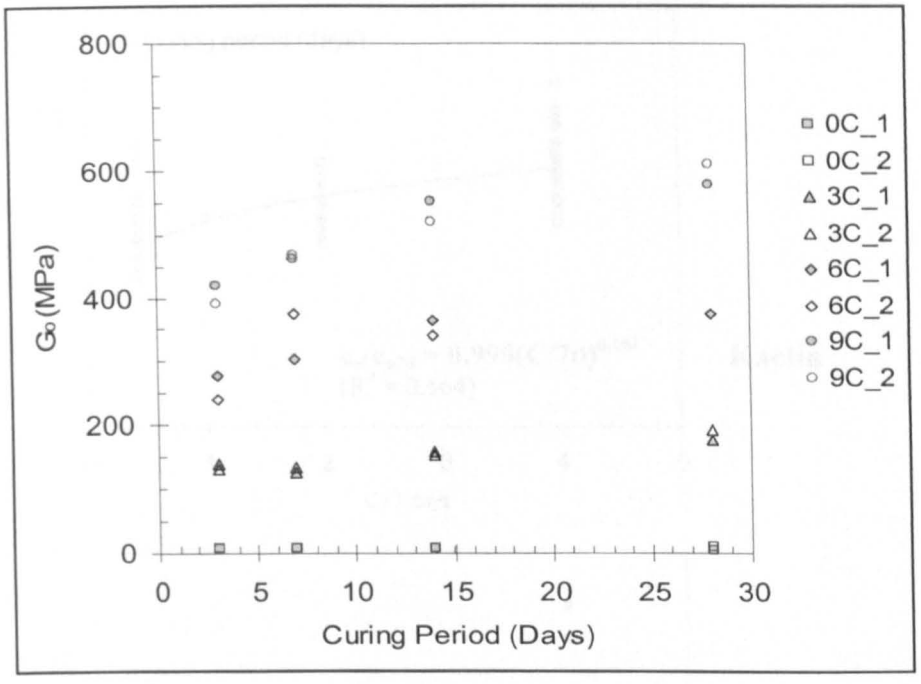

Kaolin 57 % water content

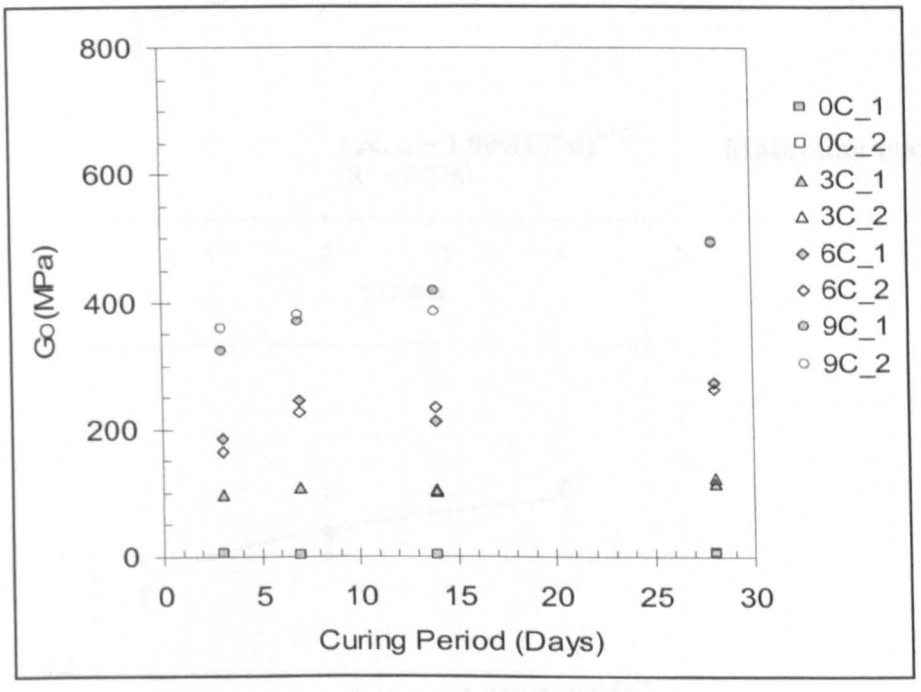

Figure 4.18b: Curing effect on kaolin samples- maximum shear modulus (G_o) - curing period (grouped according to cement contents). *(continued)*

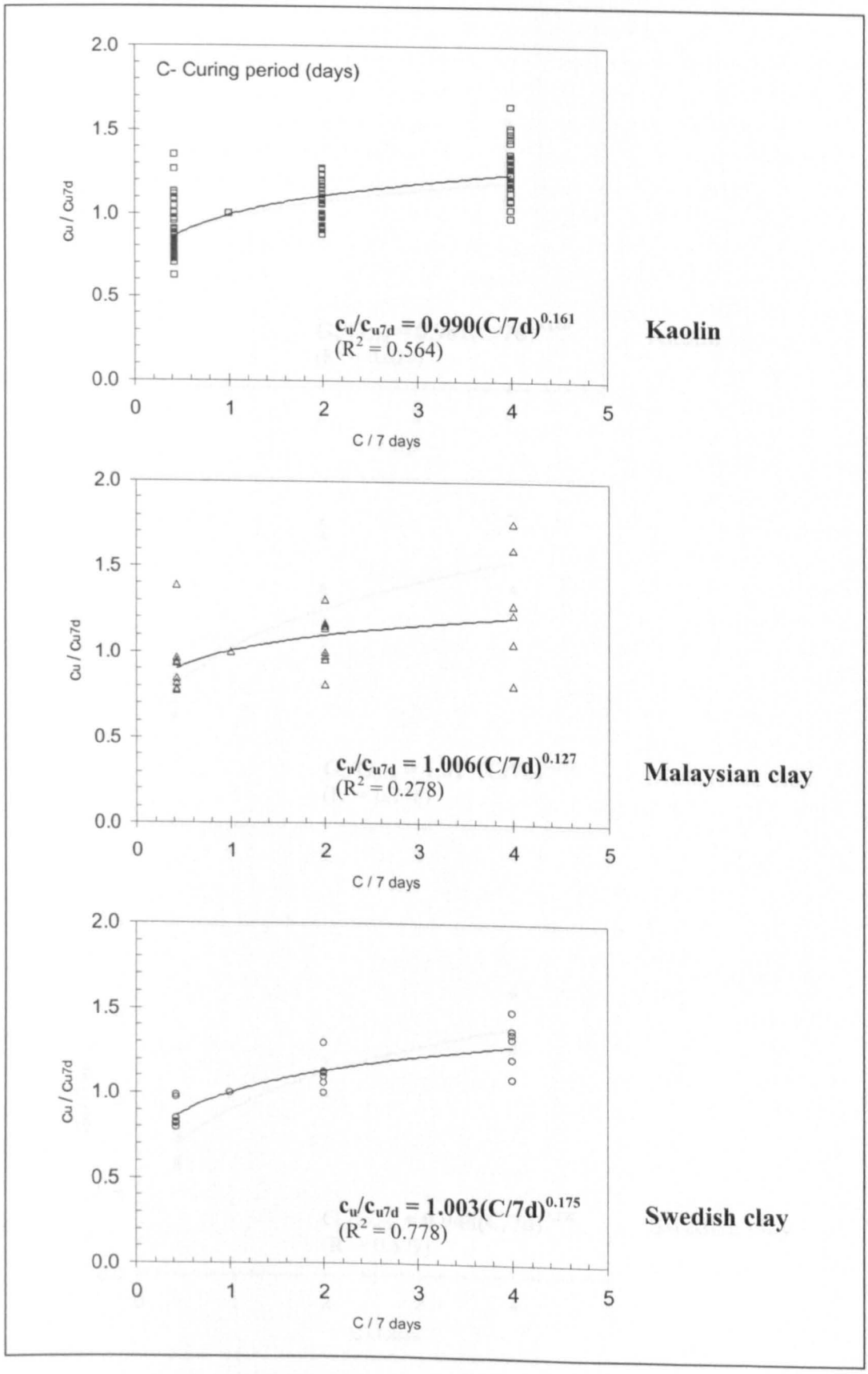

Figure 4.19a: Normalised undrained shear strength (c_u).

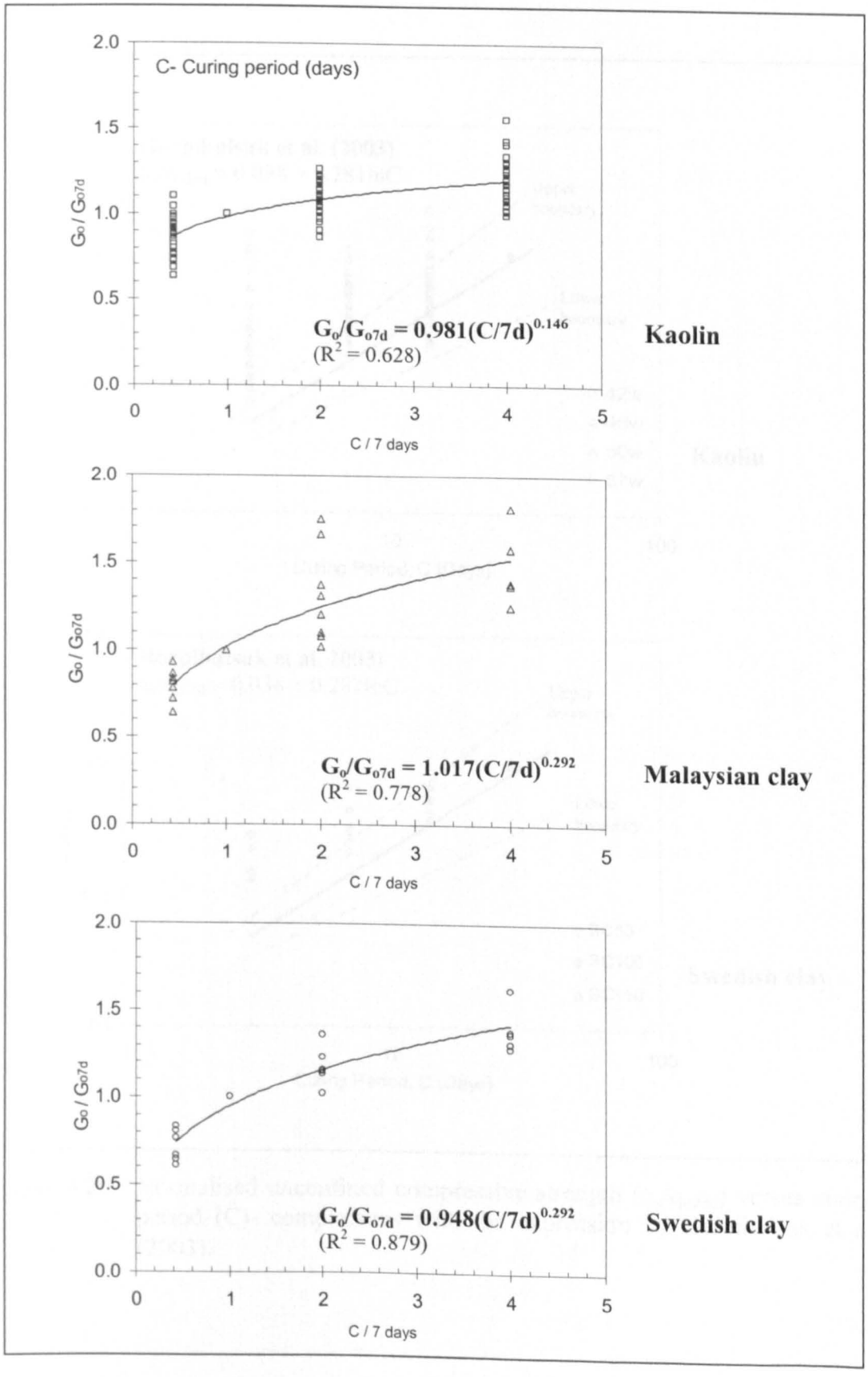

Figure 4.19b: Normalised maximum shear modulus (G_o).

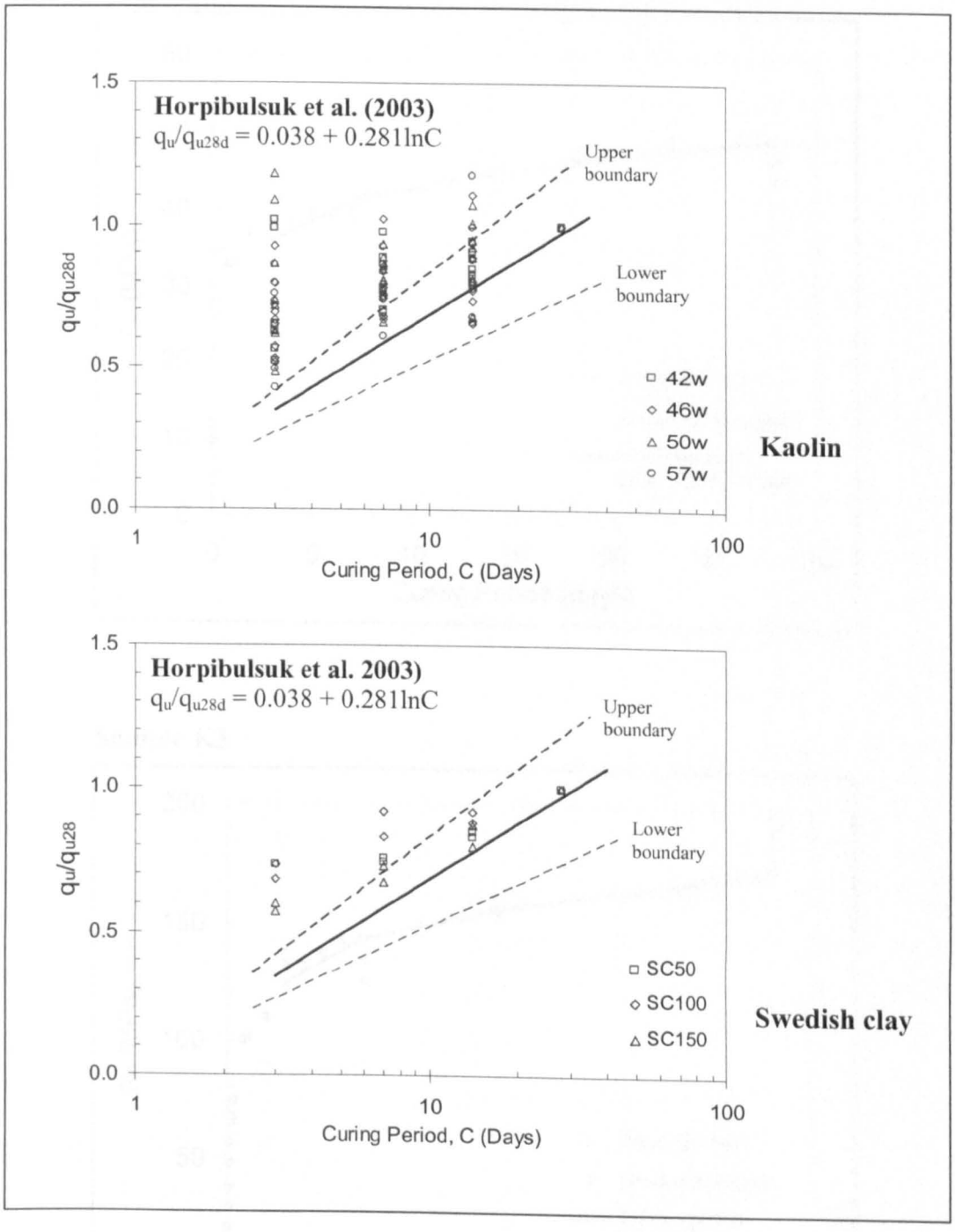

Figure 4.20: Normalised unconfined compressive strength (q_u/q_{u28d}) versus curing period (C)- comparisons with the expression by Horpibulsuk et al. (2003).

Sample K1.5

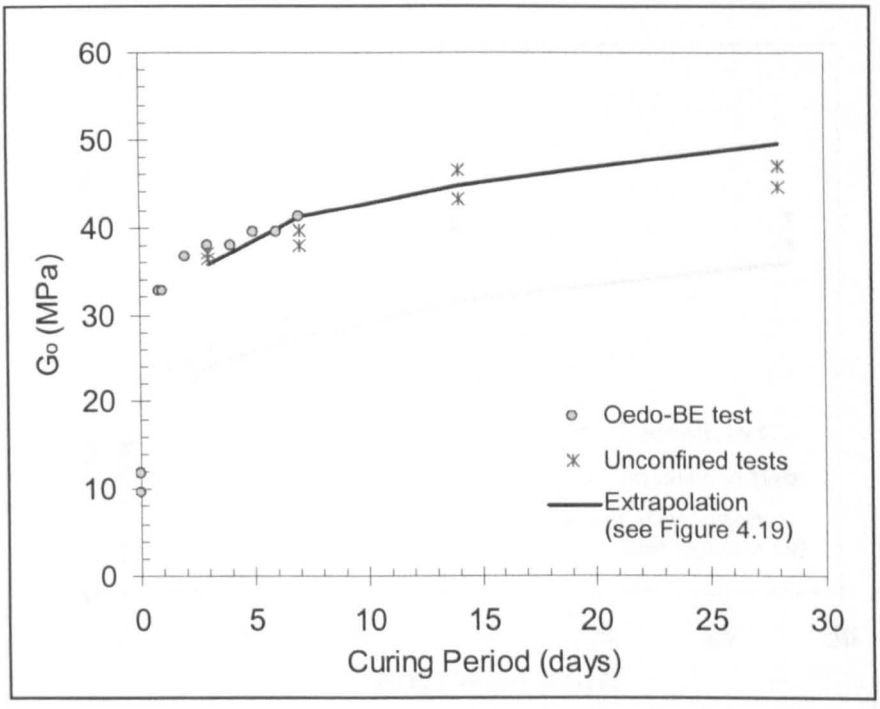

Sample K3

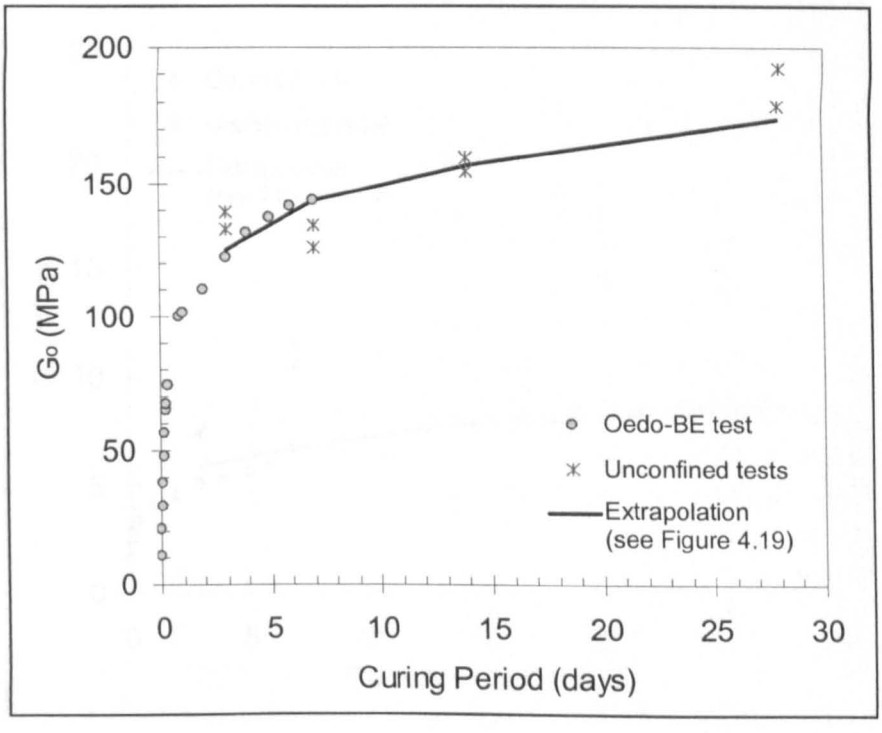

Figure 4.21: Evolution of maximum shear modulus (G_o) during curing period in the oedo-BE cell.

Sample MC1.5

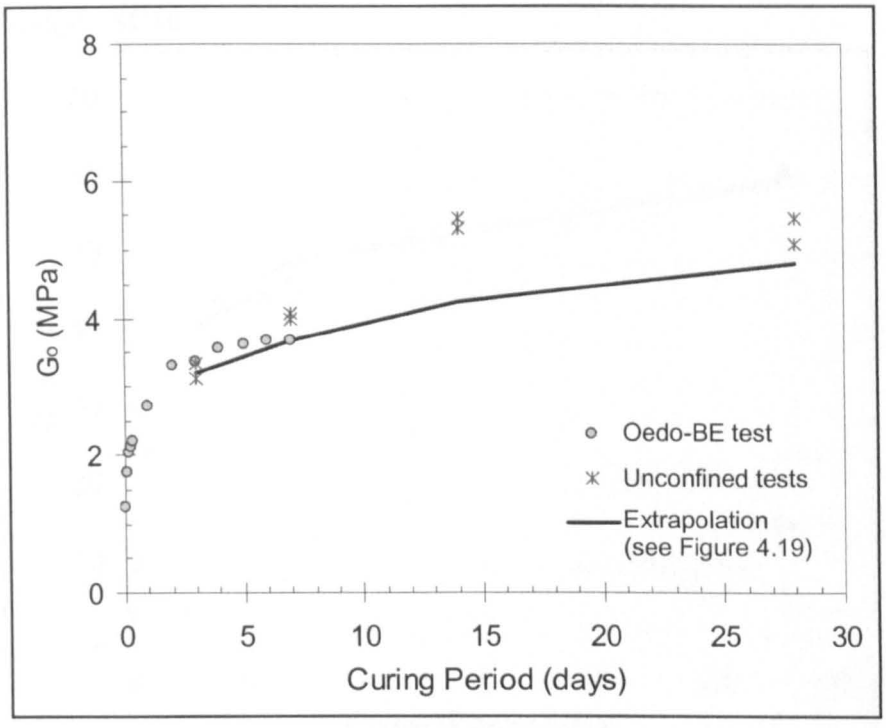

Sample MC3

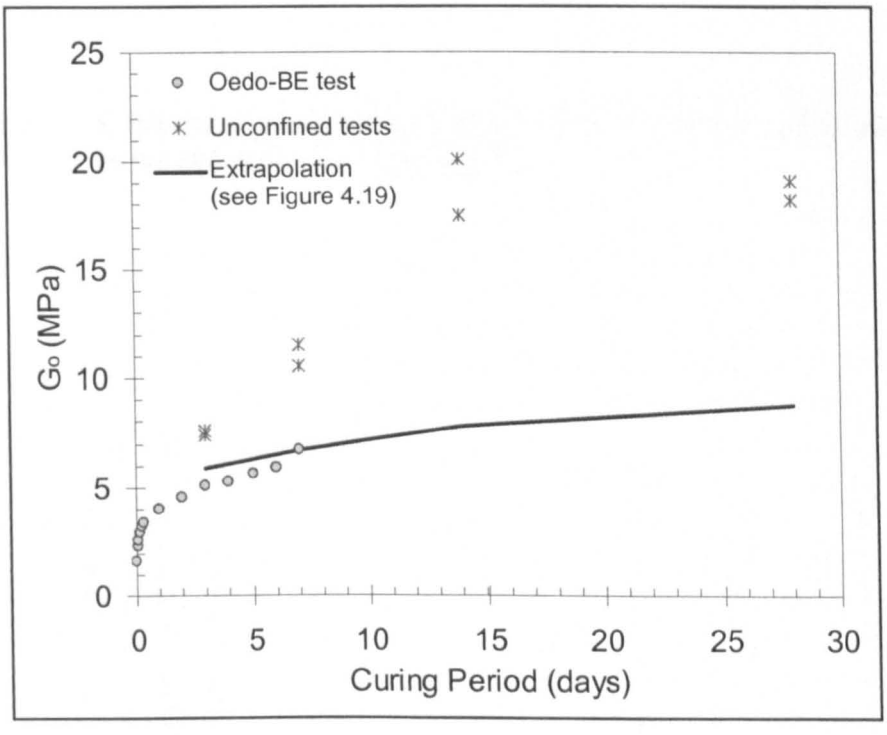

Figure 4.21: Evolution of maximum shear modulus (G_o) during curing period in the oedo-BE cell. *(continued)*

Sample SC10

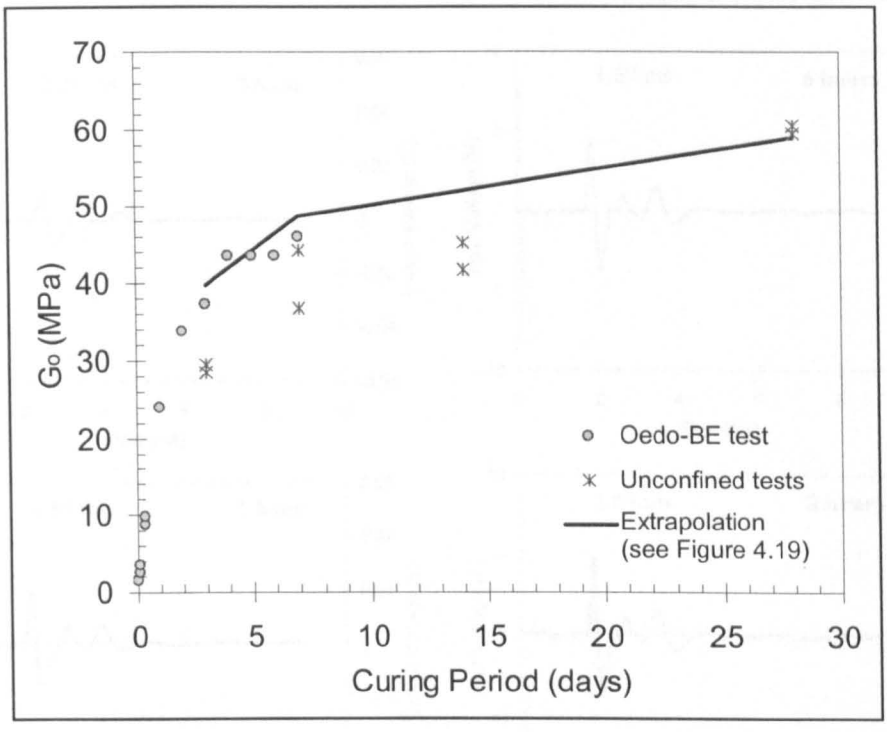

Figure 4.21: Evolution of maximum shear modulus (G_o) during curing period in the oedo-BE cell. *(continued)*

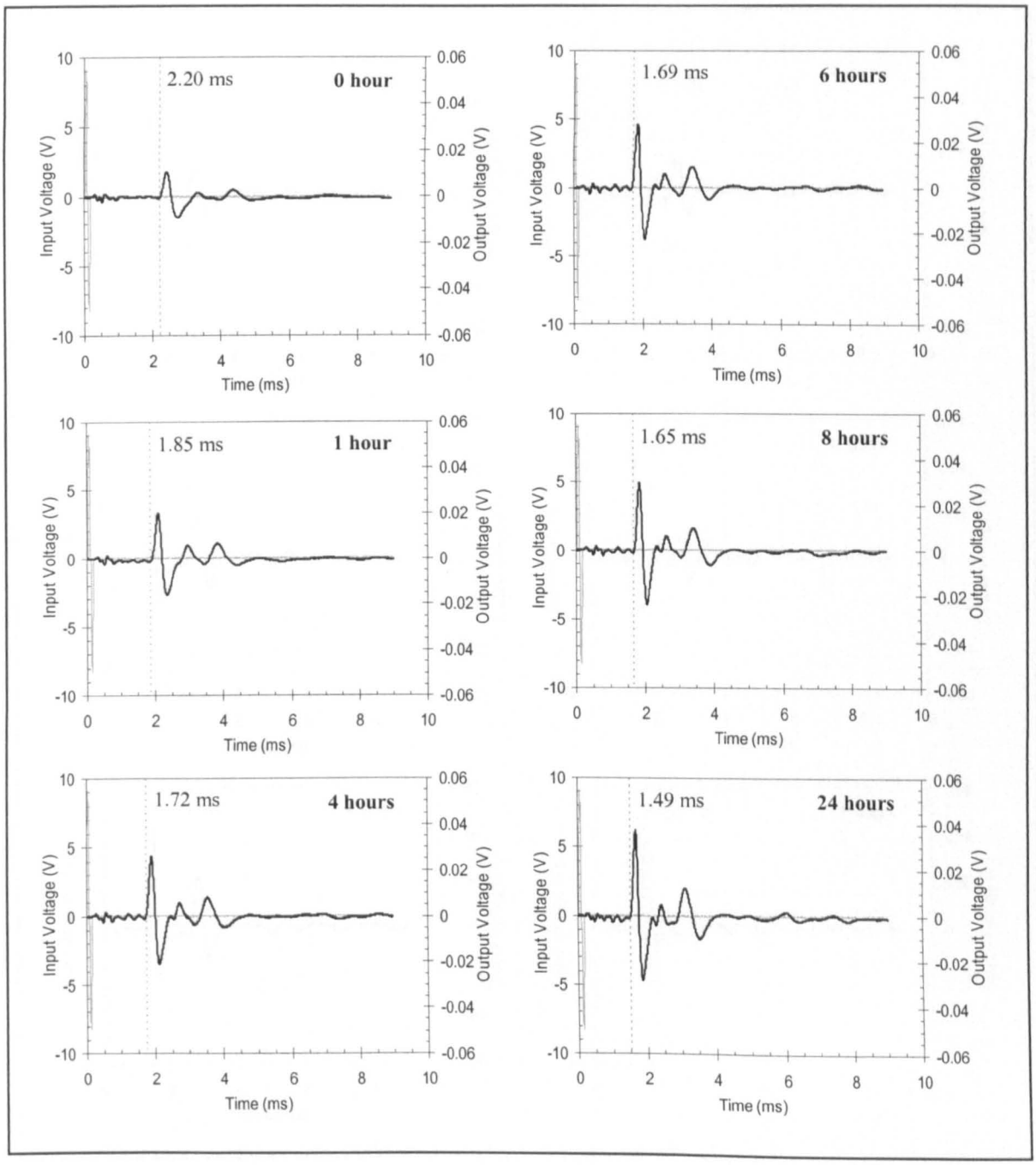

Figure 4.22: Received shear wave signals recorded during curing period in the oedo-BE cell (Sample MC1.5, f_{in} = 7 kHz).

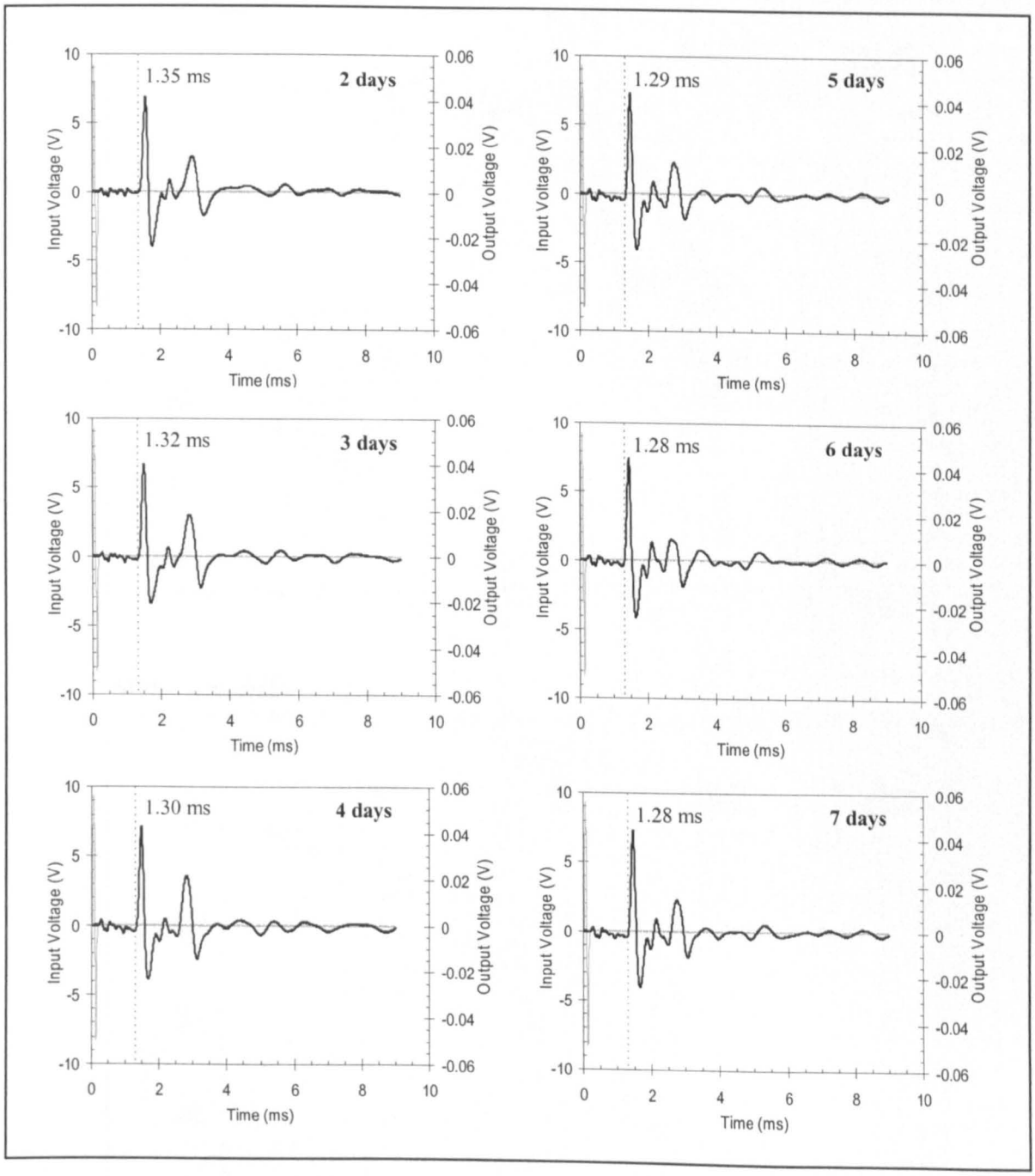

Figure 4.22: Received shear wave signals recorded during curing period in the oedo-BE cell (Sample MC1.5, f_{in} = 7 kHz). *(continued)*

Kaolin (see Table 3.5 for sample descriptions)

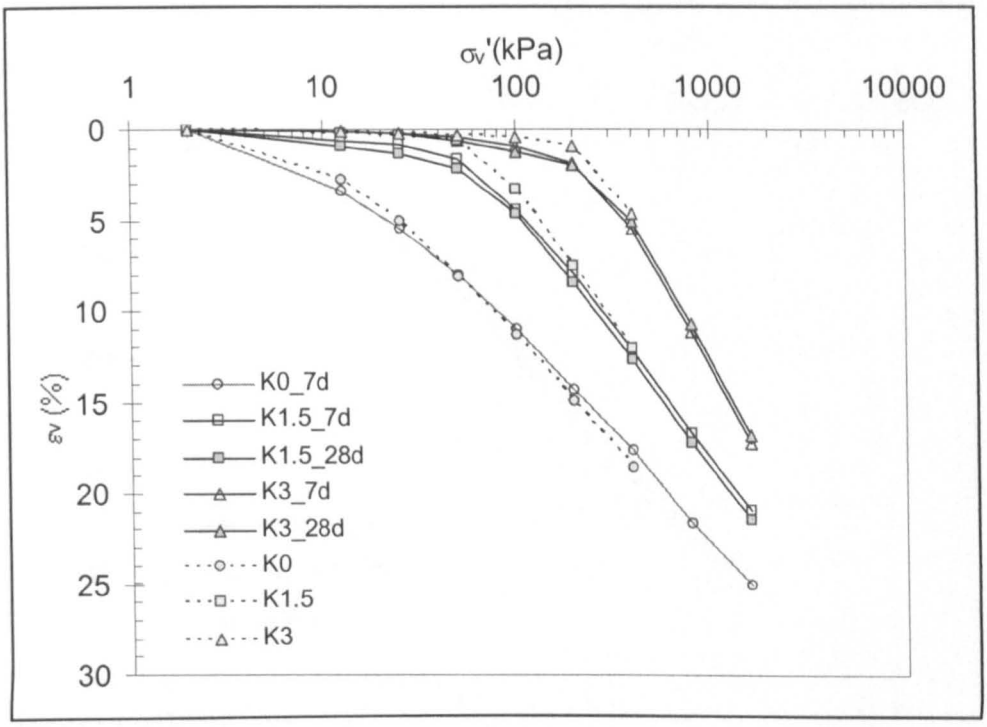

Malaysian clay

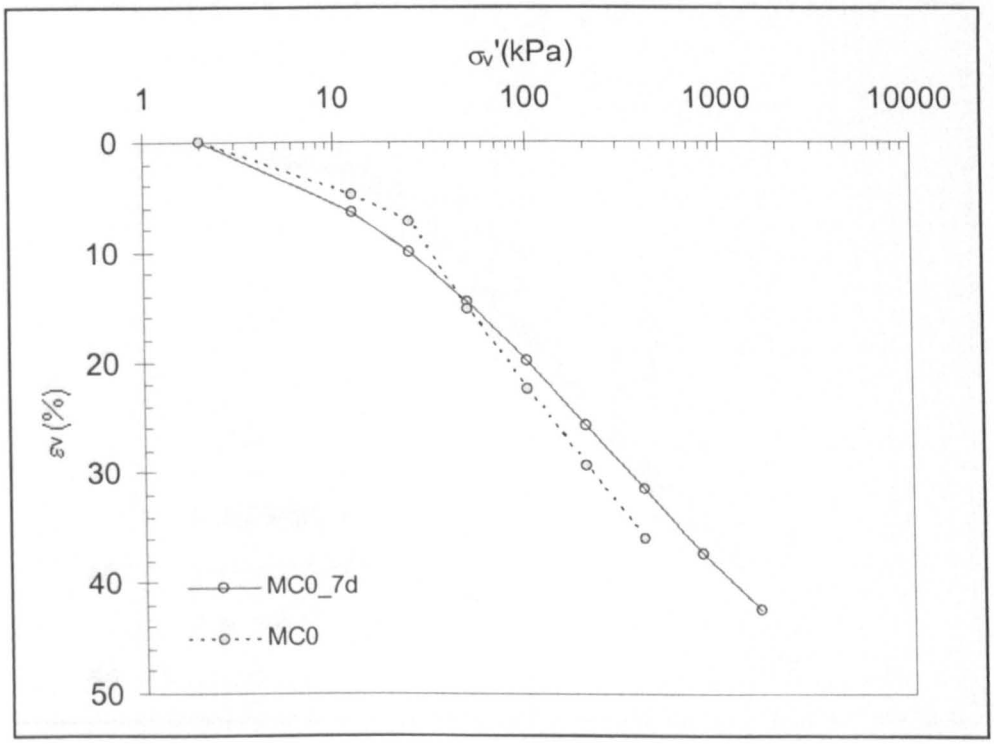

Figure 4.23: Compression curves from oedo-BE and standard oedometer tests.

(see Table 3.5 for sample descriptions)

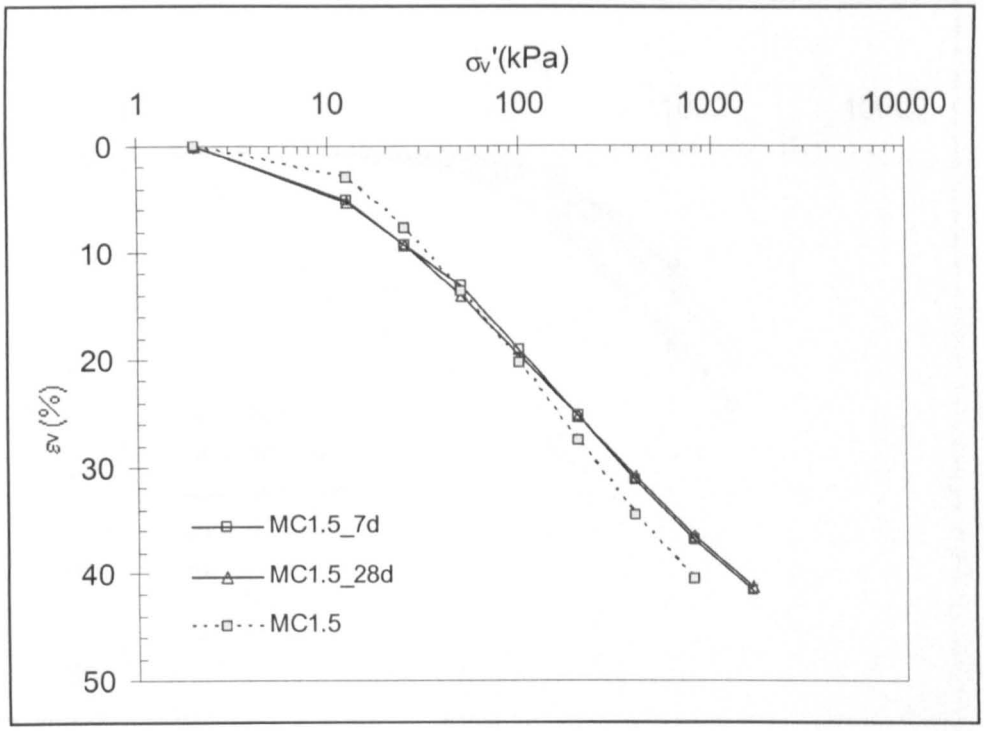

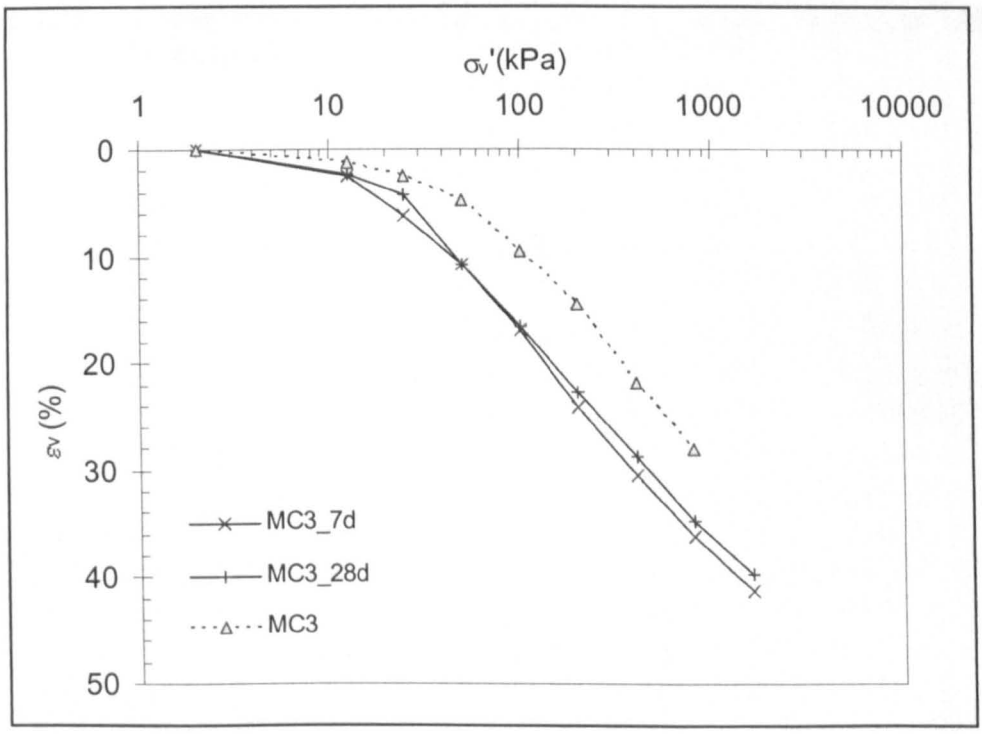

Figure 4.23: Compression curves from oedo-BE and standard oedometer tests. *(continued)*

Swedish clay (see Table 3.5 for sample descriptions)

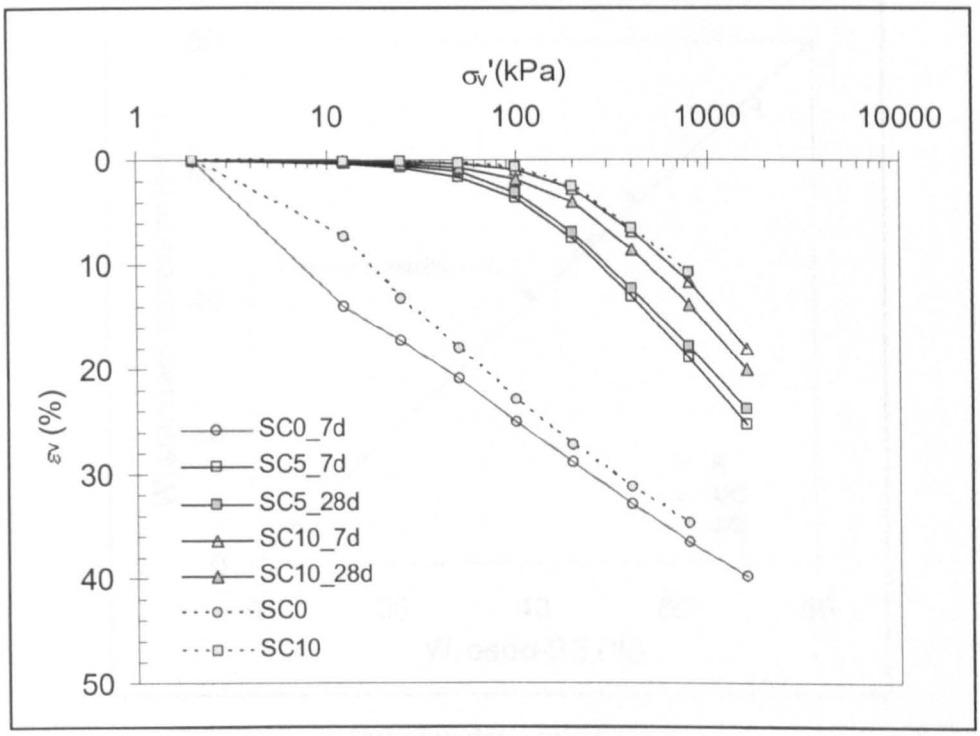

Figure 4.23: Compression curves from oedo-BE and standard oedometer tests. *(continued)*

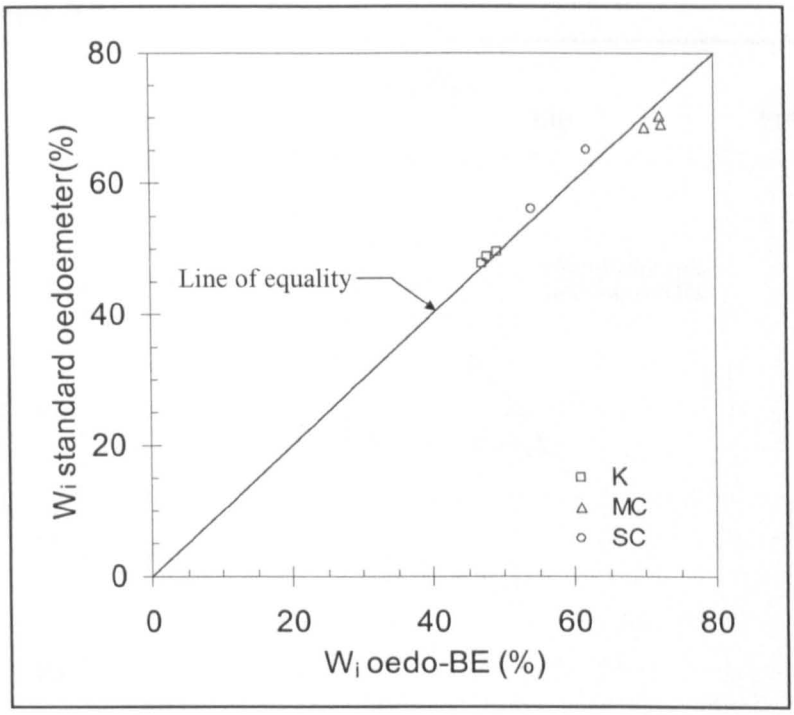

a. Initial water content (w_i)

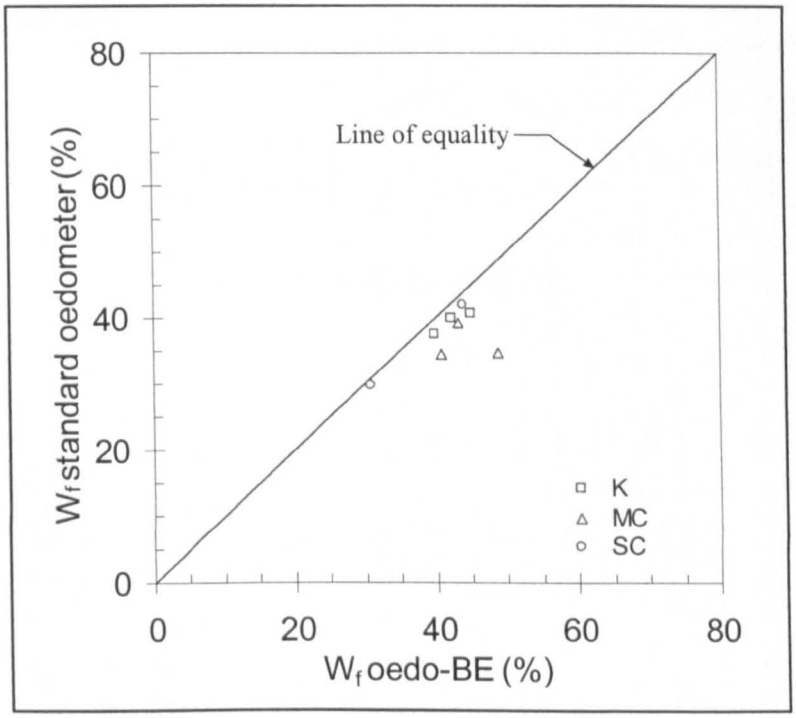

b. Final water content (w_f)

Figure 4.24: Comparison of initial and final water contents of oedo-BE and standard oedometer test samples.

Sample K0

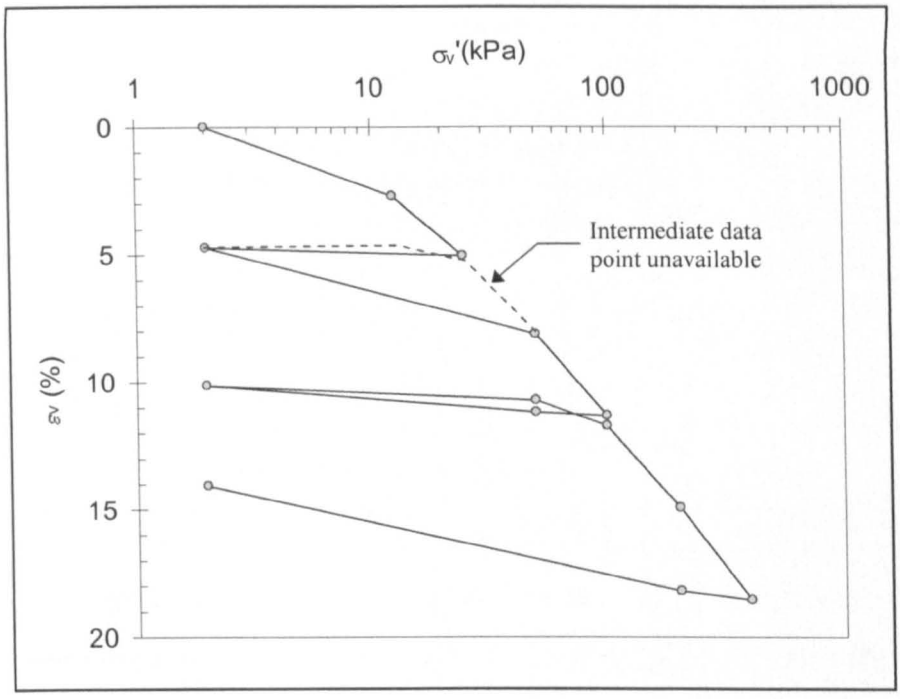

Sample K1.5

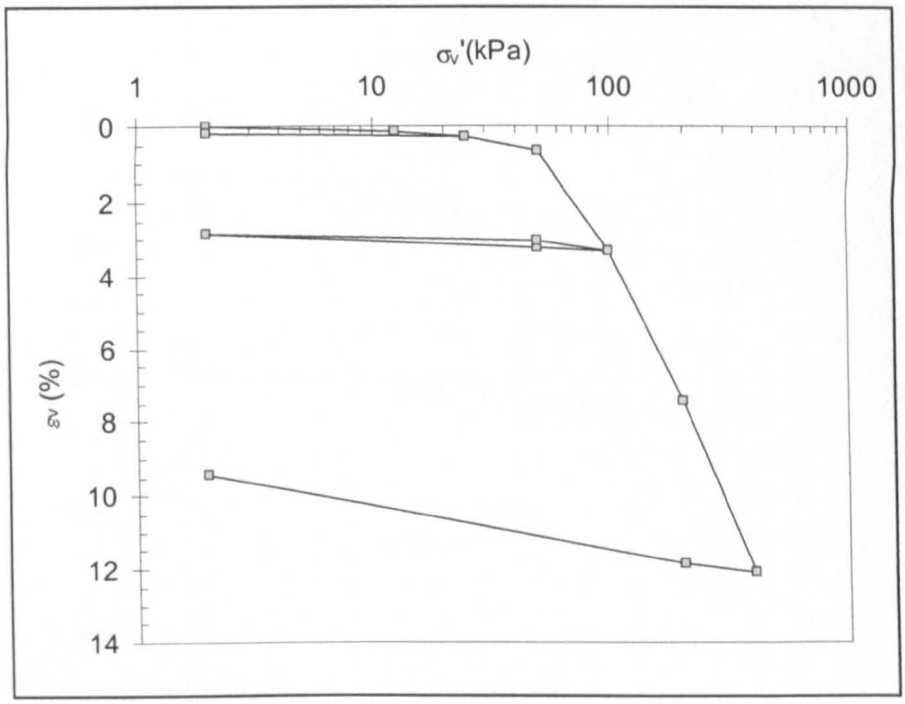

Figure 4.25: Compression curves from Oedo-BE tests- with all loading, unloading and reloading data.

Sample K3

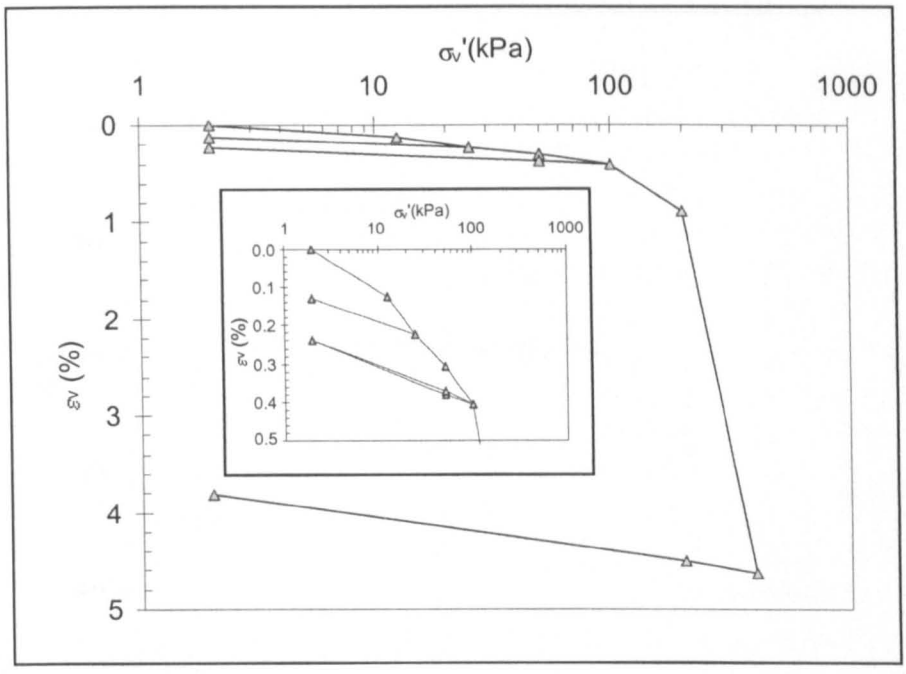

Sample MC0

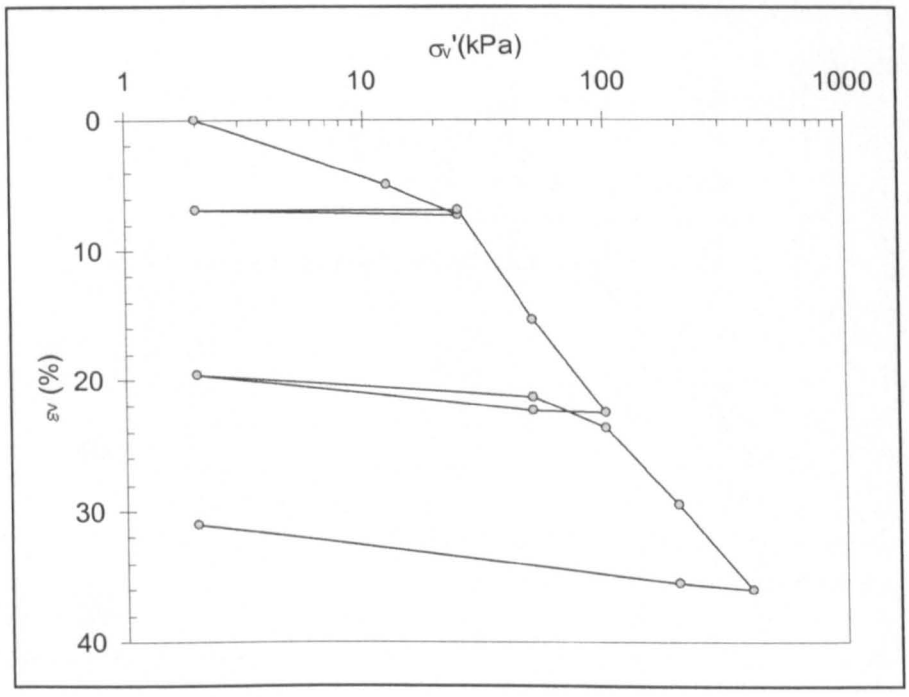

Figure 4.25: Compression curves from Oedo-BE tests- with all loading, unloading and reloading data. *(continued)*

Sample MC1.5

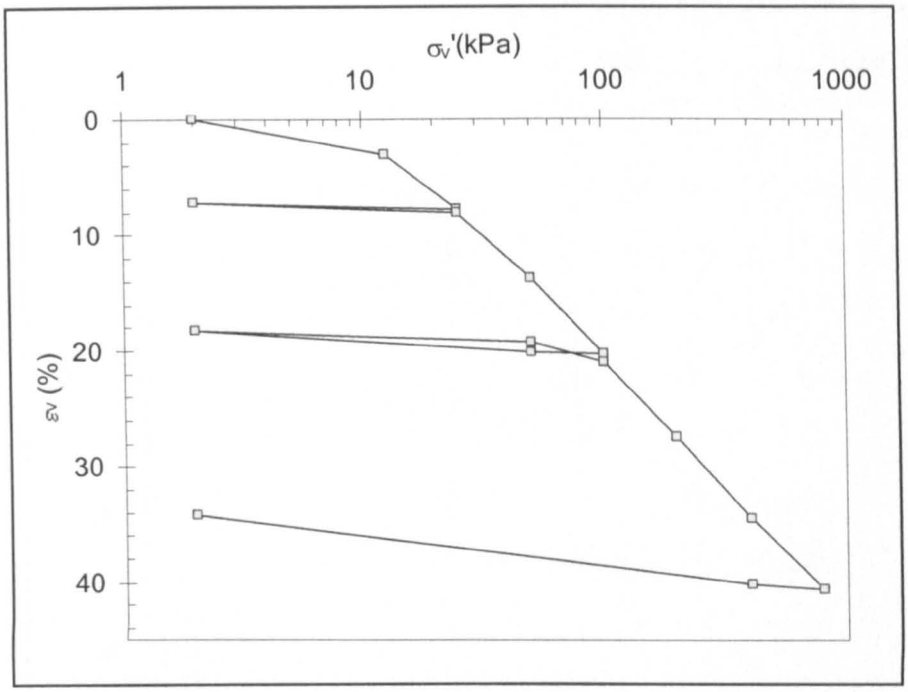

Sample MC3

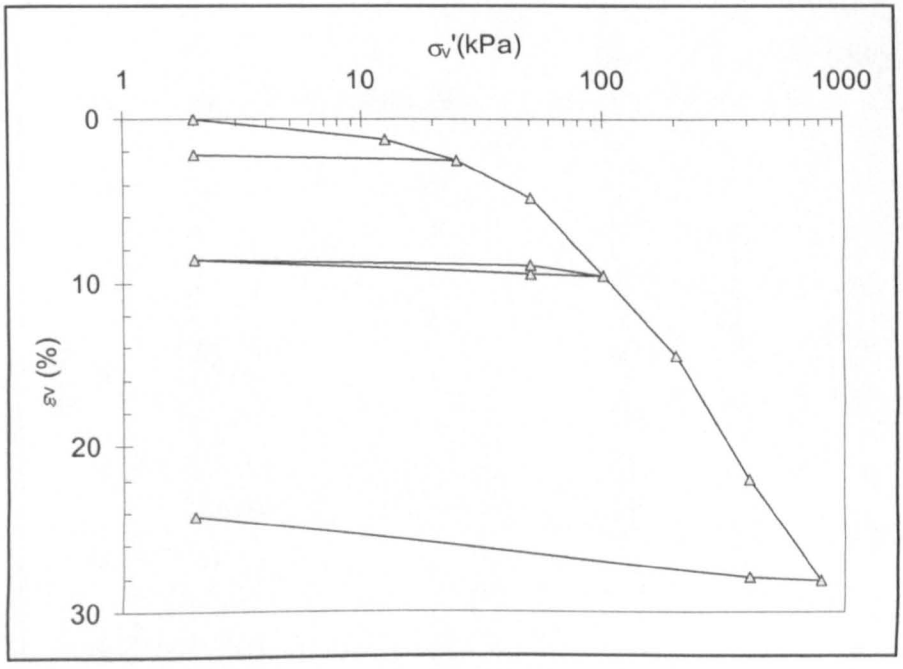

Figure 4.25: Compression curves from Oedo-BE tests- with all loading, unloading and reloading data. *(continued)*

Sample SC0

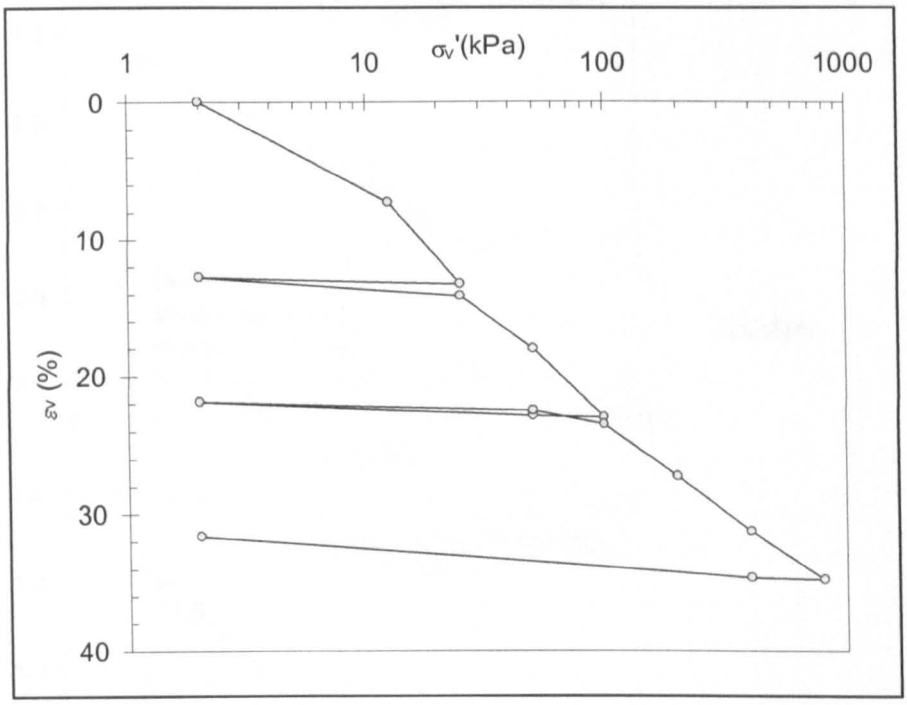

Sample SC10

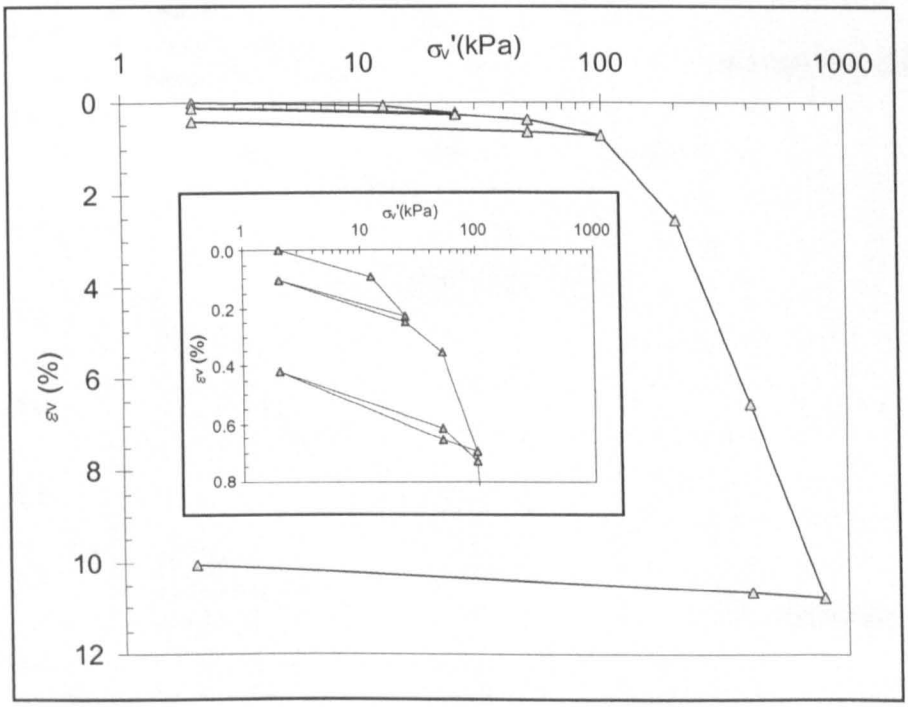

Figure 4.25: Compression curves from Oedo-BE tests- with all loading, unloading and reloading data. *(continued)*

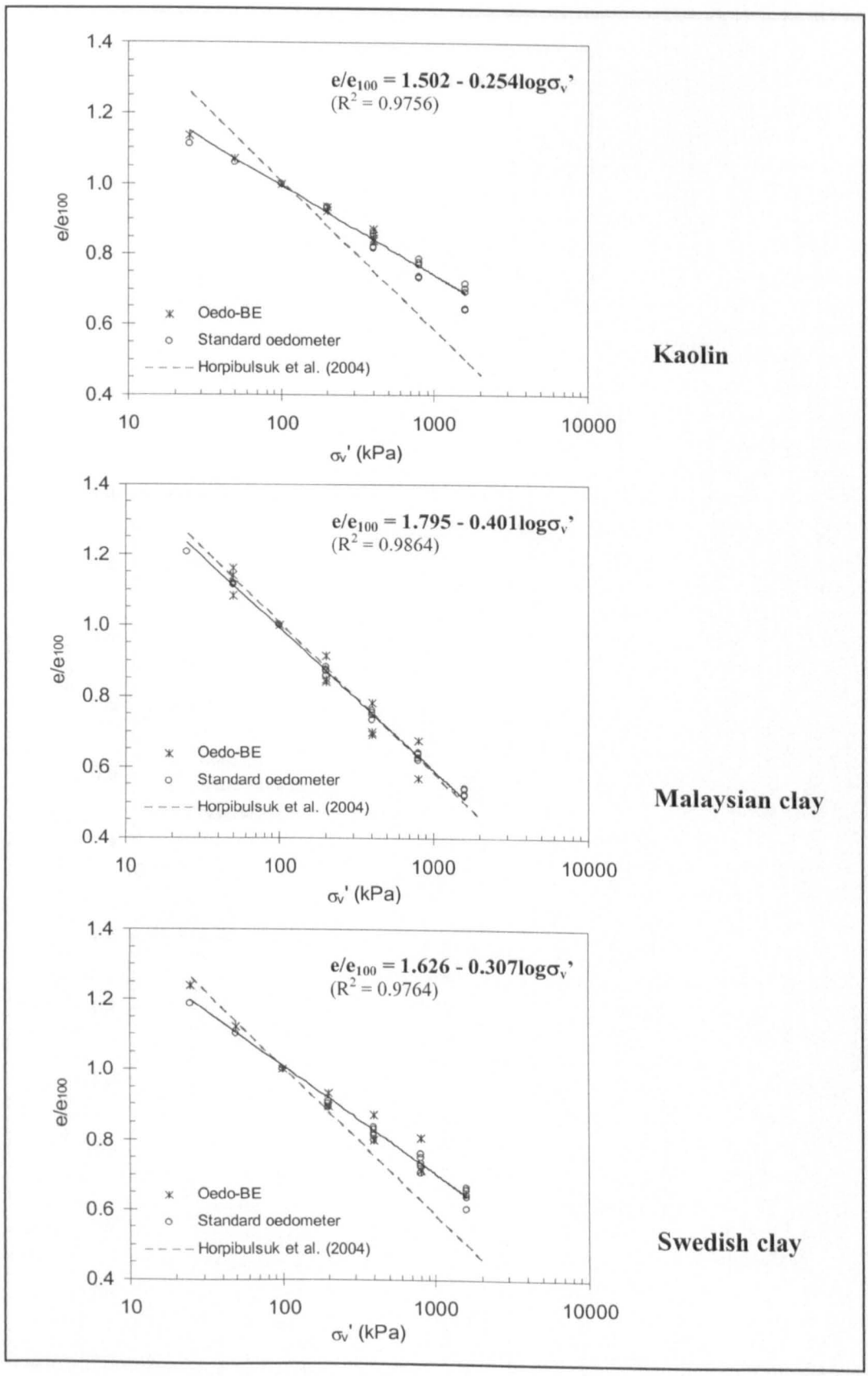

a. Worked forward with settlement data based on e_o.

Figure 4.26: $e/e_{100} - \sigma_v'$ plots- comparisons with the correlation by Horpibulsuk et al. (2004).

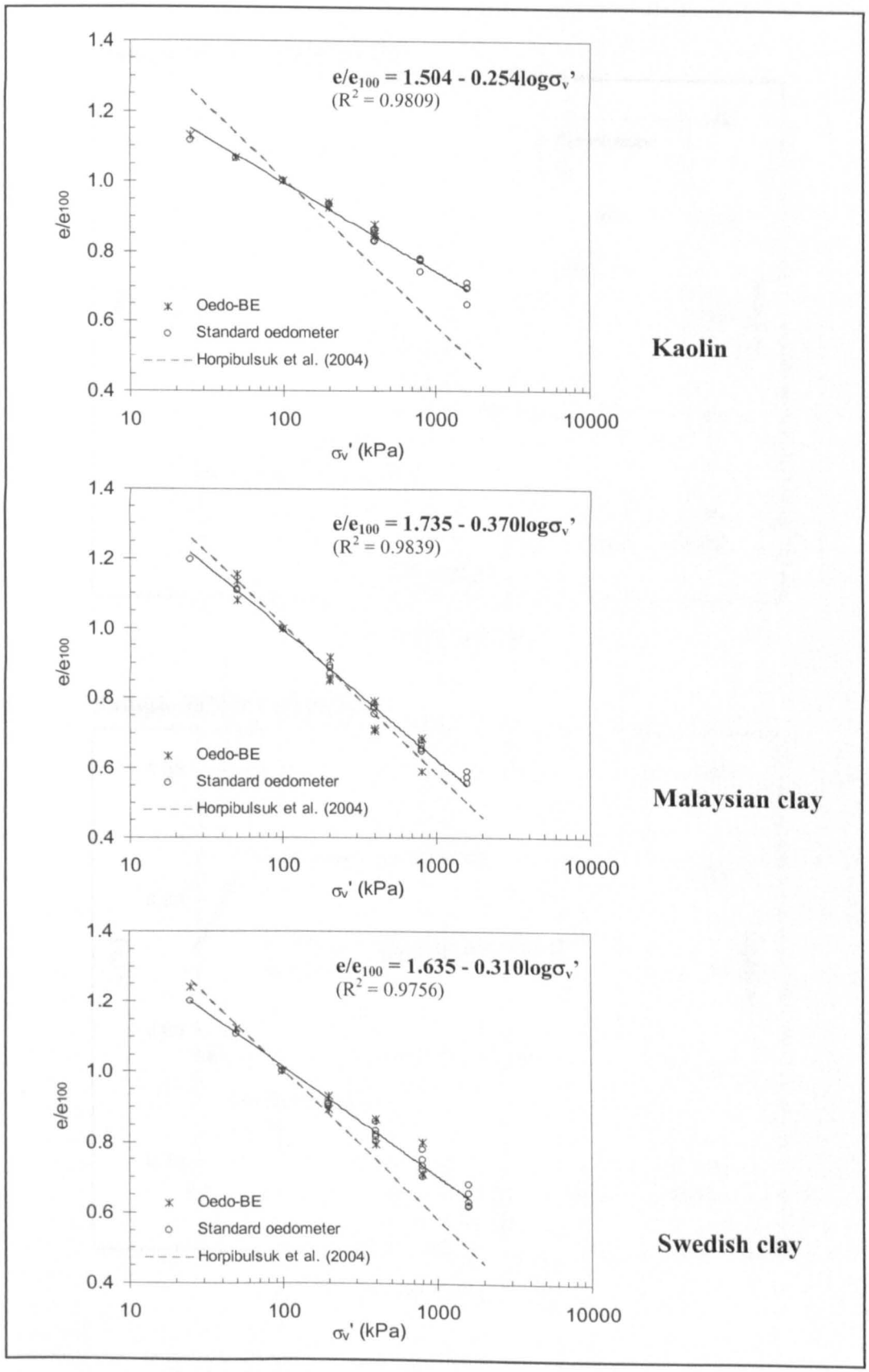

b. Worked backwards with settlement data based on e_f ($S_{rf} = S_{ro}$).

Figure 4.26: $e/e_{100} - \sigma_v'$ plots- comparisons with the correlation by Horpibulsuk et al. (2004). *(continued)*

Sample SC10: 200-400 kPa

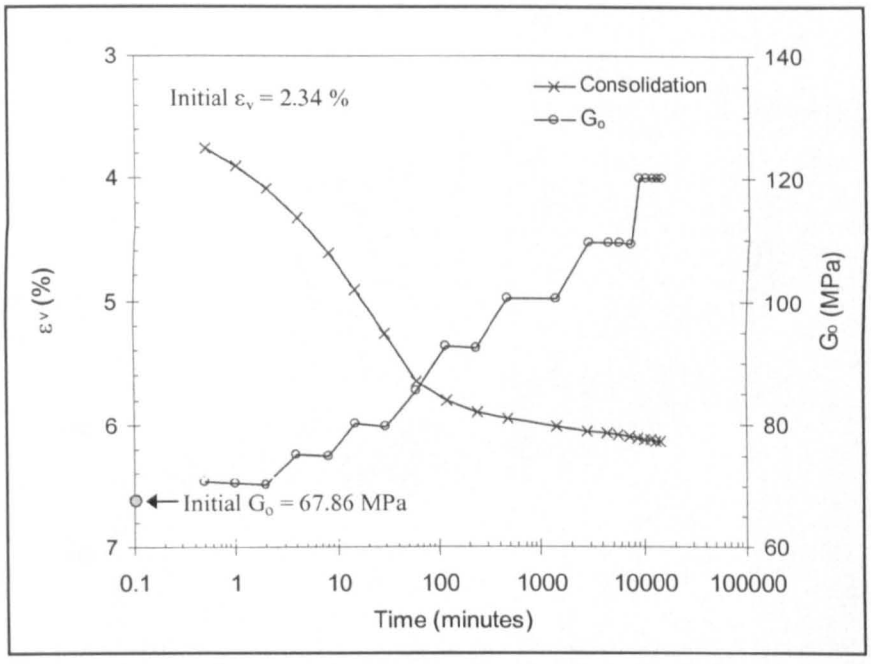

a. A loading stage.

Sample SC10: 100-50 kPa

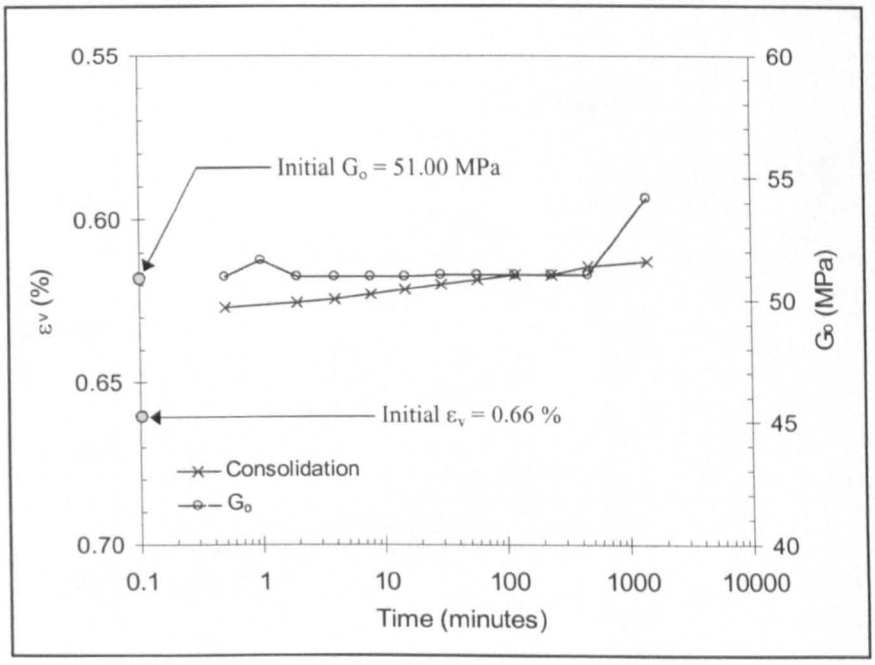

b. An unloading stage.

Figure 4.27: Change of maximum shear modulus (G_o) in a single loading or unloading stage.

Sample SC10

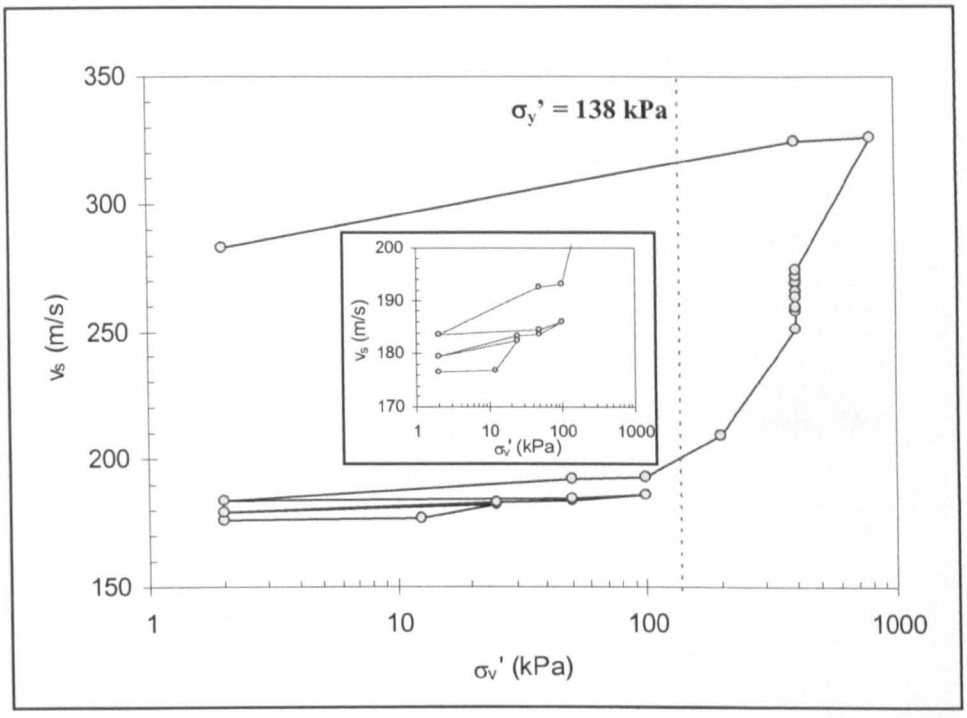

a. $v_s - \sigma_v'$.

Sample SC10

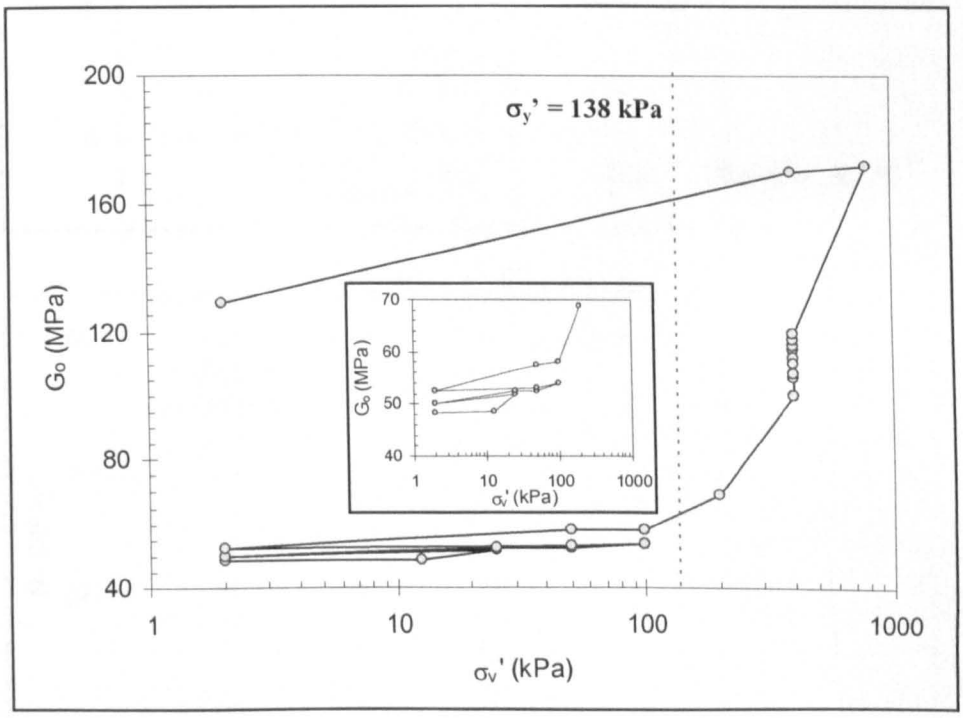

b. $G_o - \sigma_v'$.

Figure 4.28: Change of shear wave velocity (v_s) and maximum shear modulus (G_o) with effective vertical stress (σ_v') in a test.

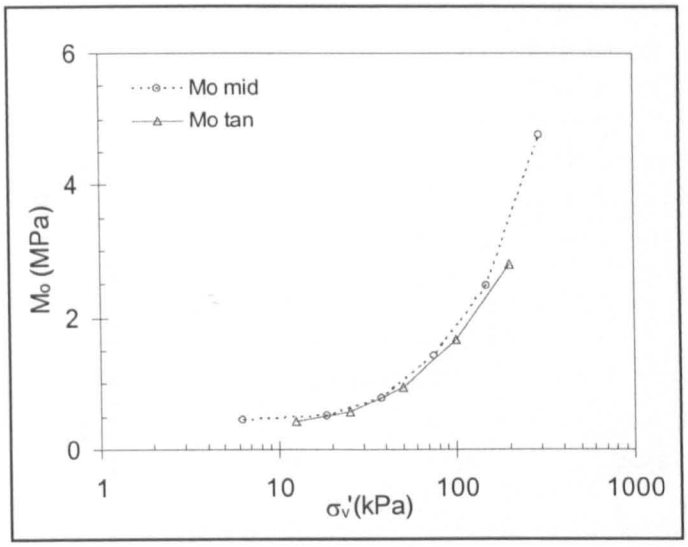

Kaolin: K0

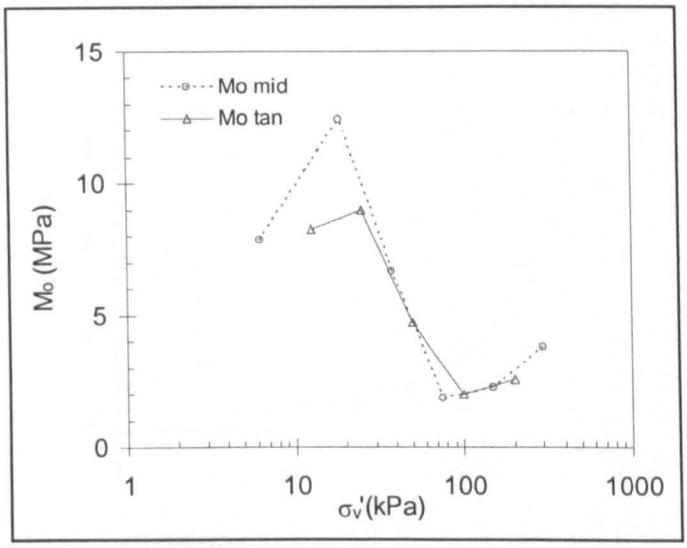

Kaolin: K1.5

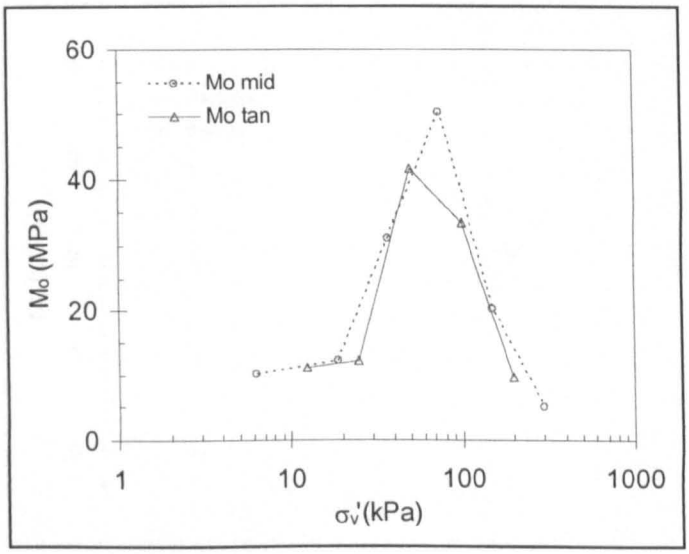

Kaolin: K3

Figure 4.29: Change of constrained modulus (M_o) with effective vertical stress (σ_v') in oedo-BE tests.

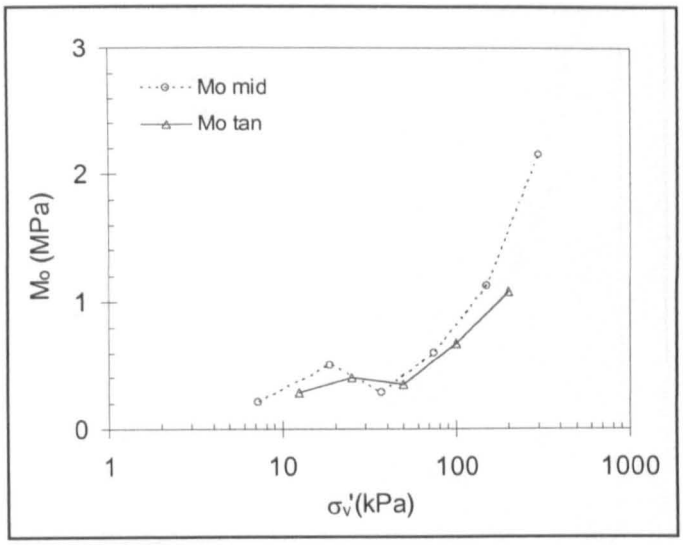

Malaysian clay: MC0

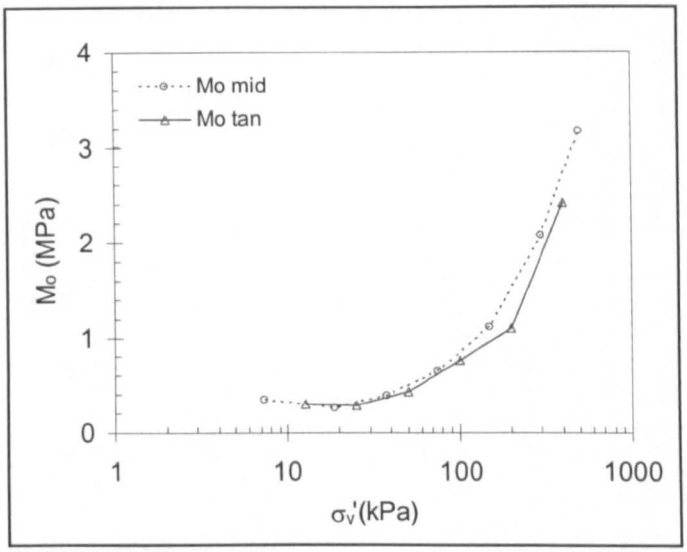

Malaysian clay: MC1.5

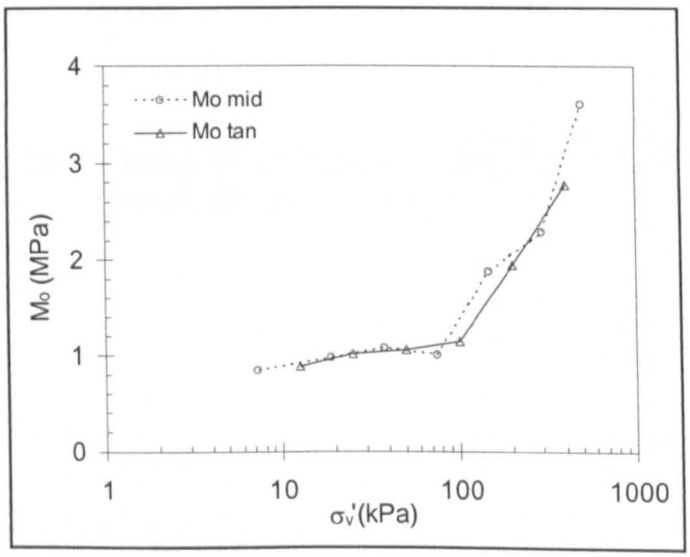

Malaysian clay: MC3

Figure 4.29: Change of constrained modulus (M_o) with effective vertical stress (σ_v') in oedo-BE tests. *(continued)*

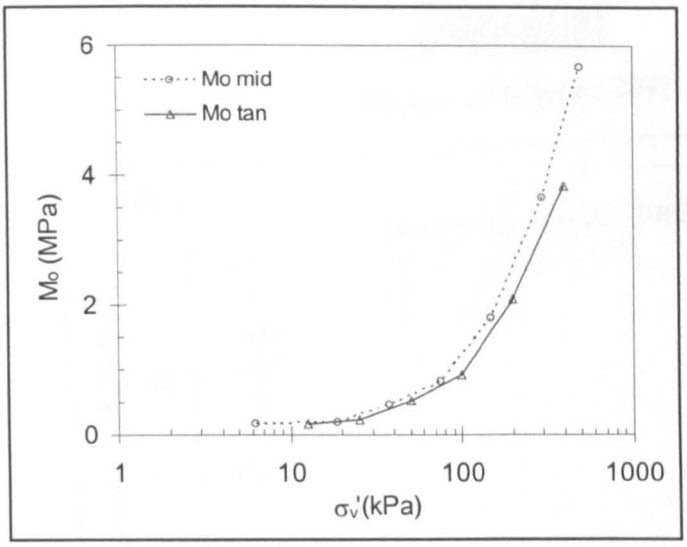

Swedish clay: SC0

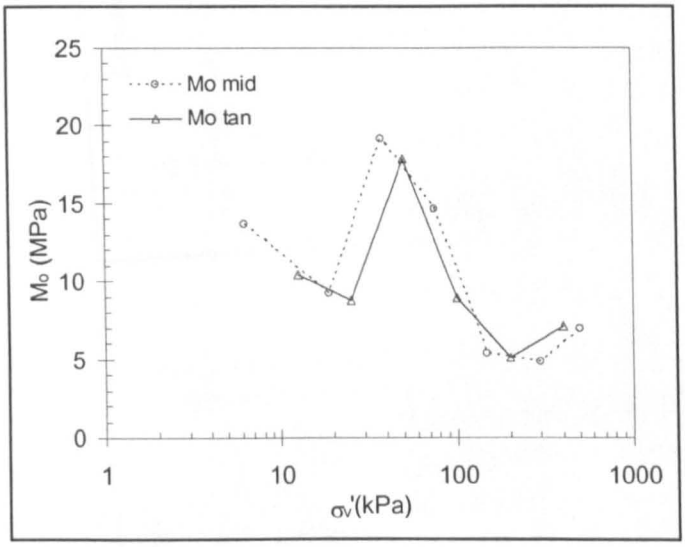

Swedish clay: SC10

Figure 4.29: Change of constrained modulus (M_o) with effective vertical stress (σ_v') in oedo-BE tests. *(continued)*

ERRATUM

Figure 4.30 (page 204)

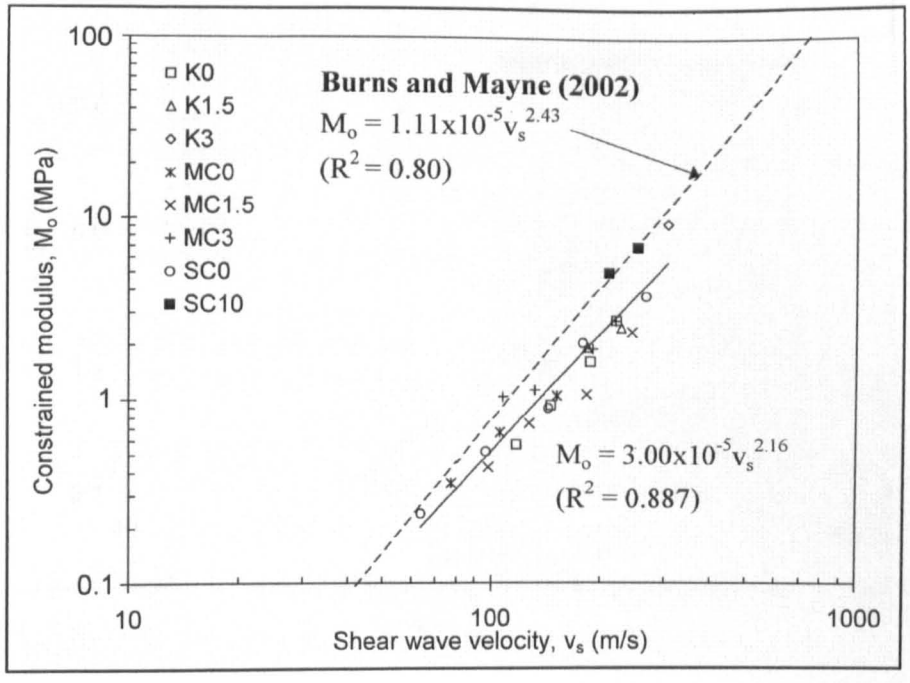

a. M_o- v_s.

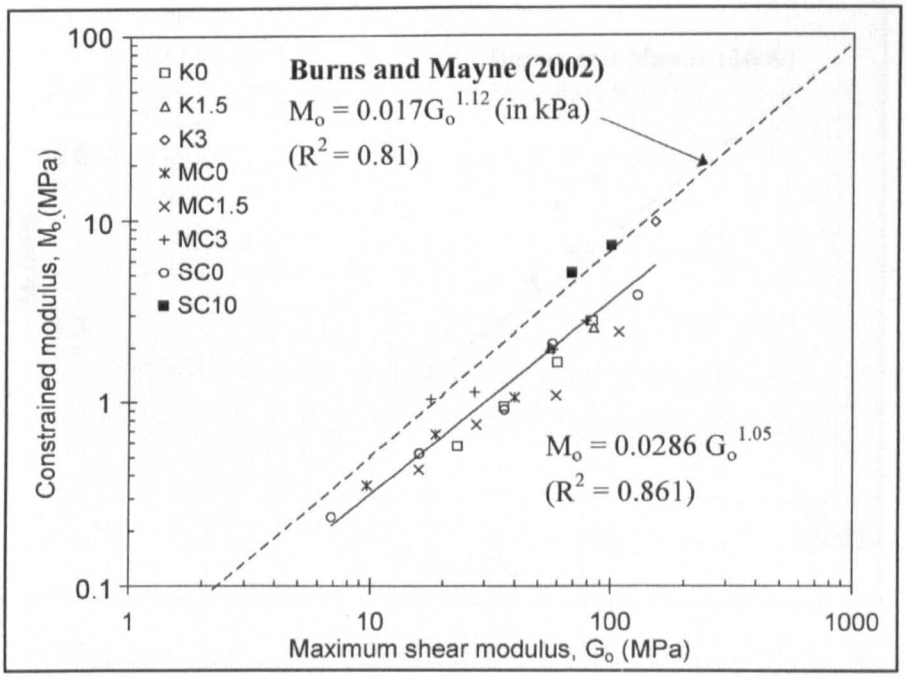

b. M_o- G_o.

Figure 4.30: Correlations of constrained modulus (M_o) with shear wave velocity (v_s) and maximum shear modulus (G_o)- comparisons with the correlations by Burns and Mayne (2002).

Sample K1.5

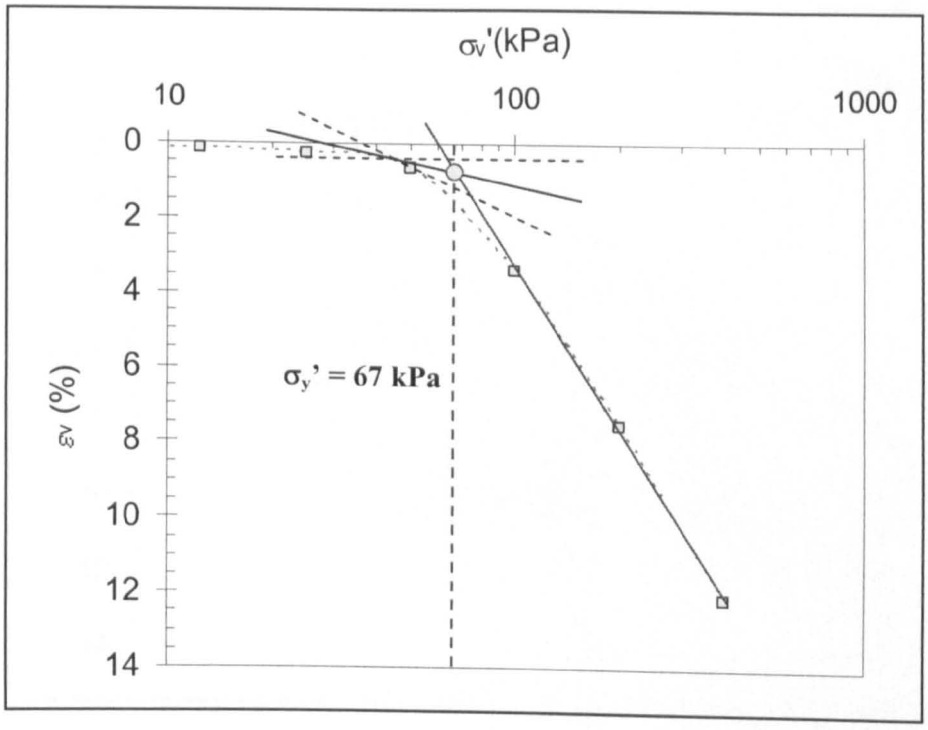

Figure 4.31: Determination of effective yield stress (σ_y')- Casagrande's method.

Sample K1.5

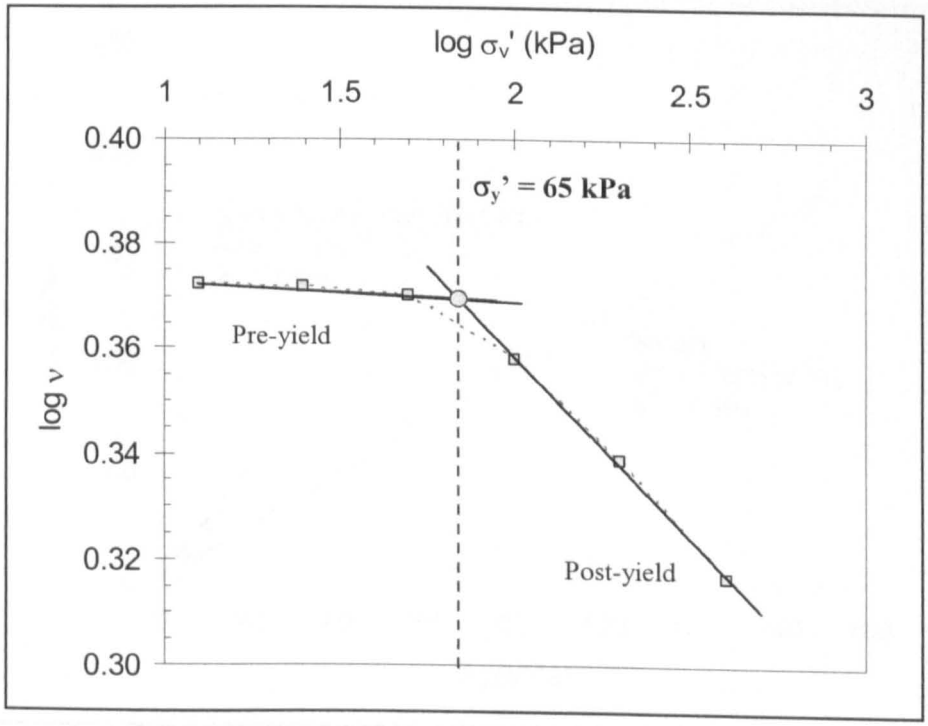

Figure 4.32: Determination of effective yield stress (σ_y')- Butterfield's method.

Sample K1.5

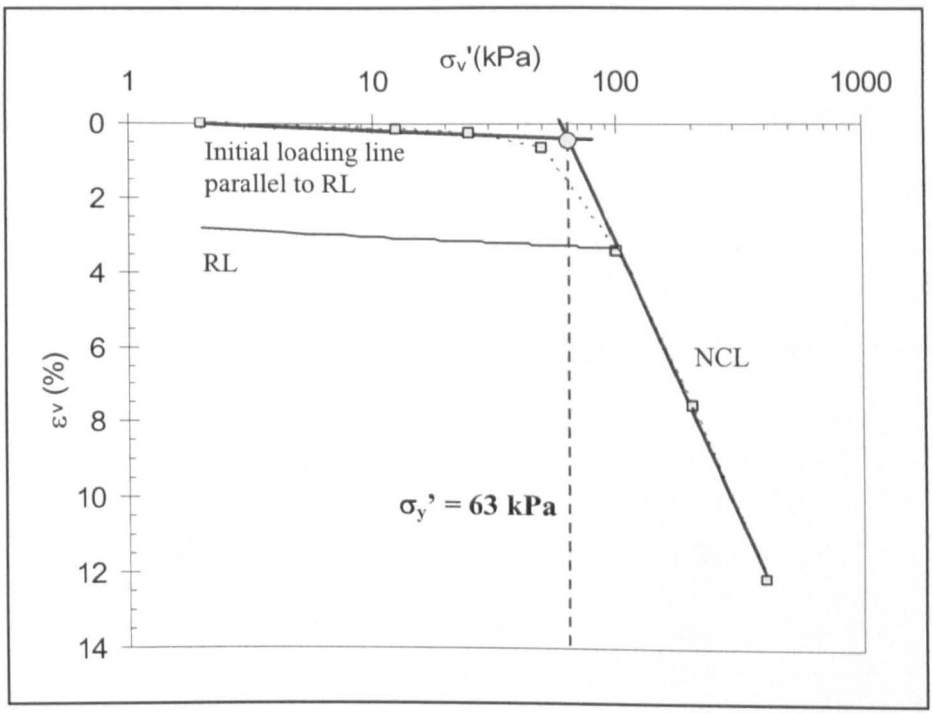

Figure 4.33: Determination of effective yield stress (σ_y')- reloading line (RL) fitting method.

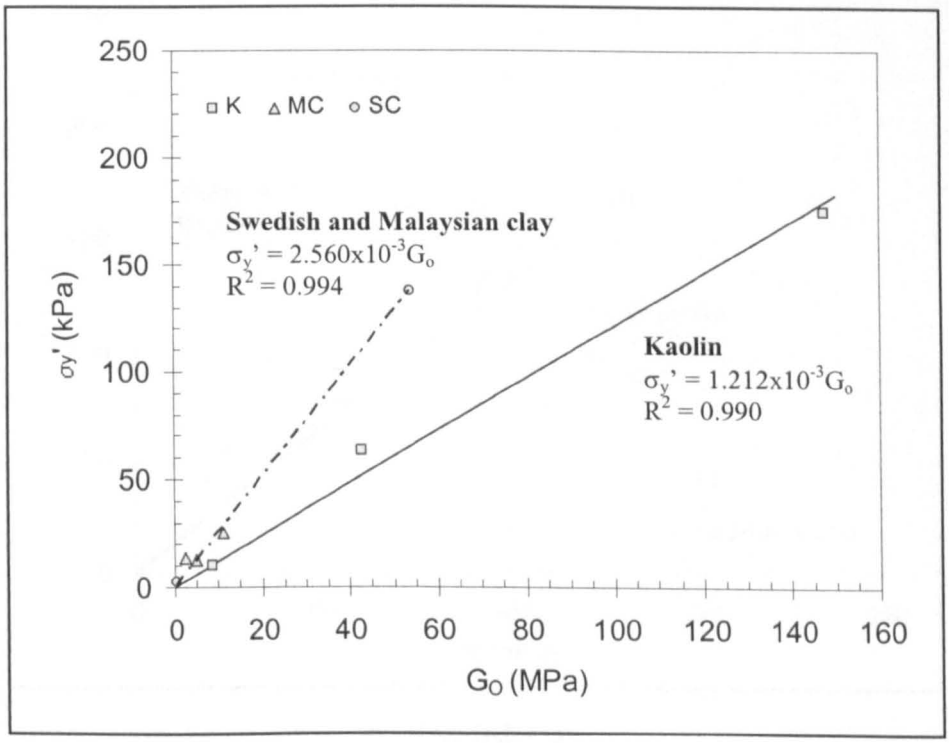

Figure 4.34: Correlation of effective yield stress (σ_y') with maximum shear modulus (G_o).

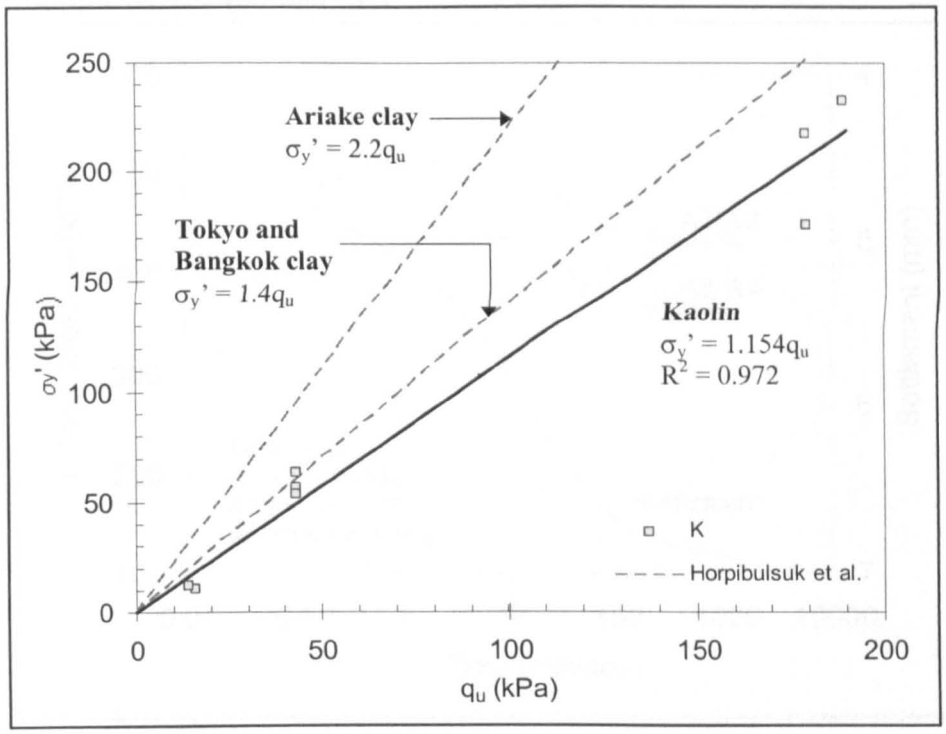

a. Kaolin

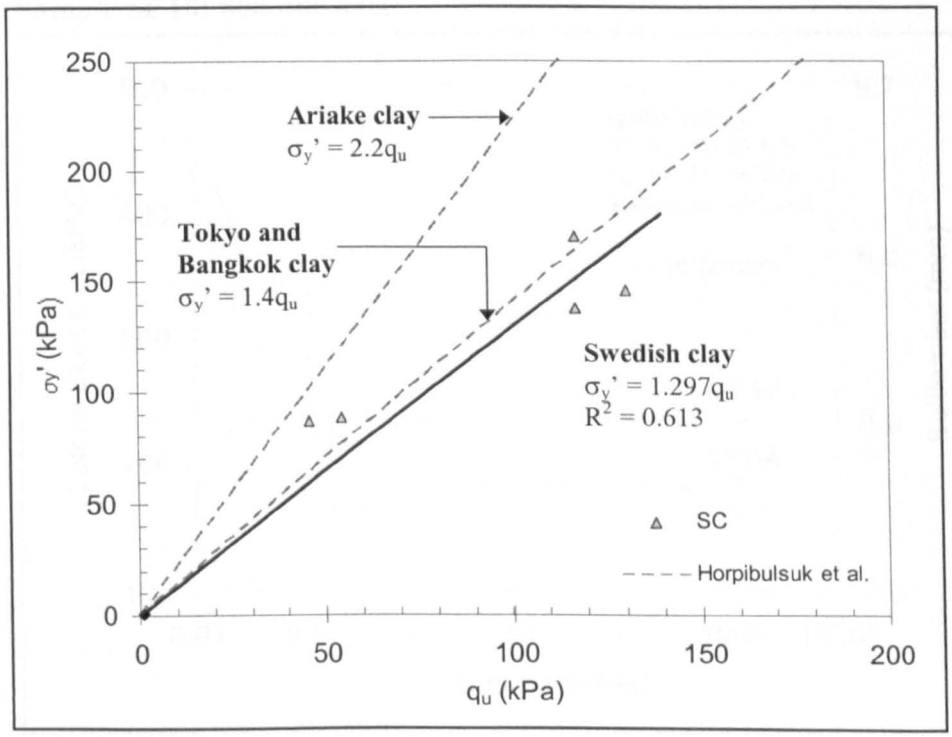

b. Swedish clay

Figure 4.35: Correlation of effective yield stress (σ_y') with unconfined compressive strength (q_u)- comparisons with the correlations by Horpibulsuk et al. (2004).

Sample SC10: 400-800 kPa

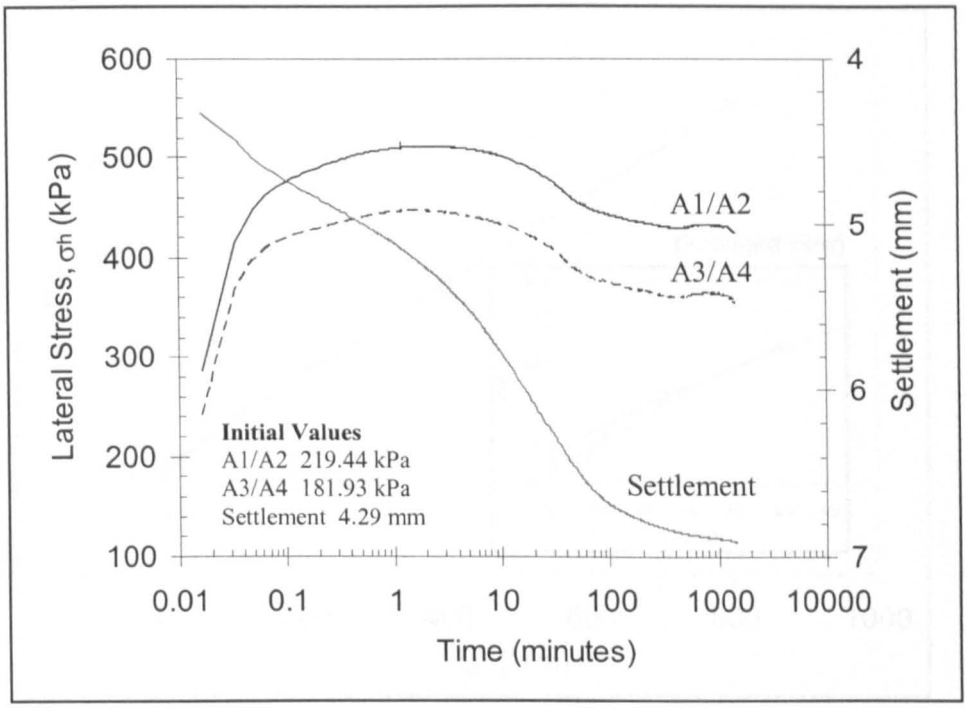

a. Loading stage.

Sample SC10: 800-400 kPa

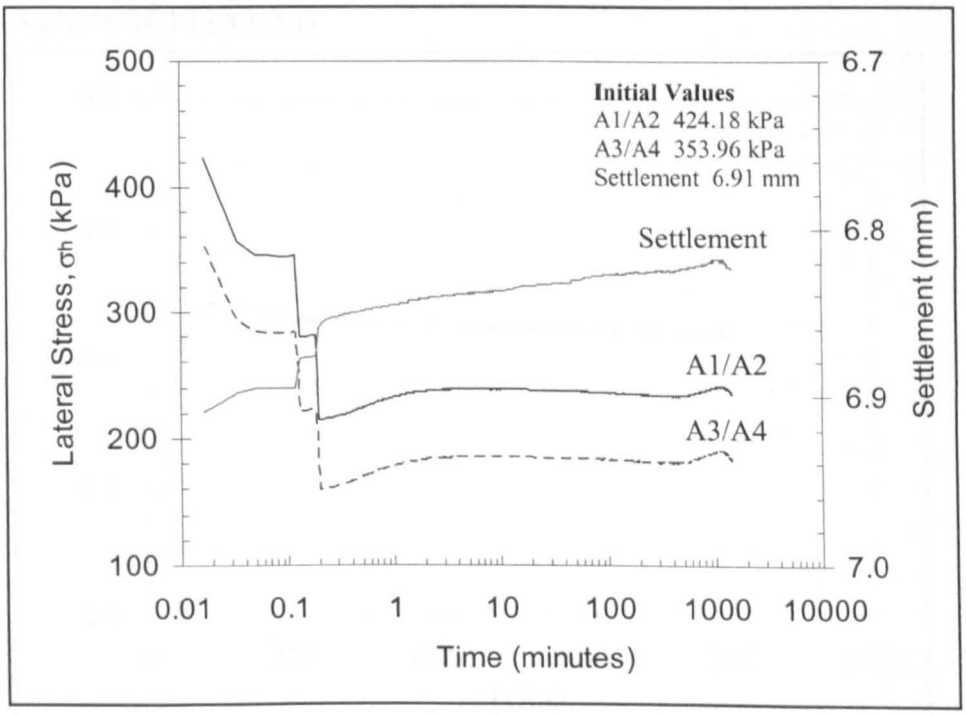

b. Unloading stage.

Figure 4.36: Change of lateral stress (σ_h) in a single loading or unloading stage.

Sample SC10 (A3/A4)

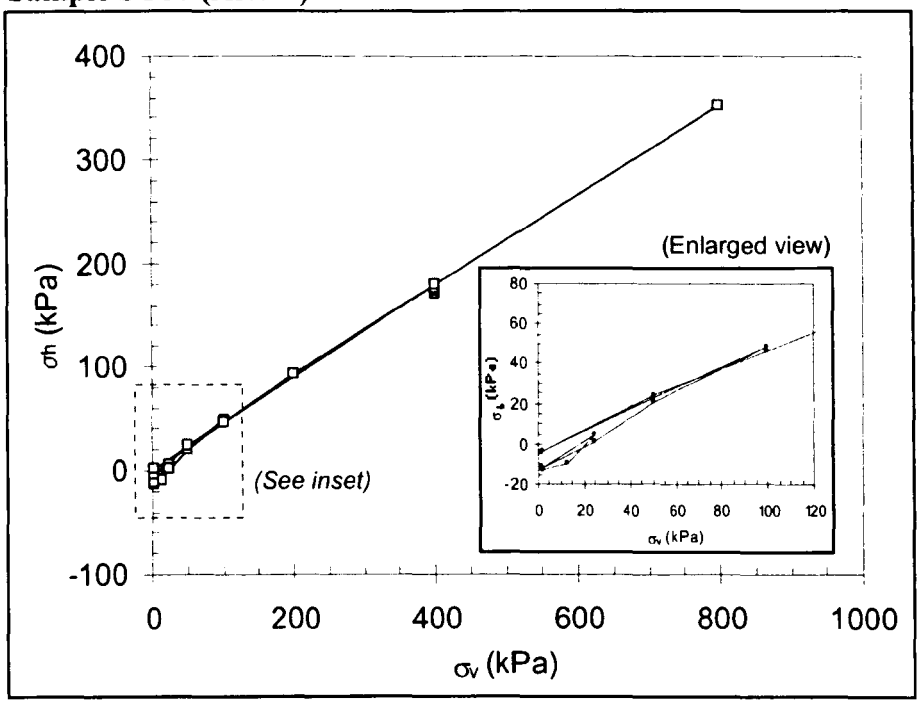

Figure 4.37: Change of total lateral stress (σ_h) with total vertical stress (σ_v) in a test.

Sample SC10 (A3/A4)

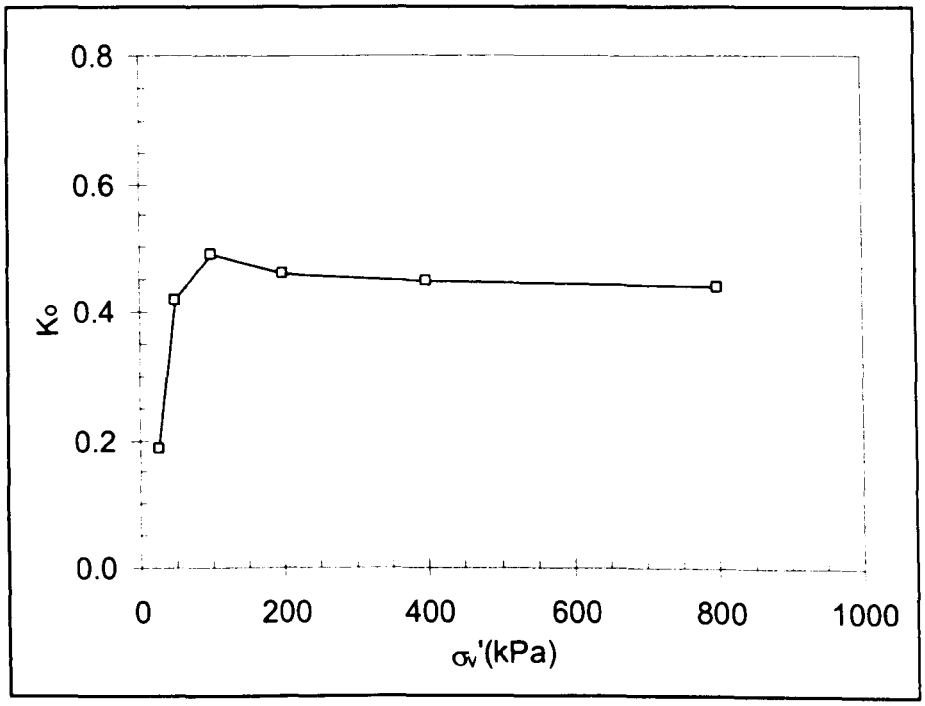

Figure 4.38: Change of coefficient of earth pressure at rest (K_o) with effective vertical stress (σ_v') in a test.

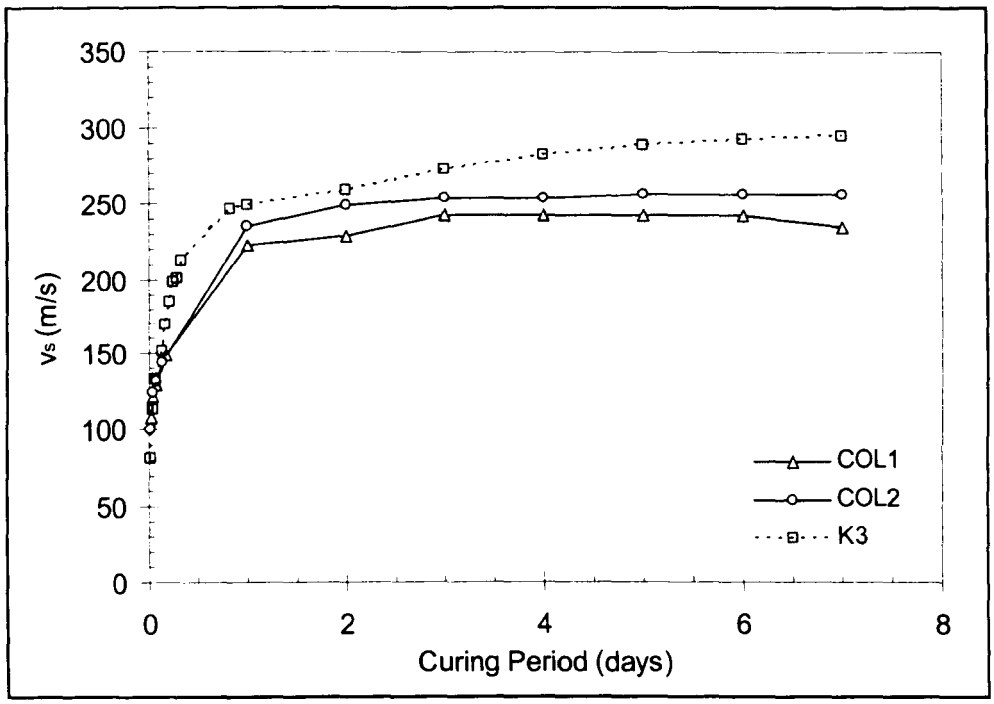

a. Kaolin samples: K3, COL1 and COL2.

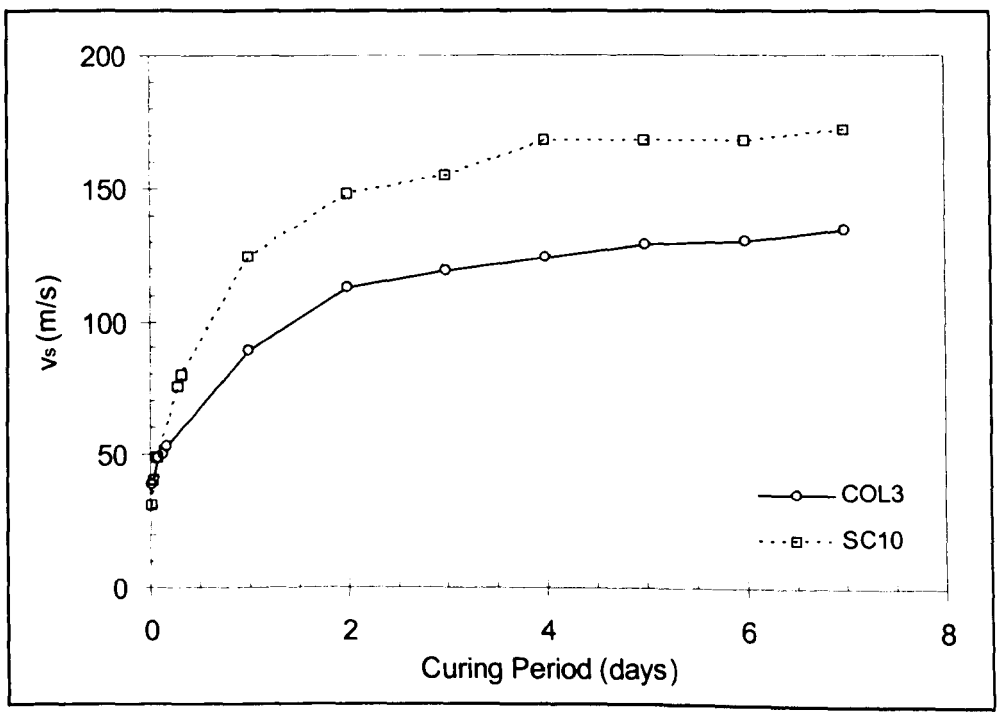

b. Swedish clay samples: SC10 and COL3.

Figure 4.39: Evolution of shear wave velocity (v_s) during curing period in column tests.

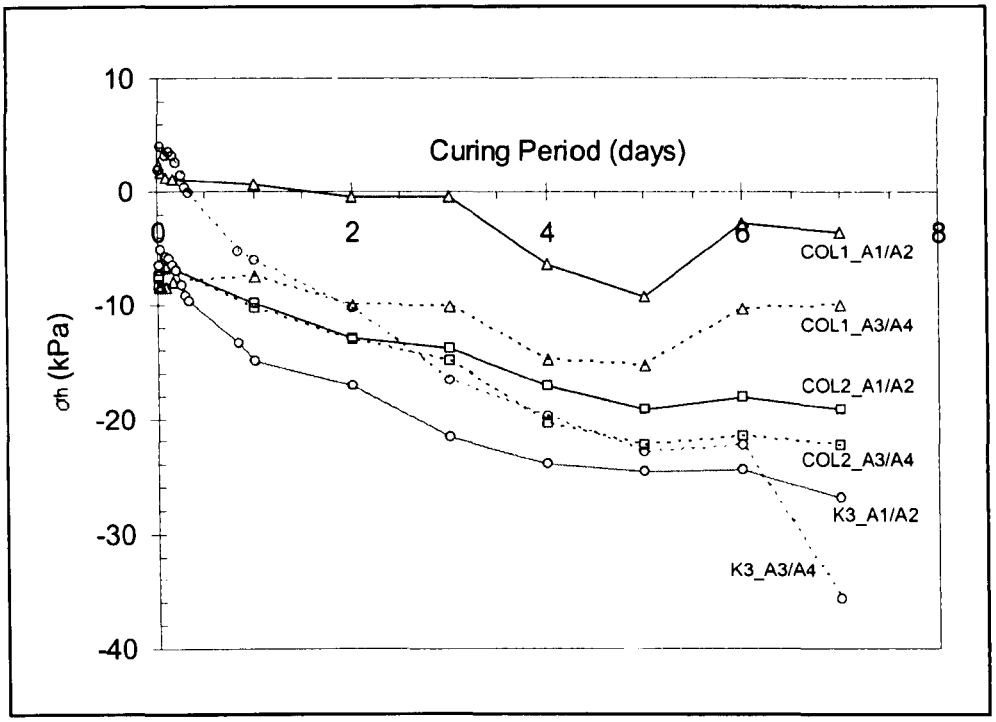

a. Kaolin samples: K3, COL1 and COL2.

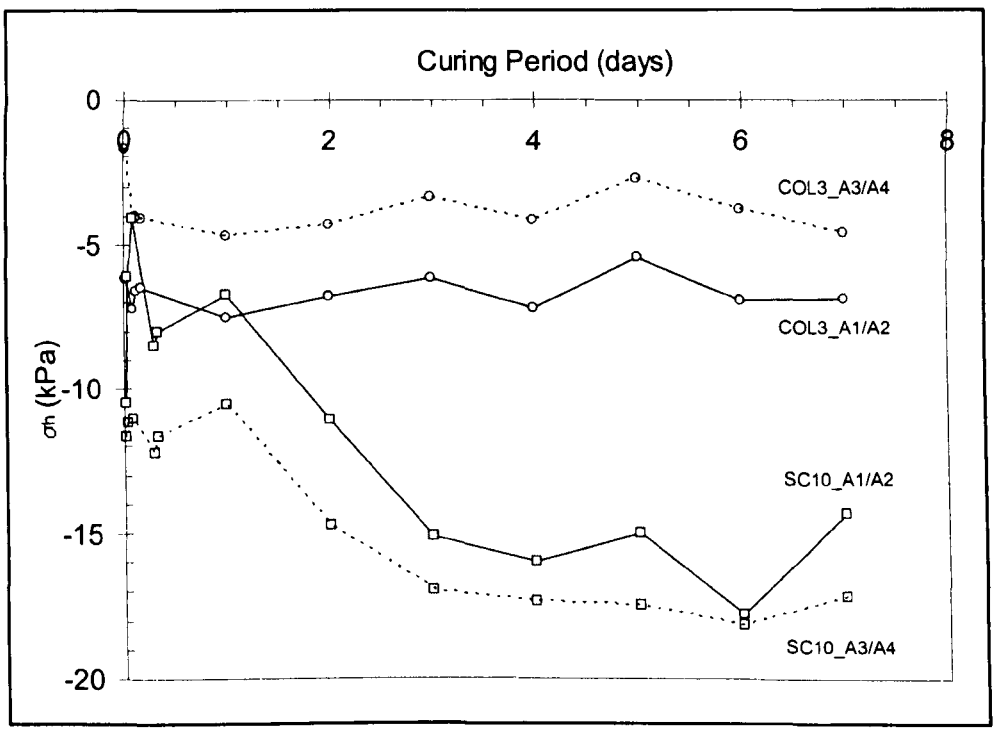

b. Swedish clay samples: SC10 and COL3.

Figure 4.40: Evolution of lateral stress (σ_h) during curing period in column tests.

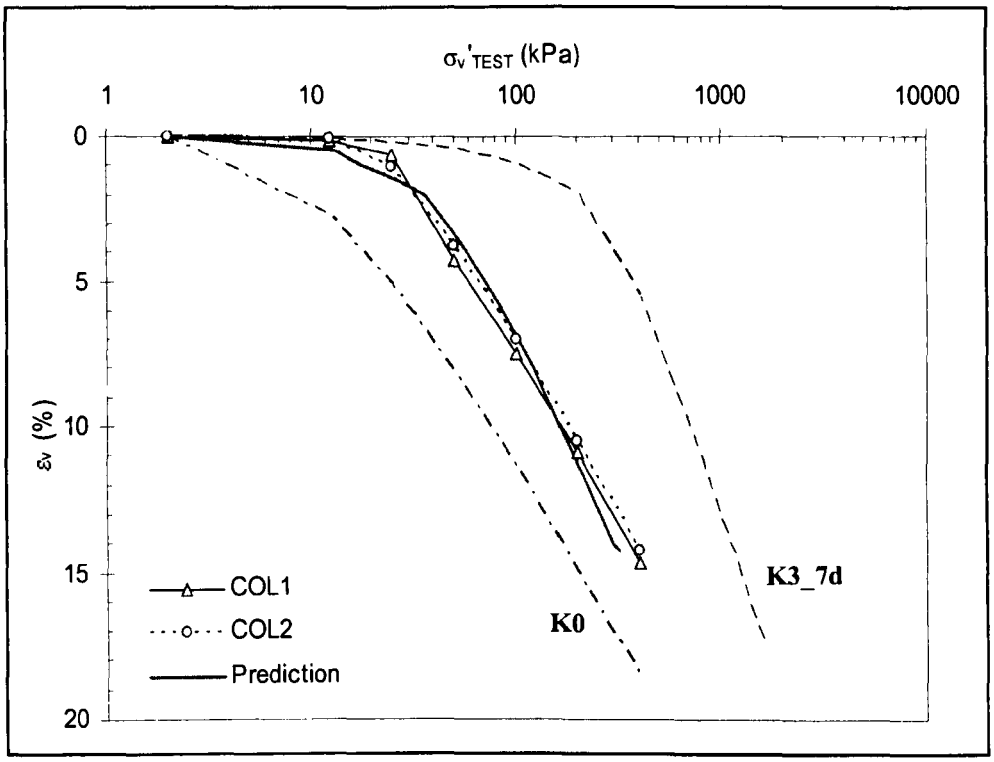

a. Kaolin samples: K0, K3, COL1 and COL2.

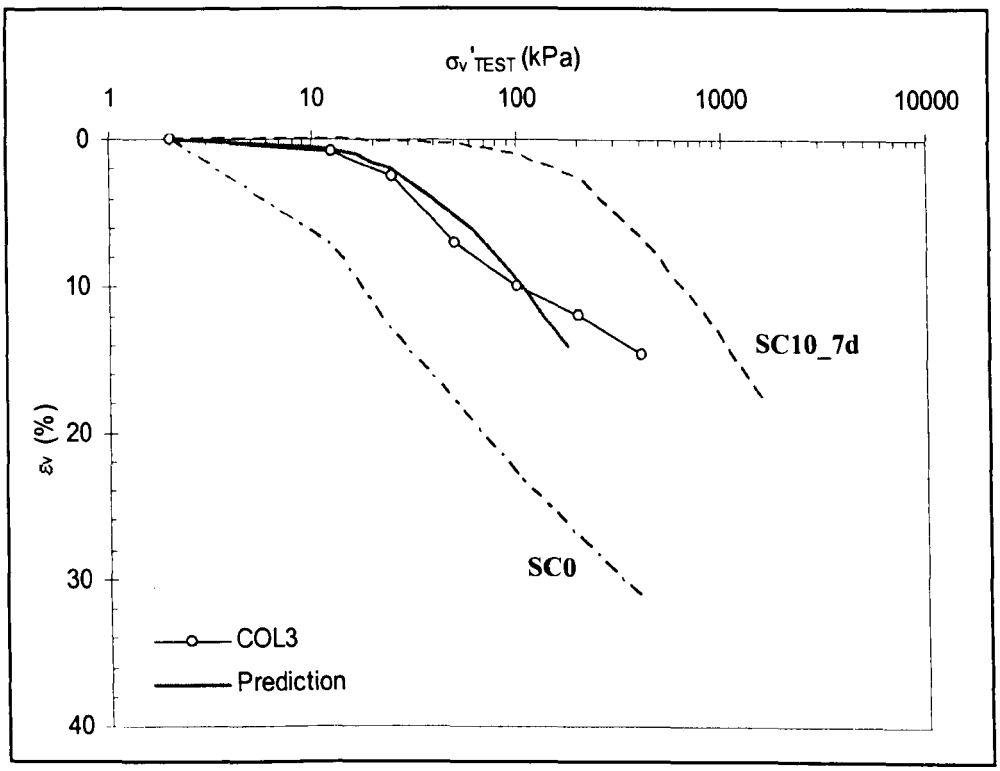

b. Swedish clay samples: SC0, SC10 and COL3.

Figure 4.41: Compression curves from column tests, including the predicted curves (see Table 4.11).

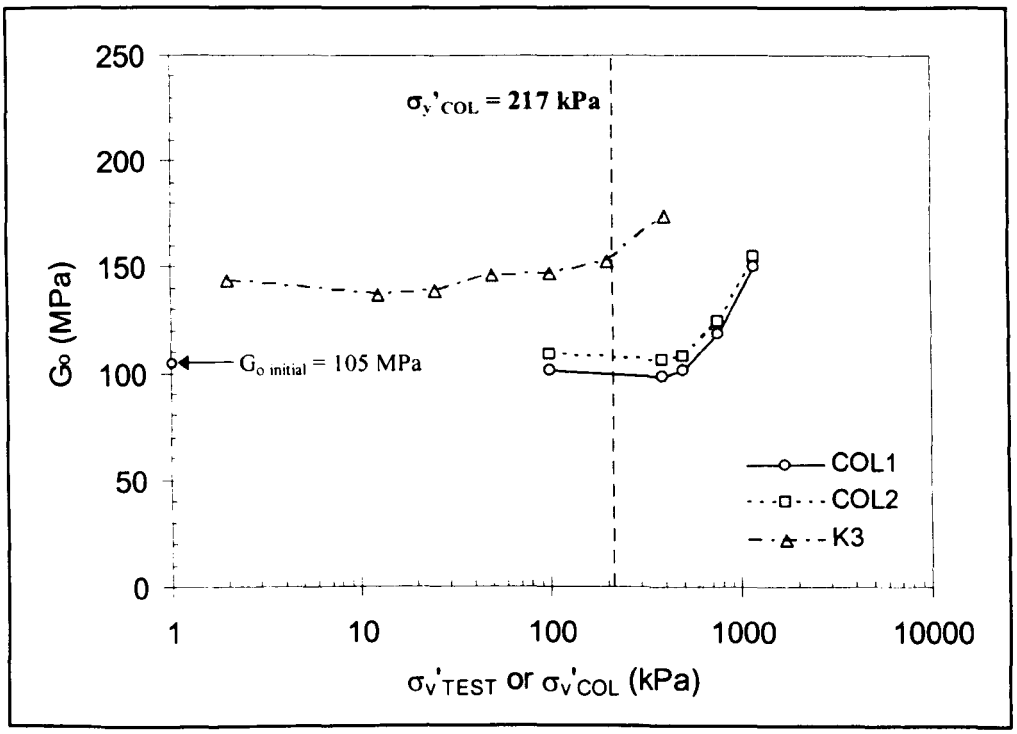

a. Kaolin samples: K3, COL1 and COL2.

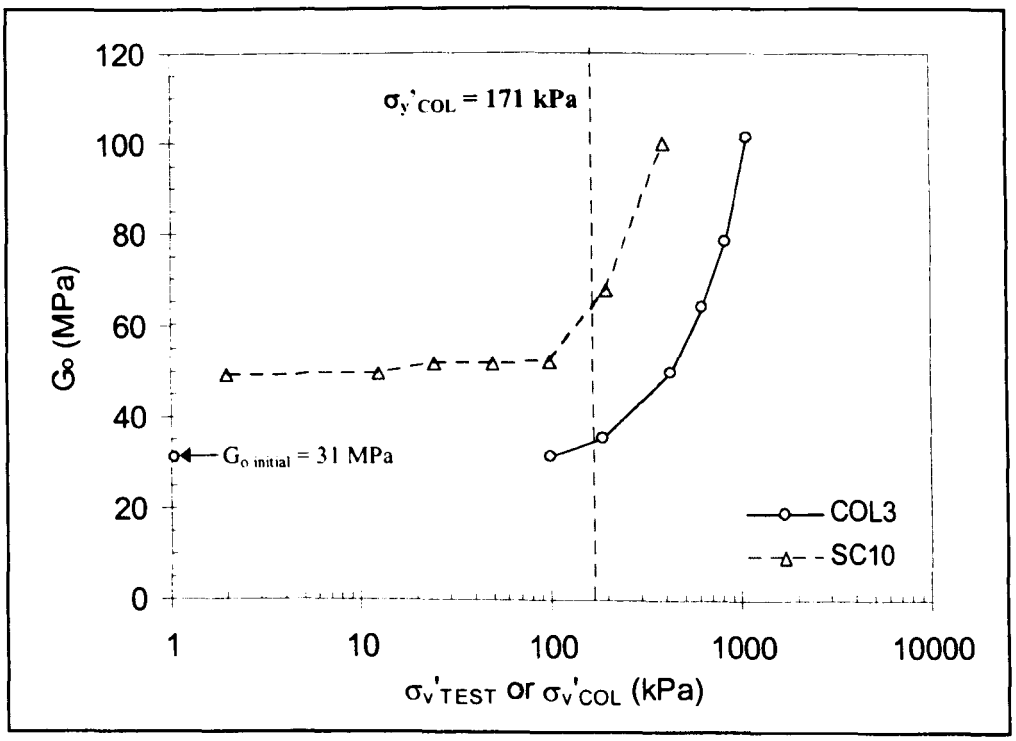

b. Swedish clay samples: SC10 and COL3.

Figure 4.42: Change of maximum shear modulus (G_o) with effective vertical stress in column tests.

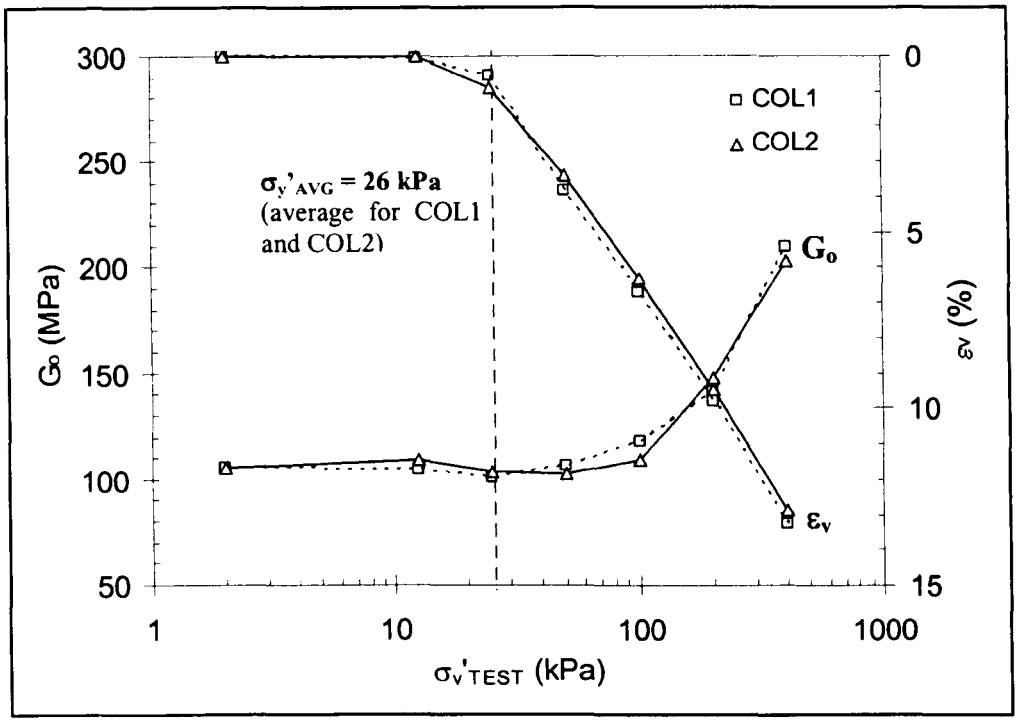

a. Kaolin samples: COL1 and COL2.

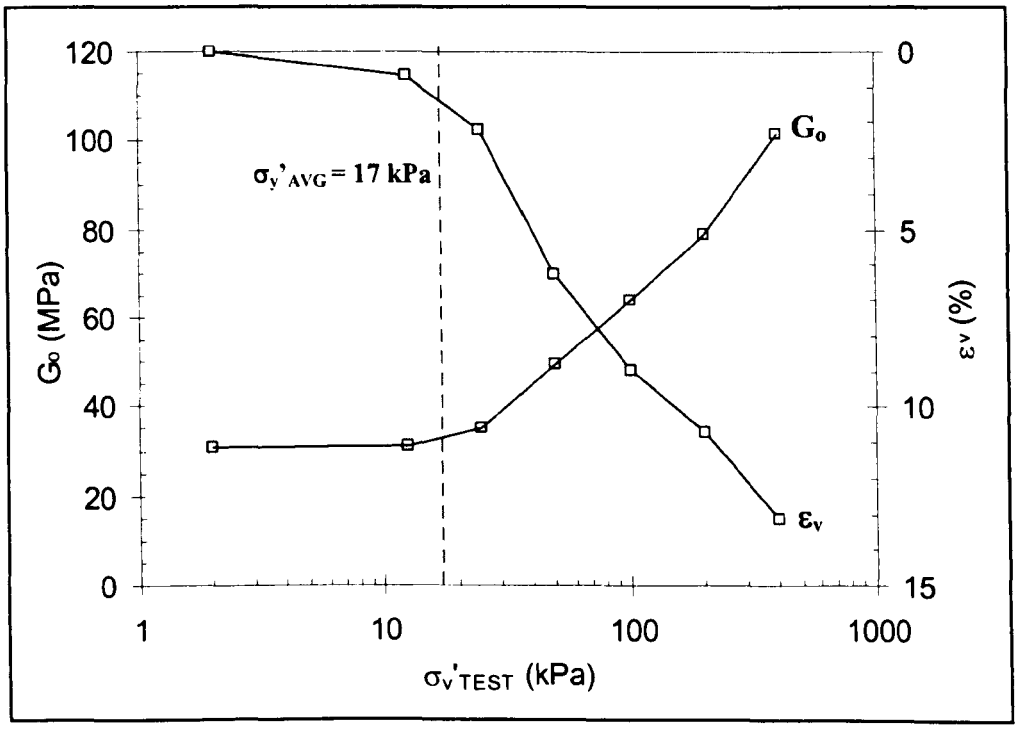

b. Swedish clay samples: COL3.

Figure 4.43: Change of maximum shear modulus (G_o) and vertical strain (ε_v) with effective vertical stress ($\sigma_v'_{TEST}$) in column tests.

Sample COL1 (A3/A4)

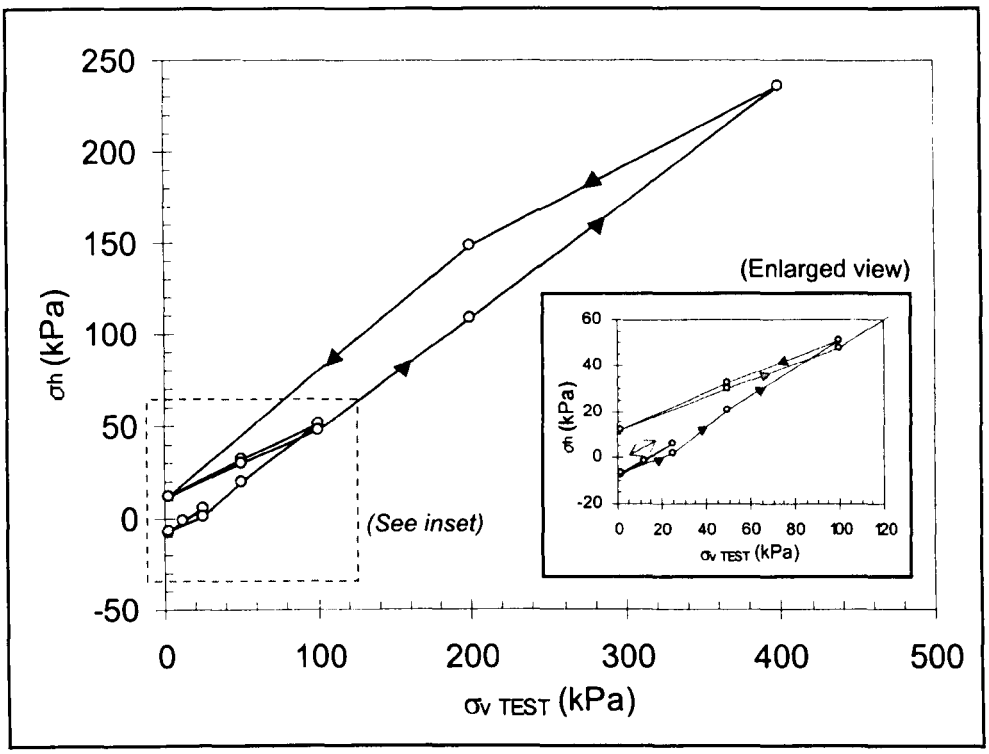

Figure 4.44: Change of total lateral stress (σ_h) with total vertical stress (σ_{vTEST}) in a column test.

Sample COL1 (A3/A4)

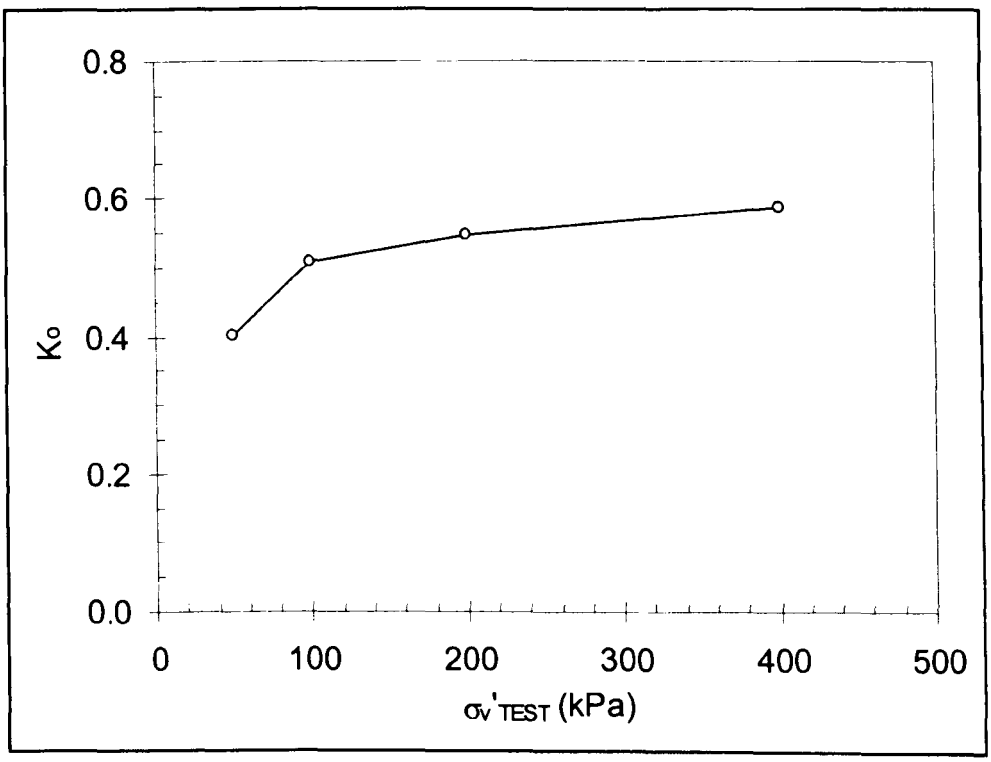

Figure 4.45: Change of coefficient of earth pressure at rest (K_o) with effective vertical stress ($\sigma_v'_{TEST}$) in a column test.

Chapter 5
Conclusions

5.1 Introduction

In the preceding chapters, research into the properties of stabilised clays has been described with the aim of achieving the objectives listed in Section 1.2. The testing mainly comprised unconfined compressive strength tests accompanied by BE tests, and one-dimensional compressibility tests, incorporating shear wave velocity and lateral stress measurements. A total of three clays was tested: one artificial clay (kaolin) and two natural clays (Malaysian and Swedish clays). Based on the results and experience gathered from the laboratory work, this chapter summarizes the main findings and gives recommendations for future studies. The main findings are subdivided into key conclusions to highlight the most important outcomes of the research, followed by other findings (presented approximately in their order of appearance in the thesis), and then the most important practical implications of the research are listed.

5.2 Main findings

5.2.1 Key conclusions

Listed below are the findings considered to be of most importance in the thesis:

[1] There is evidently a strong relationship between the undrained shear strength and shear wave velocity (or maximum shear modulus, G_o) of stabilised soils (Section 4.2.4). The correlation was different for each clay, and a polynomial relationship was found to fit the data slightly better than a linear one.

[2] The shear wave velocity, and hence G_o, was found to be a good indicator of the processes involved during a one-dimensional compression test (Section 4.3.5). G_o remained mostly unchanged pre-yield, and increased markedly with yielding of the sample. Before yield, cementation apparently reduced settlement (reduced alteration of structure) and therefore maintained the G_o values. During a loading stage, with the breakdown of the cementation bonds, considerable settlements were accompanied by a significant rise in G_o, i.e. the effect of increased effective stress eclipsed that of the destroyed cementation.

However G_o did not appear to level off with time as secondary compression set in. During an unloading stage, G_o decreased with the reduction of effective stress, but the drop in G_o was less with the highly cemented samples.

[3] The constrained modulus, M_o, was correlated with G_o, and the results compared with the correlation for natural clays published by Burns and Mayne (2002) (Section 4.3.5). It was found that only data from the normally consolidated range fitted the relationship, suggesting the need to differentiate between data for normally consolidated and overconsolidated soils.

[4] A correlation between σ_y' and q_u (unconfined compressive strength) was established for each clay tested, and compared with those proposed by Horpibulsuk et al. (2004) (Section 4.3.7). The observed disagreement was attributed to the different clays studied, and also the different methods used to define σ_y'. A tentative relationship between σ_y' and G_o was presented, following the hypothesis that, since strength (i.e. q_u and undrained shear strength, c_u) is proven to be related to G_o, and strength is also shown to correlate with σ_y', σ_y' should be a function of G_o (Section 4.3.7).

[5] The evolution of σ_h during a loading or unloading stage was found to depend on the processes occurring within the sample (Section 4.3.8). Upon loading, σ_h generally showed a sudden surge, reflecting an increase of pore pressure, then gradually decreased during primary consolidation, and finally levelled off during secondary compression. In an unloading stage, σ_h was found to drop markedly at the start, but remained relatively constant during swelling of the samples. A smaller reduction in σ_h was observed in samples with higher binder contents, suggesting that cementation could be a contributing factor to the higher locked-in lateral stresses.

[6] Model column tests were successfully carried out in the oedo-BE cell (Section 4.4). Taking an equal strain approach (Baker 2000), the stresses acting on the column and surrounding unstabilised soil were predicted to differ greatly (Section 4.4.2). With the same approach, a good prediction of the compression curve of the composite system could be made with information from the individual tests on the homogeneous base clay and stabilised clay samples.

5.2.2 Other findings

The following are other findings listed according to their order of appearance in the thesis:

[1] Bender element probes were successfully fabricated in-house, using piezoelectric bimorph ceramics with suitable wiring systems (Section 3.3). The probes were used in unconfined samples and were also incorporated in an instrumented oedometer cell.

[2] Various factors were found to affect the measurement of shear wave velocity. The main factors were the input frequency, sample geometry, near-field effects and attenuation (Section 4.2.1). The quality of the received signals was found to be satisfactory when the input frequency was kept high enough to achieve $\lambda/D_{50} > 3$ (ASTM Standard 2845-95 2000). In terms of the sample geometry, less dispersion was found when fulfilling the criterion $D/\lambda \geq 5$, as given by Wasley (1973) and mentioned in the ASTM Standard 2845-95 (2000). Also, the present work readily complied with the recommendation of keeping the sample height at least 10 times D_{50}, ensuring accurate definition of the average shear wave velocity propagating through the soil samples (ASTM Standard 2845-95 2000). Near-field effects and attenuation were found to be reduced when the ratio L/λ was kept between 2 and 4 (the upper limit caters for attenuation while the lower limit is for avoiding near-field effects), as suggested by Sánchez-Salinero et al. (1986).

[3] Different methods were used to determine the shear arrival time, working in either the time domain or the frequency domain (Section 4.2.2). Although some other researchers have claimed that frequency domain methods are more reliable, similar observations were not made in the present work. Visual picking of the arrival time in the time domain was found to be equally good, and had the advantage of being easier and faster.

[4] Laboratory shear strength measurements of the stabilised samples with the vane shear apparatus did not agree well with those obtained with the unconfined compressive strength tests (Section 4.2.3). The vane strength was consistently larger than the unconfined compressive strength test measurements.

[5] The stabilised soils generally showed high peak or failure strengths at low failure strains, but there did not appear to be a strong correlation between the two parameters (Section 4.2.3).

[6] Various factors were shown to affect the strength and stiffness improvement of the stabilised soils, the main ones being the water content, stabiliser content and curing

period (Section 4.2.5). The higher the initial water content, the lower the final strength and stiffness were found to be. However, at a given stabiliser content, the proportional improvement was more significant for samples with a higher water content. This improvement was most marked in the first week, after which the rate of strength and stiffness increase declined.

[7] A thin-walled, floating ring type instrumented oedometer was designed and successfully commissioned (Section 3.4). The apparatus incorporated measurements of lateral stress and shear wave velocity using strain gauge circuits and bender element probes respectively.

[8] A curing period of 7 days prior to the one-dimensional compression tests was found to suffice for stabilised soil samples (Section 4.3.1). This was based on the strength and stiffness improvement characteristics of the stabilised materials observed in the unconfined tests, and validated with standard oedometer tests on samples of different ages.

[9] The observed compressibility behaviour of the stabilised clays was not very different from that of unstabilised soils (Section 4.3.3). Settlement in the pre-yield range was negligible compared to that in the post-yield or normal consolidation range, indicating the importance of utilising the stiffness of stabilised columns at stresses lower than the pre-yield stresses.

[10] The void ratio (e) and degree of saturation (S_r) of the oedometer samples were difficult to ascertain with accuracy, due to the on-going hydration process of the stabiliser in the samples as well as bedding errors (Section 4.3.4). However, the G_s values of the cemented samples were found to be largely unchanged, probably due to the small quantities of stabiliser present.

[11] In comparison with the proposed normalised relationship based on the e/e_{100} - σ_v' (effective vertical stress) plot by Horpibulsuk et al. (2004), data from the present work suggest that separate correlations could exist for different clays (Section 4.3.4.1).

[12] Various methods were employed to define the effective yield stress (σ_y'), including well established methods and an adaptation by the Author (Section 4.3.6). The adaptation involved using the slope of the first unloading-reloading loop (loading data only) post-yield to correct for the initial loading path, where the intersection of the fitted reloading line and the virgin compression line was taken as the effective yield stress. The reliability of the conventional graphical methods was thought to be significantly

compromised by the characteristics of the compression curves, which did not always suggest a well defined yield point.

[13] In spite of the attempt to install two identical strain gauge circuits on the oedo-BE cell wall, the lateral stress (σ_h) measurements were not always in agreement (Section 4.3.8). This was most probably caused by a differential stress distribution along the circumference of the cell due to jamming of the o-rings by material squeezed out from the cell. Occasional unacceptable discrepancies were attributed to possible electrical anomalies in the circuits.

[14] Assuming that all excess pore pressure was dissipated by the end of each loading or unloading stage, values of the coefficient of earth pressure at-rest, K_o, were obtained (Section 4.3.8). Because suction (negative total lateral stress, σ_h) was found to be prevalent at lower stresses, the resulting erroneous negative K_o values were disregarded. In general, the K_o values for the cemented soils during normal consolidation were slightly lower than those of the unstabilised base clays, corresponding with the expected reduction of K_o with stronger materials (Section 4.3.8). However, it is acknowledged that the K_o values established in the present work might be a little too low, due to friction losses in the test set-up and lack of saturation of the samples.

[15] The G_o value, at any given σ_v' in the model column tests, was observed to be consistently lower than that of the homogeneous samples, though the general trends of G_o - σ_v' were similar (Section 4.4.3). This discrepancy was attributed to the different sample preparation methods, curing environments and test conditions.

5.2.3 Practical implications

The following practical implications of the research are considered most important:

[1] A c_u – G_o correlation is useful for estimating the in situ strength based on shear wave velocity measurements. The convenience of field seismic testing, used together with such a relationship, could significantly improve the quality control and quality assurance of stabilised columns.

[2] Small quantities of binders can usefully reduce settlement and this could make deep mixing a more cost-effective stabilisation method. In addition, with small quantities of binders (i.e. < 10 %), a prolonged curing period beyond 7 days does not make much further contribution to reducing compressibility. However it is cautioned that using a small

amount of binder is only justifiable when 'stabilisation', and not just 'modification' is achieved.

[3] The monitoring of G_o evolution in a one-dimensional compression test can provide useful complementary information on the behaviour of stabilised soils under loading.

[4] The correlation between $M_o - G_o$ in the normally consolidated range can be directly applied to estimate the compressibility of stabilised soils, by conducting only the measurement of G_o.

[5] An equal strain assumption is sufficient to make reasonable predictions of the one-dimensional compressibility of a composite system, as recommended by Baker (2000).

5.3 Recommendations for further studies

[1] If further testing of a similar nature is to be carried out, the following suggestions could be adopted:

- The initial consumption of lime (ICL) test can be conducted to estimate the minimum amount of binders (e.g. cement or lime-cement) required to achieve stabilisation.
- Revised compaction procedures should be assigned to the different test samples, in order to produce samples with more closely comparable initial properties.
- The discrepancy between strength measurements using the unconfined compressive strength test and the vane shear test (Section 4.2.3) requires further study to be fully understood.
- O-rings in the top cap and base of the instrumented oedometer could be omitted by having a tighter clearance between the ring and the caps. In some circumstances the o-rings might have been detrimental to the lateral stress measurements (Section 4.3.8).

[2] Local strain measurements on homogeneous stabilised samples could be carried out in a triaxial cell under K_o loading to eliminate the effect of bedding errors, especially on the relatively small pre-yield settlements. Larger scale model column tests could also be conducted in a large triaxial cell, again with local strain measurements.

[3] The effect of stress history on G_0 could be further explored to establish an empirical model for stabilised soils. Since G_0 is known to strongly correlate with strength and large strain compressibility, such models could be very useful to make a quick estimation of the stabilised soil response with applied stresses, via a non-destructive assessment method.

[4] For designing stabilised column systems, a simple equal strain approach based on experimental data appears to be sufficient to make realistic predictions of the system's one-dimensional compressibility. However, more columnar inclusion tests with various soils are necessary to validate this design approach.

[5] Field measurements are ultimately required to validate the correlations established in the laboratory.

References

Abdelhamid, M.S. and Krizek, R.J. (1976). At-rest lateral earth pressure of a consolidating clay. ASCE Journal of Geotechnical Engineering Division, Vol. 192, No. 7, pp. 721-738.

Afifi, S.S. and Woods, D.R. (1971). Long term pressure effect on shear modulus of soils. ASCE Journal of Soil Mechanics and Foundations, Vol. 97, No. SM10, pp. 1445-1460.

Al-Tabbaa, A. and Boes, N. (2002). Pilot in situ auger mixing treatment of a contaminated site, Part 4: Performance at five years. Proceedings of Institution of Civil Engineers-Geotechnical Engineering Division, Vol. 155, No. 3, pp. 187-202.

American Society for Testing and Materials (ASTM). (2000). Standard test methods for one-dimensional consolidation properties of soils using incremental loading (D2435-96). 2000 Annual Book of ASTM Standards, Vol. 04.08.

American Society for Testing and Materials (ASTM). (2000). Laboratory determination of pulse velocities and ultrasonic elastic constants of rocks (D2845-95). 2000 Annual Book of ASTM Standards, Vol. 04.08.

Andersson, R., Torbjörn, C. and Leppanen, M. (2001). Hydraulic cement based binders for mass stabilisation of organic soils. Soft Ground Technology- Proceedings of the Soft Ground Technology Conference (Sponsored by United Engineering Foundation and the Geo-Institute of American Society of Civil Engineers), Noordwikerhout, Netherlands, pp. 158-169.

Ando, Y., Tsuboi, H., Yamamoto, M., Harada, K. and Nozu, M. (1995). Recent soil improvement methods for preventing liquefaction. Proceedings of Earthquake Geotechnical Engineering. Balkema: Rotterdam, pp.1011-1016.

Andrawes, K.Z. and El-Sohby, M.A. (1973). Factors affecting coefficient of earth pressure K_o. ASCE Journal of Soil Mechanics and Foundation Division, Vol. 99, No. SM7, pp. 527-539.

Arroyo, M. (2001). Pulse Tests In Soil Samples. Ph.D. thesis, University of Bristol.

Arulnathan, R., Boulanger, R.W. and Riemer, M.F. (1998). Analysis of bender element tests. ASTM Geotechnical Testing Journal, Vol. 21, No. 2, pp. 120-131.

Axelsson, M. and Larsson, S. (2003). Column penetration tests for lime-cement columns in deep mixing– experiences in Sweden. ASCE Geotechnical Special Publication, No.120, No. 1, pp. 681-694.

Bahrekazemi, M., Bodare, A. and Smekal, A. (2003). Lime-cement stabilization of soft soils, an efficient method against train-induced ground vibrations. Proceedings of the 13th. European Conference on Soil Mechanics and Geotechnical Engineering, Prague, Czech Republic, Vol. 1, pp. 565-572.

Baker, S. (2000). Deformation behaviour of lime/cement column stabilised clay. Rapport 7, Swedish Deep Stabilisation Research Centre. Chalmers: Linköping.

Baker, S., Liedberg, N.S.D. and Sällfors, G. (1997). Deformation properties of lime cement stabilised soil in the working state. Proceedings of the 14th. International Conference on Soil Mechanics and Foundation Engineering, Hamburg, Germany, Vol. 3, pp. 1667-1672.

Bergado, D.T., Lorenzo, G.A., Yip, P.L. and Pun, A. (2003). Deep mixing method using cement admixture at higher water content as foundation of hexagonal wire reinforced embankment. Proceedings of the 2nd. International Conference on Advances in Soft Soil Engineering and Technology, Putrajaya, Malaysia, pp. 317-334.

Bishop, A.W. (1958). Test requirements for measuring coefficient of earth pressure at rest. Proceedings of Conference on Earth Pressure Problems, Brussels, Belgium, Vol. 1, pp. 2-14.

Bjerrum, L. and Lo, K.Y. (1963). Effects of aging on the shear strength properties of a normally consolidated clay. Géotechnique, Vol. 13, No. 2, pp. 147-157.

Boman, P., Broms, B., Paus, K. and Söderlind, G. (1980). Lime column method- follow up observations in the town block 'Myren', Huddinge. BFR, Doc. D: 1980, Stockholm.

Braaten, A., Aabøe, R and Oset, F. (1999). Development of in-situ control methods for lime-cement columns. Proceedings of the International Conference on Dry Mix Methods for Deep Soil Stabilization, Stockholm, pp. 295-301.

Brignoli, E.G.M., Marino, G. and Stokoe, K.H., II. (1996). Measurement of shear waves in laboratory specimens by means of piezoelectric transducers. ASTM Geotechnical Testing Journal, Vol. 29, No. 4, pp. 384–397.

Brillouin, L. (1960). Wave Propagation and Group Velocity. Academic Press: London.

British Standards Institution (BSI). (1990). BS1377: British Standard Methods of Test for Soils for Civil Engineering Purposes. Part 5: Compressibility, permeability and durability tests.

British Standards Institution (BSI). (1990). BS1377: British Standard Methods of Test for Soils for Civil Engineering Purposes. Part 7: Shear strength tests (total stress).

British Standards Institution (BSI). (1990). BS1377: British Standard Methods of Test for Soils for Civil Engineering Purposes. Part 8: Shear strength tests (effective stress).

Brocanelli, D. and Rinaldi, V. (1998). Measurement of low-strain material damping and wave velocity with bender elements in the frequency domain. Canadian Geotechnical Journal, Vol. 35, No. 6, pp. 1032-1040

Broms, B.B. and Boman, P. (1977). Stabilisation of soil with lime columns. Royal Institute of Technology, Stockholm, Sweden.

Brooker, E.W. and Ireland, H.O. (1965). Earth pressure at rest related to stress history. Canadian Geotechnical Journal, Vol. 35, No. 6, pp. 1032-1040.

Budhu, M. (2000). Soil Mechanics and Foundations. John Wiley & Sons, Inc.: USA.

Burke, G.K., Brengola, A.F. and Triplett, R.E. (2002). Soil mixing: a new approach to soft soil stabilization for structural support. ASCE Geotechnical Special Publication, No. 113, pp. 190-203.

Burke, G.K. and Sehn, A.L. (2005). An analysis of single axis wet mix performance. Proceedings of the International Conference on Deep Mixing Best Practice and Recent Advances, Stockholm, Vol. 1, pp. 41-46.

Burns, S.E. and Mayne, P.W. (2002). Interpretation of seismic piezocone results for the estimation of hydraulic conductivity in clays. ASTM Geotechnical Testing Journal, Vol. 25, No. 3, pp. 334-341.

Butterfield, R. (1979). A natural compression law for soils (an advance on e - logp'). Géotchnique, Vol. 29, No. 4, pp. 469-480.

Callister, W. D., Jr. (1991). Materials Science and Engineering: An Introduction (2^{nd}. edition). John Wiley & Sons, Inc.: New York, pp. 738.

Casagrande, A. (1936). The determination of the pre-consolidation load and its practical significance. Proceedings of the 1^{st}. International Conference on Soil Mechanics and Foundation Engineering, Cambridge, Massachusetts, USA, Vol. 3, pp. 60-64.

Clayton, C.R.I., Theron, M. and Best, A.I. (2004). The measurement of vertical shear-wave velocity using side-mounted bender elements in the triaxial apparatus. Géoechnique, Vol. 54, No. 7, pp. 495-498.

Dyvik, R. and Madshus, C. (1985). Lab measurements of G_{max} using bender elements. Proceedings of the conference on the Advances in the Art of Testing Soil under Cyclic Conditions. ASCE Geotechnical Engineering Division, New York, pp. 186-196.

Edil, T.B. and Dhowian, A.W. (1981). At-rest lateral pressure of peat soils. ASCE Journal of Geotechnical Engineering Division, Vol. 107, No. 2, pp. 201-217.

EuroSoilStab. (2002). Development of design and construction methods to stabilize soft organic soils (design guide soft soil stabilisation). European Commission, Industrial and Material Technologies programme (Brite-EuRam III), Brussels.

Fam, M. and Santamarina, C. (1995). Study of geoprocesses with complementary mechanical and electromagnetic wave measurements in an oedometer. ASTM Geotechnical Testing Journal, Vol. 18, No. 3, pp. 307-314.

Fam, M. and Santamarina, C. (1996). Study Of Clay-Cement Slurries With Mechanical And Electromagnetic Waves. ASCE Journal of Geotechnical Engineering Division, Vol. 122, No. 5, pp. 365-373.

Feng, T.W. (2002). Effects of small cement content on consolidation behaviour of a Lacustrine clay. ASTM Geotechnical Testing Journal, Vol. 25, No. 1, pp. 53-60.

Fioravante, V. and Capoferri, R. (2001). On the use of multi-directional piezoelectric transducers in triaxial testing. ASTM Geotechnical Testing Journal. Vol. 24, No. 3, pp. 243–255.

Foti, S. and Butcher, T. (2004) General report: Geophysical methods applied to geotechnical engineering. Proceedings of the 2nd. International Conference on Geotechnical and Geophysical Site Characterization (ISC-2), Porto, Portugal, pp. 409-418.

Futaki, M., Nakano, K. and Hagino, Y. (1996). Design strength of soil-cement columns as foundation ground for structures. Proceedings of the 2nd. International Conference on Ground Improvement Geosystems (IS-Tokyo'96), Tokyo, Japan, pp. 481-484.

Goto, T., Shimizu, K. and Chaen, T. (2000). Quality estimation of deep mixing columns by pile integrity tester. Proceedings of the 4th. International Conference on Ground Improvement Geosystems (GIGS), Helsinki, Finland, pp. 31-38.

Graff, K.F. (1975). Wave motion in elastic solids. Clarendon Press: Oxford.

Greening, P.D., Nash, D.F.T., Benahmed, N., Ferreira, C. and Viana da Fonseca, A. (2003). Comparison of shear wave velocity measurements in different materials using time and frequency domain techniques. Proceedings of the 3rd. International Symposium on Deformation Characteristics of Geomaterials, Lyon, France, pp. 381-386.

Greening, P.D. and Nash, D.F.T. (2004). Frequency domain determination of G_o using bender elements. ASTM Geotechnical Testing Journal, Vol. 27, No. 3, pp. 288-294.

Halkola, H. (1983). In situ investigations of deep stabilised soil. Proceedings of the 8th. European Conference on Soil Mechanics and Foundation Engineering, Helsinki, Finland, Vol. 2, pp. 33-36.

Halkola, H. (1999). Keynote lecture: Quality control for dry mix methods. Proceedings of the International Conference on Dry Mix Methods for Deep Stabilization, Stockholm, Sweden, pp. 285-294.

Hansson, T., Parry, L., Graham, M., Troughton, V. and Eriksson, H. (2001). Limix, a dry deep mixing system used at Channel Tunnel Rail Link Contract 440. Underground Construction, London.

Hardin, B.O. and Black, W.L. (1969). Vibration modulus of normally consolidated clay. ASCE Journal of Soil Mechanics and Foundation Division, Vol. 95, No. SM6, pp. 1531-1537.

Hirai, T., Ise, J., Kusakari, T., Gotou, M. and Hibi, Y. (1996). Development and application of deep mixing soil stabilisation method to control displacement of adjacent ground. Proceedings of the 2nd. International Conference on Ground Improvement Geosystems (IS-Tokyo'96), Tokyo, Japan, pp. 485-490.

Hiraide, A., Baba, K. and Azuma, H. (1996). Quality assessment of stabilized soil by S-wave logging. Proceedings of the 2nd. International Conference on Ground Improvement Geosystems (IS-Tokyo'96), Tokyo, Japan, pp. 603-606.

Hird, C.C. and Chan, C.M. (2005). Correlation of shear wave velocity with unconfined compressive strength of cement-stabilised clay. Proceedings of the International Conference on Deep Mixing Best Practice and Recent Advances, Stockholm, Sweden, Vol. 1, pp. 79-85.

Holm, G. (2001). Deep mixing. Soft Ground Technology- Proceedings of the Soft Ground Technology Conference (Sponsored by United Engineering Foundation and Geo-Institute of American Society of Civil Engineers), Noordwikerhout, Netherlands, pp.105-122.

Horpibulsuk, S., Miura, N. and Nagaraj, T. S. (2003). Assessment of strength development in cement-admixed high water content clays with Abram's Law as a basis. Géotechnique, Vol. 53, No. 4, pp. 439-444.

Horpibulsuk, S., Bergado, D.T. and Lorenzo, G.A. (2004). Compressibility of cement-admixed clay at high water content. Géotechnique, Vol. 54, No. 2, pp. 151-154.

Hosoya, Y., Ogino, T., Nasu, T., Kohata, Y., Hibi, Y. and Makihara, Y. (1996). Japanese Geotechnical Society Technical Report- An evaluation of strength of soils improved by DMM. Proceedings of the 2nd. International Conference on Ground Improvement Geosystems (IS-Tokyo'96), Tokyo, Japan, Vol. 2, pp. 919-924.

Hughes, J.M.O., Esrig, M.I. and Hardman, M. (2001). Quality control of dry lime cement columns by pressuremeter test. ASCE Geotechnical Special Publication, No. 113, pp. 419-432.

Huidén, E.J. (1999). Soil stabilisation for embankment of Botlek Railway tunnel in the Netherlands. Proceedings of the International Conference on Dry Mix Methods for Deep Stabilization, Stockholm, Sweden, pp. 45-50.

Huttunen, E., Kujala, K. and Vesa, H. (1996). Assessment of the quality of stabilized peat and clay. Proceedings of the 2nd. International Conference on Ground Improvement Geosystems (IS-Tokyo'96), Tokyo, Japan, pp. 607-612.

Ideal Engineering Laboratory Ltd. (Malaysia). (2002). Site investigation report for the proposed development at Kolej Universiti Teknologi Tun Hussein Onn (KUiTTHO), Johor, Malaysia.

IMERYS Minerals Ltd. (UK). (2005). Data sheet for Speswhite kaolin.

Jaky, J. (1944). The coefficient of earth pressure at rest. Journal of the Society of Hungarian Architecture and Engineers, Vol. 78, No. 22, pp. 355-358.

Jamiolkowski, M., Lancellotta, R. and Lo Presti, D.C.F. (1995). Remarks on the stiffness at small strains of six Italian clays. Development in Deep Foundations and Ground Improvement Schemes, Balkema: Rotterdam.

Jovičić V., Coop, M.R. and Simic, M. (1996). Objective criteria for determining G_{max} from bender element tests. Géotechnique, Vol. 46, No. 2, pp. 357-362.

Kakihara, Y., Hiraide, A. and Baba, K. (1996). Behaviour of nearby soil during improvement works by deep mixing method. Proceedings of the 2nd. International Conference on Ground Improvement Geosystems (IS-Tokyo'96), Tokyo, Japan, pp. 625-630.

Kamimura, K., Kami, C., Takahashi, T. and Hara, T. (2005). Development of large diameter deep mixing method with reduced displacement due to mixing (Cement Deep Mixing- Low Displacement and Control, CDM-LODIC). Proceedings of the International Conference on Deep Mixing Best Practice and Recent Advances, Stockholm, Sweden, Vol. 1, pp.533-537.

Kawasaki, K., Niina, A., Saitoh, S., Suzuki, Y. and Honjyo, Y. (1981). Deep mixing method using cement hardening agent. Proceedings of the 10th. Internaional Conference on Soil Mechanics and Foundation Engineering, Stockholm, Sweden, Vol. 3, pp. 721–724.

Kitazume, M. (2005). State of Practice Reports: Field and laboratory investigations, properties of binders and stabilised soils. Proceedings of the International Conference on Deep Mixing Best Practice and Recent Advances, Stockholm, Sweden, Vol. 2, pp. 660-684.

Kitsunezaki, C. (1980). A new method for shear wave logging. Geophysics, Vol. 45, pp. 1489-1506.

Kivelö, M. (1998). Stabilization of embankments on soft soil with lime-cement columns. Doctoral thesis, Royal Institute of Technology, Stockholm, Sweden.

KYOWA Electronic Instruments Co. Ltd. (Japan). (2003). Data sheet for strain gauge KYOWA KFG-5-120-C1-16.

Larsson, S. (2003). Mixing processes for ground improvement by deep mixing. Doctoral thesis. Royal Institute of Technology, Stockholm, Sweden.

Larsson, S. (2005). State of Practice Report: Execution, monitoring and quality control. Proceedings of the International Conference on Deep Mixing Best Practice and Recent Advances, Stockholm, Sweden, Vol. 2, pp.732-786.

Lawrence, F.V. (1963). Propagation of ultrasonic waves through sand. Research Report R63-8, Massachusetts Institute of Technology, Cambridge, MA.

Lawrence, F.V. (1965). Ultrasonic shear wave velocity in sand and clay. Research Report R65-05, Soil Publication No. 175, Massachusetts Institute of Technology, Cambridge, MA.

Lawson, C.H., Spink, T.W., Crawshaw, J.S. and Essler, R.D. (2005). Verification of dry soil mixing at Port of Tilbury, UK. Proceedings of the International Conference on Deep Mixing Best Practice and Recent Advances, Stockholm, Sweden, Vol. 1, pp. 453-462.

Lee, F-H, Lee, Y., Chew, S-H and Yong, K-Y. (2005). Strength and modulus of marine clay-cement mixes. ASCE Journal of Geotechnical and Geoenvironmental Engineering division. Vol. 131, No. 2, pp. 178-186.

Leong, E-C, Yeo, S-H and Rahardjo, H. (2004). Measurements of wave velocities and attenuation using an ultrasonic test system. Canadian Geotechnical Journal, Vol. 41, No. 5, pp. 844-860.

Lin, K.Q. and Wong, J.H. (1999). Use of deep mixing to reduce settlements at bridge approaches. ASCE Journal of Geotechnical and Geoenvironmental Engineering Division, Vol. 125, No. 4, pp. 309-320.

Lings, M.L. and Greening, P.D. (2001). A novel bender/extender for soil testing. Géotechnique, Vol. 51, No. 8, pp. 713–717.

Lorenzo, G.A. and Bergado, D.T. (2004). Fundamental parameters of cement-admixed clay- new approach. ASCE Journal of Geotechnical and Geoenvironmental Engineering division. Vol. 130, No. 10, pp. 1042-1050.

Lutsch, A. (1959). The experimental determination of the extent and degree of fracture of rock faces by means of an ultrasonic pulse reflection method. Journal of the South African Institute of Mining and Metallurgy, Vol. 59, No. 8, pp. 412-419.

Mancuso, C. and Vinale, F. (1988). Propagazione delle onde sismiche: teoria e misura in sito. Atti del Convegno del Gruppo Nazionale di Coordinamento per gli Studi di Ingegneria Geotecnica, Monselice, pp. 115-138. Rome: Consiglio Nazionale delle Ricerche. (in Italian)

Massarsch, K.R. (2005). Deformation properties of stabilized soil columns. Proceedings of the International Conference on Deep Mixing Best Practice and Recent Advances, Stockholm, Sweden, Vol. 1, pp. 129-144.

Masuda, T., Shimizu, M. and Aizawa, F. (1996). Evaluation of ground deformation due to deep mixing in adjacent construction activities. Proceedings of the 2nd. International Conference on Ground Improvement Geosystems (IS-Tokyo'96), Tokyo, Japan, pp. 515-520.

Matthews, M.C. and Clayton, C.R.I., (2000). The use of field geophysical techniques to determine geotechnical stiffness parameters. Proceedings of the Institution of Civil Engineers- Geotechnical Engineering Division, Vol. 143, No. 1, pp. 31-42.

Mattsson, H. (2005). Personal communication.

Mattsson, H., Larsson, R., Holm, G., Dannewitz, N. and Eriksson, H. (2005). Down-hole technique improves quality control on dry mix columns. Proceedings of the International Conference on Deep Mixing Best Practice and Recent Advances, Stockholm, Sweden, Vol. 1, pp. 581-592.

Menzies, B.K., Sutton, H. and Davies, R.E. (1977). A new system for automatically simulating K_o consolidation and K_o swelling in the conventional triaxial cell. Géotechnique, Vol. 27, No. 1, pp. 593-596.

Miura, N., Horpibulsuk, S. and Nagaraj, T.S. (2001). Engineering behaviour of cement stabilised clay at high water content. Soils and Foundations, Vol. 41, No. 5, pp. 33-45.

Moore, C.A. (1971). Effect of mica on K_o compressibility of two soils. ASCE Journal of Soil Mehanics and Foundation Engineering, Vol. 97, No. SM3, pp. 1275-1292.

Neville, A.M. (1995). Properties of Concrete (4^{th}. edition). Harlow: Longman.

Newlin, C.W. (1965). Lateral stresses during one-dimensional consolidation. Ph.D. thesis, Northwestern University, Evanston.

Nicholson, P.J., Mitchell, J.K., Bahner, E.W. and Moriwaki, Y. (1998). Design of composite gravity wall constructed by soil mixing. Soil Improvement for Big Digs, ASCE Geotechnical Special Publication, No. 81, pp. 27-40.

Nishikawa, J., Tada, S. and Yamaguchi, S. (1996). Strength evaluation based on logging in ground stabilized by deep mixing method. Proceedings of the 2^{nd}. International Conference on Ground Improvement Geosystems (IS-Tokyo'96), Tokyo, Japan, pp. 649-652.

O'Rourke, T.D. and McGinn, A.J. (2004). Case history of deep soil stabilization for Boston central artery. ASCE Geotechnical Special Publication, No. 126, pp. 77-136.

Pennington, D.S., Nash, D.F.T. and Lings, M.L. (2001). Horizontally mounted bender elements for measuring anisotropic shear moduli in triaxial clay specimens. ASTM Geotechnical Testing Journal, Vol. 24, No. 2, pp. 133-144.

Porbaha, A. (2002). State of the art in quality assessment of deep mixing technology. Ground Improvement, Vol. 6, No. 3, pp. 95-120.

Porbaha, A., Ghaheri, F. and Puppala, A.J. (2005). Soil cement properties from borehole geophysics correlated with laboratory tests. Proceedings of the International Conference on Deep Mixing Best Practice and Recent Advances, Stockholm, Sweden, Vol. 1, pp. 605-611.

Porbaha, A., Yamane, N. and Taguchi, H. (2001). In situ measurement of artificially cemented ground properties. Proceedings of the 1st. International Conference on In-situ Measurement of Soil Properties and Case Histories, Bali, Indonesia, pp. 219-223.

Porbaha, A. Zen, K. and Kobayashi, M. (1999). Deep mixing technology for liquefaction mitigation. Journal of Infrastructure Systems, Vol. 5, No. 1, pp. 21-34.

Raju, V.R. and Arulrajah, A. (2003). Ground treatment using dry deep soil mixing for a railway embankment in Malaysia. Proceedings of the 2nd. International Conference on Advances in Soft Soil Engineering and Technology, Putrajaya, Malaysia, pp. 589-607.

Rampello, S. and Callisto, L. (2003). Predicted and observed performance of an oil tank founded on soil-cement columns in clayey soils. Soils and Foundations, Vol. 43, No. 4, pp. 229-241.

Rathmayer, H. (1996). Deep mixing methods for soft subsoil improvement in the Nordic countries. Proceedings of the 2nd. International Conference on Ground Improvement Geosystems (IS-Tokyo'96), Tokyo, Japan, Vol. 1, pp. 869-877.

Roark, R.J. and Young, W.C. (1975). Formulas For Stress And Strain (5th. edition). McGraw-Hill: New York, pp. 446-455.

Rogers, C.D.F., Glendinning, S. and Roff, T.E.J. (1997). Lime modification of clay soils for construction expediency. Proceedings of Institution of Civil Engineers- Geotechnical Engineering Division, Vol. 125, No. 4, pp. 242-249.

Rossato, G., Ninis, N.L. and Jardine, R.J. (1992). Properties of some kaolin-based model clay soils. ASTM Geotechnical Testing Journal, Vol. 15, No. 2, pp. 166-179.

Sanchez-Salinero, I., Roesset, J.M. and Stokoe, K.H., II. (1986). Analytical studies of body wave propagation and attenuation. Geotechnical Engineering GR86-15, University of Texas, Austin.

Santamarina, J.C., Klein, K.A. and Fam, M.A. (2001). Soils and Waves. John Wiley & Sons, Inc.: Chichester, England.

Schaefer, V.R., Abramson, L.W., Drumheller, J.C. and Sharp, K.D. (1997). Ground improvement, ground reinforcement and ground treatment: developments 1987-1997. ASCE Geotechnical Special Publication, No. 69, pp. 616.

Schmertmann, J.H. (1953). Estimating the true consolidation behaviour of clay from laboratory test results. ASCE Journal of Geotechnical Engineering Division, Vol. 79, pp. 1-26.

Schmertmann, J.H. (1991). The mechanical aging of soils. ASCE Journal of Geotechnical Engineering Division, Vol. 117, No. 9, pp. 1288-1330.

Schultheiss, P.J. (1981). Simultaneous measurements of P & S wave velocities during conventional laboratory soil testing procedures. Marine Geotechnical Engineering, Vol. 4, No. 4, pp. 343-367.

Shatilo, A.P. (1992). Seismic phase unwrapping: methods, results, problems. Geophysical Prospecting, Vol. 40, pp. 211-225.

Shen, S.L. and Miura, M.N. (1999). Soil fracturing of the surrounding clay during deep mixing column installation. Soils and Foundations, Vol. 39, No. 5, pp. 13-22.

Shibuya, S., Yamashita, S., Watabe, Y. and Lo Presti, D.C.F. (2004). In situ seismic survey in characterising engineering properties of natural ground. Proceedings of the 2nd. International Conference on Site Characterisation (ISC'2), Porto, Portugal, Vol. 1, pp. 167-185.

Shirley, D.J. and Anderson, A.L. (1975). Acoustical and engineering properties of sediments. Report No. ARL-TR-75-58, Applied Research Laboratories, University of Texas, Austin.

Singh, R., Henkel, D.J. and Sangery, D.A. (1973). Shear and K_o swelling of overconsolidated clay. Proceedings of the 8th. International Conference on Soil Mechanics and Foundation Engineering, Moscow, Vol. 1, pp. 367-376.

Skempton, A.W. (1948). Vane tests in the alluvial plain of the River Forth near Grangemouth. Géotehnique, Vol. 1, No. 2, pp. 111-124.

Stephenson, R.W. (1977). Ultrasonic testing for determining dynamic soil moduli. Dynamic Geotechnical Testing- a symposium sponsored by ASTM Committee D-18 on Soil and Rock for Engineering Purposes, ASTM, Denver, Colorado, pp. 179-195.

Strassburger, E. (1982). Use of piezoelectric transducers for stiffness and density measurements of soils. M. S. thesis, University of Texas, Austin.

Tan, T-S, Goh, T-L and Yong, K-Y. (2002). Properties of Singapore marine clays improved by cement mixing. ASTM Geotechnical Testing Journal, Vol. 25, No. 4, pp. 422-433.

Teachavorasinskun, S. and Amornwithayalax, T. (2002). Elastic shear modulus of Bangkok clay during undrained triaxial compression. Geoechnique, Vol. 52, No. 7, pp. 537-540.

Terzaghi, K. (1934). Large retaining wall testing. Engineering News Record, Vol. 112, pp. 136-140.

Terzaghi, K., Peck, R.B. and Mesri, G. (1996). Soil Mechanics in Engineering Practice (3rd. edition). John Wiley & sons, Inc.: New York.

Theron, M., Clayton, C.R.I. and Best, A.I. (2003). Interpretation of side-mounted bender element results using phase shift and group velocity. Proceedings of the 3rd. International Symposium on Deformation Characteristics of Geomaterials, Lyon, pp. 127-132.

Thill, R.E. and Peng, S.S. (1969). Statistical comparison of the pulse and resonance methods for determining elastic moduli. Report of Investigations RI 7831, U.S Bureau of Mines, Washington, D.C.

Thomann, T.G. and Hryciw, R.D. (1990). Laboratory measurements of small strain shear modulus under K_o conditions. ASTM Geotechnical testing Journal, Vol. 13, No. 2, pp. 97-105.

Ting, C.M.R., Sills, G.C. and Wijeyesekera, D.C. (1994). Development of K_o in soft soils. Géotechnique, Vol. 24, No. 1, pp. 101-109.

Topolnicki, M. (2004). In situ soil mixing. Ground Improvement (2nd. Edition). Spon Press: Oxon, pp. 331-428.

Torstensson, B-A. (1980) The BAT lime column probe for in situ testing of quality of lime columns. Lindén Alimak AB, Skellefteå.

Toth, P.S. (1993). In situ soil mixing. Ground Improvement (1st. edition). Chapman & Hall: Florida, pp. 193-204.

Uddin, K., Balasubramaniam, A.S. and Bergado, D.T. (1997). Engineering behaviour of cement-treated Bangkok soft clay. ASTM Geotechnical Testing Journal, Vol. 28, No. 1, pp. 89-119.

Vähääho, I. (2000). Deep wet mixing test at old city bay in Helsinki. Proceedings of the 4th. International Conference on Ground Improvement Geosystems (GIGS), Helsinki, pp. 55-62.

Viggiani, G. and Atkinson, J.H. (1995). Interpretation of bender element tests. Géotechnique, Vol. 45, No. 1, pp. 149–154.

Vriend, A.C., de Kort, P.J.C.M. and Colmorgen, E. (2000). Soil improvement at the Botlek railway tunnel project, Potterdam, Netherlands. ASTM Geotechnical Special Publication, No. 112, pp. 472-483.

Wasley, R.J. (1973). Stress wave propagation in solids. Marcel Dekker, Inc.: New York.

Wood, D.M. (1990). Soil behaviour and critical state soil mechanics. Cambridge University Press: Cambridge, UK.

Wroth, C.P. (1984). The interpretation of in situ soil tests. Géotechnique, Vol. 34, No. 4, pp. 449-489.

Yesiller, N., Hanson, J.L. and Usmen, M.A. (2000). Ultrasonic assessment of stabilised soils. Soft Ground Technology- Proceedings of the Soft Ground Technology Conference (Sponsored by United Engineering Foundation and the Geo-Institute of American Society of Civil Engineers), Noordwikerhout, Netherlands, pp. 170-181.

Zhu, F., Clark, J.I. and Paulin, M.J. (1995). Factors affecting at-rest lateral stress in artificially cemented sands. Canadian Geotechnical Journal, Vol. 32, No. 2, pp. 195-203.

Appendix A

Fabrication of Bender Element (BE) Probes

i. Preparation of the piezoelectric ceramics

Material:

- Bimorph PZT-5A piezoceramic strips, 69 mm x 10 mm x 0.5 mm, with series and parallel polarisation *(Morgan Electro Ceramics)*, Figure A1- an opposite-sense polarised / series ceramic, appropriately wired, was used for the receiver and a same-sense polarised / parallel one for the transmitter (Lings and Greening 2001)

Tools / Equipment (Figure A2):

- 15 cm ruler and 75 mm engineering square
- Scriber
- Handheld drill with diamond wheel cutter
- Diamond plated files
- Bench vice / toolmaker's clamp

1. Using the ruler and engineering square, lengths of 16 mm were measured and marked with a scriber on the ceramic strip. The strips were carefully labelled to avoid having the *series* and *parallel* ceramics mixed up.
2. The ceramic strips were then clamped lightly and cut with a diamond wheel cutter along the marked lines.
3. Edges of the cut ceramic strips were filed with a diamond plated file, with the bottom corners smoothened to fit the recess in the potting mould.
4. For the *parallel* ceramic, the ceramic surface of the bottom right-hand corner (the area of an equal sided triangle of 3 mm x 3 mm) was filed off to the centre metal shim for cable connection.

ii. Preparation of the screened coaxial cable

Material:

- RG178B/U coaxial cable- 1.8 mm diameter, silver-plated, copper-clad steel stranded conductor 7/0.1 mm with extended PTFE (polytetrafluoroethlene)

insulation, screen of silver-plated copper wire mesh and FEP (fluorinated ethylene propylene) outer sheath *(RS Components Ltd.)*

Tools / Equipment:

- 15 cm ruler
- Cable cutter and stripper
- Syringe needle

1. 1 m long of the coaxial cable was measured and cut from the reel.
2. The outer FEP sheath was cut back to 4 mm at one end.
3. The exposed silver-plated wire screen mesh was then unwoven with a syringe needle gently to avoid severing the strands, starting at the end and working backwards circumferentially.
4. The unwoven mesh was divided into three equal parts and wound into separate strips.
5. For the *serial* connection, two of the strips were removed.
6. For the *parallel* connection, only one of the strips was cut off.
7. The remaining strips were measured and trimmed to 3 mm each.
8. Next 2 mm of the extended (inner) PTFE insulation was measured and cut back to expose 2 mm of the centre steel stranded conductor.
9. All the bared wires were tinned for subsequent soldering on the ceramic.

iii. Wiring the ceramic

Materials:

- Prepared ceramics
- Prepared coaxial cables
- Cleaner degreaser- ITW Chemtronics Electro-wash PR *(RS Components Ltd.)*

Tools / Equipment:

- Soldering station with temperature control
- Bench vice / toolmaker's clamp

1. Holding the ceramic in the clamp, it was degreased with the degreaser using cotton buds.
2. The temperature of the soldering tip was set to 300°C (the piezoelectric ceramic had a Curie temperature of ≈ 330°C, beyond which it could lose its polarisation).

3. The tinned bared wires were soldered on to the ceramic according to type of ceramic and connection desired. Prolonged heating was avoided to at all times to protect the ceramic from depolarisation as mentioned above.
   For the *serial* connection, the two wires were soldered on to each side of the ceramic.
   For the *parallel* connection, the centre steel strand was soldered on to the metal shim (the little filed triangular patch on the ceramic), while the remaining two strips were soldered on to opposite sides of the ceramic.
4. A quick check using a multimeter was performed to ensure there was no short circuit within the connections.
5. Connecting the other end of the cable to a function generator, the wired ceramic, which could then be called a 'bender element', was excited and checked for 'singing'-vibration of the ceramic giving a soft humming, evidence that the connections were sound.

iv. Preparation of the resin mixture for encapsulation

Material:

- Araldite HY951 hardener (8-10 *pbw)
- Araldite MY753 resin (100 pbw)

**pbw- parts by weight*

Tools / Equipment:

- Disposable petri dishes
- 2 ml disposable syringes and needles

1. Using separate 2 ml syringes, 20 ml of MY753 and 2 ml of HY951 were deposited in a petri dish.
2. The two parts were quickly mixed into an even mixture (mixture has a low viscosity and a recommended standing period of 30 minutes).
3. The mixture was then drawn into the syringe, ready for potting the bender elements in the mould.

v. Encapsulating the bender element

Materials:

- Bender elements
- Resin mixture

- Liquid release agent- ITW Devcon *(RS Components Ltd.)*
- Cleaner degreaser- ITW Chemtronics Electro-wash PR *(RS Components Ltd.)*

Tools / Equipment:

- Aluminium split potting mould (designed and fabricated in-house) (see Figures 3.1 and 3.2)
- 2 ml disposable syringes and needles
- Miniature G-clamp
- Files

1. Liquid release agent was applied on the inner surfaces of the mould, including the holes for the screws to prevent the resin holding the mould together upon setting.
2. The bender element and a short length of the cable (which was to be encapsulated in resin within the mould) were degreased too.
3. The bender element was then placed in the bottom half of the mould with care, ensuring that the rounded corners were secured in position.
4. Next the top half of the mould was put on and the four counter-sunk screws were inserted and tightened to hold the mould firmly together.
5. Inclining the mould at approximately 45°, the syringe needle was inserted through the needle access on the mould and the resin was slowly discharged into the mould. The mould was lightly tamped while injecting the resin to avoid entrapping air bubbles in the encapsulation process.
6. As the resin rose to the brim, the mould was gently returned to the vertical position.
7. Just as the resin reached the brim of the mould, the needle was withdrawn slowly and the needle access sealed with a wooden peg (trimmed from a matchstick).
8. Holding the protruding cable in the centre position with a miniature G-clamp and a short length of wire (for tying the cable to the G-clamp), the mould was placed in the oven at 105°C for 1 hour.
9. After the curing period of an hour, the mould was taken out of the oven and allowed to cool down to room temperature.
10. Once the mould was cool enough to be handled with bare hands, the mould was dismantled and the encapsulated bender element was extracted carefully.
11. Excess resin protrusion of 1 mm at the end (lengthwise) and peripheral uneven edges were trimmed off with a file as a finishing touch.

12. Again, connecting the cable to a function generator, the now encapsulated bender element was excited and checked for 'singing'.

vi. Potting the bender element in a brass cup

Materials:

- Encapsulated bender element
- Resin mixture
- Brass cup, 20 mm external diameter, 20 mm deep, with pre-drilled 2 mm cable access at the base
- Liquid release agent- ITW Devcon *(RS Components Ltd.)*
- Cleaner degreaser- ITW Chemtronics Electro-wash PR *(RS Components Ltd.)*

Tools / Equipment:

- Perspex 2-part potting holder with screw to hold bender element in position (fabricated in-house)
- 2 ml syringes and needles
- 10 ml syringe and needle
- Files
- Bench vice / toolmaker's clamp

1. The same mixture of resin was prepared, but with increased quantities- 40 ml of MY753 and 4 ml of HY951. The mixture was drawn into a 10 ml syringe for the subsequent potting.
2. Liquid release agent was applied on the interior of the potting holder, while the encapsulated bender element was cleaned with degreaser to ensure good adhesion.
3. With the brass cup clamped, the bender element was kept in the centre of the cup with a protrusion of 7 mm from the rim with the potting holder (by adjusting the screw on the holder, see Figure A2). The cable outlet at the base of the brass cup was sealed with plasticine to avoid leakage of the resin.
4. Resin was then slowly introduced into the brass cup through the needle access on the top cap of the holder.
5. Overflowing of the resin was kept at bay by not filling the cup right to the brim. Also, leaving a gap between the surface of the resin and the potting holder avoided the problem of the holder being stuck firmly to the resin upon setting.

6. The resin was then left to set at room temperature for 12 hours (overnight curing was found adequate for secure removal of the top half of the holder).
7. The top half of the holder was removed and the brass cup was topped up with resin to the brim, achieving as flat a surface as possible. Unfortunately, heaving at the peripherals of the bender element was often inevitable.
8. A continuation of another 24 hours curing period at room temperature was allowed for.
9. Finally, excess resin that 'heaved' around the bender element was trimmed off with a file to flush with the rim of the brass cup.

vii. Connecting the BNC plug

Material:

- RG178 BNC (Bayonet Neill Conringman) clamp plug *(RS Components Ltd.)*

Tools / Equipment:

- 15 cm ruler
- Cable cutter and stripper
- Syringe needle
- Bench vice / toolmaker's clamp

1. Referring to the instructions enclosed in the BNC clamp plug pack, parts of the plug were assembled in the correct order: connector body, centre contact or bayonet, insulator, braid clamp, gasket, washer and nut (from front to back).
2. The cable was trimmed and stripped to the required dimensions: 9 mm of FEP insulator, 2.5 mm of the wire screen mesh, unwoven (with the syringe needle) and folded back, 2.5 mm of PTFE insulator and 4 mm of bared centre connector.
3. The cable was put through all parts of the connector except the bayonet and connector body, which were to be put on later.
4. With the bayonet held inversely in the clamp, the centre steel strand was soldered on to it.
5. The connector body was then put over the bayonet and the nut was tightened to hold all the parts in one piece. The connector was ready to be plugged on.

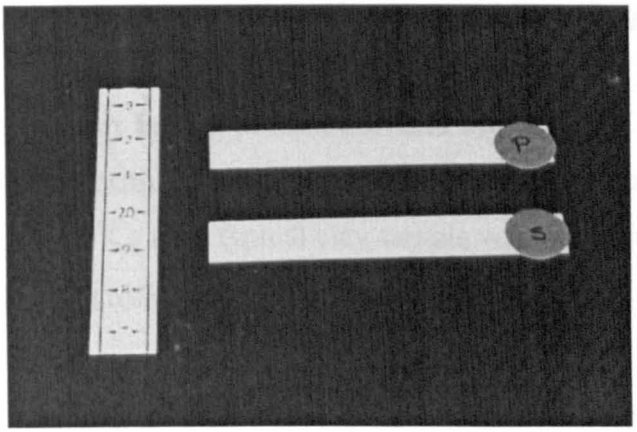

Figure A1: Bimorph PZT-5A piezoceramic strips.

Figure A2: Some materials, accessories and tools for making bender element probes (left to right)-

Back: 75 mm square, 15 cm ruler, wire stripper, wire cutter, diamond-plated file, syringe and needle.

Front: BE potting holder, BNC plug, brass cup, diamond wheel cutter.

Appendix B

Calculations for Hoop Strain and Strain Gauge Voltage Output of Oedo-BE Ring

i. Hoop strain induced by lateral pressure within the oedo-BE ring

Using Jaky's (1944) expression for normally consolidated clay, the coefficient of lateral earth pressure at rest, K_o, for a typical clay sample was estimated.

Taking the angle of shearing resistance, $\phi' = 25^o$,

$$[K_o = 1 - \sin \phi'] \quad \text{(Eq. 4.12)}$$

$$\Rightarrow \quad K_o = 1 - \sin (25^o)$$

$$\mathbf{K_o = 0.577}$$

At maximum vertical stress, σ_v = 800 kPa, the internal pressure or lateral stress, σ_h was calculated as follows:

$$[K_o = \sigma_h/\sigma_v'] \quad \text{(Eq. 4.11)}$$

$$\Rightarrow \quad 0.577 = \sigma_h / 800$$

$$\mathbf{\sigma_h = 462\ kPa}$$

Based on the maximum internal pressure of 462 kPa, the hoop stress and corresponding hoop strain were obtained using the following equation for a thin-walled cylinder (e.g. Roark and Young 1975).

$$[\sigma_h = \sigma_c t / r], \quad \text{(Eq. B1)}$$

where σ_h = internal pressure or lateral stress
= 462 kPa

σ_c = hoop stress

t = wall thickness

r = radius of cylinder

$$\Rightarrow \quad 462\ \text{kPa} = \sigma_c\ (0.0008\ \text{m}) / (0.05\ \text{m})$$

$$\sigma_c = \mathbf{28875\ kPa}$$

$$[E = \sigma_c / \varepsilon_c] \qquad \text{(Eq. B2)}$$

where E = Young's modulus (stainless steel Type 316)
= 193 MPa (Callister 1991)
ε_c = hoop strain

$$\Rightarrow \quad 193 \times 10^6\ \text{kPa} = 28875\ \text{kPa} / \varepsilon_c$$

$$\varepsilon_c = 1.496 \times 10^{-4}$$

$$\boldsymbol{\varepsilon_c = 1.496 \times 10^{-2}\ \%}$$

A plot of the hoop strain induced by σ_h of 462 kPa against various wall thicknesses is shown in Figure B1. It was important to have a wall that was as thin as was practically possible, yet sufficiently robust to endure repeated use.

ii. Estimation of strain gauge voltage output

The gauges were organised in a Wheatstone full-bridge circuit to achieve maximum voltage output (Figure B2). Two similar circuits were mounted on the ring, with a total of eight strain gauges. This was primarily to ensure a backup should either of the circuits malfunction. Each circuit consisted of four gauges, with a pair on opposite sides of the ring. In each pair, the gauges were arranged perpendicular to one another: the horizontally orientated gauge measured the hoop strain while its vertical counterpart registered the vertical strain.

The calculations were essentially based on Ohm's law, as briefly explained below.

Ohm's Law: The electrical current in any conductor is proportional to the potential difference (voltage) between its ends, with all other factors remaining constant.

$$[V = IR] \qquad \text{(Eq. B3)}$$

where V = potential difference = input voltage (V_{in})
I = current
R = resistance

Referring to Figure B2 and taking Poisson's ratio, ν, as 0.3 (Callister 1991) for the ring, estimated outputs for both arms of the full-bridge circuit (i.e. 2-3-1 and 2-4-1) were as follow:

Horizontal gauges: $R_{24} = R + \delta R$

$R_{14} = R - 0.3\delta R$

Vertical gauges: $R_{13} = R + \delta R$

$R_{23} = R - 0.3\delta R$

$$I_{241} = V / (R_{24} + R_{14})$$

$$\Rightarrow I_{241} = V_{in} / (R + \delta R) + (R - 0.3\delta R)$$

$$\mathbf{I_{241} = V_{in} / (2R + 0.7\delta R)}$$

$$V_{24} = I_{241} R_{24}$$

$$\Rightarrow V_{24} = V_{in} (R + \delta R) / (2R + 0.7\delta R)$$

$$\mathbf{V_{24} = (V_{in}R + V_{in}\delta R) / (2R + 0.7\delta R)}$$

$$I_{231} = V / (R_{23} + R_{13})$$

$$\Rightarrow I_{231} = V_{in} / (R - 0.3\delta R) + (R + \delta R)$$

$$\mathbf{I_{231} = V_{in} / (2R + 0.7\delta R)}$$

$$V_{23} = I_{231} R_{23}$$

$$\Rightarrow V_{23} = V_{in} (R - 0.3\delta R) / (2R + 0.7\delta R)$$

$$\mathbf{V_{23} = (V_{in}R - 0.3V_{in}\delta R) / (2R + 0.7\delta R)}$$

$$V_{out} = \pm V_{23} - V_{24}$$

$$\Rightarrow V_{out} = \pm [(V_{in}R - 0.3V_{in}\delta R) / (2R + 0.7\delta R)] - [(V_{in}R + V_{in}\delta R) / (2R + 0.7\delta R)]$$

$$\mathbf{V_{out} = \pm (1.3V_{in}\delta R) / (2R + 0.7\delta R)}$$

For negligibly small values of δR, $(2R + 0.7\delta R) \approx 2R$.

$$\Rightarrow \mathbf{V_{out} = \pm (1.3V_{in}\delta R) / 2R}$$

Gauge factor, $GF = 2.14$ (Table 3.4)

$[GF = (\delta R/R) / \varepsilon]$ (Eq. B4)

$\therefore \quad \mathbf{V_{out} = \pm 0.65\ V_{in}\ GF\ \varepsilon}$

For V_{in} of ±5 V and an amplification factor of 1000, as used for the 'original' circuits, the output voltage was estimated as follows:

$$V_{out} = \pm 0.65\ (5)\ (2.14)\ (1.496 \times 10^{-4}) \times (1000)$$

$$\mathbf{V_{out} = \pm 1.04\ V}$$

This in turn produced a calibration factor of 444 kN/m^2/V as shown in the calibration chart, Figure B3.

As for the 'new' circuits, V_{in} remained ±5 V but the amplification factor used was 500, hence the output voltage was halved as shown below:

$$V_{out} = \pm 0.65\ (5)\ (2.14)\ (1.496 \times 10^{-4}) \times (500)$$

$$\mathbf{V_{out} = \pm 0.52\ V}$$

The calibration factor was therefore doubled to 888 kN/m^2/V, as shown in Figure B4.

In comparison with the actual calibration factors from both circuits (Table 3.5), these predicted factors were consistently 4.5 to 11.5 % lower. Some plausible explanations were discussed in section 3.4.1.

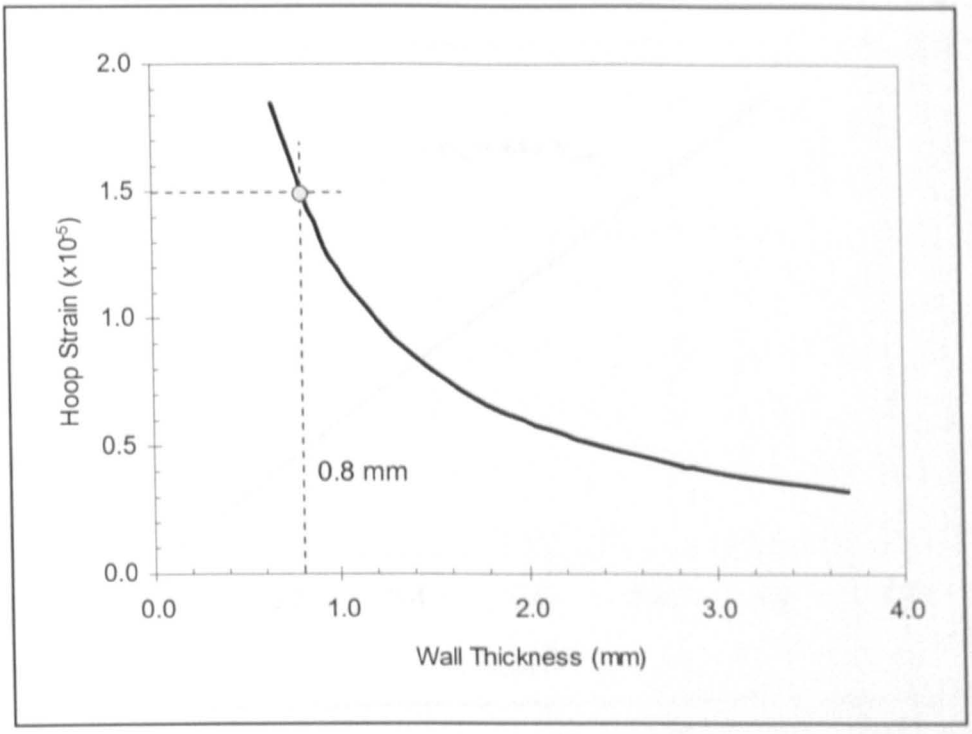

Figure B1: Hoop strain – wall thickness plot.

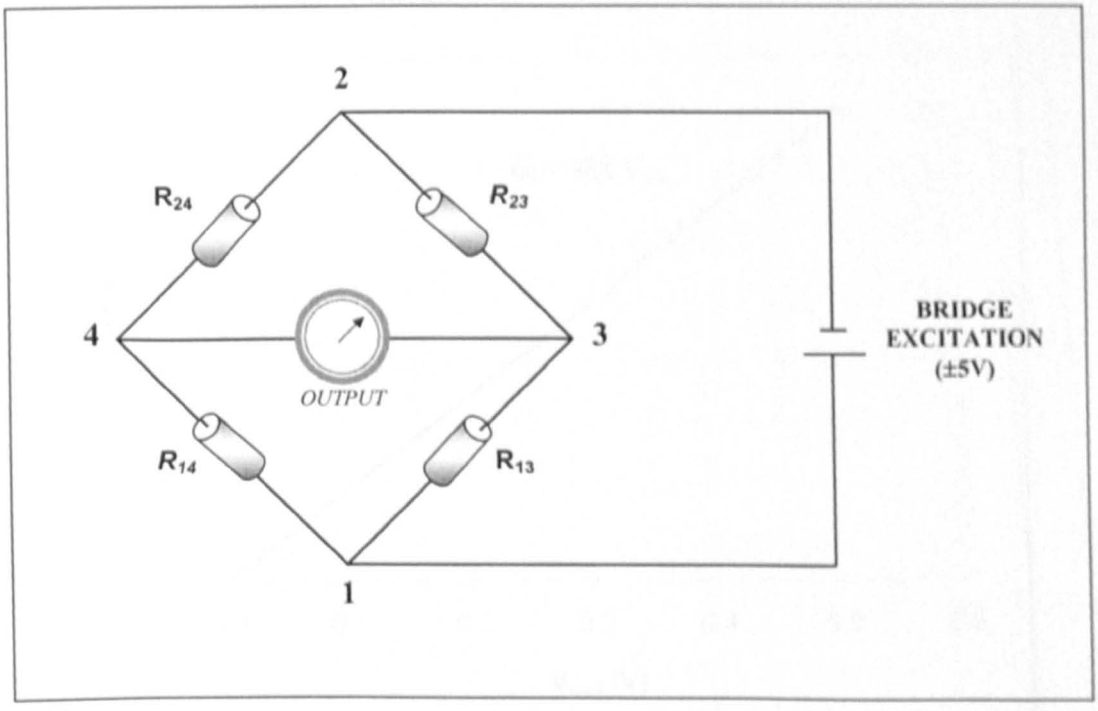

Figure B2: Wheatstone full-bridge circuit for the strain gauges.

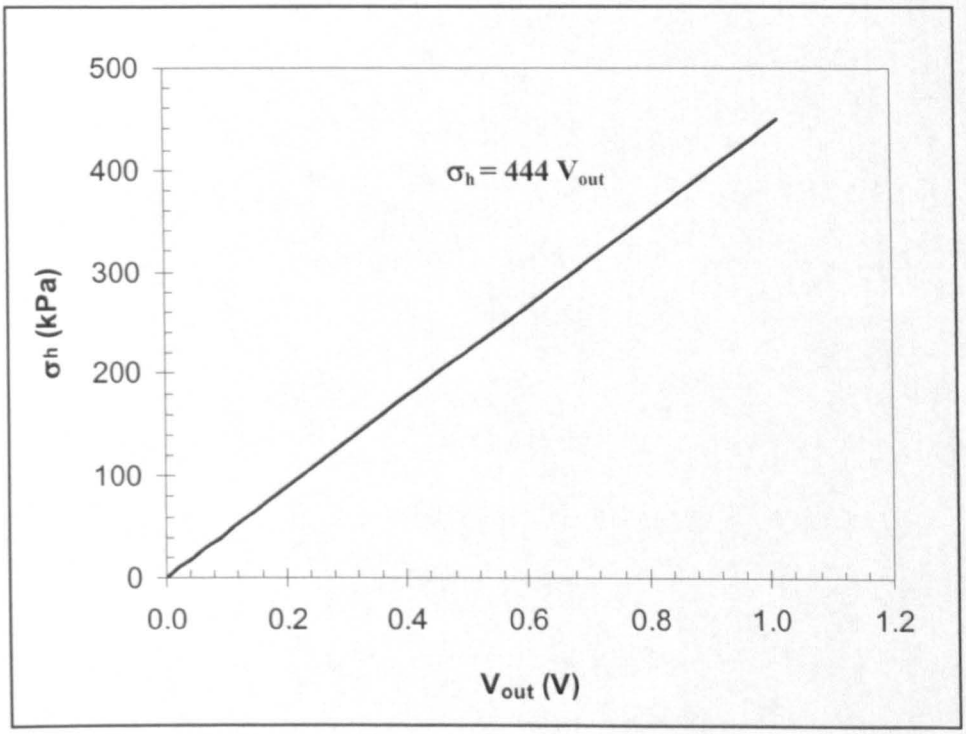

Figure B3: Predicted calibration chart- with amplification factor of 1000.

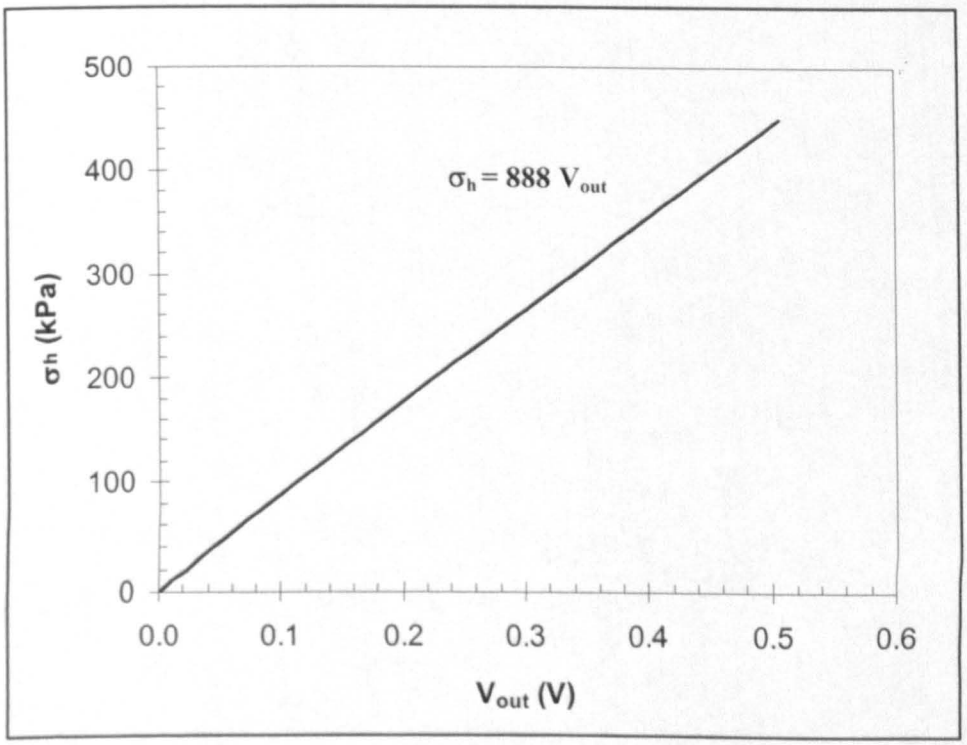

Figure B4: Predicted calibration chart- with amplification factor of 500.